

Utah State University

DigitalCommons@USU

---

All Graduate Theses and Dissertations

Graduate Studies

---

5-2016

## Computational Chemistry of Non-Covalent Interaction and Its Application in Chemical Catalysis

Vincent de Paul Nzuwah Nziko  
*Utah State University*

Follow this and additional works at: <https://digitalcommons.usu.edu/etd>

 Part of the [Chemistry Commons](#)

---

### Recommended Citation

Nziko, Vincent de Paul Nzuwah, "Computational Chemistry of Non-Covalent Interaction and Its Application in Chemical Catalysis" (2016). *All Graduate Theses and Dissertations*. 5248.  
<https://digitalcommons.usu.edu/etd/5248>

This Dissertation is brought to you for free and open access by the Graduate Studies at DigitalCommons@USU. It has been accepted for inclusion in All Graduate Theses and Dissertations by an authorized administrator of DigitalCommons@USU. For more information, please contact [digitalcommons@usu.edu](mailto:digitalcommons@usu.edu).



COMPUTATIONAL CHEMISTRY OF NON-COVALENT INTERACTION AND ITS  
APPLICATION IN CHEMICAL CATALYSIS

by

Vincent de Paul Nzuwah Nziko

A dissertation submitted in partial fulfillment  
of the requirements for the degree

of

DOCTOR OF PHILOSOPHY

in

Chemistry

Approved:

---

Steve Scheiner  
Major Professor

---

Alexander I. Boldyrev  
Committee Member

---

Alvan Hengge  
Committee Member

---

T.C. Shen  
Committee Member

---

Cheng-Wei Tom Chang  
Committee Member

---

Mark R. McLellan  
Vice President for Research and  
Dean of the School of Graduate Studies

UTAH STATE UNIVERSITY  
Logan, Utah

2016

Copyright © Vincent de Paul Nzuwah Nziko 2016

All Rights Reserved

## ABSTRACT

Computational Chemistry of Non-Covalent Interaction and its Application in Chemical  
Catalysis

by

Vincent de Paul Nzuwah Nziko, Doctor of Philosophy

Utah State University, 2016

Major Professor: Dr. Steve Scheiner  
Department: Chemistry and Biochemistry

Unconventional non-covalent interactions such as halogen, chalcogen, and tetrel bonds are gaining interest in several domains including but not limited to drug design, as well as novel catalyst design. Non-covalent interactions are known as weak forces of interactions when they are considered on an individual basis, but on a molecular basis, these effects become important such that their prevalence can be seen in the construction of large biomolecules like proteins, DNA and RNA. In this work, the fundamental aspects of these interactions are looked upon using *ab initio* and Density Functional Theory (DFT). An essential aspect of chalcogen bonds involving Sulfur as donor atom with nitrogen, oxygen and  $\pi$ -system as electron sources was examined. These bonds are strong with binding energy that varies from a minimum of 3 kcal/mol in some  $\pi$ -system to 19 kcal/mol in primary amine systems. Decomposition of the total interaction energy reveals that the induction energy constitutes more than half of the total interaction energy. The shortness and strength of some of the chalcogen bond interactions suggest these interactions may in

some cases be described as weak covalent bonds. A comparative study of  $\pi$ -hole tetrel bonding with  $\sigma$ -hole halogen bonds in complexes of XCN ( $X = \text{F, Cl, Br, I}$ ) and ammonia shows that the  $\pi$ -hole geometry is favored for  $X = \text{F}$ , and the  $\sigma$ -hole structure is preferred for the heavier halogens. Also, the potential use of these non-covalent interactions in organic catalysis was explored. The energy barrier of the Aza-Diels-Alder reaction is substantially lowered by the introduction of an imidazolium catalyst with either a Hydrogen or halogen (X) atom in the 2-position.

(269 pages)

## PUBLIC ABSTRACT

Computational Chemistry of Non-Covalent Interaction and its Application in Chemical  
Catalysis

Vincent de Paul Nzuwah Nziko

Known to be weaker than conventional covalent bonds, non-covalent bonds, especially hydrogen bond, has shown to be of great importance in molecular structures such as DNA, RNA, proteins and other organic frameworks. In this dissertation, we looked at non-covalent interactions other than the hydrogen bond. Replacement of the bridging hydrogen atom in a typical hydrogen bond by other atoms such as halogen, chalcogen and tetrel lead to the formation of interactions which are comparable in strength to the hydrogen bond. Unlike the hydrogen bond which arises mainly from electrostatics, these unconventional interactions mostly result from induction. Besides studying the fundamentals of these interactions, potential applications of these forces especially in organic catalysis are also explored.

## DEDICATION

I would like to dedicate this work to my Family.

## ACKNOWLEDGMENTS

There are many people to whom I will like to express my significant thanks for enabling me go through this stage of life and completing this work. In that respect, I would like to express my sincere gratitude to my advisor Professor Steve Scheiner for giving me a new name “Victor” also for his guidance, motivation, and advice throughout my research and study in his group. Your expertise and mentorship have enabled me to develop professional skills that will benefit me in many aspects of my career for the years to come. My thesis committee has significantly enhanced my graduate experience. In this regard, I am grateful to Dr. Alexander I. Boldyrev, Dr. Alvan Hengge, Dr. Tom Chang and Dr. T. C. Shen for their valuable suggestions, meaningful discussions, and valuable insights. Special thanks to Dr. Tapas Kar for his constant help and support during my research work.

I am thankful to Binod Nepal, Upendra Adhikari, Sandra Lundell, Alex Ivanov, Timur Galeev, Ivan Popov, Nimesh Khadka and Marina Fosso for their help, camaraderie, and discussion during my studies here.

I will also like to thank the Department of Chemistry and Biochemistry at Utah State University for providing me with the possibility to pursue my graduate education as well as offering me teaching assistantships.

I am thankful to the Division of Research Computing in the Office of Research and Graduate Studies at Utah State University for the use of their computer and storage facilities.



## CONTENTS

	Page
ABSTRACT.....	iii
PUBLIC ABSTRACT .....	v
DEDICATION.....	vi
ACKNOWLEDGMENTS .....	vii
LIST OF TABLES.....	xi
LIST OF FIGURES .....	xiv
LIST OF SCHEMES.....	xviii
ABBREVIATION.....	xix
CHAPTER	
1. INTRODUCTION .....	1
References.....	11
2. CHALCOGEN BONDING BETWEEN TETRAVALENT SF <sub>4</sub> AND AMINES.....	18
Abstract .....	18
2-1. Introduction .....	18
2-2. Computational Method .....	20
2-3. Results .....	21
2-4. Summary .....	28
References.....	31
3. INTRAMOLECULAR S··O CHALCOGEN BOND AS STABILIZING FACTOR IN GEOMETRY OF SUBSTITUTED PHENYL-SF <sub>3</sub> MOLECULES .....	48
Abstract .....	48
3-1. Introduction .....	48
3-2. Methods.....	52
3-3. Results and Discussion.....	52
3-4. Conclusion .....	63
References.....	65

4. S·· $\pi$ CHALCOGEN BOND BETWEEN SF <sub>2</sub> or SF <sub>4</sub> AND C-C MULTIPLE BOND .....	75
Abstract .....	75
4-1. Introduction .....	75
4-2. Theoretical Methods .....	78
4-3. Results .....	79
4-4. Discussion .....	86
4-5. Conclusion .....	89
References .....	90
5. INTERACTION BETWEEN THIOUREA AND IMINES:PRELUDE TO CATALYSIS .....	109
Abstract .....	109
5-1. Introduction .....	109
5-2. Computational Methods .....	111
5-3. Results .....	113
5-4. Discussion .....	122
References .....	124
6. COMPARISON OF $\pi$ -HOLE TETREL BONDING WITH $\sigma$ -HOLE HALOGEN BONDS IN COMPLEXES OF XCN (X = F, Cl, Br, I) AND NH <sub>3</sub> .....	140
Abstract .....	140
6-1. Introduction .....	140
6-2. Methods .....	143
6-3. Results .....	144
6-4. Discussion and Conclusion .....	151
References .....	153
7. CATALYSIS OF THE AZA-DIELS-ALDER REACTION BY HYDROGEN AND HALOGEN BONDS .....	169
Abstract .....	169
7-1. Introduction .....	169
7-2. Computational methods .....	172
7-3. Results .....	173
7-4. Discussion and Summary .....	189
References .....	191
8. EFFECT OF ANGULAR DEFORMATION ON THE ENERGETICS OF THE S <sub>N</sub> 2 REACTION .....	204

Abstract .....	204
8-1. Introduction .....	204
8-2. Theoretical Methods.....	206
8-3. Results .....	207
8-4. Discussion and Summary.....	210
References.....	212
9. SUMMARY .....	220
References.....	226
APPENDICES .....	228
APPENDIX A. Copyright permissions .....	229
CURRICULUM VITAE .....	246
Education .....	246
Research Experience .....	246
Teaching Experience .....	246
Expertise: .....	247
Publications (16) .....	248
Poster Presentation (05) .....	250

## LIST OF TABLES

Table		Page
2-1	Energetic (kcal/mol) and geometric aspects of alkylamine:SF <sub>4</sub> complexe .....	40
2-2	Energetic (kcal/mol) and geometric aspects of heteroaromatic amine:SF <sub>4</sub> complexes .....	40
2-3	Properties of divalent and trivalent S complexes .....	41
2-4	Extrema in the molecular electrostatic potentials (kcal/mol), on an isodensity surface corresponding to 0.001 au. ....	41
2-5	NBO second order perturbation energy (kcal/mol) for complexes with SF <sub>4</sub> .....	42
2-6	Changes in NBO atomic charges (me) within SF <sub>4</sub> that occur upon formation of complex with indicated amine .....	42
3-1	Relative energies, O...S interatomic distances, and interaction angle in configurations containing a S...O bond. ....	69
3-2	NBO E(2) (kcal/mol) for transfer from O lone pairs to $\sigma^*(\text{SF})$ antibonding orbital. ....	69
3-3	Changes in r(S-F) bond lengths (mÅ) of indicated molecules. ....	70
3-4	Changes in NBO atomic charges (me) of F atoms of indicated molecules. ....	70
3-5	Energetic (kcal/mol), geometric, and electronic properties of substituted derivatives of 1B. ....	71
4-1	Geometric aspects (Å, degs) of complexes, optimized at MP2/aug-cc-pVDZ leve .....	101
4-2	Binding Energies (Eb), kcal/mol .....	101
4-3	NBO values of E(2) (kcal/mol) for indicated charge transfers, with aug-cc-pVDZ basis set. ....	102
4-4	NBO interorbitala and totalb charge transfer (me) with aug-cc-pVDZ basis set. ....	102

4-5	Values of density and its Laplacian (au) at AIM bond critical points.....	103
4-6	Binding Energies (Eb), kcal/mol, computed at various levels of theory <sup>a</sup> .....	103
5-1	Electron density ( $10^{-2}$ au) at indicated AIM bond critical point .....	128
5-2	Interaction energies (kcal/mol) for complexes of thiourea with CH <sub>2</sub> NH calculated with aug-cc-pV(X)Z basis set.....	128
5-3	Interaction energies (kcal/mol) for complexes of thiourea with NHCHOH.....	128
5-4	Interaction energies (kcal/mol) for complexes of thiourea with CH <sub>2</sub> NOH.....	129
5-5	Interaction energies (kcal/mol) for complexes of thiourea with CH <sub>2</sub> NNH <sub>2</sub> .....	129
5-6	Changes in C-N bond length of imines (mÅ) caused by formation of indicated heterodimer .....	129
6-1	Energetic and geometric aspects of $\pi$ -hole complexes XCN $\cdots$ NH <sub>3</sub> .....	161
6-2	Energetic and geometric aspects of $\sigma$ -hole complexes NCX $\cdots$ NH <sub>3</sub> .....	161
6-3	SAPT components (kcal/mol) of total interaction energy of $\pi$ -hole complexes XCN $\cdots$ NH <sub>3</sub> .....	161
6-4	SAPT components (kcal/mol) of total interaction energy of $\sigma$ -hole complexes NCX $\cdots$ NH <sub>3</sub> .....	162
6-5	Interaction Energies (kcal/mol) of $\pi$ -hole complexes XCN $\cdots$ NH <sub>3</sub> calculated at various levels.....	162
6-6	Interaction Energies (kcal/mol) of $\sigma$ -hole complexes NCX $\cdots$ NH <sub>3</sub> calculated at various levels.....	162
6-7	Interaction energies (kcal/mol) of five heterotrimer geometries of XCN(NH <sub>3</sub> ) <sub>2</sub> .....	163
6-8	Three-body term $\Delta_3E$ (kcal/mol) of heterotrimers of XCN(NH <sub>3</sub> ) <sub>2</sub> .....	163
7-1	Interatomic distances (Å)Interatomic distances (Å).....	195

7-2	Energetics (kcal/mol) of aza-Diels-Alder reaction with various substitutions on catalyst .....	195
7-3	NBO values of E(2) (kcal/mol) between imine and diene within the TS .....	196
7-4	NBO group charges (e)NBO group charges (e) .....	196
7-5	Energy eigenvalues (au) of the $\pi^*$ imine LUMO in complex with indicated catalyst .....	197
7-6	Attractive SAPT components (kcal/mol) of the interaction energy between imine and catalyst, prior to introduction of diene .....	197
7-7	Free energies (kcal/mol) of aza-Diels-Alder reaction in the endo conformation with various substitutions on catalyst, evaluated at 298 K and 1 atm. ....	197
7-8	Free energies (kcal/mol) of aza-Diels-Alder reaction in the exo conformation with various substitutions on catalyst, evaluated at 298 K and 1 atm. ....	198
7-9	Energies (kcal/mol) computed at the MP2 level with the aug-cc-pVDZ basis set for the.....	198
7-10	Interatomic distances ( $\text{\AA}$ ) of exo conformation.....	199
7-11	Energetics (kcal/mol) of Diels-Alder reaction in the exo conformation .....	199
7-12	NBO values of E(2) (kcal/mol) between imine and diene within the TS in the exo. ....	199
7-13	NBO charges in the exo conformation.....	200
7-14	Energy eigenvalues (au) of the $\pi^*$ imine LUMO in complex with indicated catalyst in .....	200
8-1	$\theta(\text{F}\cdots\text{C}\cdots\text{I})$ angle in the transition state for $(\text{X}\cdots\text{CH}_2\text{R}\cdots\text{I})$ -.....	215
8-2	Calculated energy barriers to $\text{S}_{\text{N}}2$ reaction (kcal/mol).....	215
8-3	Distortion constant $k$ ( $\text{cal}\cdot\text{mol}^{-1}\text{deg}^{-2}$ ) fit to Eq (1).....	216

## LIST OF FIGURES

Figure		Page
1-1	a) Schematic representation of a Hydrogen bond b) NBO charge transfer in a typical water dimer.....	3
2-1	Atomic labeling used to define geometries of complexes of amines with SF <sub>4</sub> . ....	43
2-2	Heteroaromatic amines a) pyridine, b) pyrazine, c) pyridazine, d) pyrimidine, and e) imidazole used in this study. ....	43
2-3	SAPT components of interaction energy of indicated amine with SF <sub>4</sub> . ....	44
2-4	Interaction energies of amines with SF <sub>4</sub> calculated by SAPT (blue) and MP2 (red). Broken red line refers to binding energy at MP2 level. ....	45
2-5	MEP of HSF, SF <sub>2</sub> , and SF <sub>4</sub> , all calculated on isodensity surface of $\rho=0.001$ au.....	45
2-6	Overlap between NBO N lone pair orbital and a) $\sigma^*(\text{SFa})$ b) $\sigma^*(\text{SFb})$ .....	46
2-7	Variation of $E(2)$ for transfer from N lone pair into $\sigma^*(\text{SFa})$ and $\sigma^*(\text{SFb})$ antibonding orbitals, as function of rotation of SF <sub>4</sub> around S-Fb axis, $\phi(\text{N}\cdots\text{SFbFa})$ .....	46
2-8	Rearrangement of electron density in a) NH <sub>3</sub> $\cdots$ SF <sub>4</sub> and b) imidazole $\cdots$ SF <sub>4</sub> complexes. Purple and yellow regions correspond respectively to increases and decreases, contours are $\pm 0.003$ au. ....	47
3-1	Optimized geometries of various minima. Distances in Å.....	72
3-2	Optimized geometries of various minima of molecules containing two -CH <sub>2</sub> OCH <sub>3</sub> groups. Distances in Å. ....	73
3-3	Molecules used to evaluate density redistribution patterns and isodesmic values of S $\cdots$ O bond energies. ....	73

3-4	Electron density redistribution of molecule 1B, using isodesmic system in Fig 3-3. Purple regions indicate density increase, and losses are shown in yellow. Isocontour illustrated is $\pm 0.0015$ au. ....	74
4-1	Optimized geometries of SF <sub>2</sub> with ethyne, ethylene, cis-butadiene, trans-butadiene, and benzene. Distances in Å. Small purple sphere represents midpoint of indicated bond. ....	104
4-2	Optimized geometries of SF <sub>4</sub> with ethyne, ethylene, cis-butadiene, trans-butadiene, and benzene. Distances in Å. Small purple sphere represents midpoint of indicated bond. ....	105
4-3	Attractive SAPT components of interaction energies of alkenes with a) SF <sub>2</sub> and b) SF <sub>4</sub> . ES=electrostatic, IND=induction, DISP=dispersion. ....	106
4-4	Diagrammatic representations of relevant NBO orbitals of SF <sub>2</sub> and cis-butadiene. Red and blue lobes indicate opposite sign of each wave function. ....	107
4-5	Electron density redistributions accompanying formation of indicated complexes. Purple and yellow regions indicate gain and loss of density, respectively. Contours shown represent $\pm 0.001$ au. ....	108
5-1	Molecular electrostatic potentials (MEPs) of a) thiourea, b) CH <sub>2</sub> NH, c) NHCHOH, d) CH <sub>2</sub> NOH, and e) CH <sub>2</sub> NNH <sub>2</sub> , all on a surface corresponding to 1.5 x vdW radii. Colors vary from -0.04 au (red) to +0.04 au (blue). Red/black dots indicate positions of V <sub>s,max</sub> . ....	130
5-2	Optimized geometries of complexes of thiourea with CH <sub>2</sub> NH. Red number refers to interaction energy (kcal/mol) evaluated at the CCSD(T)/CBS level. Distances are in Å, and angles in degs. The NBO value of E(2) is in kcal/mol. ....	131
5-3	Optimized geometries of complexes of thiourea with NHCHOH. Red number refers to interaction energy (kcal/mol) evaluated at the CCSD(T)/CBS level. Distances are in Å, and angles in degs. The NBO value of E(2) is in kcal/mol. ....	132
5-4	Optimized geometries of complexes of thiourea with CH <sub>2</sub> NOH. Red number refers to interaction energy (kcal/mol) evaluated at the CCSD(T)/CBS level. Distances are in Å, and angles in degs. The NBO value of E(2) is in kcal/mol. ....	133



5-5	Optimized geometries of complexes of thiourea with CH <sub>2</sub> NNH <sub>2</sub> . Red number refers to interaction energy (kcal/mol) evaluated at the CCSD(T)/CBS level. Distances are in Å, and angles in degs. The NBO value of E(2) is in kcal/mol.....	134
5-6	Optimized geometries of complexes of thiourea with NHCHOH with NH trans to CH number refers to interaction energy (kcal/mol) evaluated at the CCSD(T)/CBS .....	134
5-7	SAPT partitioning of interaction energies in complexes of thiourea with a) CH <sub>2</sub> NH, b) NHCHOH, c) CH <sub>2</sub> NOH, and d) CH <sub>2</sub> NNH <sub>2</sub> .....	135
5-8	Calculated electron density shifts calculated at MP2/aug-cc-pVDZ level for complexes of thiourea with CH <sub>2</sub> NH. Blue and red regions refer respectively to gain and loss of electron density upon complexation. Contours represent ±0.001 au.....	136
5-9	Calculated electron density shifts calculated at MP2/aug-cc-pVDZ level for complexes of thiourea with NHCHOH. Blue and red regions refer respectively to gain and loss of electron density upon complexation. Contours represent ±0.001 au.....	137
5-10	Calculated electron density shifts calculated at MP2/aug-cc-pVDZ level for complexes of thiourea with CH <sub>2</sub> NOH. Blue and red regions refer respectively to gain and loss of electron density upon complexation. Contours represent ±0.001 au.....	138
5-11	Calculated electron density shifts calculated at MP2/aug-cc-pVDZ level for complexes of thiourea with CH <sub>2</sub> NNH <sub>2</sub> . Blue and red regions refer respectively to gain and loss of electron density upon complexation. Contours represent ±0.001 au.....	139
6-1	Molecular electrostatic potentials (MEPs) of XCN molecules. Black and blue dots respectively indicate positions of maxima and minima on the 0.001 au isodensity surface, with values displayed in kcal/mol. ....	164
6-2	Optimized geometries of $\pi$ -hole (top) and $\sigma$ -hole (bottom) dimers of NH <sub>3</sub> with XCN. Distances are in Å. Blue numbers refer to NBO values of E(2), in kcal/mol, for transfer from N lone pair to $\pi^*(\text{CN})$ (top) and $\sigma^*(\text{XC})$ (bottom). Number to right of slash ind.....	164

6-3	Electron density shifts that arise from formation of $\pi$ -hole complexes. Yellow and green regions respectively correspond to gain and loss of electron density, on the $\pm 0.0005$ au contour. ....	165
6-4	Optimized geometries of 2:1 heterotrimers of $\text{NH}_3$ with FCN. Red number indicates total interaction energy in kcal/mol. Distances are in Å in black. Blue numbers refer to NBO values of $E(2)$ , in kcal/mol, for transfer from N lone pair to $\pi^*(\text{CN})$ or $\sigma^*(\text{XC})$ . ....	165
6-5	Optimized geometries of 2:1 heterotrimers of $\text{NH}_3$ with ClCN. Red number indicates total interaction energy in kcal/mol. Distances are in Å in black. Blue numbers refer to NBO values of $E(2)$ , in kcal/mol, for transfer from N lone pair to $\pi^*(\text{CN})$ or $\sigma^*(\text{XC})$ .....	166
6-6	Optimized geometries of 2:1 heterotrimers of $\text{NH}_3$ with BrCN. Red number indicates total interaction energy in kcal/mol. Distances are in Å in black. Blue numbers refer to NBO values of $E(2)$ , in kcal/mol, for transfer from N lone pair to $\pi^*(\text{CN})$ or $\sigma^*(\text{XC})$ .....	167
6-7	Optimized geometries of 2:1 heterotrimers of $\text{NH}_3$ with ICN. Red number indicates total interaction energy in kcal/mol. Distances are in Å in black. Blue numbers refer to NBO values of $E(2)$ , in kcal/mol, for transfer from N lone pair to $\pi^*(\text{CN})$ or $\sigma^*(\text{XC})$ .. ....	168
7-1	Energy diagram of aza-Diels-Alder reaction of diene with imine (Im) and catalyst (cat).....	201
7-2	Encounter complex, transition state (TS) and product with no catalyst (top), H-bonding catalyst (middle), and I-bonding catalyst (bottom). Distances in Å. ....	202
7-3	Deformation energies (kcal/mol) of imine (green) and diene (black), catalyst (brown), and interaction energy (blue) of reaction with indicated catalyst. Total activation energy in red.....	203
8-1	Transition state geometries of $\text{S}_{\text{N}}2$ reactions, with F- as nucleophile. ....	218
8-2	Dependence of activation energy $E_1$ to angular distortion. ....	219

## LIST OF SCHEMES

Schemes	Page
3-1 Structure of a)DAST b) Deoxofluor, and c) 4-tert-Butyl-2,6-bis(methoxy)sulfur trifluoride .....	72
7-1 Aza Diels-Alder Reaction .....	201
8-1 Molecules considered for S <sub>N</sub> 2 reaction involving replacement of I by nucleophile. ....	217

## ABBREVIATION

Abbreviation	Definition
MP2	Second Order Moller-Plesset Perturbation Theory
NBO	Natural Bond Orbital
SAPT	Symmetry Adapted Perturbation Theory
EX	Exchange Repulsion
ES	Electrostatic
IND	Induction
DISP	Dispersion
EXIND	Exchange Repulsion Induction
EXDISP	Exchange Repulsion Dispersion
GIAO	Gauge Independent Atomic Orbital
CPCM	Conductor Polarized Continuum Model
NMA	N-Methyl Acetamide
CCSD(T)	Coupled Cluster Single Double (Triple)
DFT	Density Functional Theory

## CHAPTER 1

### INTRODUCTION

Noncovalent interactions are weak forces of attraction formed between two different entities or among the various fragments of the same entity. Although noncovalent interactions are much weaker than covalent bonds which result in the formation of molecules, non-covalent interactions play a critical role in the existence of molecular clusters like those present in bio-molecular systems and supramolecular systems.<sup>1-11</sup>

A clearer theoretical and experimental process of covalent bond formation was set in place following the Lewis definition of a covalent bond.<sup>12</sup> Unlike covalent interactions, non-covalent interactions still don't have a unified formulation; this is due in part to the variety of formation of non-covalent interactions leading to various ways of classifying this interaction. Covalent interactions are strong and their energetic values are on the order of hundreds of kcal/mol. On the other hand, noncovalent interaction ranges from weak van der Waals forces, which arise due to London dispersion, to relatively strong hydrogen bonds. On an individual basis, non-covalent interactions seem weak but cumulatively the energies of non-covalent interaction are momentous. Breaking and forming of covalent bonds generally lead to a chemical change whereas disruption or formation of non-covalent bonds brings about a physical phenomenon. The ambiguity in the definition of non-covalent interaction is a subject of interest within the scientific community which strives to provide a unified definition of non-covalent interaction. The importance of non-covalent interactions can never be overemphasized; they are useful in the organization of biomolecules like DNA, RNA, and proteins as well supramolecular chemistry and

catalysis. Non-covalent interactions are also shown to be responsible for the conformational preference of some small molecules as well as play a non-negligible role in the physical and chemical properties of molecules.<sup>13-21</sup>

The advancement in computing power has led to the development of reliable computational tools that are currently used to characterize a non-covalent interaction. These tools include but are not limited to Energetics, Energy decomposition, Cooperativity, Electrostatic potential, Atoms in Molecules, Natural Bond orbital (NBO), and Electron density redistribution. One may regard the interaction energy as the most important piece of information in the study of non-covalent interactions. When two monomers A and B are allowed to interact, the interaction energy generated as a result of their aggregation is calculated as difference between the energy of the AB complex and the sum of the energies of monomer A and monomer B. The resulting interaction energy is usually over estimated due to orbital overlap in the AB complex. This over estimation is usually corrected using the counter poise procedure. The interaction energy is often believed to originate from electrostatic, charge transfer (induction) and/or dispersion. The origin of the interaction energy can be ascertained via Symmetry Adapted Perturbation Theory (SAPT) analysis, Kitaura and Morokuma method or Natural Energy Decomposition analysis (NEDA). The perturbation of monomers upon complexation usually leads to electron redistribution which can be visualized as density shift maps. The electron density redistribution is obtained by subtracting the sum of densities of the monomers prior to interaction from the total electron density of the complex.

There are several types of non-covalent interactions namely van der Waals

interactions, hydrophobic interactions, ion-induced dipole, dipole-induced dipole and hydrogen bonds: each type differs in geometry, strength, and specificity. Amongst these interactions, the van der Waal interaction will stand on the lower end of an energy classification table. The van der Waal interaction is often at times used loosely for the totality of intermolecular interaction. The London forces are a special type of van der Waals interactions which originate from the interactive forces between instantaneous multipoles in molecules without permanent dipoles. The strength of the London-van der Waal interaction is a function of the polarizability of the molecules. London dispersion forces were shown to be solely responsible for keeping He atoms bound to each other.<sup>22</sup>

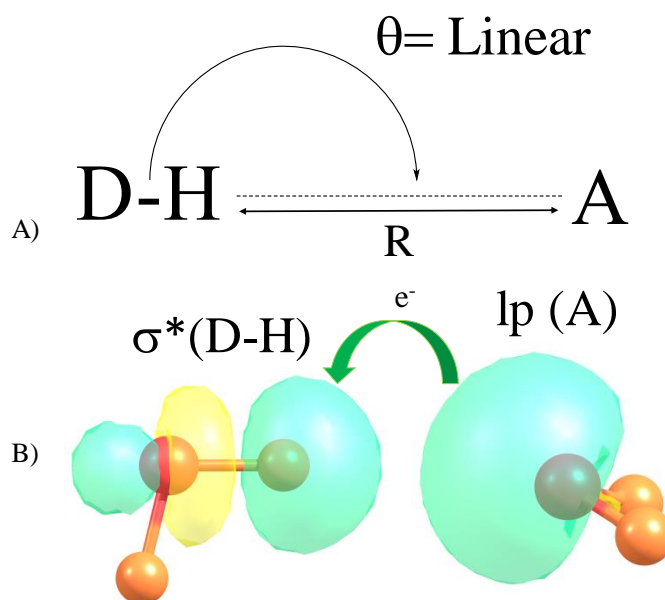


Figure 1-1. a) Schematic representation of a Hydrogen bond b) NBO charge transfer in a typical water dimer

Arguably, the most intensively studied and well-understood type of noncovalent interaction is the H-bond.<sup>23-32</sup> Historically, the H-bond was thought to be formed between a H atom covalently bonded to an electronegative atom such as N, O and /or F and another

electronegative atom. Figure 1-1 shows a pictorial representation of a typical H-bond where D is the proton donor or electron acceptor and A could be referred either as proton acceptor or electron donor.<sup>33-37</sup> Recent scientific investigations of the H-bond have open doors to a broader scope of the H-bond to include less electronegative atoms such as Cl, S, P, C as well as metals to act as proton donors. Dihydrogen bonds are special types of H-bonds in which a partially negatively charged H atom is able to engage in a H-bond with another H atom.<sup>38-41</sup>

H-bond is often believed to be electrostatic in nature as electrostatic attraction constitutes the major component of such interaction. Other attractive interactions that make up the H-bond include charge transfer or induction and dispersion interactions. The antibonding orbital of D-H ( $\sigma^*$ ) accepts electrons from the lone pair or  $\pi$ -orbital of an electron donor such as A as is the case in Figure 1-1 b. This charge transfers to the  $\sigma^*(\text{D-H})$  leads to the elongation of the D-H bond that results in a red shift of the D-H stretching frequency. This important observation is particularly useful for the experimental study of the H bond.

Geometrically, the angle subtended by the atoms D, H and A represented as  $\theta$  in Figure 1-1a should be linear. This arrangement facilitates the transfer of charge into the  $\sigma^*(\text{D-H})$ . Deviation of up to  $30^\circ$  from linearity has been observed, and this usually leads to a reduction in interaction energy strength. The distance ( $r$ ) between the bridging H and the electron donor A is less than the sum of the van der Waals radii of atom H and A. This distance generally correlates with the strength of the interaction energy.

Replacement of the bridging H-atom in an H bond by a member of the halogen



family notably Cl, Br and I lead to the formation of a novel type of non-covalent interaction which is similar to the H-bond known as the halogen bond.<sup>42-49</sup> The existence of the halogen bond was revealed in the 1800s, with the successful identification of the  $\text{NH}_3 \cdot \text{I}_2$  adduct.<sup>50-</sup><sup>54</sup> Energetically, the halogen bond stands as a strong rival to the H bond. Halogens are known to be electronegative atoms. When covalently bonded to a more electronegative group or atom as in D-X, where X is a halogen and D a more electronegative atom or group, its molecular electrostatic potential shows a region of positive potential in the vicinity of the halogen atom and along the extension of D-X bond. This area is termed an  $\sigma$ -hole<sup>43</sup>. This positively charged  $\sigma$ -hole can undergo electrostatic interaction with other electronegative atoms or with a source of  $\pi$  electrons. The similarity in  $\sigma^*(\text{D-H})$  with  $\sigma^*(\text{D-X})$  orbital suggest that this orbital can also act as an electron sink hence leading to an elongation of the D-X bond. In addition to the electrostatic attraction, other energetic components such as charge transfer or induction and dispersion component are also responsible for the strong nature of the halogen bond. Halogen bonding has much interest these days especially and it is being investigated for a range of functional applications including isomer separation, nonlinear optics, drug design, anion binding in solution and solid state, protein-ligand complexation and control reactions in the solid state.<sup>55-70</sup> In the early 2000s,<sup>71-73</sup> ultra-high resolution crystallographic analysis of the inhibitor IDD594 with aldose reductase clearly accounts for the short Br---O contacts. Howard et al <sup>71</sup> observed that the Br atom that is covalently bonded to an aromatic group of the inhibitor is 2.97 Å away from the hydroxyl O of the Thr113 in the protein. This distance is less than the sum of the van der Waals radii of Br and O-atoms hence satisfying the interaction

distance for halogen bond formation. The C-Br...O bond angle was reported to be  $152.8^\circ$  which shows a  $28^\circ$  deviation from linearity. Previous work in our group on other systems that possess halogen bond has shown that these interactions weaken as the interaction angle gets further away from linearity<sup>76</sup>. When Thr113 was mutated with Tyr residue, an amino acid which lacks the hydroxyl O, interestingly the inhibitor (IDD594) specificity for aldose reductase was lost in preference to the aldehyde reductase. This study has promoted more interest towards halogen bonds in ligand-enzymes interactions with over 700 PDB structures that show features that are characteristic of halogen bond.

The existence of the  $\sigma$ -hole is not only limited to the halogen atoms; members of the tetrel, pnictogen and chalcogen families also show this interesting feature and the resulting interactions are named after their group name.<sup>74-75</sup> The chalcogen bond is formed when a member of the chalcogen family replaces H-atom as the bridging atom in Figure 1-1a. Sulfur stands out as the default atom used in the study of chalcogen interactions. A comparative study of the chalcogen bond involving sulfur with hydrogen and halogen bonds was previously investigated in our group.<sup>76</sup> The electro positivity of S-atom in  $\text{SH}_2$  was achieved by systematic replacement of one H-atom by a halogen (X), this enabled the S to bind strongly with the N of  $\text{NH}_3$ . The binding energies were comparable to and sometimes stronger than that in a typical water dimer. When  $\text{X}=\text{F}$ , the FS...N geometry represented the global minimum on the HSF/ $\text{NH}_3$  potential energy surface. In this study, the S...N minimum was more stable than geometries containing a halogen bond. Many proteins possess amino acids with the S-S, S-H or the C-S covalent bond. The S-H bond in oxidoreductases such as thioredoxin utilizes this group as an active center.<sup>77</sup> Improvement

in spectroscopic instrumentation has enabled the observation of non-covalent interactions of the type S--- $\pi$  and S---X (X=O, N and S). These interactions have pertinent directionality and the S-atom act as electron acceptor.<sup>78-79</sup> Chopra et al<sup>80</sup> used computational tools to explore the role of substitution in the formation of XHSe---O/N chalcogen bonds with water and ammonia as electron donors' atoms. In this study, they found out that the strength of these interactions are strongly dependent on the electron withdrawing and electron donating potential of the substituent X an observation similar to a previous study on XHS---N interaction conducted by Adhikari and Scheiner.<sup>77</sup> Taylor et al<sup>81</sup> provided quantitative experimental data regarding the strength of chalcogen bond in the solution phase. Using UV-vis, <sup>1</sup>H, and <sup>19</sup>F NMR spectroscopy, they were able to trace the chalcogen bonding interactions between synthesized benzotelluradiazoles and a variety of Lewis bases including Cl<sup>-</sup>, Br<sup>-</sup>, I<sup>-</sup>, NO<sub>3</sub><sup>-</sup>. The data obtained from this study were compared to the values obtained from dispersion corrected B97-D3 calculations and were found to give good agreement with the experimental free energies of the chalcogen bonding. With respect to chalcogen bond, prior study of its interaction has centered on the divalent bonding situation for example SO<sub>2</sub>, HSF, and thiazole nucleosides.<sup>82-84</sup> Chalcogens especially S atom can engage in higher order bonding, for example, tetravalent S in H<sub>2</sub>SO<sub>4</sub> or SF<sub>4</sub>. In regard to this, this dissertation will address the following questions: Do the S---X (X= Lewis base) chalcogen bond exist in tetravalent S? Are the directional propensities of tetravalent S similar to those observed in divalent S? Can the tetravalent S chalcogen bond control molecular structure? Is the S chalcogen bond relevant in organic synthesis?

By analysis of the molecular electrostatic potential of CH<sub>3</sub>X where X is an

electronegative group, one notices a region of electronic charge depletion and accumulation around the C-atom and X-atoms respectively. This electron depleted region is similar to that observed along the extension of the D-X bond (X=halogen, D more electronegative than X) and can receive charge from electron rich sources. Similarly, this region is referred to as an  $\sigma$ -hole.<sup>85</sup> The term carbon bond or tetrel bond is used to describe interaction involving this  $\sigma$ -hole. These sought of interaction existed as far back as the reaction involving C-atom exist notably substitution nucleophilic reactions, but it is just of recent that these interactions have gained theoretical interest.<sup>85</sup> Despite it, relative short existence, much more is known about this interaction now. Using high-level ab initio computations, Grabowski<sup>85</sup> explored the detailed role played by the tetrel bond in a typical  $S_N2$  reaction in 2014. A competitive and cooperative study between tetrel and chalcogen bond was conducted by Cheng<sup>85</sup> using  $F_2CX$  (X=Se and Te) as an electron acceptor and HCN and  $NH_3$  as electron donors. He noticed that when X=Se, the tetrel bond formation was preferred over the chalcogen bond formation. But this observation was reversed when Te was used.

Despite the advances in experimental techniques such as microwave spectroscopy, IR, UV-vis and NMR in providing a better understanding of non-covalent interactions, a complete picture of these interactions at the molecular level is still not possible with the above mentioned techniques. A great number of computational publications are available in this area that aimed at complementing the limited experimental data available, yet many aspects of this topic are still devoid of clear understanding. Therefore, this dissertation will focus on the fundamentals of hydrogen, halogen, chalcogen and tetrel bonds in some

selected systems. The above interactions play important roles in molecular recognition, protein folding, structure parking as well as in organic catalysis. The latter will constitute another focal point of this dissertation as there is increased interest in the use of non-covalent interaction in catalysis. For example, the Jacobsen group<sup>86</sup> has successfully demonstrated using both experimental and computational methods that chiral bifunctional urea can catalyze the Povarov reaction via hydrogen bonding. In 2008, an important step in the application of the use of halogen bonds in catalysis was achieved by Bolm's group.<sup>87</sup> They demonstrated using experimental techniques that fluorinated alkyl halides could catalyze the reduction of substituted quinolones by Hantzsch esters. More so, Takeda and co-workers<sup>88</sup> considered a range of related halogen bonding agents in connection with the Diels-Alder reaction. They used a halogen substituted imidazolium salt as a catalyst in the Aza-Diels-Alder reaction. Their comparison of the closely related catalyst suggests that the reaction rate ought to match the expected order of halogen bond strength but left certain other issues incompletely resolved, and they suggested further studies of the details of the reaction mechanism. Despite these achievements in organocatalysis, many aspects such as detailed information about their reaction mechanism and specifically about the involvement of halogen bonds in this catalysis remain unknown. Therefore, this work will serve as a complement to the experimentation by using quantum calculations to elucidate fine detailed structures and energy of transient species such as the transition state, as well as any intermediates in the course of the reaction. A brief overview of each chapter in this dissertation is presented below.

In Chapter 2, a tetravalent sulfur, molecule in this particular case sulfur tetrafluoride

(SF<sub>4</sub>), is used as the prototype sulfur donor for a chalcogen interaction. Alkyl and aromatic amines were used as chalcogen bond acceptors. In this study, we aimed at filling the gap in the study of chalcogen bond. It was noticed that this bond is a strong one with binding energy ranging from 7-14 kcal/mol. Chapter 3 further looks into chalcogen bonds but from a different perspective. Here, the focus is mainly on the use of chalcogen bond as the primary stabilizing factor of substituted phenyl-SF<sub>3</sub> molecules. A comparative study of the sulfur valency was done in chapter 4, where divalent and tetravalent sulfur molecules were allowed to interact with both aromatic and non-aromatic p-systems. The catalytic importance of H-bond was illustrated in chapter 5. Here, the hydrogen bond interaction between thiourea and imines caused the C=N bond of the imine to elongate hence activating hence causing the imine to become susceptible to any nucleophilic attack. The halogen bond is rapidly gaining interest due in part to its similarity to the hydrogen bond. In chapter 6, the cooperative nature of this interaction with  $\pi$ -hole tetrel bond was studied using cyanogen halides as electron acceptor and ammonia as the electron donor. A comparative study of the halogen bond with tetrel was also conducted in this work and it turns out that the p-hole tetrel bonds are generally weaker than their halogen counterpart. Chapter 7 looks into the use of halogen bonds for catalysis, in this particular case, the catalysis of the Aza-Diels-Alder reaction. This work attempts to provide information about this reaction and specifically about the involvement of any halogen bond in its catalysis. The direct influence of the strength of the halogen bond is studied by a comparison of I with Br and Cl as the halogen atom on the catalyst. In order to extract further information about the influence of a halogen bond, we also consider an analogous catalyst which

replaces the halogen by H, i.e. comparison of halogen bond with the hydrogen bond.

## References

- (1) Hobza, P.; Zahradnik, R. *Weak Intermolecular Interactions in Chemistry and Biology*; Elsevier Scientific: Amsterdam, **1980**.
- (2) Hobza, P.; Muller-Dethlefs, K. *Non-Covalent Interactions*; RSC: Cambridge, **2010**.
- (3) Hobza, P.; Zahradnik, R.; Müller-Dethlefs, K. *Collect. Czech. Chem. Commun.* **2006**, 71, 443–531
- (4) Kaplan, I. G. *Theory of Molecular Interactions*; Elsevier: Amsterdam, **1986**.
- (5) Müller-Dethlefs, K.; Hobza, P. *Chem. Rev.* **2000**, 100, 143-147.
- (6) Stone, A. J. *The Theory of Intermolecular Forces*; Oxford University Press: Oxford, **2002**.
- (7) Gilson, M. K.; Mihailescu, M. *Biophys. J.* **2004**, 87, 23-36.
- (8) Kollman, P. A. *Acc. Chem. Res.* **1977**, 10, 365-371.
- (9) Beran, G. J. O. *Chem. Rev.* **2016**, 116, 5567.
- (10) Singhal, D.; Curatolo, W. *Advanced Drug Delivery Reviews* **2004**, 56, 335
- (11) Sharon, A.; Maulik, Prakas R.; Vithana, C.; Ohashi, Y.; Ram, Vishnu J. *Eur. J. Org. Chem.* **2004**, 2004, 886.
- (12) Lewis, G. N. *J. Am. Chem. Soc.* **1931**, 53, 1367.
- (13) Warshel, A.; Papazyan, A.; Kollman, P. A. *Science* **1995**, 269, 102-104.
- (14) Duncan, R.; Kopecek, J. *Adv. Polym. Sci.* **1984**, 57, 51-101
- (15) Lehn, J-M. *Angew. Chem., Int. Ed. Engl.* **1988**, 27, 89-112; *ibid.* 1990, 29, 1304-1319.

- (16) Huck, W. T. S.; Prins, L. J.; Fokkens, R. H.; Nibbering, N. M.; van Veggel, F. C. J.M.; Reinhoudt, D. N. *J. Am. Chem. Soc.* **1998**, 120, 6240-6246
- (17) Beer, P. D.; Gale, P. A.; Smith, D. K. *Supramolecular Chemistry*; Oxford University Press: New York, **1999**
- (18) Naoda, K.; Mori, H.; Oh, J.; Park, K. H.; Kim, D.; Osuka, A. *J. Org. Chem.* **2015**, 80, 11726.
- (19) Matczak-Jon, E.; Videnova-Adrabińska, V.; Burzyńska, A.; Kafarski, P.; Lis, T. *Chem. Eur. J.* **2005**, 11, 2357.
- (20) Sharon, A.; Maulik, Prakas R.; Vithana, C.; Ohashi, Y.; Ram, Vishnu J. *Eur. J. Org. Chem.* **2004**, 2004, 886.
- (21) Thomas, S. P.; Veccham, S. P. K. P.; Farrugia, L. J.; Guru Row, T. N. *Cryst. Growth Res.* **2015**, 15, 2110.
- (22) Aziz, R. A.; Slaman, M. J. *J. Chem. Phys.* **1991**, 94, 8047.
- (23) Lassettre, E. N. *Chem. Rev.* **1937**, 20, 259.
- (24) Jeffrey, G. A. *An Introduction to Hydrogen Bonding*; Oxford University Press, **1997**.
- (25) Scheiner, S. *Acc. Chem. Res.* **2013**, 46, 280.
- (26) Scheiner, S. *Molecular interactions: from van der Waals to strongly bound complexes*; Wiley, **1997**.
- (27) Scheiner, S. *Noncovalent Forces*; Springer International Publishing, **2015**
- (28) Scheiner, S. *Hydrogen Bonding: A Theoretical Perspective*; Oxford University Press, **1997**.
- (29) Schuster, P. *Hydrogen Bonds*; Springer-Verlag: Berlin, **1984**; Vol. 120.



- (30) Gilli, G.; Gilli, P. *The Nature of the Hydrogen Bond*; Oxford University Press:Oxford, UK, **2009**.
- (31) Alabugin, I. V.; Manoharan, M.; Peabody, S.; Weinhold, F. *J. Am. Chem. Soc.* **2003**, 125, 5973-5987.
- (32) Hernández-Soto, H.; Weinhold, F.; Francisco, J. S. *J. Chem. Phys.* **2007**, 127,164102.
- (33) Grzechnik, K.; Rutkowski, K.; Mielke, Z. *J. Mol. Struct.* **2012**, 1009, 96-102.
- (34) Gu, Y.; Kar, T.; Scheiner, S. *J. Am. Chem. Soc.* **1999**, 121, 9411-9422.
- (35) Howard, N. W.; Legon, A. C. *J. Chem. Phys.* **1986**, 85, 6898-6904
- (36) Scheiner, S., *The CH--O Hydrogen Bond. A Historical Account. In Theory and Applications of Computational Chemistry: The First 40 Years*; Dykstra, C. E.; Frenking, G.; Kim, K. S.; Scuseria, G. E., Eds.; Elsevier: Amsterdam, **2005**; pp 831-857
- (37) Takahashi, O.; Kohno, Y.; Nishio, M. *Chem. Rev.* **2010**, 110, 6049-6076.
- (38) Arunan, E.; Desiraju, G.R.; Klein, R.A.; Sadlej, J.; Scheiner, S.; Alkorta, I.; Clary,D.C.; Crabtree, R.H.; Dannenberg, J.J.; Hobza, P.; Kjaergaard, H.G.; Legon, A.C.;Mennucci, B.; Nesbitt, D.J. *Pure Appl. Chem.* **2011**, 83, 1619-1636
- (39) Kar, T.; Scheiner, S. *J. Chem. Phys.* **2003**, 119, 1473-1482
- (40) Solimannejad, M.; Scheiner, S. *J. Phys. Chem. A* **2005**, 109, 11933-11935.
- (41) Belkova, N. V.; Shubina, E. S.; Epstein, L. M. *Acc. Chem. Res.* **2005**, 38, 624-631.
- (42) Cavallo, G.; Metrangolo, P.; Milani, R.; Pilati, T.; Priimagi, A.; Resnati, G.; Terraneo, G. *Chem. Rev.* **2016**, 116, 2478.
- (43) Politzer, P.; Lane, P.; Concha, M. C.; Ma, Y.; Murray, J. S. *J. Mol. Model.* **2007**,

13, 305.

(44) Wolters, L. P.; Schyman, P.; Pavan, M. J.; Jorgensen, W. L.; Bickelhaupt, F. M.; Kozuch, S. *WIREs Comput Mol Sci* **2014**, 4, 523.

(45) Nguyen, H. L.; Horton, P. N.; Hursthouse, M. B.; Legon, A. C.; Bruce, D. W. *J. Am. Chem. Soc.* **2004**, 126, 16-17.

(46) Alkorta, I.; Rozas, S.; Elguero, J. *J. Phys. Chem. A* **1998**, 102, 9278-9285.

(47) Politzer, P.; Murray, J. S.; Clark, T. *Phys. Chem. Chem. Phys.* **2010**, 12, 7748-7757.

(48) Caronna, T.; Liantonio, R.; Logothetis, T. A.; Metrangolo, P.; Pilati, T.; Resnati, G. *J. Am. Chem. Soc.* **2004**, 126, 4500-4501.

(49) Glaser, R.; Chen, N.; Wu, H.; Knotts, N.; Kaupp, M. *J. Am. Chem. Soc.* **2004**, 126, 4412-4419.

(50) Glaser, R.; Chen, N.; Wu, H.; Knotts, N.; Kaupp, M. *J. Am. Chem. Soc.* **2004**, 126, 4412-4419.

(51) Colin, M. *Ann. Chim.* **1814**, 91, 252– 272

(52) Guthrie, F. *J. Chem. Soc.* **1863**, 16, 239– 244.

(53) Remsen, I.; Norris, J. F. *Am. Chem. J.* **1896**, 18, 90– 96.

(54) Benesi, H. A.; Hildebrand, J. H. *J. Am. Chem. Soc.* **1948**, 70, 2832– 2833.

(55) Benesi, H. A.; Hildebrand, J. H. *J. Am. Chem. Soc.* **1949**, 71, 2703– 2707.

(56) Bertani, R.; Metrangolo, P.; Moiana, A.; Perez, E.; Pilati, T.; Resnati, G.; Ricollattes, I.; Sassi, A. *Adv. Mater.* **2002**, 14, 1197– 1201.

(57) Nguyen, H. L.; Horton, P. N.; Hursthouse, M. B.; Legon, A. C.; Bruce, D. W. *J. Am. Chem. Soc.* **2003**, 126, 16– 17.

(58) Fourmigué, M.; Batail, P. *Chem. Rev.* **2004**, 104, 5379– 5418.

- (59) Cariati, E.; Forni, A.; Biella, S.; Metrangolo, P.; Meyer, F.; Resnati, G.; Righetto, S.; Tordin, E.; Ugo, R. *Chem. Commun.* **2007**, 2590–2592.
- (60) Sarma, J. A. R. P.; Allen, F. H.; Hoy, V. J.; Howard, J. A. K.; Thaimattam, R.; Biradha, K.; Desiraju, G. R. *Chem. Commun.* **1997**, 101–102.
- (61) Cariati, E.; Cavallo, G.; Forni, A.; Leem, G.; Metrangolo, P.; Meyer, F.; Pilati, T.; Resnati, G.; Righetto, S.; Terraneo, G.; Tordin, E. *Cryst. Growth Des.* **2011**, 11, 5642–5648.
- (62) Farina, A.; Meille, S. V.; Messina, M. T.; Metrangolo, P.; Resnati, G.; Vecchio, G. *Angew. Chem., Int. Ed.* **1999**, 38, 2433–2436.
- (63) Takeuchi, T.; Minato, Y.; Takase, M.; Shinmori, H. *Tetrahedron Lett.* **2005**, 46, 9025–9027.
- (64) Marras, G.; Metrangolo, P.; Meyer, F.; Pilati, T.; Resnati, G.; Vij, A. *New J. Chem.* **2006**, 30, 1397–1402.
- (65) Bruckmann, A.; Pena, M.; Bolm, C. *Synlett* **2008**, 2008, 900–902.
- (66) Walter, S. M.; Kniep, F.; Herdtweck, E.; Huber, S. M. *Angew. Chem., Int. Ed.* **2011**, 50, 7187–7191.
- (67) Kniep, F.; Jungbauer, S. H.; Zhang, Q.; Walter, S. M.; Schindler, S.; Schnapperelle, I.; Herdtweck, E.; Huber, S. M. *Angew. Chem., Int. Ed.* **2013**, 52, 7028–7032.
- (68) Beweries, T.; Brammer, L.; Jasim, N. A.; McGrady, J. E.; Perutz, R. N.; Whitwood, A. C. *J. Am. Chem. Soc.* **2011**, 133, 14338–14348.
- (69) Lu, Y.; Wang, Y.; Zhu, W. *Phys. Chem. Chem. Phys.* **2010**, 12, 4543–4551.
- (70) Matter, H.; Nazaré, M.; Güssregen, S.; Will, D. W.; Schreuder, H.; Bauer, A.; Urmann, M.; Ritter, K.; Wagner, M.; Wehner, V. *Angew. Chem., Int. Ed.* **2009**, 48, 2911–

2916.

- (71) Auffinger, P.; Hays, F. A.; Westhof, E.; Ho, P. S. *Proc. Natl. Acad. Sci. U. S. A.* **2004**, 101, 16789–16794.
- (72) Howard, E. I.; Sanishvili, R.; Cachau, R. E.; Mitschler, A.; Chevrier, B.; Barth, P.; Lamour, V.; Van Zandt, M.; Sibley, E.; Bon, C. *Struct., Funct., Genet.* **2004**, 55, 792–804.
- (73) Muzet, N.; Guillot, B.; Jelsch, C.; Howard, E.; Lecomte, C. *Proc. Natl. Acad. Sci. U. S. A.* **2003**, 100, 8742–8747.
- (74) Hays, F. A.; Vargason, J. M.; Ho, P. S. *Biochemistry* **2003**, 42, 9586–9597.
- (75) Solimannejad, M.; Gharabaghi, M.; Scheiner, S. *J. Chem. Phys.* **2011**, 134, 024312
- (76) Scheiner, S. *Phys. Chem. Chem. Phys.* **2011**, 13, 13860-13872.
- (77) Adhikari, U.; Scheiner, S. *Chem. Phys. Lett.* **2011**, 514, 36–39.
- (78) Nordberg J, Arner ESJ. *Free Rad. Biol. Med.* **2001**, 31, 1287-1312.
- (79) Bhattachary R, Pal, D.; Chakrabati, P; *Protein Eng. Des. Sel.* **2004**, 17, 795-808
- (80) Shukla, R.; Chopra, D. *J. Phys. Chem. B* **2015**, 119, 14857–14870.
- (81) Garrett, G.; Gibson, G.; Straus, R.; Seferos, D.; Taylo, M. *J. Am. Chem. Soc.* **2015**, 137, 4126–4133.
- (82) Bauzá, A.; Alkorta, I.; Frontera, A.; Elguero, J. *J. Chem. Theory Comput.* **2013**, 9, 5201-5210.
- (83) Iwaoka, M.; Takemoto, S.; Tomoda, S. *J. Am. Chem. Soc.* **2002**, 124, 10613-10620.
- (84) Rosenfield, R. E.; Parthasarathy, R.; Dunitz, J. D. *J. Am. Chem. Soc.* **1977**, 99, 4860-4862.
- (85) Chakrabati, P.; Bhattachary R.; *Prog. Biophys. Mol. Biol.* **2007**, 95, 83 -137.
- (86) Xu, H.; Zuend, S. J.; Woll, M. G.; Tao, Y.; Jacobsen, E. N. *Science* **2010**, 327, 986.

- (87) Bruckmann, A.; Pena, M. A.; Bolm, C. *Synlett* **2008**, 2008, 900.
- (88) Takeda, Y.; Hisakuni, D.; Lin, C.-H.; Minakata, S. *Org. Lett.* **2015**, 17, 318.

## CHAPTER 2

CHALCOGEN BONDING BETWEEN TETRAVALENT SF<sub>4</sub> AND AMINES<sup>1</sup>**Abstract**

The N··S chalcogen bond between SF<sub>4</sub> and a series of alkyl and arylamines is examined via ab initio calculations. This bond is a strong one, with a binding energy that varies from a minimum of 7 kcal/mol for NH<sub>3</sub> to 14 kcal/mol for trimethylamine. Its strength derives in large measure from charge transfer from the N lone pair into the  $\sigma^*(\text{SF})$  antibonding orbitals involving the two equatorial F atoms, one of which is disposed directly opposite the N atom. Decomposition of the total interaction energy reveals that the induction energy constitutes more than half of the total attraction. The positive region of the molecular electrostatic potential of SF<sub>4</sub> that lies directly opposite the equatorial F atoms is attracted to the N lone pair, but the magnitude of this negative region on each amine is a poor predictor of the binding energy. The shortness and strength of the N··S bond in the dimethylamine··SF<sub>4</sub> complex suggests it may better be described as a weak covalent bond.

**2-1. Introduction**

Of the various noncovalent bonds, the H-bond is arguably the most important and prevalent. It is typically formulated as the positioning of two molecules such that the H atom of one molecule, A-H, acts as a bridge to an atom D of another molecule. Although its earliest conception applied highly electronegative atoms like O, F, and N as donor and

---

<sup>1</sup> Coauthored by Vincent de Paul Nzuwah Nziko and Steve Scheiner. Reproduced with permission from *J. Phys. Chem. A* **2014**, *118*, 10849-10856. Copyright 2014, American Chemical Society.

acceptors <sup>1-3</sup>, a great deal of work since that time has broadened the picture to include other atoms such as C, S and Cl <sup>4-13</sup>. In addition, the proton need not interact with a lone pair of the acceptor atom, but also with other electron sources such as the  $\pi$ -systems of unsaturated molecules.

It is not only a proton which can serve as a bridge between two molecules. The anisotropic charge distribution around halogen atoms (X) allow them to act in a similar capacity <sup>14-25</sup>. More specifically, there is a positive pole region directly along the extension of each R-X covalent bond, surrounded by an equator of negative charge. This positive region, commonly termed a  $\sigma$ -hole, is able to interact attractively with a negatively charged atom of another molecule. The stability of this halogen bond is augmented by charge transfer into the  $\sigma^*(RX)$  antibonding orbital, precisely analogous to the case of a H-bond. And like its congener H-bond, the halogen bond can also be quite strong. This phenomenon is not limited to halogen atoms, but a similar set of physical forces allow the much less electronegative pnictogen family (N, P, As, etc.) to participate in bonds of comparable strength and similar origin <sup>26-35</sup>.

Unsurprisingly, the chalcogen family is not excluded from this sort of noncovalent bonding. A chalcogen bond is formed when a member of this family of atoms (e.g. S or Se) engages in an attractive and direct noncovalent interaction with an electronegative atom like N or O <sup>36-44</sup>. The importance of chalcogen bonds has been underscored by their strength, which is comparable to, and sometimes exceeds that of HBs. For instance, there is a direct interaction of S of FHS with N of NH<sub>3</sub>, forming a strong S $\cdots$ N noncovalent bond <sup>45</sup> with a binding energy of 8 kcal/mol.

With respect to S, prior study of its chalcogen bonding has centered on the divalent bonding situation, e.g. SO<sub>2</sub>, HSF, thioethers, or thiazole nucleosides<sup>30, 41, 46-53</sup>. But unlike its congener O, the S atom commonly engages in higher order bonding, as for example the tetravalent S in H<sub>2</sub>SO<sub>4</sub> or SF<sub>4</sub>.

The present study is thus meant to fill this gap in our present knowledge about S chalcogen bonding. SF<sub>4</sub> is taken as the prototypical tetravalent S molecule. Experimentally, SF<sub>4</sub> is widely used in fluorination of alcohols, aldehydes, ketones and carboxylic acids<sup>54-55</sup>. SF<sub>4</sub> is reacted with primary amines to yield sulfur difluoro imide and sulfur diimides. Although alternative methods for the synthesis of these compounds exist, the most common one is the reaction<sup>56-58</sup> of compounds containing the primary amino group (NH<sub>2</sub>) with SF<sub>4</sub>. This tetravalent S is allowed to interact with a series of electron donor amines, covering a range of both alkylamines and N-containing heteroaromatic rings. It is found that the S··N chalcogen bonds are all quite strong, greater in magnitude than the prototypical H-bond within a water dimer. Indeed, the binding energy ranges up to as much as 14 kcal/mol, so that some of these interactions may be considered as having crossed the threshold from noncovalent to weak covalent S–N bond.

## 2-2. Computational Method

Calculations were carried out with the Gaussian09 program<sup>59</sup>. Geometries were fully optimized at the MP2/aug-cc-pVDZ level. This method has demonstrated its reliability for a range of non-covalent interactions<sup>17, 26, 60-65</sup>. Harmonic vibrational frequencies verified the characterization of minima. The binding energy, E<sub>b</sub>, was calculated as the difference between the total energy of the complex and the sum of the isolated



optimized monomers. Interaction energy  $\Delta E$  was defined relative to the monomers in their geometries within the context of the complex. Basis set superposition error (BSSE) was corrected via the counterpoise technique <sup>66</sup>. Molecular electrostatic potentials (MEPs) were calculated on the electron density isosurface of 0.001 au, and extrema evaluated using the WFA-SAS program <sup>67</sup>. The interaction energy was dissected using SAPT methodology <sup>68</sup>. The SAPT0 calculations <sup>68-69</sup> were carried out at the HF/cc-pVDZ computational level, using the MOLPRO program <sup>70</sup>. The Natural Bond Order (NBO) method <sup>71-72</sup> was used to evaluate charge transfer effects using the NBO-3 program, incorporated in the Gaussian09 program.

### 2-3. Results

The optimized structure of  $\text{H}_3\text{N}\cdots\text{SF}_4$  is illustrated in Figure 2-1, which is representative of all of these heterodimers involving an alkylamine.  $F_a$  and  $F_b$  are the equatorial F atoms, with  $F_a$  lying nearly opposite the N atom,  $F_c$  represents one of the two symmetrically disposed axial F atoms. The first row of Table 2-1 indicates the binding energy grows rapidly as methyl groups are added, from a minimum of 6.62 kcal/mol for  $\text{NH}_3$  and peaking at 14.39 kcal/mol for trimethylamine (TMA). The enhanced strength arising from each methyl addition is consistent with the idea that alkyl groups are electron-releasing, and can hence facilitate the donation of electron charge from the amine. The next row shows a corresponding contraction of the intermolecular separation with each succeeding increase in binding energy, with the exception of a small increase for TMA. The N atom sits nearly exactly opposite one of the two equatorial F atoms of  $\text{SF}_4$ , with a  $\theta(\text{N}\cdots\text{SF}_a)$  angle within  $10^\circ$  of  $180^\circ$ . Concomitant with the binding, there is a stretch in this

S-F<sub>a</sub> bond, between 18 and 66 mÅ, and this stretch correlates with the overall binding energy. The other equatorial S-F<sub>b</sub> and axial S-F<sub>c</sub> bonds also undergo a stretch, albeit not quite as large. The full thermodynamic quantities in the remaining rows of Table 2-1 indicate that the zero-point vibrational energies introduce a small decrease in the magnitude of  $\Delta E$  on going to  $\Delta H$ . When the entropic loss is factored in,  $\Delta G$  hovers around zero (slightly positive for the three most weakly bound complexes, and slightly negative for TMA), suggesting the presence of the dimer even at room temperature.

A similar sort of analysis was also carried out for a set of N-containing heteroaromatics shown in Figure 2-2. Pyridine is a six-membered ring containing a single N. Pyrazine, pyridazine, and pyrimidine add a second N to the ring, in the 1,4, 1,2, and 1,3 positions, respectively. Imidazole retains two N atoms but reduces the ring size to five atoms. The properties of their complexes with SF<sub>4</sub> are reported in Table 2-1 where it may first be noted that the binding energies all vary within the relatively narrow range of 7.4 to 9.4 kcal/mol. This range makes these complexes intermediate in strength between NH<sub>3</sub> and CH<sub>3</sub>NH<sub>2</sub>. Pyridine forms the strongest complex, followed by the substituted rings, of which pyridazine with its adjacent N atom forms the strongest. The five-membered ring of imidazole is stronger still, despite the presence of two N atoms. Like the binding energies, the intermolecular R(N $\cdots$ S) distances are also fairly similar to one another, with the general trend of shorter distances associated with strong bonds. Also like the alkylamines, the S-F bonds elongate upon formation of each complex.  $\Delta H$  lies in the range between -6.2 and -8.2 kcal/mol, while  $\Delta G$  is positive, between 2.7 and 4.2 kcal/mol.

### 2-3.1. Energy Decomposition

The total interaction energy in each of these dimers was dissected via SAPT to provide the various attractive and repulsive components. These quantities are displayed graphically in Figure 2-3 from which one can quickly see their relative magnitudes. It is immediately clear that induction makes the largest contribution to the binding followed by electrostatic and then dispersion. The magnitudes of these quantities vary from one system to the next, but their relative proportions are surprisingly constant. Specifically, the induction accounts for more than half of the total attractive force (52-63%), compared to 29-37% arising from electrostatics, and 8-12% from dispersion.

It is instructive to compare the total interaction energy as calculated by SAPT and that from MP2, with appropriate counterpoise correction. The SAPT values are displayed in Figure 2-4 as the solid blue line. The MP2 binding energies from Table 2-1 and Table 2-2 are indicated by the broken red curve, but it must be recalled that these two quantities correspond to different properties. The binding energy  $E_b$  makes reference to the monomers in their optimized geometries, whereas the interaction energy  $\Delta E$  is calculated with respect to the monomers in their geometries within the context of the complex.  $E_b$  and  $\Delta E$  thus differ by what is sometimes termed the “distortion energy”, the energy required for the monomers to alter their geometry from their optimized structure to that within the complex. Since the SAPT quantities refer to  $\Delta E$ , the distortion energy is removed from the MP2 quantities, thereby presenting the MP2 values of  $\Delta E$  as the solid red curve in Figure 2-4, so as to facilitate a valid comparison.

One may observe first that the distortion energy, the difference between the solid

and broken red curves in Figure 2-4, is fairly small for  $\text{NH}_3$ , but grows as methyl groups are added. The heteroaromatics also present a fairly large, but nearly uniform distortion energy, most notably imidazole where it is 5.3 kcal/mol. Turning next to the comparison between SAPT and MP2, the solid red and blue curves are fairly similar. The largest difference occurs for  $(\text{CH}_3)_3\text{N}$  which is perhaps a product of the steric repulsion between the three methyl groups and the F atoms and the S lone pair of  $\text{SF}_4$ .

The importance of induction as well as electrostatics is also underscored by their ability to predict the total interaction energy. IND is linearly related to the full SAPT interaction energy, with a correlation coefficient  $R^2$  of 0.88, as is ES. The correlation improves when these two components are compared with the MP2 values of  $\Delta E$ , with  $R^2 = 0.95$ . Although small in magnitude, DISP also scales linearly with  $\Delta E$ , with  $R^2 = 0.97$ .

### 2-3.2. Comparison of Tetravalent with Divalent S

As this work represents the first examination of the chalcogen bonds formed by tetravalent S, it would be informative to draw a comparison with the more common divalent S. The properties of the complexes formed by  $\text{SF}_4$  with both  $\text{NH}_3$  and trimethylamine, are displayed in Table 2-3, and are compared with those in which  $\text{SF}_4$  is replaced by both  $\text{H}_2\text{S}$  and  $\text{HSF}$ . The first three rows of the table indicate the strong similarities of the three complexes involving  $\text{NH}_3$ , with a small advantage for  $\text{FHS}$ . Adding three methyl groups to the amine approximately doubles the strength of the interaction, but shows even less of a distinction between the divalent and tetravalent S complexes, even though the intermolecular distance is slightly longer in the latter case.

### 2-3.3. Molecular Electrostatic Potentials

With regard to the electrostatic segment of the interaction energy, examination of the molecular potentials of the various electron donors all show a negative region in the vicinity of the N atoms. These regions can be quantitatively assessed via the value of the most negative point on a surface that corresponds to an isodensity contour of 0.001 au. The values of this quantity,  $V_{s,min}$ , are presented in the first column of Table 2-4. The alkylamines in the first four rows show a diminishing trend as methyl groups are added. This trend is opposite to the pattern of binding energies in Table 2-1, or even the ES terms in the SAPT decomposition. Within the context of the heteroaromatics,  $V_{s,min}$  varies as pyrazine < pyridazine < pyridine < pyrimidine < imidazole which again differs from the binding energies in Table 2-2, where for example, pyrimidine is the most weakly bound, and pyridine the strongest. In summary, then,  $V_{s,min}$  is a poor indicator of binding strength, or even of the electrostatic component.

On the positive side, MEPs do offer some insight into the similarity between divalent and tetravalent S with respect to its chalcogen bonding. The MEPs are illustrated in Figure 2-5 for divalent  $H_2S$  and  $FHS$ , followed by tetravalent  $SF_4$ . The similarities are evident. All potentials contain a red (negative) area along the extension of the S-F bonds, particularly the axial SF bonds of  $SF_4$ .

More importantly, there is a blue (positive) region near the S atom, along the extension of each F-S bond, a so-called  $\sigma$ -hole. Quantitation of this hole via an evaluation of  $V_{s,max}$ , the maximum of this potential on the  $\rho=0.001$  au isodensity contour, leads to the values reported in Table 2-4. It is immediately plain that the depth of this hole is nearly

independent of the valency of the S atom. Whether  $\text{H}_2\text{S}$ ,  $\text{FSH}$ , or  $\text{SF}_4$ ,  $V_{\text{s,max}}$  lies within the narrow range of 39 to 42 kcal/mol. It should be finally noted that there is no positive  $\sigma$ -hole opposite the axial F atoms of  $\text{SF}_4$ , due to the presence of one axial F atom directly opposite the other.

#### 2-3.4. Charge Rearrangement

Treatment of the wave function via the NBO method leads to localized orbitals which provide insights into the chemical nature of noncovalent interactions. In particular, the overlap of the N lone pair of the amine with the  $\text{F}_\text{a}\text{-S } \sigma^*$  antibonding orbital allows charge transfer/hyperconjugation from the former to the latter. This transfer has been shown to be a dominant factor in the formation of chalcogen bonds such as these. The magnitude of this transfer is listed in the first column of Table 2-5 as a perturbation energy  $E^\text{a}(2)$ . This quantity is rather large, ranging from a minimum of 14.7 kcal/mol for  $\text{NH}_3$  all the way up above 40 kcal/mol for methylamine and trimethylamine. The heteroaromatics also display large values of  $E(2)$ , between 25 and 37 kcal/mol. Indeed, this interaction is so strong that in the case of dimethylamine, NBO assesses that there is a covalent bond linking the S and N atoms.

In a particularly interesting finding, the  $\sigma^*(\text{F}_\text{a}\text{S})$  antibonding orbital, for which  $\text{F}_\text{a}$  lies opposite the N atom, is not the only one which can accept charge. Its overlap with the N lone pair is obvious in Figure 2-6a, but one can see in Figure 2-6b that the same N lone pair can also engage with  $\sigma^*(\text{F}_\text{b}\text{S})$  wherein  $\text{F}_\text{b}$  is the other equatorial F atom of  $\text{SF}_4$ . Whereas  $\text{F}_\text{a}$  lies nearly opposite the N lone pair, so the  $\sigma^*(\text{SF}_\text{a})$  orbital points directly at N, the roughly  $80^\circ \theta(\text{N}\cdots\text{SF}_\text{b})$  angle reduces the overlap with this antibonding orbital. The amount

of hyperconjugation associated with this second antibond is reported in the second column of Table 2-5 as  $E^b(2)$ , and can be as large as 50% of  $E^a(2)$  ( $N_{lp} \rightarrow \sigma^*(F_aS)$ ), so its effect cannot be ignored.

As a means of further probing the influence of the two SF antibonding orbitals, the SF<sub>4</sub> molecule was pivoted around the S-F<sub>b</sub> axis by an angle  $\phi$ , holding fixed the other geometrical parameters of the pyridine··SF<sub>4</sub> complex. Based on the diagrams in Figure 2-6, this rotation ought to have little effect upon the overlap between the N lone pair and the  $\sigma^*(SF_b)$  orbital, but it would misalign the lone pair with  $\sigma^*(SF_a)$ . The values of  $E(2)$  computed during this rotation support this supposition. As may be seen in Figure 2-7,  $E^b(2)$  remains nearly constant over a  $\pm 20^\circ$  misalignment, while  $E^a(2)$  suffers an erosion of some 16%.

In addition to the transfer from one specific localized orbital to another, there are charge rearrangements that involve the entire complex. The redistribution of total electron density that accompanies the formation of the NH<sub>3</sub>··SF<sub>4</sub> complex is displayed in Figure 2-8a where increases in density correspond to purple and losses to yellow. One may note first that there is a charge buildup directly between the N and S atoms, in approximately the position of the center of what may be termed a noncovalent N··S bond. A larger yellow region of loss occurs immediately to the left of the S. This pattern is typical of halogen, chalcogen, and pnictogen bonds. A purple charge buildup may be noted behind the S atom, corresponding to a  $\sigma^*(SF_b)$  antibonding orbital.

It is especially interesting to note that the four F atoms of SF<sub>4</sub> are all surrounded by a purple region of charge gain. This pattern does not much distinguish between the two

equatorial F atoms whose  $\sigma^*(\text{SF})$  antibonding orbital accept charge from the amine, and the equatorial F atoms that do not. And indeed, the NBO atomic charges of these F atoms all become more negative, as reported in Table 2-6. Figure 2-8b displays the charge redistribution of the imidazole $\cdots$ SF<sub>4</sub> complex which is very much like that for the simpler NH<sub>3</sub> amine. And again, all four SF<sub>4</sub> F atoms acquire additional density, which is verified by NBO atomic charges in Table 2-6. This pattern is in fact characteristic of all of the complexes examined here, whether alkylamine or heteroaromatic amine. And this similarity in charge redistribution is also consistent with the observation that all four S-F bonds of SF<sub>4</sub> elongate upon formation of the complex. In fact, there is a fairly strong linear relationship between the change in charge on the F<sub>a</sub> atom, and its elongation, with a correlation coefficient  $R^2$  of 0.955. In terms of the hyperconjugation, the strength of the S-F bond might be measured in terms of the populations of its  $\sigma$  and  $\sigma^*$  orbitals. Since the former would act to strengthen this bond, and  $\sigma^*$  to weaken it, the overall effect can be assessed as  $(\sigma - \sigma^*)$ . This population difference is also linearly related to  $\Delta r(\text{SF}_a)$ , with  $R^2=0.945$ . Correlations exist for the other S-F bond lengths as well, but are of poorer quality.

## 2-4. Summary

All of the amines, both alkyl and heteroaromatic, engage in strong chalcogen-bonds with SF<sub>4</sub>. The alkylamine binding is very sensitive to the number of methyl groups; binding energies vary from 6.6 kcal/mol for NH<sub>3</sub> to 14.4 kcal/mol for trimethylamine. Heteroaromatics are less sensitive to the nature of the ring, all binding in the range between 7 and 9 kcal/mol. In all cases, one of the equatorial S-F bonds is arranged directly opposite



the approaching N atom. It is into this  $\sigma^*(\text{S-F})$  antibonding orbital that the N lone pair transfers some of its charge, which acts as a strong stabilizing influence on the complex. There is a lesser, but significant, amount of charge that is deposited into the  $\sigma^*(\text{S-F})$  antibonding orbital of the other equatorial F atom of  $\text{SF}_4$ . The associated induction energy is the largest contributor to the binding of these complexes, constituting more than half of the total attractive energy, followed by electrostatic, and then dispersion energy.

Examination of the charge rearrangements that accompany formation of each complex shows that the charge transferred from the amine to the  $\text{SF}_4$  molecule is ultimately distributed among all four F atoms, as well as the central S atom. The ensuing increase in the partial negative charge on these F atoms explains the elongation of the S-F bonds. The molecular electrostatic potentials surrounding each monomer furnish some useful information about the binding. For example, the N lone pair is attracted to a positive region of the  $\text{SF}_4$  potential that lies directly opposite each of the equatorial F atoms. However, the quantitative assessment of the former negative N area is poorly correlated with the total interaction energy, or even the full electrostatic component.

The especially strong interaction in the complex between dimethylamine and  $\text{SF}_4$  leads to the conclusion that the  $\text{N}\cdots\text{S}$  bond is approaching the regime where it might be better thought of as a covalent bond. The binding energy is 13 kcal/mol, and the  $\text{R}(\text{N-S})$  distance is only 2.16 Å. The charge transferred from amine to  $\text{SF}_4$  upon formation of this N-S bond is some 0.23 e, exceeding what is normally observed in a noncovalent bond. There is experimental confirmation of some of our most important findings.  $\text{SF}_4$  was found by a recent crystal structure determination<sup>73</sup> to bind to an amine in the manner described

here. In its complex with triethylamine, one of the equatorial F atoms of SF<sub>4</sub> lies 173° away from the N atom, within 2° of the structure described here with trimethylamine. Also quite similar is the R(N··S) distance of 2.38 Å, only slightly longer than the equivalent distance in our calculated TMA complex. Also confirmed by this crystal structure is the elongation of all of the S-F bonds upon formation of the complex.

There is an indication in the literature that a tetravalent S can engage in a chalcogen bond with an O atom as well. The complex between water and SO<sub>2</sub>(CH<sub>3</sub>)<sub>2</sub> contains what would appear at least geometrically to be a S··O chalcogen bond, of length 3.34 Å, and with the water O atom situated opposite one of the two O covalently bonded to S <sup>74</sup>. However, there was little analysis of the nature of any possible S··O bond; furthermore, the energy of this bond could not be disentangled from the combined effects of several H-bonds.

## References

- (1) Joesten, M. D.; Schaad, L. J. *Hydrogen Bonding*. Marcel Dekker: New York, 1974; p 622.
- (2) Schuster, P.; Zundel, G.; Sandorfy, C. *The Hydrogen Bond. Recent Developments in Theory and Experiments*. North-Holland Publishing Co.: Amsterdam, 1976.
- (3) Schuster, P. *Hydrogen Bonds*. Springer-Verlag: Berlin, 1984; Vol. 120, p 117.
- (4) Nishio, M.; Umezawa, Y.; Honda, K.; Tsuboyama, S.; Suezawa, H. CH/p Hydrogen Bonds in Organic and Organometallic Chemistry. *CrystEngComm* **2009**, *11*, 1757-1788.
- (5) van der Veken, B. J.; Delanoye, S. N.; Michielsen, B.; Herrebout, W. A. A Cryospectroscopic Study of the Blue-Shifting C–H $\cdots$ O Bonded Complexes of Pentafluoroethane with Dimethyl Ether-D<sub>6</sub>, Acetone-D<sub>6</sub> and Oxirane-D<sub>4</sub>. *J. Mol. Struct.* **2010**, *976*, 97-104.
- (6) Scheiner, S.; Gu, Y.; Kar, T. Evaluation of the H-Bonding Properties of CH $\cdots$ O Interactions Based Upon NMR Spectra. *J. Mol. Struct. (Theochem)* **2000**, *500*, 441-452.
- (7) Karpfen, A.; Kryachko, E. S. The Dimers of Glyoxal and Acrolein with H<sub>2</sub>O and HF: Negative Intramolecular Coupling and Blue-Shifted C–H Stretch. *Chem. Phys. Lett.* **2010**, *489*, 39-43.
- (8) Gu, Y.; Kar, T.; Scheiner, S. Comparison of the CH $\cdots$ N and CH $\cdots$ O Interactions Involving Substituted Alkanes. *J. Mol. Struct.* **2000**, *552*, 17-31.
- (9) Domagala, M.; Grabowski, S. J. Hydrocarbons as Proton Donors in C–H $\cdots$ N and C–H $\cdots$ S Hydrogen Bonds. *Chem. Phys.* **2010**, *367*, 1-6.

- (10) Arunan, E.; Desiraju, G. R.; Klein, R. A.; Sadlej, J.; Scheiner, S.; Alkorta, I.; Clary, D. C.; Crabtree, R. H.; Dannenberg, J. J.; Hobza, P.; Kjaergaard, H. G.; Legon, A. C.; Mennucci, B.; Nesbitt, D. J. Definition of the Hydrogen Bond. *Pure Appl. Chem.* **2011**, *83*, 1637-1641.
- (11) Latajka, Z.; Scheiner, S. Structure, Energetics and Vibrational Spectrum of H<sub>2</sub>O-HCl. *J. Chem. Phys.* **1987**, *87*, 5928-5936.
- (12) Biswal, H. S.; Gloaguen, E.; Loquais, Y.; Tardivel, B.; Mons, M. Strength of NH...S Hydrogen Bonds in Methionine Residues Revealed by Gas-Phase IR/UV Spectroscopy. *J. Phys. Chem. Lett.* **2012**, *3*, 755-759.
- (13) Scheiner, S.; Grabowski, S. J.; Kar, T. Influence of Hybridization and Substitution Upon the Properties of the CH...O Hydrogen Bond. *J. Phys. Chem. A* **2001**, *105*, 10607-10612.
- (14) Riley, K. E.; Hobza, P. Investigations into the Nature of Halogen Bonding Including Symmetry Adapted Perturbation Theory Analyses. *J. Chem. Theory Comput.* **2008**, *4*, 232-242.
- (15) Alkorta, I.; Blanco, F.; Solimannejad, M.; Elguero, J. Competition of Hydrogen Bonds and Halogen Bonds in Complexes of Hypohalous Acids with Nitrogenated Bases. *J. Phys. Chem. A* **2008**, *112*, 10856-10863.
- (16) Karpfen, A. Theoretical Characterization of the Trends in Halogen Bonding. In *Halogen Bonding. Fundamentals and Applications*, Metrangolo, P.; Resnati, G., Eds. Springer: Berlin, 2008; Vol. 126, pp 1-15.
- (17) Hauchecorne, D.; Herrebout, W. A. Experimental Characterization of C-X...Y-C (X = Br, I; Y = F, Cl) Halogen-Halogen Bonds. *J. Phys. Chem. A* **2013**, *117*, 11548-11557.

- (18) Zierkiewicz, W.; Michalska, D.; Zeegers-Huyskens, T. Theoretical Investigation of the Conformation, Acidity, Basicity and Hydrogen Bonding Ability of Halogenated Ethers. *Phys. Chem. Chem. Phys.* **2010**, *12*, 13681-13691.
- (19) Parisini, E.; Metrangolo, P.; Pilati, T.; Resnati, G.; Terraneo, G. Halogen Bonding in Halocarbon–Protein Complexes: A Structural Survey. *Chem. Soc. Rev.* **2011**, *40*, 2267-2278.
- (20) Stephens, S. L.; Walker, N. R.; Legon, A. C. Internal Rotation and Halogen Bonds in  $\text{CF}_3\text{I}\cdots\text{NH}_3$  and  $\text{CF}_3\text{I}\cdots\text{N}(\text{CH}_3)_3$  Probed by Broadband Rotational Spectroscopy. *Phys. Chem. Chem. Phys.* **2011**, *13*, 20736-20744.
- (21) Grabowski, S. J. QTAIM Characteristics of Halogen Bond and Related Interactions. *J. Phys. Chem. A* **2012**, *116*, 1838-1845.
- (22) Evangelisti, L.; Feng, G.; Gou, Q.; Grabow, J.-U.; Caminati, W. Halogen Bond and Free Internal Rotation: The Microwave Spectrum of  $\text{CF}_3\text{Cl}$ –Dimethyl Ether. *J. Phys. Chem. A* **2014**, *118*, 579-582.
- (23) Riley, K. E.; Murray, J. S.; Fanfrlík, J.; Rezáč, J.; Solá, R. J.; Concha, M. C.; Ramos, F. M.; Politzer, P. Halogen Bond Tunability II: The Varying Roles of Electrostatic and Dispersion Contributions to Attraction in Halogen Bonds. *J. Mol. Model.* **2013**, *19*, 4651-4659.
- (24) Solimannejad, M.; Malekani, M. Substituent Effects on the Cooperativity of Halogen Bonding. *J. Phys. Chem. A* **2013**, *117*, 5551-5557.
- (25) Stone, A. J. Are Halogen Bonded Structures Electrostatically Driven? *J. Am. Chem. Soc.* **2013**, *135*, 7005-7009.

- (26) Sanchez-Sanz, G.; Trujillo, C.; Alkorta, I.; Elguero, J. Intramolecular Pnictogen Interactions in Phosphorus and Arsenic Analogues of Proton Sponges. *Phys. Chem. Chem. Phys.* **2014**, *16*, 15900-15909.
- (27) Robertson, A. P. M.; Gray, P. A.; Burford, N. Interpnictogen Cations: Exploring New Vistas in Coordination Chemistry. *Angew. Chem. Int. Ed.* **2014**, *53*, 6050-6069.
- (28) Scheiner, S. A New Noncovalent Force: Comparison of P $\cdots$ N Interaction with Hydrogen and Halogen Bonds. *J. Chem. Phys.* **2011**, *134*, 094315.
- (29) Del Bene, J. E.; Alkorta, I.; Elguero, J. Influence of Substituent Effects on the Formation of P $\cdots$ Cl Pnictogen Bonds or Halogen Bonds. *J. Phys. Chem. A* **2014**, *118*, 2360-2366.
- (30) Bauzá, A.; Alkorta, I.; Frontera, A.; Elguero, J. On the Reliability of Pure and Hybrid DFT Methods for the Evaluation of Halogen, Chalcogen, and Pnictogen Bonds Involving Anionic and Neutral Electron Donors. *J. Chem. Theory Comput.* **2013**, *9*, 5201-5210.
- (31) Scheiner, S. The Pnictogen Bond: Its Relation to Hydrogen, Halogen, and Other Noncovalent Bonds. *Acc. Chem. Res.* **2013**, *46*, 280-288.
- (32) Grabowski, S. J. s-Hole Bond Versus Hydrogen Bond: From Tetravalent to Pentavalent N, P, and As Atoms. *Chem. Eur. J.* **2013**, *19*, 14600-14611.
- (33) Zahn, S.; Frank, R.; Hey-Hawkins, E.; Kirchner, B. Pnictogen Bonds: A New Molecular Linker? *Chem. Eur. J.* **2011**, *17*, 6034-6038.
- (34) Moilanen, J.; Ganesamoorthy, C.; Balakrishna, M. S.; Tuononen, H. M. Weak Interactions between Trivalent Pnictogen Centers: Computational Analysis of Bonding in Dimers X<sub>3</sub>E $\cdots$ EX<sub>3</sub> (E = Pnictogen, X = Halogen). *Inorg. Chem.* **2009**, *48*, 6740-6747.

- (35) Adhikari, U.; Scheiner, S. Comparison of  $P\cdots D$  ( $D=P,N$ ) with Other Noncovalent Bonds in Molecular Aggregates. *J. Chem. Phys.* **2011**, *135*, 184306.
- (36) Bauzá, A.; Quiñonero, D.; Deyà, P. M.; Frontera, A. Halogen Bonding Versus Chalcogen and Pnicogen Bonding: A Combined Cambridge Structural Database and Theoretical Study. *CrystEngComm* **2013**, *15*, 3137-3144.
- (37) Iwaoka, M.; Isozumi, N. Hypervalent Nonbonded Interactions of a Divalent Sulfur Atom. Implications in Protein Architecture and the Functions. *Molecules* **2012**, *17*, 7266-7283.
- (38) Sánchez-Sanz, G.; Trujillo, C.; Alkorta, I.; Elguero, J. Intermolecular Weak Interactions in Htexh Dimers ( $X=O, S, Se, Te$ ): Hydrogen Bonds, Chalcogen–Chalcogen Contacts and Chiral Discrimination. *ChemPhysChem* **2012**, *13*, 496–503.
- (39) Sanz, P.; Mó, O.; Yáñez, M. Characterization of Intramolecular Hydrogen Bonds and Competitive Chalcogen–Chalcogen Interactions on the Basis of the Topology of the Charge Density. *Phys. Chem. Chem. Phys.* **2003**, *5*, 2942-2947.
- (40) Esseffar, M. H.; Herrero, R.; Quintanilla, E.; Dávalos, J. Z.; Jiménez, P.; Abboud, J.-L. M.; Yáñez, M.; Mó, O. Activation of the Disulfide Bond and Chalcogen–Chalcogen Interactions: An Experimental (FTICR) and Computational Study. *Chem. Eur. J.* **2007**, *13*, 1796-1803.
- (41) Iwaoka, M.; Takemoto, S.; Tomoda, S. Statistical and Theoretical Investigations on the Directionality of Nonbonded  $S\cdots O$  Interactions. Implications for Molecular Design and Protein Engineering. *J. Am. Chem. Soc.* **2002**, *124*, 10613-10620.
- (42) Azofra, L. M.; Scheiner, S. Complexation of  $n$   $SO_2$  Molecules ( $n=1,2,3$ ) with Formaldehyde and Thioformaldehyde. *J. Chem. Phys.* **2014**, *140*, 034302.

- (43) Fanfrlík, J.; Přáda, A.; Padělková, Z.; Pecina, A.; Macháček, J.; Lepšík, M.; Holub, J.; Růžicka, A.; Hnyk, D.; Hobza, P. The Dominant Role of Chalcogen Bonding in the Crystal Packing of 2d/3d Aromatics. *Angew. Chem. Int. Ed.* **2014**, *53*, 10139-10142.
- (44) Adhikari, U.; Scheiner, S. Sensitivity of Pnicogen, Chalcogen, Halogen and H-Bonds to Angular Distortions. *Chem. Phys. Lett.* **2012**, *532*, 31-35.
- (45) Adhikari, U.; Scheiner, S. The S $\cdots$ N Noncovalent Interaction: Comparison with Hydrogen and Halogen Bonds. *Chem. Phys. Lett.* **2011**, *514*, 36-39.
- (46) Rosenfield, R. E.; Parthasarathy, R.; Dunitz, J. D. Directional Preferences of Nonbonded Atomic Contacts with Divalent Sulfur. 1. Electrophiles and Nucleophiles. *J. Am. Chem. Soc.* **1977**, *99*, 4860-4862.
- (47) Burling, F. T.; Goldstein, B. M. Computational Studies of Nonbonded Sulfur-Oxygen and Selenium-Oxygen Interactions in the Thiazole and Selenazole Nucleosides. *J. Am. Chem. Soc.* **1992**, *114*, 2313-2320.
- (48) Werz, D. B.; Gleiter, R.; Rominger, F. Nanotube Formation Favored by Chalcogen-Chalcogen Interactions. *J. Am. Chem. Soc.* **2002**, *124*, 10638-10639.
- (49) Jablonski, M. Energetic and Geometrical Evidence of Nonbonding Character of Some Intramolecular Halogen $\cdots$ Oxygen and Other Y $\cdots$ Y Interactions. *J. Phys. Chem. A* **2012**, *116*, 3753-3764.
- (50) Bleiholder, C.; Werz, D. B.; Koppel, H.; Gleiter, R. Theoretical Investigations on Chalcogen-Chalcogen Interactions: What Makes These Nonbonded Interactions Bonding? *J. Am. Chem. Soc.* **2006**, *128*, 2666-2674.
- (51) Esrafil, M.; Mohammadian-Sabet, F.; Solimannejad, M. A Theoretical Evidence for Mutual Influence between S $\cdots$ N(C) and Hydrogen/Lithium/Halogen Bonds:



Competition and Interplay between  $\Pi$ -Hole and  $\Sigma$ -Hole Interactions. *Struct. Chem.* **2014**, *25*, 1197-1205.

(52) George, J.; Deringer, V. L.; Dronskowski, R. Cooperativity of Halogen, Chalcogen, and Pnictogen Bonds in Infinite Molecular Chains by Electronic Structure Theory. *J. Phys. Chem. A* **2014**, *118*, 3193-3200.

(53) Sánchez-Sanz, G.; Alkorta, I.; Elguero, J. Theoretical Study of the HXYH Dimers (X, Y = O, S, Se). Hydrogen Bonding and Chalcogen–Chalcogen Interactions. *Mol. Phys.* **2011**, *109*, 2543-2552.

(54) Smith, G. L.; Mercier, H. P. A.; Schrobilgen, G. J. Ennobling an Old Molecule: Thiazyl Trifluoride ( $\text{N}\equiv\text{SF}_3$ ), a Versatile Synthone for Xe–N Bond Formation. *Inorg. Chem.* **2011**, *50*, 12359-12373.

(55) Umemoto, T.; Singh, R. P.; Xu, Y.; Saito, N. Discovery of 4-Tert-Butyl-2,6-Dimethylphenylsulfur Trifluoride as a Deoxofluorinating Agent with High Thermal Stability as Well as Unusual Resistance to Aqueous Hydrolysis, and Its Diverse Fluorination Capabilities Including Deoxofluoro-Arylsulfonylation with High Stereoselectivity. *J. Am. Chem. Soc.* **2010**, *132*, 18199-18205.

(56) Grunwell, J. R.; Dye, S. L. Novel Generation of Benzonitrile-N-Sulfide. *Tetrahedron Lett.* **1975**, *16*, 1739-1740.

(57) Patel, N. R.; Kirchmeier, R. L.; Shreeve, J. n. M. Reactions of Per- and Polyfluorinated Amines with Sulfur Compounds. *Inorg. Chem.* **1994**, *33*, 4403-4406.

(58) Goettel, J. T.; Kostiuk, N.; Gerken, M. The Solid-State Structure of  $\text{SF}_4$ : The Final Piece of the Puzzle. *Angew. Chem.* **2013**, *125*, 8195-8198.

- (59) Frisch, M. J.; Trucks, G. W.; Schlegel, H. B.; Scuseria, G. E.; Robb, M. A.; Cheeseman, J. R.; Scalmani, G.; Barone, V.; Mennucci, B.; Petersson, G. A.; et al. *Gaussian 09*, Revision B.01; Wallingford, CT, 2009.
- (60) Chen, Y.; Yao, L.; Lin, X. Theoretical Study of  $(\text{FH}_2\text{X})_n \cdot \text{Y}$  ( $\text{X} = \text{P}$  and  $\text{As}$ ,  $n = 1-4$ ,  $\text{Y} = \text{F}^-$ ,  $\text{Cl}^-$ ,  $\text{Br}^-$ ,  $\text{I}^-$ ,  $\text{NO}_3^-$  and  $\text{SO}_4^{2-}$ ): The Possibility of Anion Recognition Based on Pnictogen Bonding. *Comput. Theor. Chem.* **2014**, *1036*, 44-50.
- (61) Esrafil, M. D.; Fatehi, P.; Solimannejad, M. Mutual Interplay between Pnictogen Bond and Dihydrogen Bond in  $\text{HMH} \cdots \text{HCN} \cdots \text{PH}_2\text{X}$  Complexes ( $\text{M} = \text{Be}$ ,  $\text{Mg}$ ,  $\text{Zn}$ ;  $\text{X} = \text{H}$ ,  $\text{F}$ ,  $\text{Cl}$ ). *Comput. Theor. Chem.* **2014**, *1034*, 1-6.
- (62) Hauchecorne, D.; Nagels, N.; van der Veken, B. J.; Herrebout, W. A. C–X $\cdots$ p Halogen and C–H $\cdots$ p Hydrogen Bonding: Interactions of  $\text{CF}_3\text{X}$  ( $\text{X} = \text{Cl}$ ,  $\text{Br}$ ,  $\text{I}$  or  $\text{H}$ ) with Ethene and Propene. *Phys. Chem. Chem. Phys.* **2012**, *14*, 681-690.
- (63) Wu, W.; Lu, Y.; Liu, Y.; Li, H.; Peng, C.; Liu, H.; Zhu, W. Weak Energetic Effects between X–p and X–N Halogen Bonds: CSD Search and Theoretical Study. *Chem. Phys. Lett.* **2013**, *582*, 49-55.
- (64) Kerdawy, A. E.; Murray, J. S.; Politzer, P.; Bleiziffer, P.; Heßelmann, A.; Görling, A.; Clark, T. Directional Noncovalent Interactions: Repulsion and Dispersion. *J. Chem. Theory Comput.* **2013**, *9*, 2264-2275.
- (65) Ji, W.-Y.; Xia, X.-L.; Ren, X.-H.; Wang, F.; Wang, H.-J.; Diao, K.-S. The Non-Covalent Bindings of  $\text{CF}_2\text{Cl}_2$  with  $\text{NO}$  and  $\text{SO}_2$ . *Struct. Chem.* **2013**, *24*, 49-54.
- (66) Boys, S. F.; Bernardi, F. The Calculation of Small Molecular Interactions by the Differences of Separate Total Energies. Some Procedures with Reduced Errors. *Mol. Phys.* **1970**, *19*, 553-566.

- (67) Bulat, F.; Toro-Labbé, A.; Brinck, T.; Murray, J.; Politzer, P. Quantitative Analysis of Molecular Surfaces: Areas, Volumes, Electrostatic Potentials and Average Local Ionization Energies. *J. Mol. Model.* **2010**, *16*, 1679-1691.
- (68) Moszynski, R.; Wormer, P. E. S.; Jeziorski, B.; van der Avoird, A. Symmetry-Adapted Perturbation Theory of Nonadditive Three-Body Interactions in van der Waals Molecules. I. General Theory. *J. Chem. Phys.* **1995**, *103*, 8058-8074.
- (69) Szalewicz, K.; Jeziorski, B. Symmetry-Adapted Perturbation Theory of Intermolecular Interactions. In *Molecular Interactions. From Van der Waals to Strongly Bound Complexes*, Scheiner, S., Ed. Wiley: New York, 1997; pp 3-43.
- (70) Werner, H.-J.; Knowles, P. J.; Manby, F. R.; Schütz, M.; Celani, P.; Knizia, G.; Korona, T.; Lindh, R.; Mitrushenkov, A.; Rauhut, G.; et al. *MOLPRO*, Version 2006; 2010.
- (71) Reed, A. E.; Weinhold, F.; Curtiss, L. A.; Pochatko, D. J. Natural Bond Orbital Analysis of Molecular Interactions: Theoretical Studies of Binary Complexes of HF, H<sub>2</sub>O, NH<sub>3</sub>, N<sub>2</sub>, O<sub>2</sub>, F<sub>2</sub>, CO and CO<sub>2</sub> with HF, H<sub>2</sub>O, and NH<sub>3</sub>. *J. Chem. Phys.* **1986**, *84*, 5687-5705.
- (72) Reed, A. E.; Curtiss, L. A.; Weinhold, F. Intermolecular Interactions from a Natural Bond Orbital, Donor-Acceptor Viewpoint. *Chem. Rev.* **1988**, *88*, 899-926.
- (73) Goettel, J. T.; Chaudhary, P.; Hazendonk, P.; Mercier, H. P. A.; Gerken, M. SF<sub>4</sub>N(C<sub>2</sub>H<sub>5</sub>)<sub>3</sub>: The First Conclusively Characterized SF<sub>4</sub> Adduct with an Organic Base. *Chem. Commun.* **2012**, *48*, 9120-9122.
- (74) Clark, T.; Murray, J. S.; Lane, P.; Politzer, P. Why Are Dimethyl Sulfoxide and Dimethyl Sulfone Such Good Solvents? *J. Mol. Model.* **2008**, *14*, 689-697.

Table 2-1 Energetic (kcal/mol) and geometric aspects of alkylamine:SF<sub>4</sub> complexes

	Ammonia	Methylamine	Dimethylamine	Trimethylamine
E <sub>b</sub>	-6.62	-9.72	-13.25	-14.39
R(N...S), Å	2.571	2.188	2.158	2.227
θ(N...SF <sub>a</sub> ), degs	173.3	170.3	169.7	171.3
Δr(S-F <sub>a</sub> ), mÅ	18.5	52.9	65.9	62.4
Δr(S-F <sub>b</sub> ), mÅ	8.7	27.9	36.9	32.4
Δr(S-F <sub>c</sub> ), mÅ	22.7	43.3	43.7	45.2
ΔH (298K)	-5.26	-8.32	-11.63	-12.66
ΔS <sup>a</sup> , cal mol <sup>-1</sup> K <sup>-1</sup>	-27.00	-36.38	-39.44	-40.36
ΔG (298K)	2.80	2.47	0.12	-0.63

<sup>a</sup>Evaluated at 25°C.Table 2-2 Energetic (kcal/mol) and geometric aspects of heteroaromatic amine:SF<sub>4</sub> complexes

	Pyridine	Pyrazine	Pyridazine	Pyrimidine	Imidazole
E <sub>b</sub>	-9.39	-7.69	-8.62	-7.43	-9.14
R(N...S), Å	2.308	2.372	2.338	2.416	2.285
θ(N...SF <sub>a</sub> ), degs	171.9	172.5	173.7	173.1	172.3
Δr(S-F <sub>a</sub> ), mÅ	43.3	31.1	32.4	27.1	43.9
Δr(S-F <sub>b</sub> ), mÅ	15.5	11.5	23.7	9.0	14.6
Δr(S-F <sub>c</sub> ), mÅ	41.7	36.6	31.4	38.3	37.5
ΔH (298K)	-8.24	-6.46	-7.25	-6.23	-7.90
ΔS <sup>a</sup> , cal mol <sup>-1</sup> K <sup>-1</sup>	-33.01	-37.03	-30.46	-31.03	-35.35
ΔG (298K)	2.76	4.18	3.07	4.16	2.65

<sup>a</sup>Evaluated at 25°C.

Table 2-3 Properties of divalent and trivalent S complexes

Complex	$E_b$ kcal/mol	$R(N\cdots S)$ Å	$\theta(FS\cdots N)$ degs
$FHS\cdots NH_3^a$	-7.92	2.466	171.0
$F_2S\cdots NH_3$	-6.95	2.480	173.0
$F_4S\cdots NH_3$	-6.62	2.573	173.3
$FHS\cdots TMA$	-14.56	2.183	170.6
$F_2S\cdots TMA$	-14.48	2.158	172.3
$F_4S\cdots TMA$	-14.39	2.227	171.3

Table 2-4 Extrema in the molecular electrostatic potentials (kcal/mol), on an isodensity surface corresponding to 0.001 au.

	$V_{s,min}$		$V_{s,max}$
$NH_3$	-39.39	$H_2S$	+42.15
Methylamine	-38.04	$FHS$	+39.16
Dimethylamine	-35.63	$SF_4$	+42.19
Trimethylamine	-33.45		
Pyridine	-29.76		
Pyrazine	-23.10		
Pyridazine	-25.45		
Pyrimidine	-35.60		
Imidazole	-36.27		

Table 2-5 NBO second order perturbation energy (kcal/mol) for complexes with SF<sub>4</sub>

	E <sup>a</sup> (2) <sup>a</sup>	E <sup>b</sup> (2) <sup>b</sup>	E <sup>a</sup> (2) + E <sup>b</sup> (2)	θ(N··SF <sub>a</sub> ), degs	θ(N··SF <sub>b</sub> ), degs
Ammonia	14.68	3.70	18.48	173.3	77.4
Methylamine	41.49	16.77	58.26	170.3	80.6
Dimethylamine	NA <sup>c</sup>	NA <sup>c</sup>	NA <sup>c</sup>	169.7	81.2
Trimethylamine	41.28	20.65	61.93	171.3	81.7
Pyridine	36.57	11.79	48.36	171.9	80.2
Pyrazine	27.76	8.13	36.89	172.5	79.5
Pyridazine	27.80	9.60	37.4	173.7	80.4
Pyrimidine	24.59	6.93	31.52	173.1	79.4
Imidazole	37.10	9.46	46.56	172.3	80.6

<sup>a</sup>NBO perturbation energy corresponding to N<sub>lp</sub>---σ\*(S-F<sub>a</sub>). <sup>b</sup>NBO perturbation energy corresponding to N<sub>lp</sub>---σ\*(S-F<sub>b</sub>).

<sup>c</sup>The interaction is strong enough that NBO places a covalent bond between N and S, i.e. considers the entire system as one unit.

Table 2-6 Changes in NBO atomic charges (me) within SF<sub>4</sub> that occur upon formation of complex with indicated amine

	S	F <sub>a</sub>	F <sub>b</sub>	F <sub>c</sub>
Ammonia	3.18	-23.25	-10.78	-15.01
Methylamine	-86.9	-65.45	-22.03	-21.61
Dimethylamine	-97.41	-52.89	-26.11	-27.29
TMA	-81.91	-46.64	-23.57	-18.71
Pyridine	-27.22	-41.83	-8.86	-21.01
Pyrazine	-12.50	-31.01	-6.34	-19.09
Pyridazine	-7.06	-33.69	-5.56	-15.28
Pyrimidine	-5.36	-29.29	-6.15	-22.80
Imidazole	-25.11	-38.60	-9.76	-29.32

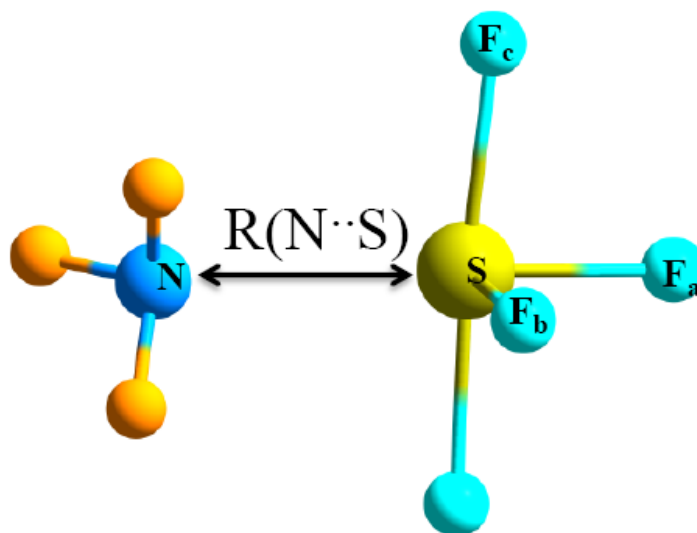


Figure 2-1 Atomic labeling used to define geometries of complexes of amines with  $\text{SF}_4$ .

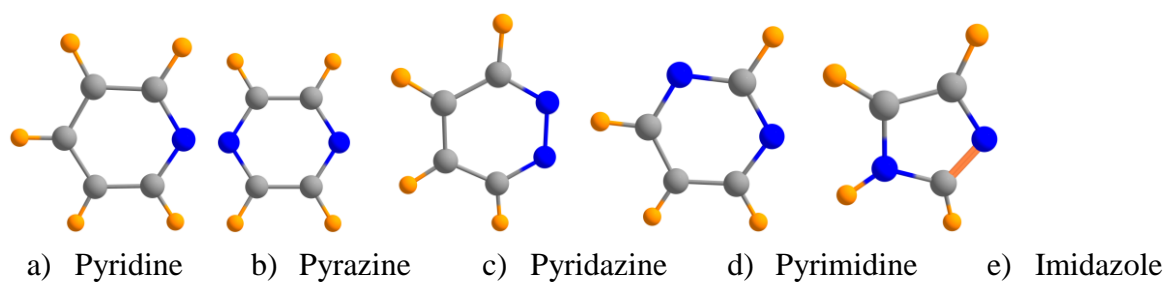


Figure 2-2 Heteroaromatic amines a) pyridine, b) pyrazine, c) pyridazine, d) pyrimidine, and e) imidazole used in this study.

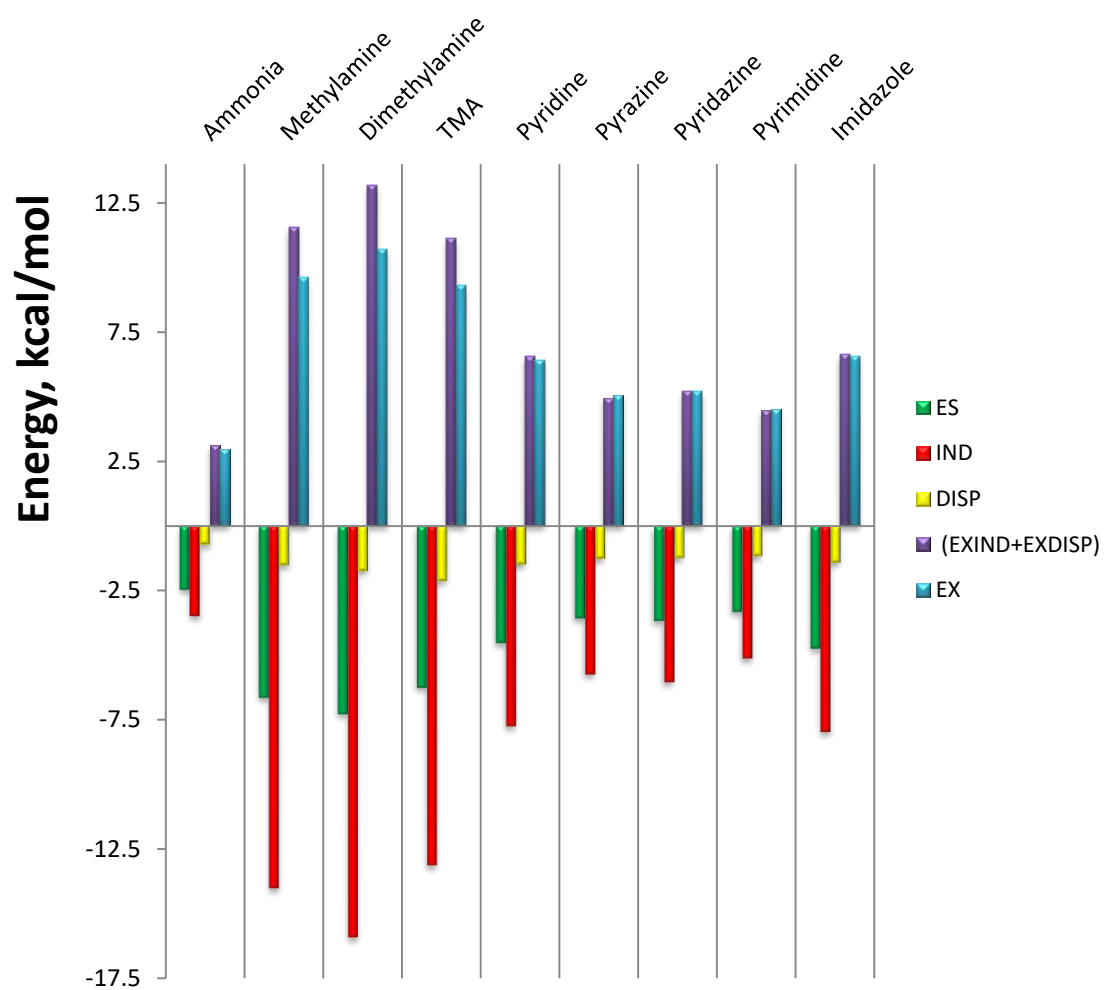


Figure 2-3 SAPT components of interaction energy of indicated amine with SF<sub>4</sub>.



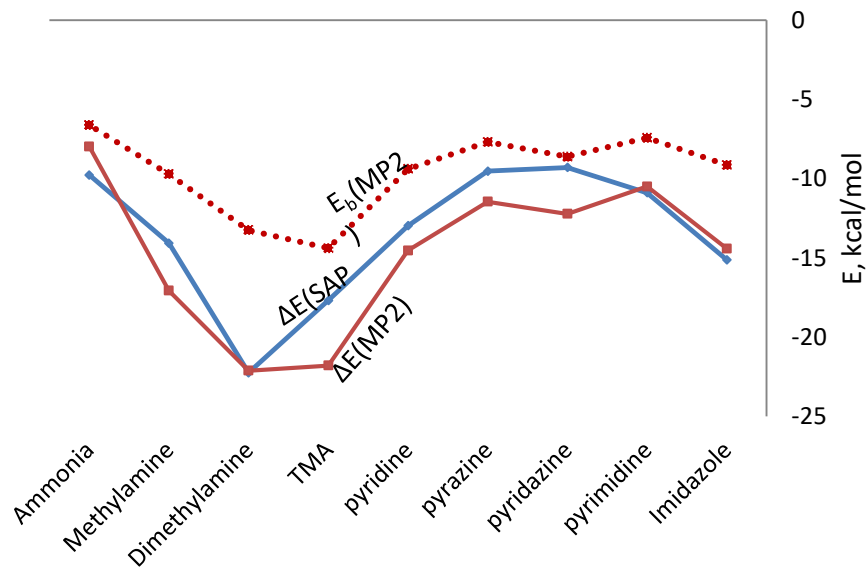


Figure 2-4 Interaction energies of amines with  $\text{SF}_4$  calculated by SAPT (blue) and MP2 (red). Broken red line refers to binding energy at MP2 level.

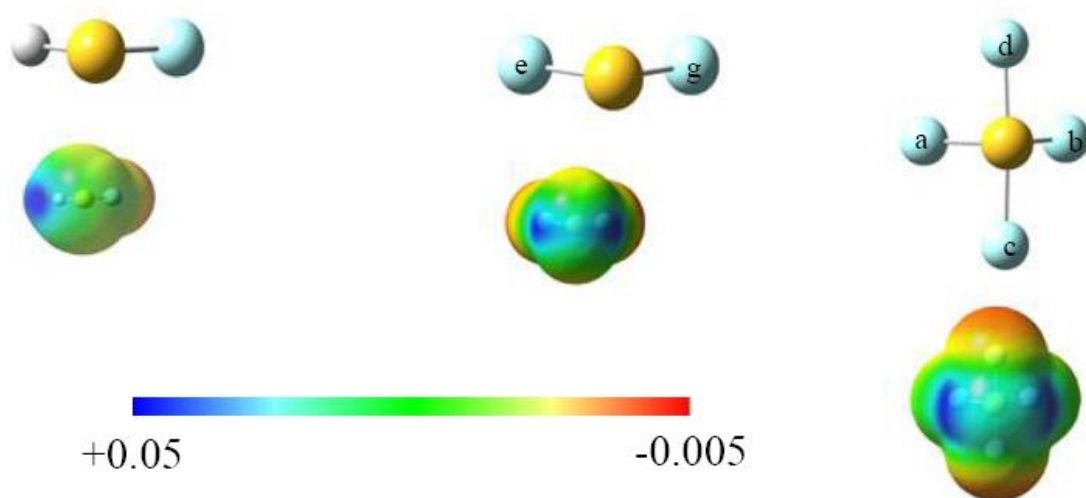


Figure 2-5 MEP of  $\text{HSF}$ ,  $\text{SF}_2$ , and  $\text{SF}_4$ , all calculated on isodensity surface of  $\rho=0.001$  au

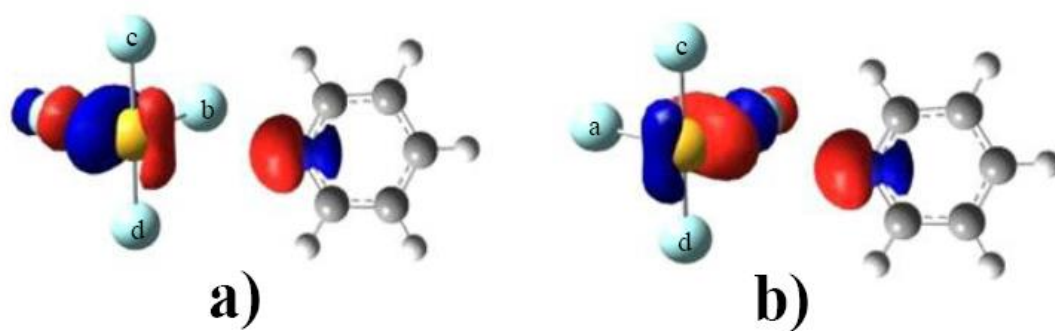


Figure 2-6 Overlap between NBO N lone pair orbital and a)  $\sigma^*(\text{SFa})$  b)  $\sigma^*(\text{SFb})$

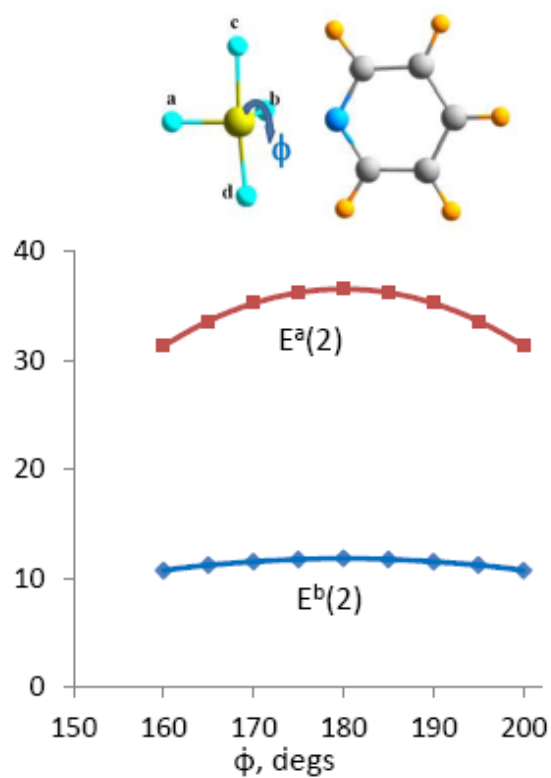


Figure 2-7 Variation of  $E(2)$  for transfer from N lone pair into  $\sigma^*(\text{SFa})$  and  $\sigma^*(\text{SFb})$  antibonding orbitals, as function of rotation of  $\text{SF}_4$  around S-Fb axis,  $\phi(\text{N} \cdots \text{SFbFa})$

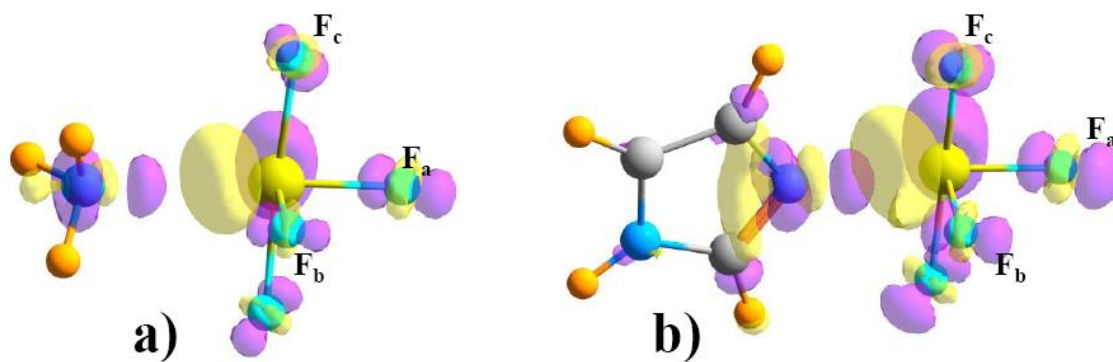


Figure 2-8 Rearrangement of electron density in a)  $\text{NH}_3 \cdots \text{SF}_4$  and b)  $\text{imidazole} \cdots \text{SF}_4$  complexes. Purple and yellow regions correspond respectively to increases and decreases, contours are  $\pm 0.003$  au.

## CHAPTER 3

INTRAMOLECULAR S··O CHALCOGEN BOND AS STABILIZING FACTOR IN  
GEOMETRY OF SUBSTITUTED PHENYL-SF<sub>3</sub> MOLECULES<sup>1</sup>**Abstract**

Density functional methods are used to examine the geometries and energetics of molecules containing a phenyl ring joined to the trigonal bipyramidal SF<sub>3</sub> framework. The phenyl ring has a strong preference for an equatorial position. This preference remains when one or two ether -CH<sub>2</sub>OCH<sub>3</sub> groups are added to the phenyl ring, *ortho* to SF<sub>3</sub>, wherein an apical structure lies nearly 30 kcal/mol higher in energy. Whether equatorial or apical, the molecule is stabilized by a S··O chalcogen bond, sometimes augmented by CH··F or CH··O H-bonds. The strength of the intramolecular S··O bond is estimated to lie in the range between 3 and 6 kcal/mol. A secondary effect of the S··O chalcogen bond is elongation of the S-F bonds. Solvation of the molecule strengthens the S··O interaction. Addition of substituents to the phenyl ring has only modest effects upon the S··O bond strength. A strengthening arises when an electron-withdrawing substituent is placed *ortho* to the ether and *meta* to SF<sub>3</sub>, while electron-releasing species produce an opposite effect.

**3-1. Introduction**

Fluorine-containing compounds are of great importance in organic synthesis, and in the pharmaceutical and agro-industries. Fluorinated compounds constitute about 25% of

---

<sup>1</sup>Coauthored by Vincent de Paul Nzuwah Nziko and Steve Scheiner. Reproduced with permission from *J. Org. Chem.* **2015**, 80, 2356-2363. Copyright 2014, American Chemical Society.

pharmaceutical and 30% of all agricultural compounds <sup>1-4</sup>. Glycosyl fluorides have been widely and effectively used for purposes of *O*- and *C*-glycosylation. The addition of a fluorine atom to a molecule can have a variety of dramatic effects on its properties, making it more selective, increasing its efficacy, or making it easier to administer <sup>2, 5-7</sup>.

The preparation of fluorinated compounds made use of SF<sub>4</sub> in order to convert alcohols, aldehydes, ketones and carboxylic acids to their respective fluorinated forms <sup>8</sup>. Due to the highly toxic and gaseous nature of SF<sub>4</sub>, other fluorinating agents with improved physical and chemical behavior were highly sought after. In the 1970s, SF<sub>4</sub> was largely replaced by dialkylaminosulfur trifluorides. One of these, diethylaminosulfur trifluoride (DAST illustrated in Scheme Ia) was effective <sup>9</sup> for deoxofluorination of alcohols and C=O containing molecules. A major drawback, however, was the thermal instability of DAST, coupled with its inability to fluorinate certain ketones. These problems have led to a number of other deoxofluorinating agents, such as deoxofluor (Scheme Ib) <sup>10</sup> and Yarovenko and Ishikawa reagents <sup>11-12</sup>, but each of these have been limited in terms of molecules they can easily fluorinate.

In 2010, Umemoto et al <sup>13</sup> reported a series of aryl fluorinated compounds with improved reactivity as deoxofluorinating agents, with high thermal stability that led to extensive applications. They suggested that the improved thermal stability of phenylsulfur trifluorides probably resulted from strong C-S bonds, compared to the weak N-S bonds in DAST and deoxofluor. A series of related compounds were tested for their efficacy, and some of the most promising molecules contained one or more ether groups bound to the phenyl, in positions adjacent to the SF<sub>3</sub> group, as for example in Scheme Ic. There was

limited structural information available about these molecules, but  $^{19}\text{F}$  and  $^1\text{H}$  NMR data strongly suggested a trigonal bipyramidal geometry around the sulfur atom. The authors suggested that the stability of this series of molecules might be due in part to coordination of electron-donating ether oxygen atoms to the electron-deficient  $\text{SF}_3$  group.

The potential of this sort of molecule as a deoxofluorinating agent leads to the necessity for better understanding of the underlying factors that make it so effective. This information ought to lead to a rational means of designing and synthesizing new systems with superior effectiveness. From a more basic perspective, there is little known about the chalcogen  $\text{S}\cdots\text{O}$  bond that has been proposed as a key ingredient in the efficacy and thermal stability of these systems. Even as information begins to accumulate about such chalcogen bonds <sup>14-30</sup>, most of this work has been aimed toward intermolecular interactions, not the sort of intramolecular bonds that are characteristic of these systems. Unlike the former, the intramolecular sort of  $\text{S}\cdots\text{O}$  bonds are saddled with a variety of inescapable geometrical restrictions that are part and parcel of each molecule. Another distinguishing feature of intramolecular bonds is the strong interdependence of the electronic structure around the sulfur and oxygen atoms, which are connected by only a few covalent bonds between them. There are a number of very important issues related to this series of molecules, their geometry, and their potential as fluorinating agents. Are there in fact intramolecular  $\text{O}\cdots\text{S}$  contacts present in these systems? How strong are these noncovalent bonds, and do they persist in different solvents? How does the presence of one such  $\text{S}\cdots\text{O}$  contact affect the properties of a second? Importantly, what are the effects of these interactions upon the neighboring  $\text{S-F}$  bonds which are the source of the fluorine atoms during the fluorination

process? How are the structure and properties affected by the presence of various substituents on the aromatic ring, and in different positions?

A straightforward means to address these important questions is via quantum chemical calculations. In this work, the molecules of interest have been built and studied in stages. First the intrinsic geometric preferences of an unsubstituted phenyl-SF<sub>3</sub> molecule are examined. We determine first whether this molecule adopts a trigonal bipyramidal geometry as is the case in the catalysts of interest: if so what is the difference in energy between an apical or equatorial placement of the phenyl group. An ether functionality is then added to the phenyl ring, as in the molecules under study. Careful examination determines whether there is indeed a S··O chalcogen bond present, and if so, how stable is this structure in comparison to other geometries. The possibility of H-bonds (HBs) of the CH··F type influencing the structure is examined as well. The system is brought into exact correspondence with the deoxofluorinating agents of interest when a second ether group is added. (The -CH<sub>2</sub>OCH<sub>3</sub> group used here corresponds to the functionality that showed the highest percent yield in the experimental work <sup>13</sup>.) Is there a S··O chalcogen bond present here also, and if so, might there be a second as well? In terms of rationally designing a more effective agent, the first step might be to add a substituent to the phenyl ring. A set of different substituents are therefore added, both electron-withdrawing and releasing. And these substituents are added to various positions on the phenyl ring to determine which would be most effective. And finally, the molecules are examined not only *in vacuo* which tells much about their intrinsic properties, but also in solution where they would normally be used.

### 3-2. Methods

Molecular systems were examined using the B3LYP variant of density functional theory, and the aug-cc-pVDZ basis set. Calculations were carried out using the Gaussian-09 package<sup>31</sup> of codes. Solvent was introduced via the PCM method<sup>32</sup>. Second-order interaction energies between molecular segments were computed using the Natural Bond Orbital (NBO) approach<sup>33-34</sup>, as implemented in Gaussian. Atoms in Molecules (AIM) methodology<sup>35</sup> was used to analyze the electron density of the system using the AIMALL<sup>36</sup> program.

### 3-3. Results and Discussion

When one fluorine atom of SF<sub>4</sub> is replaced by a phenyl group, there is only one minimum on the monosubstituted molecule's potential energy surface. As seen in Fig 3-1, the phenyl group of 1A assumes an equatorial position, wherein two of its CH groups are in near proximity to the apical fluorine atoms, with  $r(\text{H}\cdots\text{F})$  less than 2.3 Å. The optimization of this same molecule, with the phenyl group placed in an apical position decayed to the equatorial conformer 1A.

The situation changes to a certain extent when an *ortho*-H atom of the phenyl group is replaced by a -CH<sub>2</sub>OCH<sub>3</sub> ether group. There are now two equatorial arrangements that occur as minima. The more stable of the two is displayed as 1B in Fig 3-1, and contains a close approach of the ether oxygen to the sulfur atom, with  $R(\text{S}\cdots\text{O})=2.663$  Å. There is also a fairly close approach of an apical fluorine atom to a methylene proton, 2.527 Å. The stabilizing O $\cdots$ S chalcogen bond is replaced by several CH $\cdots$ F H-bonds and one CH $\cdots$ O in the other equatorial configuration 1C. But these HBs cannot compensate for the loss of the



O··S chalcogen bond, making this structure less stable than 1B by 3.8 kcal/mol.

As is indicated in Figure 3-1, and as is true for all of the structures described here, the geometry around the sulfur atom fits the description of a “see-saw”, i.e. a trigonal bipyramid with one of the equatorial sites occupied by a S lone pair. As is typical of these sorts of geometries, the bulging lone pair squeezes the bonding pairs closer together than would be the case in a full trigonal bipyramid of bonding pairs. The angles between each pair of apical S-F/C bonds were found to be within 10° of the classical 180°, and angles between apical and equatorial bonds are within 6° of the unstrained 90°. The greatest strain induced by the lone pair occurs within each pair of equatorial bond pairs, so these angles lie in the range 95-106°, smaller than the unstrained value of 120°. Noncovalent S··O chalcogen bonds occur when charge is transferred from the oxygen atom to the  $\sigma^*(\text{S-F})$  antibonding orbital which lies directly opposite the associated FH covalent bond. They do not represent a fifth covalent bond around the S which would alter its overall geometry. Nor is the formation of a chalcogen (or pnictogen or halogen) bond impeded by the presence of one or more lone pairs on the central atom in the general direction<sup>37-48</sup> of the noncovalent bond. The equatorial SF bonds have associated with them a vacant position which may be occupied by a S··O chalcogen bond. In contrast, such noncovalent bonds are not possible opposite an apical SF bond, since this position is already occupied by a second apical covalent bond.

The presence of the introduced ether group also results in the appearance of a minimum on the surface in which the substituted phenyl group occupies an apical position, albeit 27.7 kcal/mol higher in energy than the global minimum 1B. Like the latter, this

apical minimum 1D also contains a close approach of the oxygen and sulfur atoms; in this case  $R(O\cdots S)$  is 0.1 Å shorter at 2.56 Å. It is likely that it is the presence of this chalcogen bond which permits this configuration to exist as a minimum on the surface, as there is no apical minimum in the absence of the ether. Not only is  $R(S\cdots O)$  shorter in 1D than in 1B, but the NBO value of  $E(2)$ , a measure of charge transfer from the O lone pairs to the  $\sigma^*(SF)$  antibonding orbitals, is 10.81 kcal/mol in 1D, even larger than in 1B where it is 6.66 kcal/mol.

Addition of a second ether functionality to the other *ortho* position of the phenyl group imparts a more complicated character to the potential energy surface. There is still a heavy preference for equatorial placement of the phenyl. The global minimum 2A in Figure 3-2 is stabilized by three attractive interactions. One ether oxygen atom participates in a  $O\cdots S$  chalcogen bond with the sulfur atom, with  $R(O\cdots S)=2.626$  Å. A methylene H comes within 2.426 Å of an apical fluorine atom. Without a second site on S available for another  $O\cdots S$  chalcogen bond, the other ether O associates instead with a phenyl H, forming a strong  $CH\cdots O$  HB, with  $R(H\cdots O)$  as short as 2.226 Å. The second equatorial minimum 2B is less stable by 2.2 kcal/mol, and relies for its stability on HBs alone, of both the  $CH\cdots O$  and  $CH\cdots F$  varieties, some as short as 2.3 Å. Again, these HBs are unable to make this structure as stable as the one containing the chalcogen bond.

Apical positioning of the phenyl group again results in a much less stable set of minima, 28-31 kcal/mol higher in energy than the equatorial global minimum. The apical placement of the substituent opens up a second site opposite a  $S-F_e$  bond which might be occupied by a second  $O\cdots S$  chalcogen bond. And indeed, two such bonds are observed in

the most stable of the apical conformers 2C. Reducing this number of chalcogen bonds to one raises the energy in 2D and 2E, even in the presence of a  $\text{CH}\cdots\text{O}$  HB in 2D. Comparison of 2C with 2D and 2E indicates a negative cooperativity in the two  $\text{S}\cdots\text{O}$  chalcogen bonds.  $R(\text{S}\cdots\text{O})$  is longer in 2C by nearly  $0.3 \text{ \AA}$ , and the two values of  $E(2)$  are  $6.5 \text{ kcal/mol}$  in each of the  $\text{S}\cdots\text{O}$  bonds of 2C, smaller than  $17.81$  of 2D or  $16.41 \text{ kcal/mol}$  of 2E.

One can conclude that a phenyl substituent has a strong propensity to occupy an equatorial position around S. If the phenyl also contains one or more ether linkages, the oxygen atoms are drawn to form a  $\text{O}\cdots\text{S}$  chalcogen bond which will be present in the global minimum in all cases. This bond can stabilize an apical substitution to the point of becoming a true minimum, even if nearly  $30 \text{ kcal/mol}$  higher in energy than equatorial. This apical placement opens up a second site for  $\text{S}\cdots\text{O}$  chalcogen bond formation, which is indeed occupied in the substituted molecule 2C. These  $\text{S}\cdots\text{O}$  chalcogen bonds prove a stronger influence upon conformation than even short  $\text{CH}\cdots\text{O}$  or  $\text{CH}\cdots\text{F}$  HBs.

### 3-3.1. Solvation Effects

As some of the most useful behavior of these molecules occurs in solution, it is worthwhile to examine how solvation affects their properties. Table 3-1 focuses on those structures that contain a  $\text{S}\cdots\text{O}$  chalcogen bond, e.g. 1B and 1D. The data in the leftmost section of Table 3-1 shows that the introduction of solvent causes a slight lowering of the energies of the secondary minima relative to the global minimum. For example, the energy of 1D relative to 1B drops from  $27.7 \text{ kcal/mol}$  in the gas phase to  $25.0 \text{ kcal/mol}$  in dichloromethane (DCM:  $\epsilon=8.9$ ), and then to  $23.8 \text{ kcal/mol}$  in water ( $\epsilon=78$ ). Similar reductions are noted for the 2C, 2D, 2E series relative to 2A. It would appear then that

solvent allows a mild stabilization of apical geometries in comparison to the more stable equatorial structures.

The next section of Table 3-1 shows that the  $R(O\cdots S)$  distances of the chalcogen bonds undergo a contraction as solvent is introduced and becomes more polar. For example, the first row of Table 3-1 shows that the  $R(O\cdots S)$  distance in 1B is 2.663 Å *in vacuo*, contracts to 2.556 Å in dichloromethane, and then to 2.529 Å in water. This contraction is even stronger in the apical configuration 1D, where water reduces this distance by 0.24 Å. Other rows in Table 3-1 show that the reduction occurs not only when there is a single  $S\cdots O$  chalcogen bond, but also in 2C where there are two such bonds, both contracted by 0.18 Å when immersed in water. Note that the solvent-induced bond contractions are of larger magnitude in the apical structures in comparison to the equatorial, consistent with the energetic trends in Table 3-1. Another sign of growing strength of these  $S\cdots O$  noncovalent bonds in solution arises by examination of the  $\theta(O\cdots SF)$  angles which all become more linear. Again taking 1B as an example, this angle is raised from 165° in the gas phase to 173° in water.

One can also consider the NBO second order perturbation energy  $E(2)$  associated with charge transfer from the O lone pairs to the  $\sigma^*(SF)$  antibonding orbital as a measure of chalcogen bond strength. These values in the various solvation situations are reported in Table 3-2. The major component refers to the SF bond that lies directly opposite the O, whereas a smaller value is associated with the  $\sigma^*$  antibonding orbital of the other equatorial SF bond. (This secondary transfer was shown to be important in our earlier study<sup>49</sup> of the interaction of  $SF_4$  with several amines.) 1B and 2A are exceptions since the second

equatorial position is taken up not by an F but rather by the phenyl group, so there is no minor component. The important finding in Table 3-2 is that the increasing polarity of the solvent raises  $E(2)$ , consistent with the trends in the energetic and geometrical data in Table 3-1.

### 3-3.2. Internal Bond Perturbations

Prior work with the  $\text{SF}_4$  molecule<sup>49</sup> has shown that its participation in a chalcogen bond tends to lengthen all of its S-F bonds, albeit in the context of an intermolecular interaction. It was therefore of interest to examine whether the same trend occurs in the case of an intramolecular chalcogen bond. The optimized geometry of 1A was taken as the reference point for an equatorial phenyl group, but without any possibility of a S $\cdots$ O chalcogen bond. As indicated earlier, there is no corresponding apical minimum on the surface of this system in the gas phase. In order to construct such a reference structure, a restraint was introduced into the molecule, wherein  $\theta(\text{C-S-F}_a)$  was held constant at  $177.3^\circ$ , the angle which is adopted by the apical minimum in DCM solvent. This structure is illustrated as 1A' in Figure 3-1.

The left side of Table 3-3 contains the changes in the  $r(\text{SF})$  bond lengths relative to equatorial 1A whereas the apical structure 1A' was taken as the reference for molecules on the right side of the Table. Considering 1B first, this molecule contains a O $\cdots$ S chalcogen bond which stretches the S-F<sub>e</sub> bond which lies directly opposite the incoming oxygen atom, by 4.4 mÅ. One of the apical S-F bonds is stretched by 6 mÅ, but the longest stretch of 20 mÅ is associated with F<sub>a2</sub> which engages in a CH $\cdots$ F HB with a methylene proton. The pattern of a small stretch for the S-F<sub>e</sub> and longer stretches for the apical S-F bonds is

repeated in 2A, which also contains a noncovalent S $\cdots$ O bond. Neither 1C nor 2B contain such a chalcogen bond, and in both of these cases S-F<sub>e</sub> suffers a contraction rather than a stretch. One of the S-F<sub>a</sub> bonds shows little change, and the other such bond undergoes a small stretch. Thus, the S-F bond elongations associated with O $\cdots$ S chalcogen bond formation are either absent or much reduced in the absence of such a bond.

Turning to the molecules in which the phenyl group occupies an apical position, the S $\cdots$ O chalcogen bond in 1D has small but opposite effects on the two S-F<sub>e</sub> bonds, one stretching and the other contracting. It is the apical S-F bond that undergoes the largest change, stretching by 40 mÅ. This same pattern repeats in the other apical conformations 2C, 2D, and 2E, where the apical S-F bond stretches by a large amount upon formation of the S $\cdots$ O chalcogen bond, between 62 and 67 mÅ. Also common in these structures, the S-F<sub>e</sub> bonds undergo much smaller changes in length.

Perusal of data in the lower portions of Table 3-3 indicates a repeat of the patterns found within the gas phase for the most part, although these stretches generally increase in solution. For example, the S-F<sub>e</sub> bond stretch in 1B increases from 4.4 mÅ in the gas phase, to 7.8 in DCM and then to 9.3 mÅ in water. These solvent-induced enhancements are most noticeable in the stretches of the S-F<sub>a</sub> bond in the apical conformations. Elongations of 40 to 67 mÅ in the gas phase are magnified several-fold to as much as 209 mÅ in water. One might anticipate that S-F bond elongations would be tied to bond polarization making these fluorine atoms more negative. The changes in the NBO charges on the fluorine atoms reported in Table 3-4 indeed confirm this expectation. For example, the greater stretches of the apical S-F bonds in 1B, compared to equatorial, are consistent with the greater

increase of  $F_a$  negative charge. And in those cases where a S-F bond contraction is noted, e.g. 1C and 2B, the fluorine atoms become more positive. Just as the longest S-F bond stretches occur in the apical bond in aqueous phase on the lower right of Table 3-3, so too does the  $F_a$  atom gain the largest negative charge in Table 3-4.

In summary, formation of a S $\cdots$ O chalcogen bond tends to lengthen all of the S-F bonds and to increase the fluorine atom negative charge. The largest effects are associated with the apical S-F bonds. This pattern is observed whether the phenyl substituent is placed in an equatorial or apical position, but the latter results in a much larger S- $F_a$  elongation upon formation of the S $\cdots$ O chalcogen bond. These bond elongations are presumably associated with a weakening which would facilitate the transfer of one or more fluorine atoms during the deoxofluorinating process.

### 3-3.3. Electron Density Shifts

Another window through which to view the purported formation of an interaction such as a S $\cdots$ O chalcogen bond is via electron density difference maps. The construction of such a map is straightforward in the case of an intermolecular interaction, where it comprises the difference between the density of the complex and the sum of the two isolated subunits of which it is composed. But one cannot do this in the case of an intramolecular interaction where there are no isolated subunits to take as a reference. Instead, the idea of an isodesmic reaction<sup>50</sup> was used to construct this map. As indicated in Figure 3-3, C represents the molecule containing the intramolecular interaction of interest between SF<sub>3</sub> and CH<sub>2</sub>OCH<sub>3</sub>. A and B are both the same as C, but each replaces one of the two functional groups by a simple hydrogen atom. Their sum therefore contains the

density of both groups, but without the mutual interaction. The second benzene ring of this sum must be accounted for, so the density of D is added to that of C. The electron density difference map therefore is taken as the sum of (C + D), minus (A + B), which ought to focus on the shifts of density that accompany the formation of the chalcogen bond.

This density shift map is illustrated in Figure 3-4 where purple and yellow regions respectively indicate gains and losses of density that occur as a result of the formation of the intramolecular S··O noncovalent bond. Perhaps the most important aspect of this figure is the purple buildup of density between the oxygen and sulfur atoms, expected for bond formation. Also noted is a yellow density loss to the immediate left of the sulfur atom, both features that were observed earlier<sup>49</sup> for the intermolecular S··N noncovalent bond between SF<sub>4</sub> and a series of aliphatic and aromatic amines. Another similarity to the intermolecular systems is the buildup of density on the various fluorine atoms, both the one involved in the O<sub>lp</sub>→σ\*(SF) charge transfer, and the others as well. It is also worth noting the lack of substantive density rearrangement within the aromatic ring, suggesting its lack of direct involvement in the S··O chalcogen bond.

#### 3-3.4. Substituent Effects

The presence of substituents on the phenyl ring will typically affect the nature of a molecule's electronic structure. The following groups were thus added to the phenyl ring in positions *ortho*, *meta*, and *para* to the SF<sub>3</sub> group: nominally electron-withdrawing F, Cl, Br, and donating OH, NH<sub>2</sub>, NHMe and NMe<sub>2</sub>. More specifically, placing the SF<sub>3</sub> group in the 1-position and -CH<sub>2</sub>OCH<sub>3</sub> at 2, *meta* refers to 3, *para* to 4, and *ortho* to 6.

After each substitution, the -CH<sub>2</sub>OCH<sub>3</sub> group was rotated around the C-C<sub>aryl</sub> bond



to search for the minimum-energy structure. The amount of this rotation is defined by the dihedral angle  $\varphi(\text{OCCC}_S)$  where  $C_S$  refers to the C bonded to the sulfur atom. There are several local minima for different values of  $\varphi$  but the global minimum occurs at  $\varphi \sim -39^\circ$ , which corresponds to a geometry much like 1B where a O $\cdots$ S chalcogen bond is present. For *o*, *m*, and *p* derivatives, as well as the unsubstituted molecule, there is also a secondary minimum at  $\varphi \sim -130^\circ$ , only slightly higher in energy, within 1 kcal/mol of the global minimum. With regard to other local minima, *o* and *p* derivatives differ from *m*. The former molecules, like the unsubstituted one, have another minimum located at  $\varphi \sim 170^\circ$ , some 2-4 kcal/mol higher in energy than the global minimum. These structures are stabilized by a pair of weak H-bonds. One of these involves a methylene proton from the  $\text{CH}_2\text{OCH}_3$  group and a fluorine atom. The other H-bond pairs the oxygen atom of the ether group and a phenyl CH which is meta to the  $\text{SF}_3$ . The latter H-bond is not possible for the *meta*-substituted molecule, so an energy maximum occurs at this value of  $\varphi$ . But most importantly, the global minimum of all these molecules, whether substituted or not, contains the O $\cdots$ S chalcogen bond, and it is this conformation which is considered further. Some of the salient features of the various substituted molecules are presented in Table 3-5, along with the unsubstituted molecule 1B. It should perhaps be stated at the outset that most of the substituent effects are rather small. It is clear from the first column that the presence of any substituent, and in any position, shortens the  $\text{R}(\text{O}\cdots\text{S})$  distance within the chalcogen bond. The degree of this contraction is greatest for the *meta*-substituted molecules, but is only slightly sensitive to the nature of the substituent. Considering the *meta*-substituted molecules as an example, the *m*-Br molecule exhibits the shortest  $\text{R}(\text{O}\cdots\text{S})$ ,

and *m*-F the longest. But even here, the changes in this noncovalent bond length amount to less than 7%. The values of  $E(2)$  for the  $O_{lp} \rightarrow \sigma^*(SF)$  charge transfer follow a similar pattern, in that the largest values are associated with *meta* substitution, with only mild sensitivity to nature of substituent. It is notable that there is a very strong linear correlation between  $R(O \cdots S)$  and  $E(2)$ , with correlation coefficient  $R^2 = 0.991$ .

AIM analysis of the electron density reveals a bond critical point between the oxygen and sulfur atoms in all cases. The value of  $\rho$  at this point, as well as its Laplacian, are reported in the next two columns of Table 3-5. In all cases,  $\rho$  is in the 0.028 - 0.037 range, and  $\nabla^2\rho$  between 0.082 and 0.102. Both quantities lie in their upper ranges for *meta* substitution.

There is no completely unambiguous means of assessing the energy of an intramolecular interaction. Of the various prescriptions developed for approximating this property, application of an isodesmic reaction should offer a realistic, if imperfect, value. As applied to the systems of interest here, reference is again made to Figure 3-3 where C contains the full molecule and D only the phenyl ring. A and B each contain one of the two functional groups. The substituent X is included for all four segments. The difference in energy for the reaction  $A + B \rightarrow C + D$  should offer a realistic assessment of the energy of the  $S \cdots O$  chalcogen bond which is contained only in C. As indicated in the first row of Table 3-5, this  $E_{iso}$  is equal to 4.96 kcal/mol for the unsubstituted 1B. With respect to the *meta*-substituted molecules, this bond is strengthened for the halogens and OH, and weakened for  $NH_2$ ,  $NHMe$  and  $NMe_2$ . The *ortho*-substituted molecules, on the other hand, all exhibit a weaker  $S \cdots O$ . Weakening, albeit not quite as much, is also characteristic of the *para*-

substituted systems, with the exception of Br and Cl.

In summary, substitution on the aryl ring leads to a modest amount of shortening of the R(O $\cdots$ S) chalcogen bonds, in tandem with increases of the O<sub>lp</sub> $\rightarrow\sigma^*$ (S-F) charge transfer contained within E(2). These changes are largest for *m*-substitution. It may be noted that all substituents yield similar trends, at least qualitatively, even though some are generally considered electron-withdrawing and others releasing. On the other hand, all substituents manifest as electron-withdrawing within the context of the full molecules in that all are associated with a partial negative charge. For example, the NH<sub>2</sub> group acquires a charge of -0.10 in this system, even though it is commonly thought of as electron-releasing. And indeed, the AIM parameters in Table 3-5 show little difference between any of the substituents, also suggesting a chalcogen bond strengthening, albeit a very small one.

### 3-4. Conclusion

When replacing a fluorine atom of SF<sub>4</sub>, there is a strong preference for a phenyl group to occupy one of the equatorial positions. In fact, in the gas phase, there is no minimum in which the phenyl group is in an apical position. Such a minimum occurs in solution, but the apical structure is much higher in energy than the equatorial configuration. The preference for an equatorial position remains when the phenyl group is substituted with an ether -CH<sub>2</sub>OCH<sub>3</sub> group in a position *ortho* to S. The optimal geometry contains an intramolecular O $\cdots$ S chalcogen bond as a major stabilizing force. This same bond occurs as well in the apical geometry, and accounts for its existence as a true minimum of this configuration even in the gas phase. The S $\cdots$ O chalcogen bond occurs also when both *ortho* positions of the phenyl are occupied by ether groups. This bond appears to be a stronger

influence upon the structure than the various CH $\cdots$ F and CH $\cdots$ O H-bonds which it replaces. The apical geometry of this disubstituted molecule contains two O $\cdots$ S chalcogen bonds in its most stable structure.

Placing these systems within a solvent environment does not change any of the above trends. Increasing the polarizability of the solvent leads to a progressive strengthening of the chalcogen bonds. The R(S $\cdots$ O) interatomic distances contract and the NBO value of E(2) is increased. The S-F bond lengthening associated with the formation of the S $\cdots$ O chalcogen bond is enhanced in solution, as are the increases in fluorine atom negative charges. The weakening of these S-F bonds would likely facilitate the catalytic activity of these molecules as deoxofluorinating agents. Solvation also reduces the energetic differences between the apical and equatorial geometries, albeit by only a small amount.

The addition of a second substituent on the phenyl ring, in addition to the ether functionality, has only minor effects on the properties and energetics. All substituents, whether nominally electron-donating or withdrawing, and in any position on the phenyl ring, strengthen the O $\cdots$ S chalcogen bond. This conclusion is supported by a shorter R(S $\cdots$ O) distance and larger value of E(2). AIM quantities offer a slightly different conclusion: greater  $\rho$  and  $\nabla^2\rho$  at the bond critical point are substantial only for the *meta* positioning of the substituent. As an intramolecular interaction, the energy of the S $\cdots$ O noncovalent bond is difficult to define unambiguously. An isodesmic measure of this property suggests the bond is strengthened when electron-withdrawing substituents, e.g. F or Br, are placed adjacent to the ether, *meta* to SF<sub>3</sub>.

While there is little experimental structural information available about these system, it should be noted finally that the computational finding of a trigonal bipyramidal framework is consistent with NMR spectroscopic data.

## References

- (1) Hunter, L. *Beilstein J. Org. Chem.* **2010**, *6*, DOI: 10.3762/bjoc.6.38.
- (2) Müller, K.; Faeh, C.; Diederich, F. *Science* **2007**, *317*, 1881.
- (3) McGrath, N. A.; Brichacek, M.; Njardarson, J. T. *J. Chem. Ed.* **2010**, *87*, 1348.
- (4) Wang, J.; Sánchez-Roselló, M.; Aceña, J. L.; del Pozo, C.; Sorochinsky, A. E.; Fustero, S.; Soloshonok, V. A.; Liu, H. *Chem. Rev.* **2014**, *114*, 2432.
- (5) Ji, W.-Y.; Xia, X.-L.; Ren, X.-H.; Wang, F.; Wang, H.-J.; Diao, K.-S. *Struct. Chem.* **2013**, *24*, 49.
- (6) Fried, J.; Mitra, D. K.; Nagarajan, M.; Mehrotra, M. M. *J. Med. Chem.* **1980**, *23*, 234.
- (7) Rowley, M.; Hallett, D. J.; Goodacre, S.; Moyes, C.; Crawforth, J.; Sparey, T. J.; Patel, S.; Marwood, R.; Patel, S.; Thomas, S.; Hitzel, L.; O'Connor, D.; Szeto, N.; Castro, J. L.; Hutson, P. H.; MacLeod, A. M. *J. Med. Chem.* **2001**, *44*, 1603.
- (8) Hasek, W. R.; Smith, W. C.; Engelhardt, V. A. *J. Am. Chem. Soc.* **1960**, *82*, 543.
- (9) Middleton, W. J. *J. Org. Chem.* **1975**, *40*, 574.
- (10) Lal, G. S.; Pez, G. P.; Pesaresi, R. J.; Prozonic, F. M.; Cheng, H. *J. Org. Chem.* **1999**, *64*, 7048.
- (11) Yarovenko, N. N.; Raksha, M. A.; Shemanina, V. N.; Vasileva, A. S. *J. Gen. Chem. USSR* **1957**, *27*, 2246.

- (12) Takaoka, A.; Iwakiri, H.; Ishikawa, N. *Bull. Chem. Soc. Jpn.* **1979**, *52*, 3377.
- (13) Umemoto, T.; Singh, R. P.; Xu, Y.; Saito, N. *J. Am. Chem. Soc.* **2010**, *132*, 18199.
- (14) Werz, D. B.; Gleiter, R.; Rominger, F. *J. Am. Chem. Soc.* **2002**, *124*, 10638.
- (15) Sanz, P.; Yáñez, M.; Mó, O. *Chem. Eur. J.* **2003**, *9*, 4548.
- (16) Cozzolino, A. F.; Vargas-Baca, I.; Mansour, S.; Mahmoudkhani, A. H. *J. Am. Chem. Soc.* **2005**, *127*, 3184.
- (17) Gleiter, R.; Werz, D. B.; Rausch, B. *J. Chem. Eur. J.* **2006**, *9*, 2676.
- (18) Bleiholder, C.; Werz, D. B.; Koppel, H.; Gleiter, R. *J. Am. Chem. Soc.* **2006**, *128*, 2666.
- (19) Iwaoka, M.; Isozumi, N. *Molecules* **2012**, *17*, 7266.
- (20) Jablonski, M. *J. Phys. Chem. A* **2012**, *116*, 3753.
- (21) Zhao, J.-L.; Li, Q.-Z.; Liu, Z.-B.; Li, W.-Z.; Cheng, J.-B. *Mol. Phys.* **2012**, *110*, 2969.
- (22) Bauzá, A.; Quiñonero, D.; Deyà, P. M.; Frontera, A. *CrystEngComm* **2013**, *15*, 3137.
- (23) Esrafil, M. D.; Vakili, M. *Mol. Phys.* **2014**, *112*, 2746.
- (24) Begum, S.; Subramanian, R. *Phys. Chem. Chem. Phys.* **2014**, *16*, 17658.
- (25) George, J.; Deringer, V. L.; Dronskowski, R. *J. Phys. Chem. A* **2014**, *118*, 3193.
- (26) Phuong, V. T.; Trang, N. T. T.; Vo, V.; Trung, N. T. *Chem. Phys. Lett.* **2014**, *598*, 75.
- (27) Azofra, L. M.; Scheiner, S. *J. Chem. Phys.* **2014**, *140*, 034302.
- (28) Azofra, L. M.; Scheiner, S. *Phys. Chem. Chem. Phys.* **2014**, *16*, 5142.
- (29) Azofra, L. M.; Scheiner, S. *J. Phys. Chem. A* **2014**, *118*, 3835.

- (30) Azofra, L. M.; Alkorta, I.; Scheiner, S. *Phys. Chem. Chem. Phys.* **2014**, *16*, 18974.
- (31) Frisch, M. J.; Trucks, G. W.; Schlegel, H. B.; Scuseria, G. E.; Robb, M. A.; Cheeseman, J. R.; Scalmani, G.; Barone, V.; Mennucci, B.; Petersson, G. A.; Nakatsuji, H.; Caricato, M.; Li, X.; Hratchian, H. P.; Izmaylov, A. F.; Bloino, J.; Zheng, G.; Sonnenberg, J. L.; Hada, M.; Ehara, M.; Toyota, K.; Fukuda, R.; Hasegawa, J.; Ishida, M.; Nakajima, T.; Honda, Y.; Kitao, O.; Nakai, H.; Vreven, T.; Montgomery, J., J. A.; Peralta, J. E.; Ogliaro, F.; Bearpark, M.; Heyd, J. J.; Brothers, E.; Kudin, K. N.; Staroverov, V. N.; Kobayashi, R.; Normand, J.; Raghavachari, K.; Rendell, A.; Burant, J. C.; Iyengar, S. S.; Tomasi, J.; Cossi, M.; Rega, N.; Millam, J. M.; Klene, M.; Knox, J. E.; Cross, J. B.; Bakken, V.; Adamo, C.; Jaramillo, J.; Gomperts, R.; Stratmann, R. E.; Yazyev, O.; Austin, A. J.; Cammi, R.; Pomelli, C.; Ochterski, J. W.; Martin, R. L.; Morokuma, K.; Zakrzewski, V. G.; Voth, G. A.; Salvador, P.; Dannenberg, J. J.; Dapprich, S.; Daniels, A. D.; Farkas, O.; Foresman, J. B.; Ortiz, J. V.; Cioslowski, J.; Fox, D. J. *Gaussian 09*, Revision B.01; Wallingford, CT, 2009.
- (32) Barone, V.; Cossi, M. *J. Phys. Chem. A* **1998**, *102*, 1995.
- (33) Reed, A. E.; Curtiss, L. A.; Weinhold, F. *Chem. Rev.* **1988**, *88*, 899.
- (34) Reed, A. E.; Weinhold, F.; Curtiss, L. A.; Pochatko, D. J. *J. Chem. Phys.* **1986**, *84*, 5687.
- (35) Bader, R. F. W. *Atoms in Molecules, A Quantum Theory*. Clarendon Press: Oxford, 1990; Vol. 22, p 438.
- (36) Keith, T. A. *AIMALL*, TK Gristmill Software: Overland Park KS, 2013.
- (37) Grabowski, S. J. *Chem. Phys. Lett.* **2014**, *605-606*, 131.
- (38) Scheiner, S. *Acc. Chem. Res.* **2013**, *46*, 280.

- (39) Alkorta, I.; Elguero, J.; Grabowski, S. J. *Phys. Chem. Chem. Phys.* **2015**, *17*, 3261.
- (40) Sladek, V.; Škorňa, P.; Poliak, P.; Lukeš, V. *Chem. Phys. Lett.* **2015**, *619*, 7.
- (41) Solimannejad, M.; Gharabaghi, M.; Scheiner, S. J. *Chem. Phys.* **2011**, *134*, 024312.
- (42) Sánchez-Sanz, G.; Trujillo, C.; Alkorta, I.; Elguero, J. *Comput. Theor. Chem.* **2015**, *1053*, 305.
- (43) Adhikari, U.; Scheiner, S. *Chem. Phys. Lett.* **2012**, *532*, 31.
- (44) Del Bene, J. E.; Alkorta, I.; Elguero, J. *J. Phys. Chem. A* **2014**, *119*, 224.
- (45) Scheiner, S. *Phys. Chem. Chem. Phys.* **2011**, *13*, 13860.
- (46) Shahi, A.; Arunan, E. *Phys. Chem. Chem. Phys.* **2014**, *16*, 22935.
- (47) Scheiner, S. *Int. J. Quantum Chem.* **2013**, *113*, 1609.
- (48) Scheiner, S. *J. Chem. Phys.* **2011**, *134*, 094315.
- (49) Nziko, V. d. P. N.; Scheiner, S. *J. Phys. Chem. A* **2014**, *118*, 10849.
- (50) Sanchez-Sanz, G.; Trujillo, C.; Alkorta, I.; Elguero, J. *Phys. Chem. Chem. Phys.* **2014**, *16*, 15900.



Table 3-1 Relative energies, O $\cdots$ S interatomic distances, and interaction angle in configurations containing a S $\cdots$ O bond.

	E <sub>rel</sub> , kcal/mol			R(O $\cdots$ S), Å			$\theta$ (O $\cdots$ SF), degs		
	Gas	DCM	Water	Gas	DCM	Water	Gas	DCM	Water
1B	0	0	0	2.663	2.556	2.529	165.0	172.5	173.4
1D	27.7	25.0	23.8	2.561	2.370	2.317	167.6	172.0	173.1
2A	0	0	0	2.626	2.551	2.532	172.0	174.4	174.8
2C	27.7	23.3	21.7	2.710	2.583	2.529	157.4	159.7	160.8
2D	28.9	25.4	24.2	2.428	2.295	2.254	171.5	172.2	172.3
2E	30.6	26.2	24.7	2.448	2.322	2.278	171.0	171.7	172.0

Table 3-2 NBO E(2) (kcal/mol) for transfer from O lone pairs to  $\sigma^*$ (SF) antibonding orbital.

	gas		DCM		water	
	Major <sup>a</sup>	Minor <sup>b</sup>	Major	Minor	major	Minor
1B	6.66	-	9.71	-	10.67	-
1D	9.67	1.14	17.76	2.25	20.80	2.68
2A	8.35	-	9.98	-	10.69	-
2C	6.24	6.20	10.21	10.21	12.42	12.42
2D	17.59	3.58	23.19	3.97	25.73	4.48
2E	16.14	3.34	20.98	3.62	23.96	4.16

<sup>a</sup> SF bond directly opposite O

<sup>b</sup> other equatorial SF bond

Table 3-3 Changes in r(S-F) bond lengths (mÅ) of indicated molecules.

	Equatorial <sup>a</sup>				Apical <sup>b</sup>				
vacuum									
	1B	1C <sup>c</sup>	2A	2B <sup>c</sup>		1D	2C	2D	2E
e	4.4	-5.0	5.8	-4.8	e-1	8.0	-3.6	7.1	5.0
a-1	6.0	-0.5	10.6	1.6	e-2	-3.4	-3.6	-4.0	-11.7
a-2	20.5	4.5	22.3	5.4	a	40.0	66.8	64.2	62.0
DCM									
e	7.8	-8.0	6.5	-9.4	e-1	3.82	0.22	5.63	0.63
a-1	19.3	-0.2	19.2	2.5	e-2	4.20	0.22	7.64	3.85
a-2	19.3	3.9	21.3	5.1	a	119.5	156.2	135. 6	125.8
Water									
e	9.3	-8.3	7.3	-10.1	e-1	5.4	4.7	6.5	5.8
a-1	23.4	1.2	22.6	3.2	e-2	9.9	4.7	14.5	7.9
a-2	18.5	3.2	20.0	4.1	a	158.5	208.6	170.0	156.1

<sup>a</sup>relative to 1A<sup>b</sup>relative to apical geometry 1A'<sup>c</sup>no S··O bond present

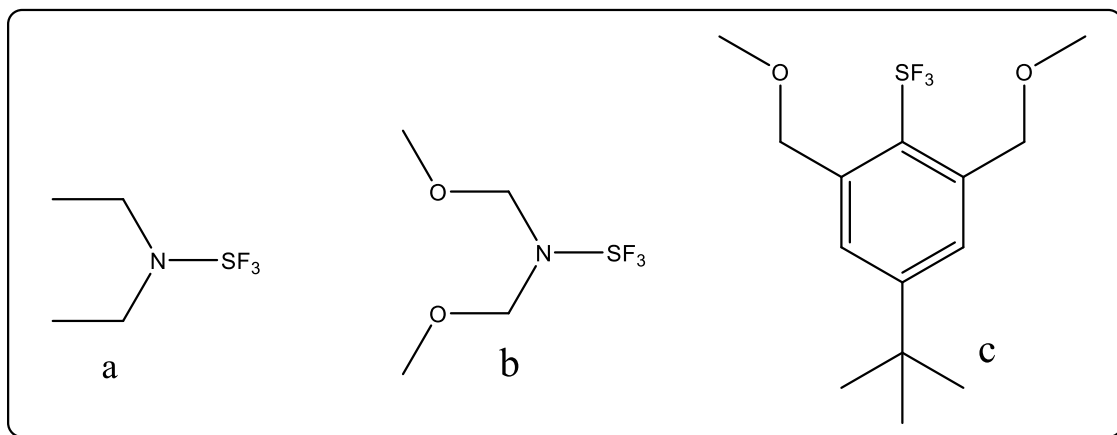
Table 3-4 Changes in NBO atomic charges (me) of F atoms of indicated molecules.

	Equatorial <sup>a</sup>				Apical <sup>b</sup>				
vacuum									
	1B	1C <sup>c</sup>	2A	2B <sup>c</sup>		1D	2C	2D	2E
e	-0.6	5.2	-0.9	4.5	e-1	-4.8	-7.4	-12.8	-5.3
a-1	-9.7	3.3	-11.2	4.8	e-2	-0.9	-7.4	4.7	-3.3
a-2	-14.5	-3.5	-14.4	0.2	a	-29.3	-56.7	-47.9	-47.4
DCM									
e	-3.3	3.4	-3.0	2.7	e-1	-3.6	-12.4	-11.4	-9.3
a-1	-12.2	4.9	-13.1	1.8	e-2	-9.5	-12.4	-18.1	-9.6
a-2	-13.8	-2.4	-14.1	-1.8	a	-57.8	-81.9	-65.6	-62.6
Water									
e	-4.5	1.1	-4.1	2.2	e-1	-3.1	-13.2	-11.0	-9.2
a-1	-12.0	3.2	-14.4	1.6	e-2	-12.1	-13.2	-16.0	-12.0
a-2	-14.8	-2.1	-12.1	-1.8	a	-69.2	-98.5	-75.1	-70.5

<sup>a</sup>relative to 1A<sup>b</sup>relative to apical geometry 1A'<sup>c</sup>no S··O bond present

Table 3-5 Energetic (kcal/mol), geometric, and electronic properties of substituted derivatives of 1B.

	R(O··S), Å	E(2)	$\rho$ , au	$\nabla^2\rho$ , au	E <sub>iso</sub>
unsub 1B	2.663	6.66	0.030	0.088	4.96
<i>meta</i>					
F	2.545	11.00	0.033	0.092	5.21
Cl	2.493	13.12	0.036	0.100	5.62
Br	2.486	13.48	0.037	0.102	6.03
OH	2.524	11.91	0.034	0.096	5.36
NH <sub>2</sub>	2.520	11.87	0.034	0.097	4.15
NHMe	2.511	12.21	0.035	0.099	4.05
NMe <sub>2</sub>	2.514	12.28	0.035	0.097	3.97
<i>para</i>					
F	2.577	9.71	0.030	0.087	4.81
Cl	2.573	9.85	0.031	0.088	5.18
Br	2.573	9.86	0.031	0.088	5.37
OH	2.587	9.33	0.029	0.085	4.43
NH <sub>2</sub>	2.601	8.82	0.028	0.083	3.88
NHMe	2.610	7.95	0.028	0.082	3.86
NMe <sub>2</sub>	2.609	8.57	0.028	0.082	3.74
<i>ortho</i>					
F	2.577	9.52	0.031	0.088	4.66
Cl	2.561	10.1	0.032	0.091	3.78
Br	2.555	10.31	0.033	0.092	3.67
OH	2.582	9.27	0.031	0.088	3.78
NH <sub>2</sub>	2.552	10.57	0.032	0.092	3.62
NHMe	2.546	10.78	0.033	0.093	3.35
NMe <sub>2</sub>	2.601	8.64	0.029	0.085	3.24



Scheme 3-1 Structure of a) DAST b) Deoxofluor, and c) 4-tert-Butyl-2,6-bis(methoxy)sulfur trifluoride

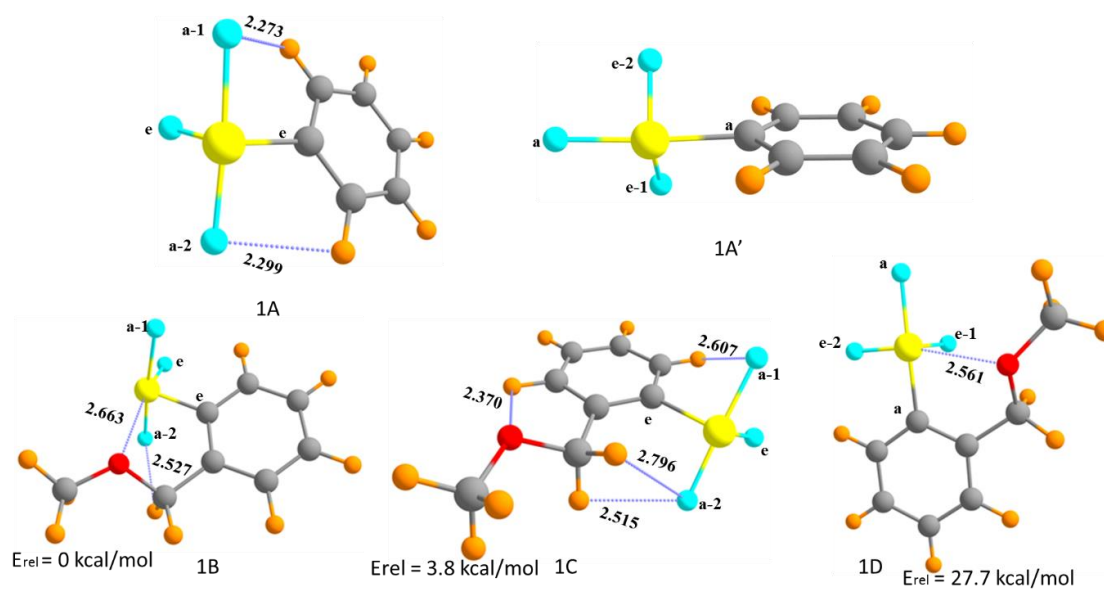


Figure 3-1 Optimized geometries of various minima. Distances in Å.

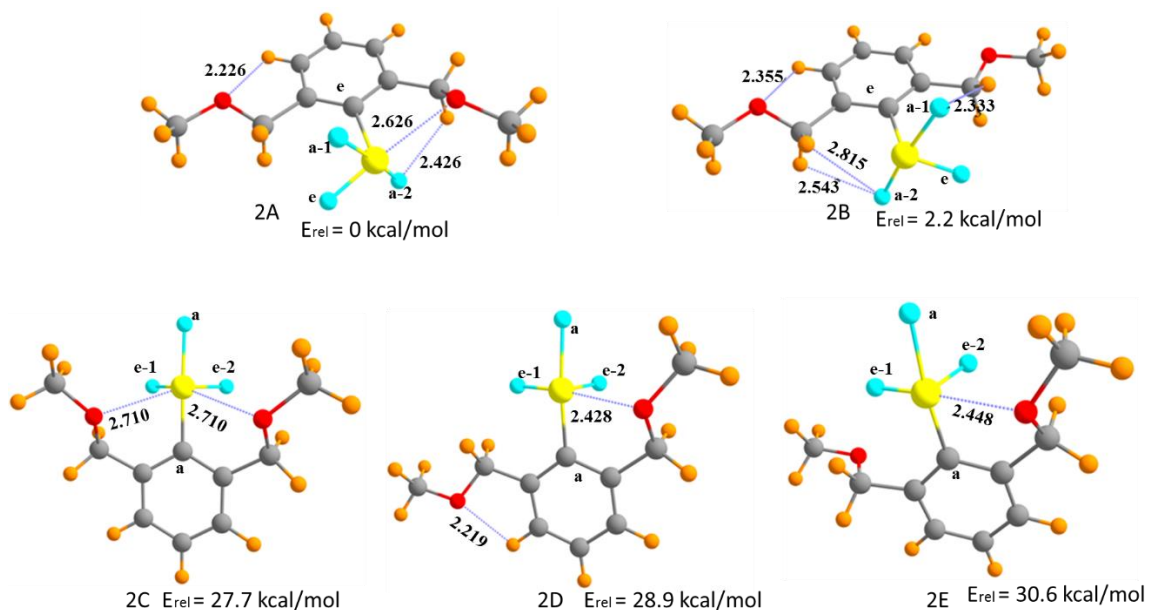


Figure 3-2 Optimized geometries of various minima of molecules containing two  $-\text{CH}_2\text{OCH}_3$  groups. Distances in Å.

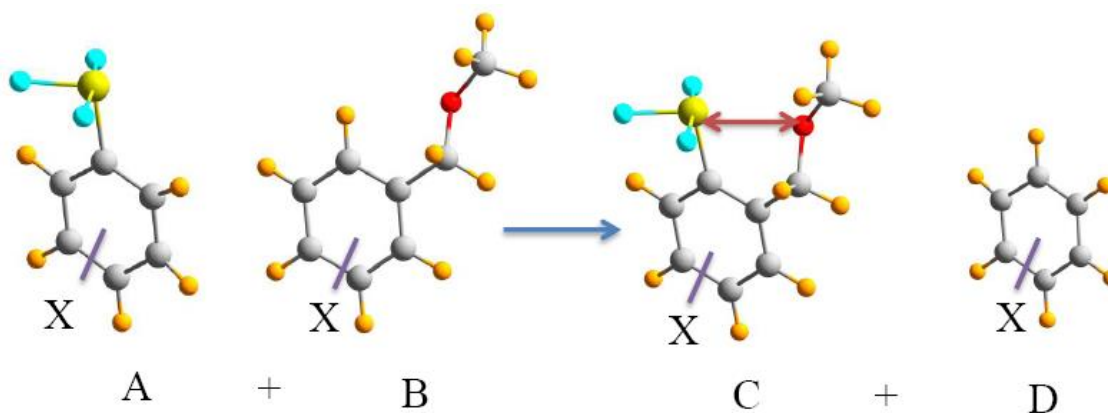


Figure 3-3 Molecules used to evaluate density redistribution patterns and isodesmic values of  $\text{S}\cdots\text{O}$  bond energies.

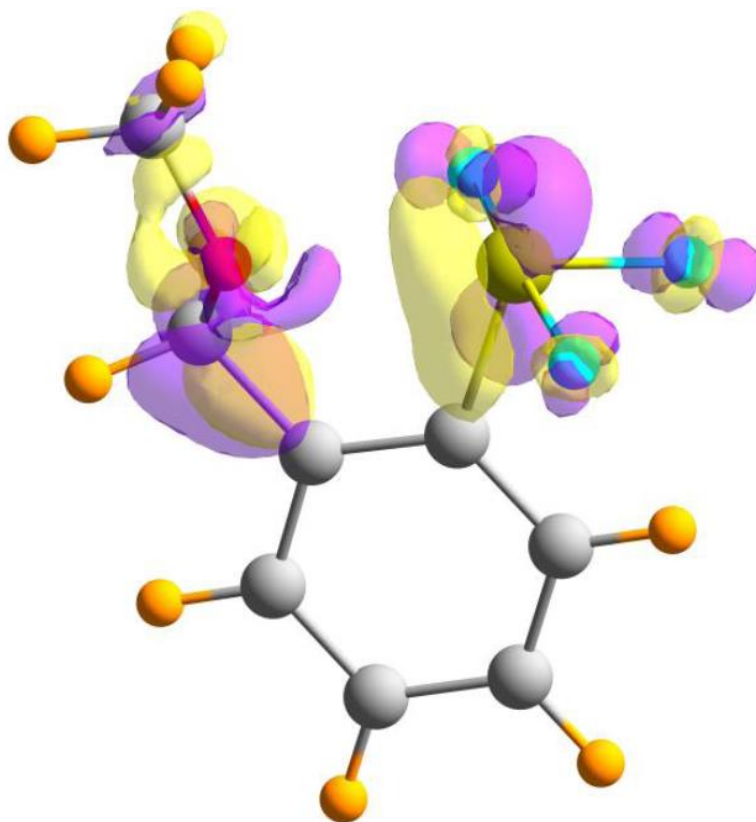


Figure 3-4 Electron density redistribution of molecule 1B, using isodesmic system in Fig 3-3. Purple regions indicate density increase, and losses are shown in yellow. Isocontour illustrated is  $\pm 0.0015$  au.

## CHAPTER 4

S··II CHALCOGEN BOND BETWEEN SF<sub>2</sub> OR SF<sub>4</sub> AND C-C MULTIPLE BOND<sup>1</sup>**Abstract**

SF<sub>2</sub> and SF<sub>4</sub> were each paired with a series of unsaturated hydrocarbons including ethene, ethyne, 1,3-butadiene, and benzene, in each case forming a chalcogen bond between the S atom and the carbon  $\pi$ -system. MP2 ab initio calculations reveal that the S atom is situated directly above one specific C=C bond, even when more than one are present. The binding energies range between 3.3 and 6.6 kcal/mol. SF<sub>2</sub> engages in a stronger, and shorter, noncovalent bond than does SF<sub>4</sub> for all systems with the exception of benzene to which SF<sub>4</sub> is more tightly bound. Cis-butadiene complexes contain the shortest chalcogen bond, even if not necessarily the strongest. The internal S-F covalent bonds elongate upon formation of each chalcogen bond. The molecules are held together largely by charge transfer forces, particularly from the C=C  $\pi$ -bonds to the  $\sigma^*(\text{SF})$  antibonding orbitals. In the case of SF<sub>2</sub>, a sulfur lone pair can transfer charge into the  $\pi^*$  MOs of the alkene, a back transfer which is more difficult for SF<sub>4</sub>.

**4-1. Introduction**

Noncovalent interactions between molecules are a quintessential ingredient in the behavior of condensed phases. They are also controlling factors<sup>1-3</sup> in molecular recognition and crystal packing, and are important building blocks of the structures adopted by

---

<sup>1</sup> Coauthored by Vincent de Paul Nzuwah Nziko and Steve Scheiner. Reproduced with permission from *J. Phys. Chem. A* **2014**, 119, 5889-5897. Copyright 2014, American Chemical Society.

molecules, and their transitions from one conformation to another. Arguably, the most intensively studied and well understood type of noncovalent interaction is the H-bond <sup>4-6</sup>, which classically involves a proton donor AH and acceptor B. While A and B were historically very electronegative atoms such as O, N, and F <sup>7-10</sup>, the restrictions on the classification as a H-bond have broadened over the years <sup>11</sup>. For example, less electronegative atoms like C can serve as proton donor atom <sup>12-14</sup>, and the acceptor can donate electron density via  $\pi$  bonds, rather than the classical lone pair. Moreover, the bridging H atom can be replaced by halogen <sup>15-24</sup>, chalcogen <sup>25-33</sup>, and pnictogen <sup>34-45</sup> atoms in the eponymously named bonds. Of these, the halogen bond has received the most attention, but knowledge is very rapidly accruing for the other two as well.

In particular, a typical chalcogen bond is formed when an atom of this family e.g. S or Se, acts as an electron acceptor from an electron donor atom or molecule. The system is stabilized by a transfer of charge from a lone pair of the donor atom to a  $\sigma^*(Y-R)$  antibonding orbital where Y represents a chalcogen atom and R is directly bonded to it. This transfer is accompanied by a Coulombic attraction between the negative electrostatic potential of the donor and a positive region that lies nearby to the chalcogen atom. (The latter is sometimes referred to as a  $\sigma$ -hole.) These attractive forces are supplemented by a certain amount of dispersion energy.

Most prior study <sup>46-56</sup> of S-chalcogen bonds has been devoted to divalent S, e.g. SH<sub>2</sub>, SF<sub>2</sub>, or S=C(CH<sub>3</sub>)<sub>2</sub>. However, S commonly engages in other valencies <sup>57</sup>, perhaps most notably engaging in four separate covalent bonds. A few recent works have begun to tackle the issue of tetravalent S and its involvement in chalcogen bonds. Our own earlier



work<sup>58</sup> showed, for example, that the S $\cdots$ N interaction involving SF<sub>4</sub> can be stronger than that of a typical H-bond. We also showed that this interaction is dominated by charge transfer; unlike the H-bond, electrostatic forces play only a supporting role. Some of these computed results were soon thereafter confirmed<sup>59</sup> by experimental measurements. It has also been typical to consider chalcogen bonds wherein a lone pair of the electron donor atom acts as the source of the charge being transferred. However, as has been shown in analogous pnictogen bonds, the  $\pi$  bonding system of alkenes can serve a similar function, with bonds that are nearly as strong as their lone-pair donor cousins.

The present work is therefore meant to fill these gaps in our understanding of the S chalcogen bond. A comparison of SF<sub>4</sub> with SF<sub>2</sub> provides direct information about the comparative effects of divalency and tetravalency. A range of different  $\pi$ -electron donors are considered. Ethene and ethyne are both simple two-C molecules with one and two  $\pi$  C-C bonds, respectively. The effects of conjugation are evaluated by enlarging the system to 1,3-butadiene, in both its cis and trans conformations. Benzene is also considered so as to compare simple conjugation of butadiene with full-fledged aromaticity. In addition to assessing the overall strength of the interaction, we are most especially concerned with understanding the fundamental origins of each. What exactly is it that makes one sort of S valency a more potent electron acceptor than another? Do both depend to the same extent upon charge transfer versus Coulombic attraction? How does a triple bond compare with a double bond in terms of electron donation, and how are these forces affected by conjugation or aromaticity? From a wider perspective, how does S compare with pnictogen atom P in terms of formation of a noncovalent bond with a  $\pi$ -donor?

## 4-2. Theoretical Methods

Quantum chemical calculations employed the Gaussian-09 <sup>60</sup> software package. Geometries of monomers and dimers were optimized at the MP2/aug-cc-pVDZ level, and were verified as minima by frequency analysis. Higher level calculations expanded the basis set to aug-cc-pVTZ and aug-cc-pVQZ, using the MP2/aug-cc-pVDZ geometries. CCSD(T) was also employed with the aug-cc-pVDZ basis set. Binding energies were derived as the difference in energy between the optimized dimer and the sum of the individual monomers in their optimized geometries. This binding energy was corrected for basis set superposition error via the counterpoise procedure <sup>61-62</sup>.

One can extrapolate the data from the ordered DZ, TZ, QZ basis sets to an estimate of complete basis set (CBS) results. Extrapolation was based on the idea <sup>63</sup> that correlation energy is roughly proportional to  $X^{-3}$  for basis sets of the aug-cc-pVXZ type. Utilizing a two-step method with triple and quadruple sets <sup>64</sup>:

$$\Delta E_{\text{MP2/CBS}} = (64 \Delta E_{\text{MP2/aug-cc-pVQZ}} - 27 \Delta E_{\text{MP2/aug-cc-pVTZ}}) / 37 \quad (1)$$

A correction was added to account for discrepancies between MP2 and CCSD(T)

$$E_{\text{CCSD(T)/CBS}} = E_{\text{MP2/CBS}} + (E_{\text{CCSD(T)/aug-cc-pVDZ}} - E_{\text{MP2/aug-cc-pVDZ}}) \quad (2)$$

The total interaction energy was dissected into various components by Symmetry-Adapted Perturbation Theory (SAPT) <sup>65-66</sup> analysis using the MOLPRO <sup>67</sup> program, at the SCF level with the aug-cc-pVDZ set. Charge transfer effects were examined via Natural Bond Orbital (NBO) formalism <sup>68-69</sup> using the NBO 3.1 procedures contained in Gaussian at the SCF level. The electron density was analyzed via the Atoms in Molecules procedure <sup>70-71</sup> to determine the positions of bond critical points, as well as the density and its

Laplacian, via the AIMALL software <sup>72</sup>. Maxima and minima of the electrostatic potential were derived via the WFA-SAS program <sup>73</sup>. Both SF<sub>2</sub> and SF<sub>4</sub> were used as electron acceptors in chalcogen bonds. They were combined with a series of  $\pi$ -bonded hydrocarbons, including ethene and ethyne, 1,3-butadiene, and benzene.

### 4-3. Results

#### 4-3.1. Geometries and Energetics

The geometries optimized at the MP2/aug-cc-pVDZ level are displayed in Figure 4-1 and Figure 4-2, and the most important structural details are reported in Table 4-1. The S atom is drawn toward the center of a particular C-C bond, designated C<sub>a</sub>-C<sub>b</sub> this central point is indicated by the small purple sphere in Figure 4-1. Where there is a single C-C bond (C<sub>2</sub>H<sub>2</sub> and C<sub>2</sub>H<sub>4</sub>), the S atom is positioned equidistant from C<sub>a</sub> and C<sub>b</sub>, but it moves off center for some of the other cases. One of the F atoms (F<sup>1</sup>) is positioned nearly apposite the C=C bond, with  $\theta(\text{F}^1\text{S}\cdots\text{m})$  angles close to 180° (m refers to CC bond midpoint). The last several rows of Table 4-1 display the changes in some of the bond lengths arising from formation of the complex.

The SF<sub>2</sub> molecule approaches more closely to the alkene than does SF<sub>4</sub>, by amounts varying between 0.03 Å (for benzene) and 0.22 Å for ethene. Whether SF<sub>2</sub> or SF<sub>4</sub>, the shortest R(S-m) intermolecular distance is associated with cis-butadiene (c-but). For SF<sub>4</sub>, the simple 2-carbon systems are further removed than butadiene, but this is less clear for SF<sub>2</sub>; benzene is most distant for SF<sub>2</sub> but roughly the same as t-but for SF<sub>4</sub>. The last three rows refer to the changes in the internal bond lengths that occur as a result of the formation

of each complex. The S-F bonds of both SF<sub>2</sub> and SF<sub>4</sub> elongate. The S-F<sup>1</sup> bond, which lies directly opposite the alkene, stretches by between 0.01 and 0.02 Å for SF<sub>2</sub>, but by less than 0.007 Å for SF<sub>4</sub>. A smaller elongation is observed in r(S-F<sup>2</sup>) which refers to the other SF bond of SF<sub>2</sub>, and to the other equatorial SF bond of SF<sub>4</sub>. Similar stretches have been observed<sup>41, 53, 55, 58, 74-75</sup> in related complexes, and are due in part to the charge transfer into the  $\sigma^*(\text{SF})$  antibonding orbitals (see below). Also undergoing a stretch are the C=C bonds participating in the chalcogen bond; the donation of charge out of its  $\pi$ -bonding orbital is a contributing factor to this bond weakening. These elongations are small in magnitude, the largest being 0.008 Å.

The binding energies of the various complexes were computed at various levels of theory, all using the geometries optimized by MP2/aug-cc-pVDZ. Focusing first on basis set size at the MP2 level, Table 4-2 shows a trend for stronger binding as the basis is enlarged from double to triple and then to quadruple- $\zeta$ . With any of these basis sets, SF<sub>2</sub> engages in a stronger noncovalent bond than does SF<sub>4</sub> for all systems with the exception of benzene where this pattern is reversed. The stronger binding by SF<sub>2</sub> fits with its pattern of shorter intermolecular distances. Computation of electron correlation via CCSD(T) yields a modest reduction in binding energy relative to MP2, as evident by a comparison of the CCSD(T)/aug-cc-pVDZ data with the values in the first two columns of Table 4-2. Importantly, CCSD(T) maintains the MP2 trend that butadiene is most strongly bound to SF<sub>2</sub>, followed by benzene, ethene, and acetylene in that order, and also that SF<sub>4</sub> forms its tightest bond with benzene, followed next by c-but > t-but > ethyne > ethene.

Extrapolation of the basis set to a complete set leads to the MP2/CBS entries in the

next pair of columns of Table 4-2. These quantities represent only a small increase over the MP2/aug-cc-pVQZ data and maintain the other MP2 trends. Adding in a correction to account for discrepancies between MP2 and CCSD(T) (via Eq 2) yields the values in the last columns of Table 4-2. These values underscore the trends that SF<sub>2</sub> forms stronger bonds than SF<sub>4</sub> with all of the alkenes, except benzene. The strongest bond of all is between SF<sub>2</sub> and cis-butadiene, nearly 7 kcal/mol. In contrast, SF<sub>4</sub> interacts most strongly with benzene, with a binding energy of 5.5 kcal/mol.

#### 4-3. 2. Energy Components and Electronic Structure

A partitioning of the total binding energy of each complex into its individual contributing factors can provide useful insights into its origins. One such means of effecting such a partition is via SAPT which leads to three attractive components. The data in Figure 4-3 obey a very similar trend in all cases. The induction (IND) energy represents the largest factor in all of the complexes examined, followed by electrostatic (ES) and then by dispersion (DISP). Comparison of Figure 4-3a with Figure 4-3b indicates that the individual components tend to be larger for the SF<sub>2</sub> complexes, even if the total binding energies are more similar. Taking the cis-butadiene electron donor as one example, the IND attraction for SF<sub>2</sub> amounts to 25 kcal/mol, while it is only 18 kcal/mol for SF<sub>4</sub>. It is also interesting that despite the similarity between the total binding energies of ethene and ethyne, the attractive components are considerably larger in the former case. As another example, although SF<sub>4</sub> is more strongly bound to benzene than to cis-butadiene, the ES and IND components in Figure 4-3b are larger for the latter.

The importance of inductive forces in these complexes warrants a more detailed

examination. NBO offers a means of assessing the energetic contribution of charge transfer between any particular pair of localized orbitals. As in most such complexes of this type, the largest contribution arises from the transfer from the occupied C-C  $\pi$  bonding orbital of the alkene to the  $\sigma^*$  antibonding S-F orbital of the SF<sup>1</sup> bond which lies opposite the alkene. The energetic consequences of this transfer are reported in the first column of Table 4-3. It may first be noted that these quantities are considerably larger for SF<sub>2</sub> than for SF<sub>4</sub>, in some cases by a factor of 2. These larger values echo the IND components in Figure 4-3, albeit not in a quantitative sense. It is of particular note that these E(2) quantities obey the same general trends as do the total binding energies in Table 4-2. For example, SF<sub>2</sub> forms its strongest complex with c-but, which also has the largest value of 10.82 kcal/mol for E(2). Likewise, the largest E(2) for SF<sub>4</sub> is associated with benzene, the most strongly bound. On the other hand, the correspondence between E<sub>b</sub> and E(2) is imperfect. Whereas E(2) for the complex of ethene with SF<sub>2</sub> is larger than for either t-butadiene or benzene, the binding energy of the former is weaker than the latter. Nor is there a perfect match between binding energy and induction energy, for which this particular charge transfer is a prime ingredient.

And indeed, it is important to note that the  $\pi_{ab} \rightarrow \sigma^*(S-F^1)$  transfer is not the only one identified by NBO analysis. Because of the shape of the  $\sigma^*$  NBO, there is some overlap between the  $\sigma^*(SF^2)$  antibonding orbital and the occupied CC  $\pi$  orbitals, as illustrated schematically in Figure 4-4a and Figure 4-4b for SF<sub>2</sub> and c-but. This overlap allows a certain, albeit smaller, amount of charge transfer which is reflected in the second and third columns of Table 4-3. In the case of butadiene, where there is a second C<sub>c</sub>-C<sub>d</sub>  $\pi$  bonding

orbital, the overlap is especially good as indicated in Figure 4-4b, resulting in the larger values in the third column.

Another sort of transfer which takes place in these complexes can be considered a back-donation <sup>74</sup> in that the charge transfers from the SF<sub>2</sub> molecule to the alkene. In particular, the S lone pair transfers charge into the CC  $\pi^*$  orbitals. The overlap of these orbitals is pictured in Figure 4-4c and Figure 4-4d, where the overlap is superior for C<sub>a</sub>-C<sub>b</sub> as compared to C<sub>c</sub>-C<sub>d</sub>, and the values of E(2) are correspondingly larger. It is immediately apparent that this back transfer is practically nonexistent for SF<sub>4</sub>. This absence is due to the different electronic structure of this molecule. SF<sub>2</sub> contains two lone pairs, one of which resembles a S  $\pi$ -orbital as illustrated in Figure 4-4. The second SF<sub>2</sub> lone pair has the characteristics of a  $\sigma$ -orbital which is very nearly orthogonal to the CC  $\pi^*$  antibonding orbitals, so contributes very little to the back donation in Table 4-3. With its greater number of covalent bonds, the S atom of SF<sub>4</sub> contains only one S lone pair. This pair resembles a sp<sup>n</sup> hybrid orbital, with a single lobe facing the alkene. As such, it is essentially orthogonal to the C<sub>a</sub>-C<sub>b</sub>  $\pi^*$  orbital, accounting for the lack of significant values of E(2) in Table 4-3. There is some small overlap with the other C<sub>c</sub>-C<sub>d</sub>  $\pi^*$  orbital of butadiene, enough to result in a small contribution to the interaction energy, but less than that for SF<sub>2</sub> with its superior overlap.

In addition to the energetic consequence of charge transfer, E(2), one can also compute the amount of charge transferred from one particular orbital to another via the NBO procedure. These transfers are displayed in Table 4-4, and reasonably mimic the E(2) values. For example, the largest values of both for the  $\pi_{ab} \rightarrow \sigma^*(S-F^1)$  transfer occur for

SF<sub>2</sub>··c-butadiene, and the smallest for SF<sub>4</sub>··ethyne. The last column of Table 4-4 contains the total charge transferred from the electron donor to the acceptor, irrespective of individual orbitals. These quantities obey the same general pattern as the individual  $\pi_{ab} \rightarrow \sigma^*(S-F^1)$  transfers: for instance, ethyne is the weakest donor to SF<sub>2</sub>, and cis-butadiene the strongest. Again, these trends are not wholly consistent with the binding energies. For example, although benzene forms a stronger complex with SF<sub>4</sub> than does c-but, the total charge transferred is considerably larger in the latter case.

The Coulombic attractive force is most accurately assessed by the electrostatic attractive term from SAPT, as described above. On the other hand, the literature contains a number of examples where the ES term, and indeed sometimes the entire binding energy itself, is closely related to the electrostatic potential at a single point around a given molecule. In particular,  $V_{s,min}$  has been commonly computed as the minimum in the potential on an isodensity contour (usually  $\rho=0.001$  au) surrounding the molecule. This quantity was computed for all of the alkenes studied here within the context of the aug-cc-pVDZ basis set. It was found that  $V_{s,min}$  is nearly the same for ethene, ethyne, and cis and trans butadiene (between -17.2 and -17.8 kcal/mol) and is only slightly larger at -19.8 kcal/mol above the benzene molecule. Likewise,  $V_{s,max}$ , the maximum in the electrostatic potential surrounding SF<sub>2</sub> and SF<sub>4</sub>, is essentially identical (+42.2 kcal/mol) for these two molecules. The hypothesis of a proportional relationship between the values of these extrema and the full ES component in Figure 4-3 is hence invalid here, and is an even poorer predictor of the full binding energy.

The AIM interpretation of the electron density is frequently used to provide an



alternate measure of the strength of an individual noncovalent interaction. In particular, the value of the density and its Laplacian at each bond critical point are typically taken as the most direct measure of the bond strength. The values of these quantities are listed in Table 4-5. They suggest that cis-butadiene forms the strongest bond, followed by its trans conformer; the weakest interaction occurs with ethyne. In all cases except benzene, SF<sub>2</sub> is predicted to form stronger bonds than SF<sub>4</sub>. These patterns are in fact, similar to those of the binding energies in Table 4-2, although there are certain discrepancies. As an example, SF<sub>4</sub> binds most tightly to benzene, as opposed to c-but which is predicted by AIM. Benzene's binding energy with SF<sub>2</sub> exceeds that of ethene or ethyne, opposite to the AIM order.

The manner in which the electron density adjusts to a given interaction offers useful clues about the fundamental aspects of the interaction. The electron density shifts were computed as the difference between the density of the full complex, and the sum of individual monomers in their same internal geometries. The increases in density arising from the interaction are illustrated as the purple regions in Figure 4-5, and losses shown in yellow, at the  $\pm 0.001$  au isocontour. Figure 4-5a and Figure 4-5b compare the changes occurring when ethene interacts with SF<sub>2</sub> and SF<sub>4</sub>, respectively. The most prominent feature is a yellow region of loss immediately below the S atom and a purple increase above the C=C bond; there are also smaller areas of charge gain around the F atoms. These redistributions are very similar to those observed earlier<sup>58</sup> when SF<sub>4</sub> interacts with the N lone pair in N-bases, although somewhat more muted here. Note also that there is very little distinction between the SF<sub>2</sub> and SF<sub>4</sub> patterns. Addition of another  $\pi$ -bond has little effect

on the charge shift pattern as the plots for HCCH look very much like those in Figure 4-5 for ethene. The patterns for butadiene emphasize the degree of asymmetry of the interaction. The purple region above the trans isomer in Figure 4-5c lies over the two central C atoms, whereas this region moves toward a terminal C-C bond for SF<sub>4</sub> in Figure 4-5d. The same shift toward a terminal C-C bond is evident for the cis isomer in Figure 4-5e. These displacements of density shift mirror the positions of the S atom in each case. The interaction of SF<sub>2</sub> with benzene is largest for one particular C-C bond rather than the center of the molecule, as is clear in Figure 4-5f.

#### 4-4. Discussion

The highly accurate CCSD(T)/CBS data computed here can serve as a benchmark by which to test the reliability of some of the more popular DFT schemes. The comparative data in Table 4-6 combine the aug-cc-pVDZ basis set with the B3LYP functional, with and without a D3 dispersion correction. Also of interest is the M06-2X functional which contains a dispersion component. It is first evident that the B3LYP method provides a very substantial underestimate of the accurate binding energies. Without dispersion B3LYP is too small by a factor of 2 or more, and even some of the trends are incorrect. The results are greatly improved after the D3 correction has been applied. SF<sub>2</sub> data are quite good, but the SF<sub>4</sub> values represent a bit of an overestimate. Importantly, the trends in the data are good for the most part. M06-2X also provides excellent reproduction of CCSD(T)/CBS data. Most quantities are slightly overestimated, but the trends are faithful.

The geometry optimizations were carried out using standard convergence thresholds. Very little difference was observed when “tight” criteria were applied. Nor is

there any substantial change observed when the version of NBO was upgraded from 3.1 to 6.0. Incorporation of the effects of electron correlation into the NBO data was examined via both B3LYP and M06-2X DFT functionals which include correlation for the SF<sub>2</sub>··ethyne system. There was a diminution of the values of E(2) but this decrease was quite small. The ability of the aug-cc-pVDZ set to adequately characterize sulfur was investigated by comparing the data with that obtained with the aug-cc-pV(D+d)Z set <sup>76</sup>. Interaction energies of SF<sub>2</sub> and SF<sub>4</sub> with both ethyne and ethene were changed by less than 0.15 kcal/mol.

There are some calculations in the literature that present relevant points of comparison. A very recent work <sup>77</sup> indicates that SFH engages in somewhat stronger S·· $\pi$  bonds with ethene and ethyne than does SF<sub>2</sub> or SF<sub>4</sub>, but is similar for butadiene and benzene. On the other hand, the intermolecular distances are uniformly shorter for SFH. In common with the SF<sub>2</sub> and SF<sub>4</sub> data, the interactions with SFH are also dominated by induction.

An earlier work <sup>74</sup> had probed the ability of these same alkenes to engage in a similar sort of interaction wherein the S atom was instead a P. Like SF<sub>2</sub> and SF<sub>4</sub> considered here, the FH<sub>2</sub>P molecule is also a potent electron acceptor. The binding energies varied from a minimum of 3.0 kcal/mol for HCCH up to 4.2 kcal/mol for benzene, in the context of the MP2/aug-cc-pVDZ level of theory. Overall, these quantities were slightly different but generally similar to the data derived here at the same level for SF<sub>2</sub> and SF<sub>4</sub>. The stretches induced by the complexation upon the P-F bond were intermediate between the S-F elongations observed here for the two S-analogues. SAPT decomposition of the FH<sub>2</sub>P

complexes also found induction to be the largest contribution, followed by ES, and then by dispersion. In fact, their quantitative values were rather similar to the quantities in Figure 4-3 for SF<sub>2</sub> and SF<sub>4</sub>. Also similar to the results here, there was a certain amount of back donation in these complexes, wherein some charge was transferred from the P lone pair into the vacant  $\pi^*$  MOs of the alkene, which added to the stability. Other work<sup>78</sup> expanded the range of pnictogen bonds to aromatic systems which included various substituents, and to As, Sb, and Bi, obtaining a binding energy as large as 8.4 kcal/mol for the combination of benzene and BiCl<sub>3</sub>.

The ability of SF<sub>4</sub> to engage in a chalcogen bond, not to a  $\pi$ -system but rather to an amine lone pair, was considered<sup>58</sup> earlier. These interactions were considerably stronger than the S $\cdots\pi$  complexes described here, varying between 6.6 and 14.4 kcal/mol. Nonetheless, many of the same features were exhibited. For example, S-F bonds were stretched upon formation of each complex. Induction was the prime attractive component, quite exceeding ES, with a much smaller DISP term. As in the  $\pi$ -donors described here, the major recipient of charge from the N lone pair was the  $\sigma^*(\text{SF}^1)$  antibonding orbital, with a secondary transfer into  $\sigma^*(\text{SF}^2)$  involving the SF bond which is not directly opposite the electron donor atom. A more recent set of calculations<sup>75</sup> showed that these same forces are in operation when the N donor is replaced by O, and when the S $\cdots$ O chalcogen bond is intramolecular.

To place some of these interactions into a larger context, these S $\cdots\pi$  bonds are considerably stronger than the CH $\cdots\pi$  H-bond that occurs when methane donates a proton<sup>79</sup> to the  $\pi$ -system of benzene. The energy of that interaction is only 1.7 kcal/mol, and

remains below 2.8 kcal/mol even when F, methyl, or other substituents replace the H atoms of the benzene. Benzene can also host a  $X\cdots\pi$  halogen bond. However, these appear to be considerably weaker than the  $S\cdots\pi$  chalcogen bonds to benzene considered here. The strongest such bond of those considered <sup>80</sup>, between benzene and  $HC\equiv CBr$ , amounted to only 3.2 kcal/mol. This work was followed by studies of halogen bonds to various aromatic systems <sup>81-82</sup>.

In a biological context, there was early evidence <sup>83</sup> that the phenyl ring of the Phe residue of proteins is attracted toward the S atom of Cys and Met. Later analysis of other protein structures <sup>84</sup> observed geometries consistent with electron donation to the S atom from aromatic systems which approach the S from a direction opposite to an S-H bond.

#### 4-5. Conclusion

Both  $SF_2$  and  $SF_4$  engage in  $S\cdots\pi$  chalcogen bonds with a range of unsaturated hydrocarbons. The S atom is situated directly above one specific  $C=C$  bond, even when more than one are present, as in butadiene or benzene. The binding energies vary from a minimum of 3.3 kcal/mol for  $SF_4\cdots$ ethene up to 6.6 kcal/mol for  $SF_2\cdots$ cis-butadiene. This range places the  $S\cdots\pi$  bond squarely along the lines of conventional H-bonds such as that in the water dimer. The interactions with the 2-carbon ethene and ethyne are strengthened by the conjugation of additional  $C=C$  bonds within the alkene. Induction energy is the largest contributor to the binding, followed by electrostatic and then dispersion. Charge transfer from the  $\pi$  bond of the alkene to the  $\sigma^*(S-F^1)$  antibonding orbital is the primary source of the binding, wherein  $F^1$  lies directly opposite the alkene. However, there are also lesser contributions from transfer to the other  $\sigma^*(SF^2)$  antibond. Additional transfer can originate

from secondary C=C  $\pi$ -bonds as in butadiene. S sulfur lone pair of SF<sub>2</sub> can align itself so as to transfer charge into the  $\pi^*$  MOs of the alkene, in what amounts to a back transfer, augmenting the strength of the chalcogen bond.

## References

- (1) Gilday, L. C.; Beer, P. D. Halogen- and Hydrogen-Bonding Catenanes for Halide-Anion Recognition. *Chem. Eur. J.* **2014**, *20*, 8379-8385.
- (2) Robinson, S. W.; Mustoe, C. L.; White, N. G.; Brown, A.; Thompson, A. L.; Kennepohl, P.; Beer, P. D. Evidence for Halogen Bond Covalency in Acyclic and Interlocked Halogen-Bonding Receptor Anion Recognition. *J. Am. Chem. Soc.* **2015**, *137*, 499-507.
- (3) Tepper, R.; Schulze, B.; Jäger, M.; Friebe, C.; Scharf, D. H.; Görls, H.; Schubert, U. S. Anion Receptors Based on Halogen Bonding with Halo-1,2,3-Triazoliums. *J. Org. Chem.* **2015**, *80*, 3139-3150.
- (4) Schuster, P.; Zundel, G.; Sandorfy, C. *The Hydrogen Bond. Recent Developments in Theory and Experiments*. North-Holland Publishing Co.: Amsterdam, 1976.
- (5) Scheiner, S. *Hydrogen Bonding: A Theoretical Perspective*. Oxford University Press: New York, 1997; p 375.
- (6) Gilli, G.; Gilli, P. *The Nature of the Hydrogen Bond*. Oxford University Press: Oxford, UK, 2009; p 313.
- (7) Vener, M. V.; Scheiner, S. Hydrogen Bonding and Proton Transfer in the Ground and Lowest Excited Singlet States of O-Hydroxyacetophenone. *J. Phys. Chem.* **1995**, *99*, 642-649.

- (8) Latajka, Z.; Scheiner, S. Structure, Energetics and Vibrational Spectrum of H<sub>2</sub>O-HCl. *J. Chem. Phys.* **1987**, *87*, 5928-5936.
- (9) Hillenbrand, E. A.; Scheiner, S. Effects of Molecular Charge and Methyl Substitution on Proton Transfers between Oxygen Atoms. *J. Am. Chem. Soc.* **1984**, *106*, 6266-6273.
- (10) Scheiner, S. Comparison of Proton Transfers in Cationic Heterodimers and Homodimers of NH<sub>3</sub> and OH<sub>2</sub>. *J. Chem. Phys.* **1982**, *77*, 4039-4050.
- (11) Arunan, E.; Desiraju, G. R.; Klein, R. A.; Sadlej, J.; Scheiner, S.; Alkorta, I.; Clary, D. C.; Crabtree, R. H.; Dannenberg, J. J.; Hobza, P. et al. Definition of the Hydrogen Bond. *Pure Appl. Chem.* **2011**, *83*, 1637-1641.
- (12) Kryachko, E.; Scheiner, S. CH $\cdots$ F Hydrogen Bonds. Dimers of Fluoromethanes. *J. Phys. Chem. A* **2004**, *108*, 2527-2535.
- (13) Scheiner, S.; Kar, T. Effect of Solvent Upon CH $\cdots$ O Hydrogen Bonds with Implications for Protein Folding. *J. Phys. Chem. B* **2005**, *109*, 3681-3689.
- (14) Scheiner, S. Relative Strengths of NH $\cdots$ O and CH $\cdots$ O Hydrogen Bonds between Polypeptide Chain Segments. *J. Phys. Chem. B* **2005**, *109*, 16132-16141.
- (15) Auffinger, P.; Hays, F. A.; Westhof, E.; Ho, P. S. Halogen Bonds in Biological Molecules. *Proc. Nat. Acad. Sci., USA* **2004**, *101*, 16789-16794.
- (16) Politzer, P.; Lane, P.; Concha, M. C.; Ma, Y.; Murray, J. S. An Overview of Halogen Bonding. *J. Mol. Model.* **2007**, *13*, 305-311.
- (17) Grabowski, S. J. s-Hole Bond Versus Hydrogen Bond: From Tetravalent to Pentavalent N, P, and As Atoms. *Chem. Eur. J.* **2013**, *19*, 14600-14611.

- (18) Bauzá, A.; Ramis, R.; Frontera, A. A Combined Theoretical and Cambridge Structural Database Study of p-Hole Pnictogen Bonding Complexes between Electron Rich Molecules and Both Nitro Compounds and Inorganic Bromides ( $\text{YO}_2\text{Br}$ ,  $\text{Y} = \text{N}, \text{P}$ , and  $\text{As}$ ). *J. Phys. Chem. A* **2014**, *118*, 2827-2834.
- (19) Viger-Gravel, J.; Leclerc, S.; Korobkov, I.; Bryce, D. L. Direct Investigation of Halogen Bonds by Solid-State Multinuclear Magnetic Resonance Spectroscopy and Molecular Orbital Analysis. *J. Am. Chem. Soc.* **2014**, *136*, 6929-6942.
- (20) Riley, K. E.; Ford Jr, C. L.; Demouchet, K. Comparison of Hydrogen Bonds, Halogen Bonds,  $\text{CH}\cdots\pi$  Interactions, and  $\text{CX}\cdots\pi$  Interactions Using High-Level Ab Initio Methods. *Chem. Phys. Lett.* **2015**, *621*, 165-170.
- (21) Gou, Q.; Feng, G.; Evangelisti, L.; Vallejo-López, M.; Spada, L.; Lesarri, A.; Cocinero, E. J.; Caminati, W. Internal Dynamics in Halogen-Bonded Adducts: A Rotational Study of Chlorotrifluoromethane–Formaldehyde. *Chem. Eur. J.* **2015**, *21*, 4148-4152.
- (22) Joseph, J. A.; McDowell, S. A. C. Comparative Computational Study of Model Halogen-Bonded Complexes of  $\text{FkrCl}$ . *J. Phys. Chem. A* **2015**, *119*, 2568-2577.
- (23) Zierkiewicz, W.; Bieńko, D. C.; Michalska, D.; Zeegers-Huyskens, T. Theoretical Investigation of the Halogen Bonded Complexes between Carbonyl Bases and Molecular Chlorine. *J. Comput. Chem.* **2015**, *36*, 821-832.
- (24) Anable, J. P.; Hird, D. E.; Stephens, S. L.; Zaleski, D. P.; Walker, N. R.; Legon, A. C. Characterisation of the Weak Halogen Bond in  $\text{N}_2\cdots\text{ICF}_3$  by Pure Rotational Spectroscopy. *Chem. Phys. Lett.* **2015**, *625*, 179-185.



- (25) Werz, D. B.; Gleiter, R.; Rominger, F. Nanotube Formation Favored by Chalcogen-Chalcogen Interactions. *J. Am. Chem. Soc.* **2002**, *124*, 10638-10639.
- (26) Sanz, P.; Mó, O.; Yáñez, M. Characterization of Intramolecular Hydrogen Bonds and Competitive Chalcogen-Chalcogen Interactions on the Basis of the Topology of the Charge Density. *Phys. Chem. Chem. Phys.* **2003**, *5*, 2942-2947.
27. Bleiholder, C.; Werz, D. B.; Koppel, H.; Gleiter, R. Theoretical Investigations on Chalcogen-Chalcogen Interactions: What Makes These Nonbonded Interactions Bonding? *J. Am. Chem. Soc.* **2006**, *128*, 2666-2674.
- (27) Cozzolino, A. F.; Vargas-Baca, I. The Supramolecular Chemistry of 1,2,5-Chalcogenadiazoles. *J. Organomet. Chem.* **2007**, *692*, 2654-2657.
- (28) Begum, S.; Subramanian, R. Bonding and Spectroscopic Properties of Complexes of SO<sub>2</sub>-O<sub>2</sub> and SO<sub>2</sub>-N<sub>2</sub> and Its Atmospheric Consequences. *Phys. Chem. Chem. Phys.* **2014**, *16*, 17658-17669.
- (29) Fanfrlík, J.; Přáda, A.; Padělková, Z.; Pecina, A.; Macháček, J.; Lepšík, M.; Holub, J.; Růžicka, A.; Hnyk, D.; Hobza, P. The Dominant Role of Chalcogen Bonding in the Crystal Packing of 2d/3d Aromatics. *Angew. Chem. Int. Ed.* **2014**, *53*, 10139-10142.
- (30) Azofra, L. M.; Scheiner, S. Complexation of n SO<sub>2</sub> Molecules (n=1,2,3) with Formaldehyde and Thioformaldehyde. *J. Chem. Phys.* **2014**, *140*, 034302.
- (31) Esrafil, M.; Mohammadian-Sabet, F. Ab Initio Calculations of Cooperativity Effects on Chalcogen Bonding: Linear Clusters of (OCS)<sub>2-8</sub> and (OCSe)<sub>2-8</sub>. *Struct. Chem.* **2015**, *26*, 199-206.
- (32) Azofra, L. M.; Scheiner, S. Complexes Containing CO<sub>2</sub> and SO<sub>2</sub>. Mixed Dimers, Trimers and Tetramers. *Phys. Chem. Chem. Phys.* **2014**, *16*, 5142-5149.

- (33) Klinkhammer, K. W.; Pyykko, P. Ab Initio Interpretation of the Closed-Shell Intermolecular E···E Attraction in Dipnictogen (H<sub>2</sub>E-EH<sub>2</sub>)<sub>2</sub> and (He-EH)<sub>2</sub> Hydride Model Dimers. *Inorg. Chem.* **1995**, *34*, 4134-4138.
- (34) Moilanen, J.; Ganesamoorthy, C.; Balakrishna, M. S.; Tuononen, H. M. Weak Interactions between Trivalent Pnictogen Centers: Computational Analysis of Bonding in Dimers X<sub>3</sub>E···EX<sub>3</sub> (E = Pnictogen, X = Halogen). *Inorg. Chem.* **2009**, *48*, 6740-6747.
- (35) Scheiner, S. A New Noncovalent Force: Comparison of P···N Interaction with Hydrogen and Halogen Bonds. *J. Chem. Phys.* **2011**, *134*, 094315.
- (36) Zahn, S.; Frank, R.; Hey-Hawkins, E.; Kirchner, B. Pnictogen Bonds: A New Molecular Linker? *Chem. Eur. J.* **2011**, *17*, 6034-6038.
- (37) Oliveira, B. G. Theoretical Estimation of Pnictogen Bonds and Hydrogen Bonds in Small Heterocyclic Complexes: Red-Shifts and Blue-Shifts Ruled by Polarization Effects. *Chem. Phys.* **2014**, *443*, 67-75.
- (38) Sarkar, S.; Pavan, M. S.; Guru Row, T. N. Experimental Validation of 'Pnictogen Bonding' in Nitrogen by Charge Density Analysis. *Phys. Chem. Chem. Phys.* **2015**, *17*, 2330-2334.
- (39) Del Bene, J. E.; Alkorta, I.; Elguero, J. Substituent Effects on the Properties of Pnictogen-Bonded Complexes H<sub>2</sub>XP:PyH<sub>2</sub>, for X, Y = F, Cl, OH, NC, CCH, CH<sub>3</sub>, CN, and H. *J. Phys. Chem. A* **2014**, *119*, 224-233.
- (40) Scheiner, S. Detailed Comparison of the Pnictogen Bond with Chalcogen, Halogen and Hydrogen Bonds. *Int. J. Quantum Chem.* **2013**, *113*, 1609-1620.

- (41) Sánchez-Sanz, G.; Trujillo, C.; Alkorta, I.; Elguero, J. Theoretical Study of Cyanophosphines: Pnicogen vs. Dipole–Dipole Interactions. *Comput. Theor. Chem.* **2015**, *1053*, 305-314.
- (42) Alkorta, I.; Elguero, J.; Grabowski, S. J. Pnicogen and Hydrogen Bonds: Complexes between  $\text{PH}_3\text{X}^+$  and  $\text{PH}_2\text{X}$  Systems. *Phys. Chem. Chem. Phys.* **2015**, *17*, 3261-3272.
- (43) Zhuo, H.; Li, Q. Novel Pnicogen Bonding Interactions with Silylene as an Electron Donor: Covalency, Unusual Substituent Effects and New Mechanisms. *Phys. Chem. Chem. Phys.* **2015**, *17*, 9153-9160.
- (44) Adhikari, U.; Scheiner, S. Sensitivity of Pnicogen, Chalcogen, Halogen and H-Bonds to Angular Distortions. *Chem. Phys. Lett.* **2012**, *532*, 31-35.
- (45) Row, T. N. G.; Parthasarathy, R. Directional Preferences of Nonbonded Atomic Contacts with Divalent Sulfur in Terms of Its Orbital Orientations. 2. Sulfur··Sulfur Interactions and Nonspherical Shape of Sulfur in Crystals. *J. Am. Chem. Soc.* **1981**, *103*, 477-479.
- (46) Burling, F. T.; Goldstein, B. M. Computational Studies of Nonbonded Sulfur-Oxygen and Selenium-Oxygen Interactions in the Thiazole and Selenazole Nucleosides. *J. Am. Chem. Soc.* **1992**, *114*, 2313-2320.
- (47) Nagao, Y.; Hirata, T.; Goto, S.; Sano, S.; Kakehi, A.; Iizuka, K.; Shiro, M. Intramolecular Nonbonded  $\text{S}\cdots\text{O}$  Interaction Recognized in (Acylimino)Thiadiazoline Derivatives as Angiotensin II Receptor Antagonists and Related Compounds. *J. Am. Chem. Soc.* **1998**, *120*, 3104-3110.

- (48) Iwaoka, M.; Takemoto, S.; Tomoda, S. Statistical and Theoretical Investigations on the Directionality of Nonbonded S $\cdots$ O Interactions. Implications for Molecular Design and Protein Engineering. *J. Am. Chem. Soc.* **2002**, *124*, 10613-10620.
- (49) Bleiholder, C.; Gleiter, R.; Werz, D. B.; Köppel, H. Theoretical Investigations on Heteronuclear Chalcogen-Chalcogen Interactions: On the Nature of Weak Bonds between Chalcogen Centers. *Inorg. Chem.* **2007**, *46*, 2249-2260.
- (50) Junming, L.; Yunxiang, L.; Subin, Y.; Weiliang, Z. Theoretical and Crystallographic Data Investigations of Noncovalent S $\cdots$ O Interactions. *Struct. Chem.* **2011**, *22*, 757-963.
- (51) Esrafil, M. D.; Vakili, M. Cooperativity Effects between  $\sigma$ -Hole Interactions: A Theoretical Evidence for Mutual Influence between Chalcogen Bond and Halogen Bond Interactions in F<sub>2</sub>S $\cdots$ NCX $\cdots$ NCY Complexes (X = F, Cl, Br, I; Y = H, F, OH). *Mol. Phys.* **2014**, *112*, 2746-2752.
- (52) Adhikari, U.; Scheiner, S. The S $\cdots$ N Noncovalent Interaction: Comparison with Hydrogen and Halogen Bonds. *Chem. Phys. Lett.* **2011**, *514*, 36-39.
- (53) Garrett, G. E.; Gibson, G. L.; Straus, R. N.; Seferos, D. S.; Taylor, M. S. Chalcogen Bonding in Solution: Interactions of Benzotelluradiazoles with Anionic and Uncharged Lewis Bases. *J. Am. Chem. Soc.* **2015**, *137*, 4126-4133.
- (54) Adhikari, U.; Scheiner, S. Substituent Effects on Cl $\cdots$ N, S $\cdots$ N, and P $\cdots$ N Noncovalent Bonds. *J. Phys. Chem. A* **2012**, *116*, 3487-3497.
- (55) Adhikari, U.; Scheiner, S. Contributions of Various Noncovalent Bonds to the Interaction between an Amide and S-Containing Molecules. *ChemPhysChem.* **2012**, *13*, 3535-3541.

- (56) Clark, T.; Murray, J. S.; Lane, P.; Politzer, P. Why Are Dimethyl Sulfoxide and Dimethyl Sulfone Such Good Solvents? *J. Mol. Model.* **2008**, *14*, 689-697.
- (57) Nziko, V. d. P. N.; Scheiner, S. Chalcogen Bonding between Tetravalent SF<sub>4</sub> and Amines. *J. Phys. Chem. A* **2014**, *118*, 10849-10856.
- (58) Chaudhary, P.; Goettel, J. T.; Mercier, H. P. A.; Sowlati-Hashjin, S.; Hazendonk, P.; Gerken, M. Lewis Acid Behavior of SF<sub>4</sub>: Synthesis, Characterization, and Computational Study of Adducts of SF<sub>4</sub> with Pyridine and Pyridine Derivatives. *Chem. Eur. J.* **2015**, *21*, 6247-6256.
- (59) Frisch, M. J.; Trucks, G. W.; Schlegel, H. B.; Scuseria, G. E.; Robb, M. A.; Cheeseman, J. R.; Scalmani, G.; Barone, V.; Mennucci, B.; Petersson, G. A. et al. *Gaussian 09*, Revision B.01; Gaussian, Inc: Wallingford CT, 2009.
- (60) Boys, S. F.; Bernardi, F. The Calculation of Small Molecular Interactions by the Differences of Separate Total Energies. Some Procedures with Reduced Errors. *Mol. Phys.* **1970**, *19*, 553-566.
- (61) Latajka, Z.; Scheiner, S. Primary and Secondary Basis Set Superposition Error at the SCF and MP2 Levels: H<sub>3</sub>N--Li<sup>+</sup> and H<sub>2</sub>O--Li<sup>+</sup>. *J. Chem. Phys.* **1987**, *87*, 1194-1204.
- (62) Helgaker, T.; Klopper, W.; Koch, H.; Noga, J. Basis-Set Convergence of Correlated Calculations on Water. *J. Chem. Phys.* **1997**, *106*, 9639-9646.
- (63) Mishra, B. K.; Karthikeyan, S.; Ramanathan, V. Tuning the C–H··· $\pi$  Interaction by Different Substitutions in Benzene–Acetylene Complexes. *J. Chem. Theory Comput.* **2012**, *8*, 1935-1942.

- (64) Szalewicz, K.; Jeziorski, B. Symmetry-Adapted Perturbation Theory of Intermolecular Interactions. In *Molecular Interactions. From Van der Waals to Strongly Bound Complexes*, Scheiner, S., Ed. Wiley: New York, 1997; pp 3-43.
- (65) Moszynski, R.; Wormer, P. E. S.; Jeziorski, B.; van der Avoird, A. Symmetry-Adapted Perturbation Theory of Nonadditive Three-Body Interactions in van der Waals Molecules. I. General Theory. *J. Chem. Phys.* **1995**, *103*, 8058-8074.
- (66) Werner, H.-J.; Knowles, P. J.; Manby, F. R.; Schütz, M.; Celani, P.; Knizia, G.; Korona, T.; Lindh, R.; Mitrushenkov, A.; Rauhut, G.; et al. *MOLPRO*, Version 2006; 2010.
- (67) Reed, A. E.; Weinhold, F.; Curtiss, L. A.; Pochatko, D. J. Natural Bond Orbital Analysis of Molecular Interactions: Theoretical Studies of Binary Complexes of HF, H<sub>2</sub>O, NH<sub>3</sub>, N<sub>2</sub>, O<sub>2</sub>, F<sub>2</sub>, CO and CO<sub>2</sub> with HF, H<sub>2</sub>O, and NH<sub>3</sub>. *J. Chem. Phys.* **1986**, *84*, 5687-5705.
- (68) Reed, A. E.; Curtiss, L. A.; Weinhold, F. Intermolecular Interactions from a Natural Bond Orbital, Donor-Acceptor Viewpoint. *Chem. Rev.* **1988**, *88*, 899-926.
- (69) Bader, R. F. W. *Atoms in Molecules, a Quantum Theory*. Clarendon Press: Oxford, 1990; Vol. 22, p 438.
- (70) Carroll, M. T.; Chang, C.; Bader, M. F. W. Prediction of the Structures of Hydrogen-Bonded Complexes Using the Laplacian of the Charge Density. *Mol. Phys.* **1988**, *63*, 387-405.
- (71) Keith, T. A. *Aimall*, TK Gristmill Software: Overland Park KS, 2013.

- (72) Bulat, F. A.; Toro-Labbé, A.; Brinck, T.; Murray, J. S.; Politzer, P. Quantitative Analysis of Molecular Surfaces: Areas, Volumes, Electrostatic Potentials and Average Local Ionization Energies. *J. Mol. Model.* **2010**, *16*, 1679-1691.
- (73) Scheiner, S.; Adhikari, U. Abilities of Different Electron Donors (D) to Engage in a P $\cdots$ D Noncovalent Interaction. *J. Phys. Chem. A* **2011**, *115*, 11101-11110.
- (74) Nziko, V. d. P. N.; Scheiner, S. Intramolecular S $\cdots$ O Chalcogen Bond as Stabilizing Factor in Geometry of Substituted Phenyl-SF<sub>3</sub> Molecules. *J. Org. Chem.* **2015**, *80*, 2356-2363.
- (75) Dunning, T. H.; Peterson, K. A.; Wilson, A. K. Gaussian Basis Sets for Use in Correlated Molecular Calculations. X. The Atoms Aluminum through Argon Revisited. *J. Chem. Phys.* **2001**, *114*, 9244-9253.
- (76) Zhou, F.; Liu, R.; Li, P.; Zhang, H. On the Properties of S $\cdots$ O and S $\cdots$ p Noncovalent Interactions: The Analysis of Geometry, Interaction Energy and Electron Density. *New J. Chem.* **2015**, *39*, 1611-1618.
- (77) Bauzá, A.; Quiñonero, D.; Deyà, P. M.; Frontera, A. Pnictogen-p Complexes: Theoretical Study and Biological Implications. *Phys. Chem. Chem. Phys.* **2012**, *14*, 14061-14066.
- (78) Karthikeyan, S.; Ramanathan, V.; Mishra, B. K. Influence of the Substituents on the CH $\cdots$ p Interaction: Benzene-Methane Complex. *J. Phys. Chem. A* **2013**, *117*, 6687-6694.
- (79) Lu, Y.-X.; Zou, J.-W.; Wang, Y.-H.; Yu, Q.-S. Theoretical Investigations of the C-X/ $\pi$  Interactions between Benzene and Some Model Halocarbons. *Chem. Phys.* **2007**, *334*, 1-7.

- (80) Matter, H.; Nazaré, M.; Güssregen, S.; Will, D. W.; Schreuder, H.; Bauer, A.; Urmann, M.; Ritter, K.; Wagner, M.; Wehner, V. Evidence for C-Cl/C-Br $\cdots$ p Interactions as an Important Contribution to Protein–Ligand Binding Affinity. *Angew. Chem. Int. Ed.* **2009**, *48*, 2911-2916.
- (81) Wallnoefer, H. G.; Fox, T.; Liedl, K. R.; Tautermann, C. S. Dispersion Dominated Halogen-p Interactions: Energies and Locations of Minima. *Phys. Chem. Chem. Phys.* **2010**, *12*, 14941-14949.
- (82) Viguera, A. R.; Serrano, L. Side-Chain Interactions between Sulfur-Containing Amino Acids and Phenylalanine in Alpha-Helices. *Biochem.* **1995**, *34*, 8771-8779.
- (83) Pal, D.; Chakrabarti, P. Non-Hydrogen Bond Interactions Involving the Methionine Sulfur Atom. *J. Biomol. Struct. Dyn.* **2001**, *19*, 115-128.



Table 4-1 Geometric aspects ( $\text{\AA}$ , degs) of complexes, optimized at MP2/aug-cc-pVDZ level

	SF <sub>2</sub>					SF <sub>4</sub>				
	ethene	ethyne	c-but	t-but	benzene	ethene	ethyne	c-but	t-but	benzene
r(S $\cdots$ C <sub>a</sub> )	2.982	3.051	2.883	3.116	3.019	3.195	3.185	3.044	3.192	3.108
r(S $\cdots$ C <sub>b</sub> )	2.982	3.051	2.830	2.903	3.136	3.195	3.185	3.049	3.046	3.108
r(S $\cdots$ m <sup>a</sup> )	2.904	2.988	2.774	2.934	2.996	3.123	3.125	2.970	3.045	3.027
$\theta(\text{F}^1\text{-S}\cdots\text{C}_a)$	166.6	168.2	166.3	171.9	177.3	167.5	168.8	171.9	169.6	165.3
$\theta(\text{F}^1\text{-S}\cdots\text{C}_b)$	166.6	168.2	161.1	160.1	152.5	167.5	168.8	160.1	163.8	165.3
$\theta(\text{F}^1\text{-S}\cdots\text{m}^a)$	177.4	178.1	171.2	172.3	164.8	177.4	179.8	171.9	174.8	173.3
$\Delta r(\text{S-F}^1) \cdot 10^{-3}$	10.6	9.6	21.0	14.7	12.5	5.0	3.0	6.9	6.0	7.1
$\Delta r(\text{S-F}^2) \cdot 10^{-3}$	7.1	3.4	14.3	10.4	8.8	1.1	1.8	4.1	3.0	5.0
$\Delta r(\text{C}_a\text{-C}_b) \cdot 10^{-3}$	2.6	1.3	5.4	3.3	2.9	4.7	1.9	7.9	3.7	1.9

<sup>a</sup>m represents midpoint of C=C bonds indicated in Figure 4-1 and Figure 4-2.

Table 4-2 Binding Energies (Eb), kcal/mol

	MP2/aug-cc-pVxZ											
x	D		T		Q		CCSD(T)/aug-cc-pVDZ		MP2/CBS		CCSD(T)/CBS	
	SF <sub>2</sub>	SF <sub>4</sub>	SF <sub>2</sub>	SF <sub>4</sub>	SF <sub>2</sub>	SF <sub>4</sub>	SF <sub>2</sub>	SF <sub>4</sub>	SF <sub>2</sub>	SF <sub>4</sub>	SF <sub>2</sub>	SF <sub>4</sub>
ethene	3.40	2.87	4.47	3.49	4.84	3.71	2.42	2.31	5.11	3.87	4.13	3.31
ethyne	2.86	2.96	3.79	3.61	4.11	3.81	2.19	2.51	4.34	3.96	3.67	3.51
c-but	6.13	4.95	7.83	6.01	8.43	6.36	3.88	3.51	8.86	6.62	6.61	5.18
t-but	4.81	4.28	5.88	5.05	6.30	5.32	3.26	3.19	6.60	5.52	5.05	4.43
benzene	4.39	5.42	5.39	6.52	5.77	6.92	2.90	3.71	6.04	7.21	4.55	5.50

Table 4-3 NBO values of E(2) (kcal/mol) for indicated charge transfers, with aug-cc-pVDZ basis set.

	$\pi_{ab} \rightarrow \sigma^*(S-F^1)$	$\pi_{ab} \rightarrow \sigma^*(S-F^2)$	$\pi_{cd} \rightarrow \sigma^*(S-F^2)$	$S_{lp} \rightarrow \pi^*_{ab}$	$S_{lp} \rightarrow \pi^*_{cd}$
SF <sub>2</sub>					
ethene	8.72	0.68	-	3.79	-
ethyne	5.12	0.45	-	2.48	-
c-but	10.82	0.85	3.11	4.30	0.80
t-but	6.48	0.57	1.72	2.07	1.13
benzene	5.69	1.72		1.10	
SF <sub>4</sub>					
ethene	3.24	0.77	-		
ethyne	2.57	0.53	-		
c-but	4.70	1.08	0.74	-	0.19
t-but	3.53	0.98	0.37	-	0.61
benzene	5.51	1.59			

Table 4-4 NBO interorbital and total charge transfer (me) with aug-cc-pVDZ basis set.

	$\pi_{ab} \rightarrow \sigma^*(S-F^1)$	$\pi_{ab} \rightarrow \sigma^*(S-F^2)$	$\pi_{cd} \rightarrow \sigma^*(S-F^2)$	$S_{lp} \rightarrow \pi^*_{ab}$	$S_{lp} \rightarrow \pi^*_{cd}$	total <sup>b</sup>
SF <sub>2</sub>						
ethene	22.0	1.8	-	9.8	-	16.1
ethyne	12.8	1.2	-	6.4	-	6.4
c-but	28.8	2.2	8.5	8.7	2.2	36.2
t-but	17.4	1.6	4.7	2.4	1.2	22.1
benzene	13.2	2.7	-	1.6		13.0
SF <sub>4</sub>						
ethene	8.2	1.9	-			12.6
ethyne	6.1	1.4	-			8.1
c-but	11.8	2.6	1.8	-	0.3	27.6
t-but	8.8	2.4	0.9	-	0.9	18.0
benzene	12.8	4.0				17.3

<sup>a</sup>calculated as  $2 \{ \langle \psi^*_{don} | F | \psi_{acc} \rangle / (\epsilon_{acc} - \epsilon_{don}) \}^2$

<sup>b</sup>sum of NBO atomic charges on electron donor molecule

Table 4-5 Values of density and its Laplacian (au) at AIM bond critical points

	SF <sub>2</sub>		SF <sub>4</sub>	
	$\rho$	$\nabla^2\rho$	$\rho$	$\nabla^2\rho$
ethene	1.649	4.535	1.252	3.136
ethyne	1.337	4.293	1.176	3.427
c-but	2.141	6.116	1.700	4.403
t-but	1.707	5.075	1.525	4.137
benzene	1.366	4.070	1.406	4.09

Table 4-6 Binding Energies (Eb), kcal/mol, computed at various levels of theory<sup>a</sup>

	CCSD(T)/ CBS		B3LYP/ aug-cc-pVDZ		B3LYP-D3/ aug-cc-pVDZ		M06-2X/ aug-cc-pVDZ	
	SF <sub>2</sub>	SF <sub>4</sub>	SF <sub>2</sub>	SF <sub>4</sub>	SF <sub>2</sub>	SF <sub>4</sub>	SF <sub>2</sub>	SF <sub>4</sub>
ethene	4.11	3.31	2.24	1.35	4.40	3.87	4.62	3.75
ethyne	3.71	3.51	2.02	1.70	3.60	3.86	4.01	3.73
c-but	6.68	5.18	3.40	2.13	6.63	6.15	6.67	5.51
t-but	5.03	4.43	2.18	1.78	4.95	5.12	5.51	4.70
benzene	4.60	5.50	1.24	1.40	4.22	5.56	4.89	6.03

<sup>a</sup>All geometries were optimized at theoretical level indicated.

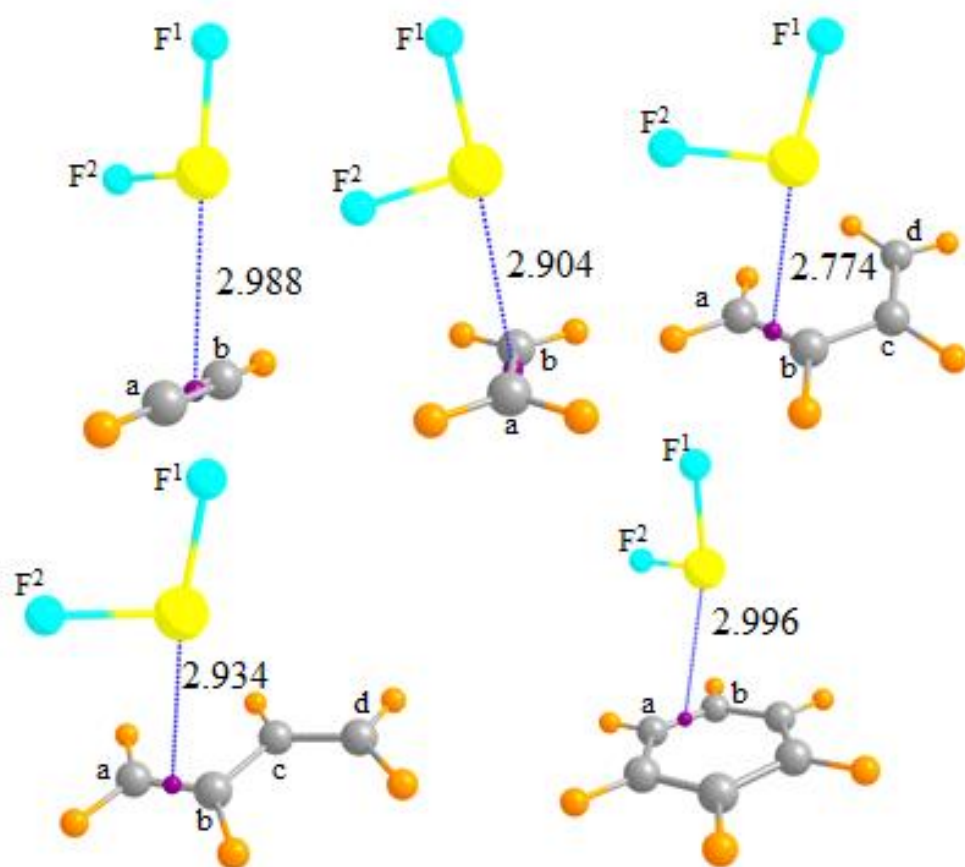


Figure 4-1 Optimized geometries of  $\text{SF}_2$  with ethyne, ethylene, cis-butadiene, trans-butadiene, and benzene. Distances in Å. Small purple sphere represents midpoint of indicated bond.

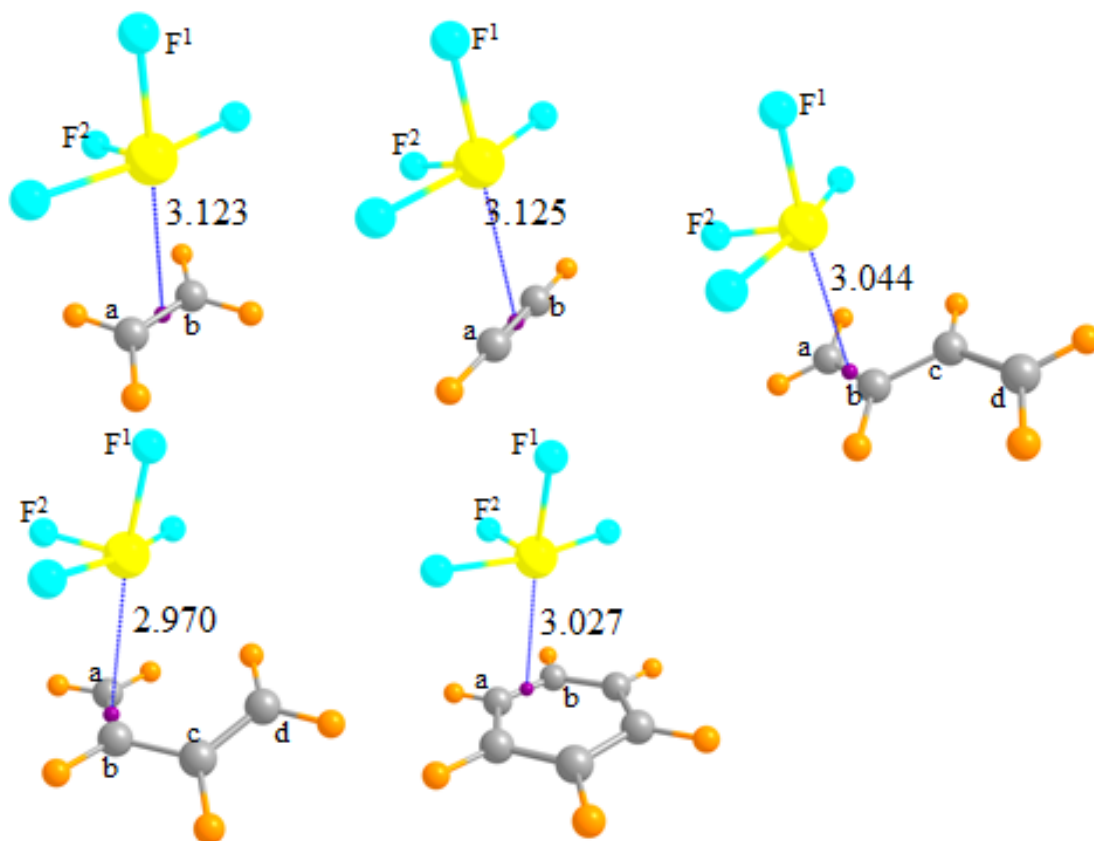


Figure 4-2 Optimized geometries of  $\text{SF}_4$  with ethyne, ethylene, cis-butadiene, trans-butadiene, and benzene. Distances in Å. Small purple sphere represents midpoint of indicated bond.

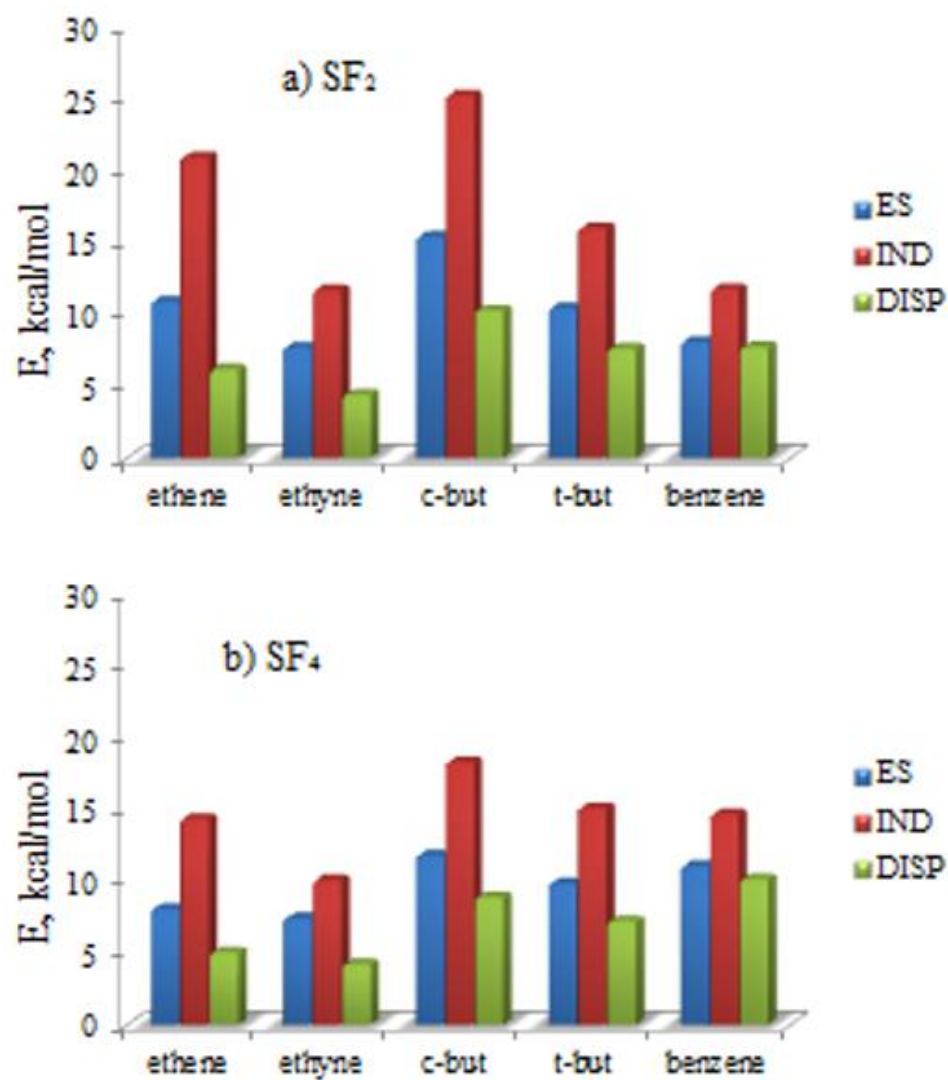


Figure 4-3 Attractive SAPT components of interaction energies of alkenes with a) SF<sub>2</sub> and b) SF<sub>4</sub>. ES=electrostatic, IND=induction, DISP=dispersion.

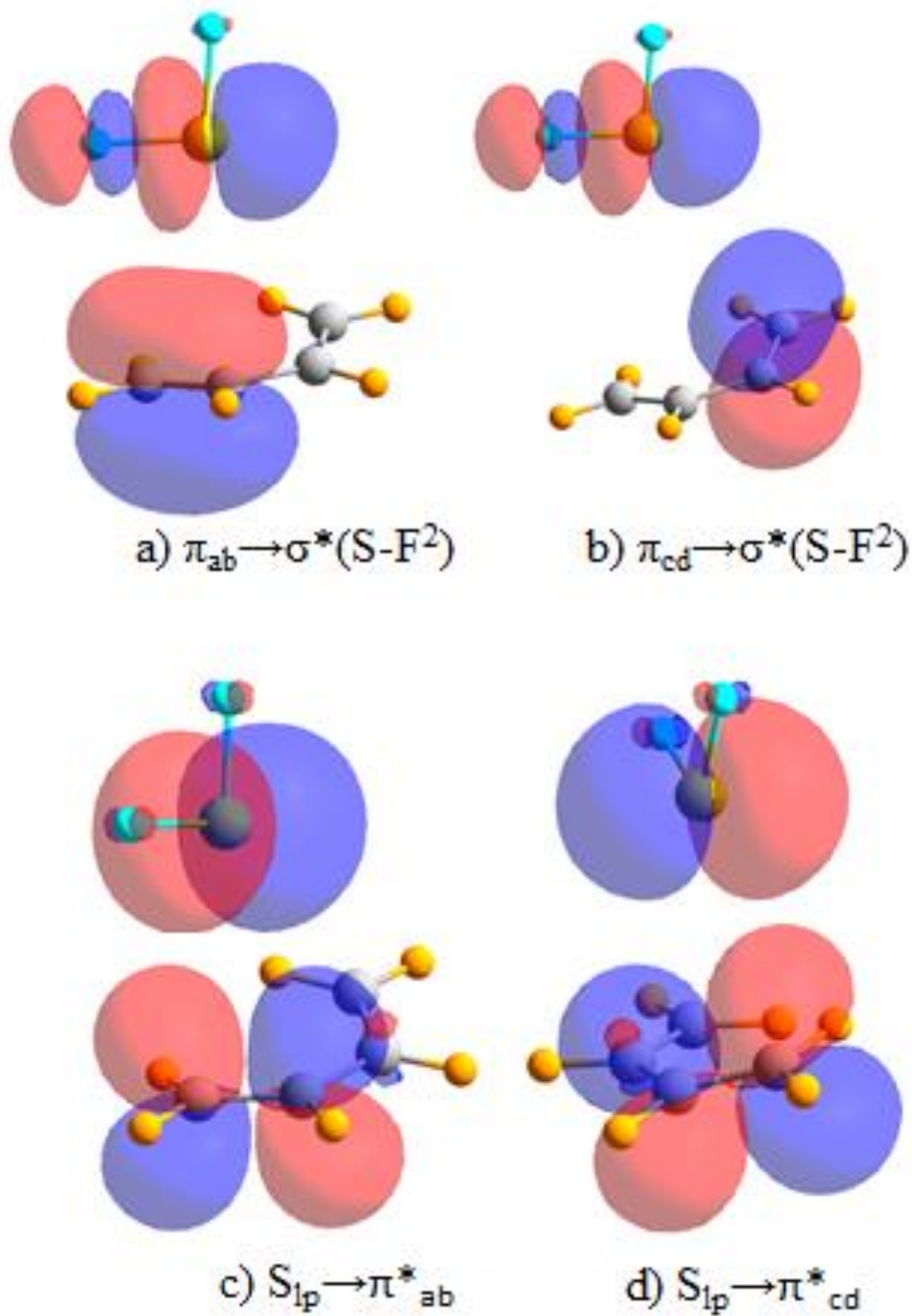


Figure 4-4 Diagrammatic representations of relevant NBO orbitals of  $SF_2$  and cis-butadiene. Red and blue lobes indicate opposite sign of each wave function.

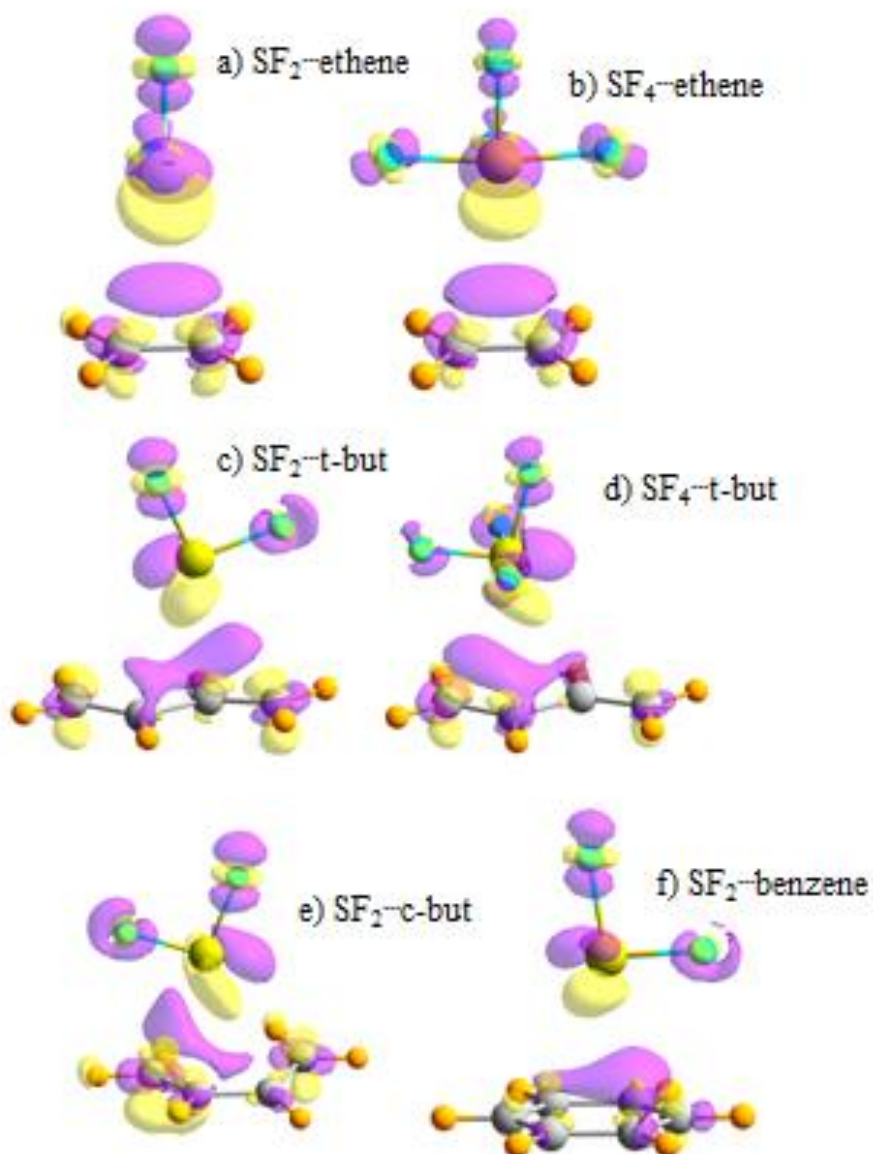


Figure 4-5 Electron density redistributions accompanying formation of indicated complexes. Purple and yellow regions indicate gain and loss of density, respectively. Contours shown represent  $\pm 0.001$  au.



## CHAPTER 5

INTERACTION BETWEEN THIOUREA AND IMINES:PRELUDE TO CATALYSIS<sup>1</sup>**Abstract**

The interaction between thiourea and a series of imines was examined via high-level ab initio calculations. For each imine, there is a set of stable complexes that represent minima on the potential energy surface. One type is characterized by a pair of symmetric NH··N HBs, with both NH groups of thiourea approaching the imine N from above and below its molecular plane. Another geometry category combines a linear NH··N with a CH··S H-bond. A third, which is less stable, has the S approaching the imine's CH<sub>2</sub> group, and a stacking arrangement is present in the fourth. Interaction energies vary from about 2 kcal/mol up to a maximum of 13.5 kcal/mol. The formation of the complex tends to elongate the C-N bond within the imine by as much as 0.004 Å, but there are certain dimers which cause a small contraction of this bond.

**5-1. Introduction**

Organocatalysis refers to the efficient use of small organic molecules containing no metallic atoms as catalysts for various asymmetric organic reactions. These catalysts have several advantages: they are environmentally friendly, cheap, insensitive to moisture and considerably less toxic, and can control the chirality of the product <sup>1-4</sup>. A common mode of organocatalysis takes advantage <sup>5</sup> of iminium ion activation, enamine activation, and

---

<sup>1</sup> Coauthored by Vincent de Paul Nzuwah Nziko and Steve Scheiner. Reproduced with permission from *J. Org. Chem.* **2015**, *80*, 10334-10341. Copyright 2014, American Chemical Society.

activation via hydrogen bonding.

Thiourea and its derivatives have emerged <sup>6-7</sup> as a very powerful class of organocatalysts in part because of their ability to form strong hydrogen bonds. The first asymmetric hydrocyanation of imines <sup>7</sup> was accomplished with the use of a thiourea-derived catalyst. The proposed reaction mechanism proceeds through the formation of a thiourea/imine hydrogen-bonded reactant complex. Thiourea derivatives have been used as catalysts for a number of reactions <sup>8-12</sup> including the aza-Baylis-Hillman reaction, Strecker reaction, Mannich reaction and Pictet-Spengler reaction. All these reactions make use of imines as a reagent which forms complexes with the thiourea derivative.

There is unfortunately a dearth of current information about the details of the complexes formed by thiourea with imines. It is not certain for example, whether thiourea engages in H-bonds (HBs) with the imine, and if so whether it serves as proton donor or acceptor. There is also the possibility that it could act as both simultaneously, i.e. NH<sub>2</sub> groups as donor, and S as acceptor. But there is no limitation that the intermolecular interactions must be HBs. The S atom has shown a propensity <sup>13-28</sup> to engage in chalcogen bonds, which would involve the S and N of the imine in a direct attraction, with no need for a bridging H atom. Still another sort of interaction would involve the  $\pi$ -systems of the two molecules in a stacked arrangement. At issue also is the way in which the complexation affects the imine. Does the interaction serve as a prelude to catalysis in some way, facilitating the entire process?

The present work is designed to provide answers to some of these questions via quantum chemical calculations which can focus on the fundamentals of the complexation

process. It is possible to determine which types of complexes might be formed upon the approach of the thiourea to the imine. The various sorts of dimers can be examined to see which are most favorable, what types of noncovalent bonds they contain, and how the interaction affects the molecular properties of each system. The prototypical imine investigated here is  $\text{CH}_2\text{NH}$ . The study broadens the scope from a standard imine to related systems as well, which may serve catalytic functions. Oximes are imines in which the imino hydrogen is replaced by a hydroxyl group, which is modeled here by  $\text{CH}_2\text{NOH}$ . Replacement by an amino lead to the hydrazone class, with  $\text{CH}_2\text{NNH}_2$  as prototype. In carbimides, a hydroxyl group is located on the imine carbon, which is modeled here by  $\text{NHCHOH}$ . Each of these molecules was paired with thiourea, so as to identify the sorts of complexes in which they can engage, and to analyze the properties of each.

## 5-2. Computational Methods

The quantum mechanical calculations were carried out using the GAUSSIAN 09 program<sup>29</sup>. Second-order Moller-Plesset perturbation theory (MP2) was used to include the effects of electron correlation. Geometries were optimized in the framework of Dunning's augmented correlation consistent polarized valence double zeta basis set (aug-cc-pVDZ). Frequency calculations confirmed that the complexes obtained correspond to true minima. The interaction energies,  $E_{\text{int}}$ , were evaluated as the difference between the energy of the complex and the sum of the energies of the two monomers, using their geometries within the optimized complex.  $E_{\text{int}}$  was corrected for basis set superposition error via the counterpoise<sup>30</sup> procedure.

Higher level calculations with larger basis sets made use of the MP2/aug-cc-pVDZ

geometries. The interaction energies were extrapolated to the complete basis set (CBS) by a methodology used by us <sup>19</sup> in our earlier work. The extrapolation is based on the idea <sup>31</sup> that correlation energy is roughly proportional to  $X^{-3}$  for basis sets of the aug-cc-pVXZ type. It utilizes a two-step method, described by Eq (1), with triple and quadruple sets <sup>32</sup>:

$$\Delta E_{\text{MP2/CBS}} = (64 \Delta E_{\text{MP2/aug-cc-pVQZ}} - 27 \Delta E_{\text{MP2/aug-cc-pVTZ}}) / 37 \quad (1)$$

A correction was added via Eq (2) to account for discrepancies between MP2 and CCSD(T)

$$E_{\text{CCSD(T)/CBS}} = E_{\text{MP2/CBS}} + (E_{\text{CCSD(T)/aug-cc-pVDZ}} - E_{\text{MP2/aug-cc-pVDZ}}) \quad (2)$$

The molecular electrostatic potential (MEP) was evaluated for the monomers in their optimized geometry at the MP2/aug-cc-pVDZ level. Electron density shifts caused by complexation were calculated as the difference between the electron density of the complex and the sum of those of the monomers, again in the geometry within the complex. The total interaction energy was dissected into various components by symmetry-adapted perturbation theory (SAPT) analysis <sup>33-34</sup> using the MOLPRO program <sup>35</sup>, at the HF/aug-cc-pVDZ level of theory. Natural bond orbital (NBO) formalism <sup>36-37</sup> provided information about interorbital charge transfer, evaluated at the M06-2X/aug-cc-pVDZ level so as to include correlation effects. The electron density was analyzed through the atoms in molecule (AIM) procedure <sup>38-39</sup> to determine the position of the bond critical points, as well as the density and its Laplacian using the AIMALL software <sup>40</sup>, at the MP2/aug-cc-pVDZ level.

### 5-3. Results

#### 5-3. 1. Monomers

The MEP of each monomer is illustrated in Figure 5-1, where red and blue regions indicate negative and positive regions, respectively. The MEP of thiourea is negative at the S atom, particularly along its lone pair direction, with  $V_{s,min} = -29.3$  kcal/mol. The most positive regions correspond to extensions of the NH bonds, rising up to a maximum of +57.8 kcal/mol for the H atoms anti to the C=S bond.

The potentials surrounding the imine molecules have certain features in common. All exhibit a negative region along the N lone pair, with the potential varying from a minimum value of -25.2 kcal/mol for  $\text{CH}_2\text{NOH}$  to a maximum of -42.6 kcal/mol for  $\text{NHCHOH}$ . Another minimum occurs near the O or N atom of the substituted imines. In the case of  $\text{CH}_2\text{NNH}_2$ ,  $V_{s,min}$  on the  $\text{NH}_2$  group slightly exceeds that on the imine N atom. Positive regions are associated with the various H atoms, most notable the OH group with a  $V_{s,max}$  of 45-57 kcal/mol; least positive are the CH protons.

#### 5-3. 2. Heterodimers

The 1:1 complexes between thiourea and each of the imines were searched for all minima, using their MEPs as a starting point, and supplemented by optimizations of randomly generated starting configurations. The searches led to a total of 19 dimers, illustrated in Figure 5-2. The interaction energy of each is displayed, along with salient geometric properties.

Beginning with the  $\text{CH}_2\text{NH}$  dimers in Figure 5-2, there are two structures with

equal energy. **A1** is characterized by a pair of equivalent  $\text{NH}\cdots\text{N}$  HBs to the same imine N proton acceptor. Each HB is 2.235 Å in length, and is distorted by 37° from linearity. The NBO value of  $E(2)$  for the charge transfer from the N lone pair to each pertinent  $\text{NH } \sigma^*$  antibonding orbital is 4.45 kcal/mol, corresponding to a HB of reasonable strength. This supposition is confirmed by the presence of a AIM bond path between the relevant atoms, with  $\rho$  at the bond critical point of 0.0166 au, as indicated by the first entry in Table 5-1. Note that this geometry pairs together the most positive region of thiourea with a negative area of  $\text{CH}_2\text{NH}$ , although the two bridging protons lie above and below the plane of  $\text{CH}_2\text{NH}$ , and thus miss  $V_{s,\text{min}}$ .

The **A2** dimer, of equivalent energy, is characterized by one linear  $\text{NH}\cdots\text{N}$  HB, supplemented by a much longer and weaker  $\text{CH}\cdots\text{S}$  HB. The greater strength of the former is accentuated by its length of less than 2 Å, and a large  $E(2)$  of 18 kcal/mol. Its  $\rho_{\text{BCP}}$  is nearly three times that of the  $\text{CH}\cdots\text{S}$  HB, and double that of the  $\text{NH}\cdots\text{N}$  HBs in **A1**. This bond strengthening relative to **A1** is due in large part to the approach of the proton along the plane of  $\text{CH}_2\text{NH}$ , wherein lies the N lone pair. In terms of monomer MEPs, the H of thiourea that is cis to S is less positive than the trans H. Likewise, the CH proton and the S exhibit smaller extrema than the atoms involved in the HBs of **A1**.

The  $\text{NH}\cdots\text{N}$  HB persists in **A3**, despite a 20° nonlinearity coupled with some stretching, but the  $\text{CH}\cdots\text{S}$  HB of **A2** is replaced by a  $\text{NH}\cdots\text{S}$  HB. This arrangement is slightly weaker than **A1** or **A2**. It might be noted that a certain amount of cooperativity will be present in **A2** and **A3** as each molecule serves as both electron donor and acceptor, whereas **A1** is likely weakened by negative cooperativity as the imine acts as double electron donor.

**A4** is considerably less stable. It contains a weak  $\text{NH}\cdots\pi$  HB wherein the  $\text{C}=\text{S}$   $\pi$ -bonding orbital serves as electron donor. The NH proton lies some 2.71 Å from the  $\text{C}=\text{S}$  midpoint, as shown in Figure 5-2. An AIM bond path connects the H and S atoms, which might appear as a  $\text{NH}\cdots\text{S}$  rather than a  $\text{NH}\cdots\pi$  HB. There is also some stabilization contributed by the interaction of the CN  $\pi$  bond of the imine and the CS  $\sigma$  antibond of thiourea, so this minimum could perhaps best be classified as a stacked structure. (There is no corresponding AIM bond path for the latter interaction.) The weakest dimer found on the thiourea/ $\text{CH}_2\text{NH}$  PES is **A5**, bound by only 1.90 kcal/mol. While initial examination of the geometry might suggest a bifurcated  $\text{CH}\cdots\text{S}$  HB, NBO analysis suggests rather a tetrel bond, wherein charge is transferred from the S lone pairs to the CN  $\sigma^*$  antibonding orbital of the imine. AIM, on the other hand, tends toward the alternate description of a symmetric bifurcated  $\text{CH}\cdots\text{S}$  HB.

As reported in the first entry of Table 5-2, the interaction energy of **A1** is 9.11 kcal/mol at the MP2/aug-cc-pVDZ level. Enlarging the basis set leads to small progressive increments up to 9.97 kcal/mol with the quadruply polarized set. Extrapolation to a complete set results in an interaction energy higher than pVDZ by 1 kcal/mol. Replacing the MP2 treatment of electron correlation by CCSD(T), on the other hand, reduces the interaction energy, by roughly 0.5 kcal/mol with the aug-cc-pVDZ set. Again extrapolation to the complete set raises this quantity, to our best estimate of 9.66 kcal/mol, which is the value displayed in Figure 5-2. A quick scan of Table 5-2 illustrates that the MP2/aug-cc-pVDZ interaction energies represent only slight underestimates of the CCSD(T)/CBS quantities for all of the dimers. Importantly, the less accurate values obey the same trends,

with generally similar energy differences from one dimer to the next.

NHCHOH replaces one of the H atoms on the C of CH<sub>2</sub>NH by an OH group. The latter is a powerful proton donor so it is no surprise that there is a OH··S HB in the most stable dimer **B1** with thiourea (see Figure 5-3). The strength of this bond is exemplified by the very large E(2) of 25.2 kcal/mol and  $\rho_{\text{BCP}}=0.0298$  au (see Table 5-1). This geometry is supplemented by a NH··O HB, shorter than OH··S but with a slightly smaller  $\rho_{\text{BCP}}$  and much smaller E(2). Together, these two HBs compose a total interaction energy of 13.5 kcal/mol. Both NH groups of thiourea act as proton donors in **B2**, with the NH··N considerably stronger than NH··O. This complex is likely disfavored by negative cooperativity since thiourea serve as double electron acceptor. Only slightly less stable is **B3**, which combines a strong NH··N with a weaker NH··S. This pair of molecules also exhibits a stacking arrangement **B4**, which is bound by 6.3 kcal/mol. The AIM bonding pattern attributes the stability of **B4** to a single C··N interaction, whereas NBO indicates a pair of charge transfers in both direction, and both involving the imine's C-N bond. **B3** is similar to **A3**, with comparable interaction energies. Examination of Table 5-3 confirms the earlier pattern that CCSD(T) interaction energies are slightly larger than MP2/aug-cc-pVDZ quantities but follow similar patterns.

The OH group in CH<sub>2</sub>NOH leads again to a OH··S HB in the global minimum of its dimers with thiourea, as illustrated in Figure 5-4, and with interaction energies presented in Table 5-4. Unlike **B1**, the second HB in **C1** is of the NH··N variety. Even though the latter HB is quite a bit stronger than the secondary HB in **B1** (E(2)=18.7 kcal/mol) the total interaction energies of these two complexes are quite similar. **C2** is reminiscent of **A2**,



although the strong  $\text{NH}\cdots\text{N}$  HB is 0.1 Å longer in **C2** and both  $E(2)$  and  $\rho_{\text{BCP}}$  are smaller. It is for this reason that the interaction energy is lower in **C2**. The pair of  $\text{NH}\cdots\text{N}$  HBs to the same imine N proton acceptor in **C3** is similar to the pattern in **A1**, although the former is more weakly bound. Note also that the two HBs in **C3** are distinctly different from one another, unlike the symmetric **A1** geometry. Although the geometry of **C4** resembles that of **A5**, NBO analysis suggests a pair of  $\text{CH}\cdots\text{S}$  HBs, and not a tetrel bond. AIM, on the other hand, suggests only one of these two HBs. Nonetheless these two complexes have equal interaction energies. It is interesting to note the absence of a stable stacked dimer for this pair of molecules.

The OH group of  $\text{CH}_2\text{NOH}$  is replaced by  $\text{NH}_2$  in  $\text{CH}_2\text{NNH}_2$ , precluding the possibility of a  $\text{OH}\cdots\text{S}$  HB. The global minimum **D1** in Figure 5-5 instead contains a pair of  $\text{NH}\cdots\text{N}$  HBs, with thiourea serving as double electron acceptor, but to two different, adjacent N atoms. As indicated in Table 5-5, this complex is bound by 9.6 kcal/mol, similar to **A1** despite the different HB pattern and the stronger  $\text{NH}\cdots\text{N}$  HBs suggested by both NBO and AIM. The pattern of **A1** is reproduced instead in **D2**, the latter of which is slightly less stable. The  $\text{NH}\cdots\text{N}/\text{CH}\cdots\text{S}$  HB pair of **A2** and **C2** arises again in **D3**, this time with an interaction energy of 8.9 kcal/mol. A new pair of HBs,  $\text{NH}\cdots\text{N}$  and  $\text{NH}\cdots\text{S}$  occur in **D4**. It is interesting to note that these four dimers have very similar interaction energies, within 1.2 kcal/mol of one another. A classic  $\text{NH}\cdots\text{N}$  HB is paired with a  $\text{CH}\cdots\pi(\text{CS})$  HB in **D5**. (The latter HB is designated  $\text{CH}\cdots\text{S}$  by AIM.) Both bonds are rather weak, and the total interaction energy is less than 5 kcal/mol. The bifurcated arrangement in **D6** is quite similar to that in **C4**, with a comparable interaction energy. The NBO and AIM data agree on the

presence of a single CH $\cdots$ S HB.

The only prior computational study of complexes between thiourea and an imine<sup>41</sup> considered CR<sup>1</sup><sub>2</sub>NCR<sup>2</sup>O, somewhat different than the imines considered here. The geometries of the dimers were optimized at the B3LYP level, with a much smaller 6-31G\* basis set. The potential energy surfaces were not examined extensively; instead only two particular geometries were considered, corresponding roughly to **B2** and **C3**. The interaction energies of 4.2 and 4.1 kcal/mol for R<sup>1</sup>=R<sup>2</sup>=H were considerably smaller than our CCSD(T)/CBS values, or even our crudest MP2/aug-cc-pVDZ results, for the corresponding structures. It would therefore appear inadvisable to apply small basis sets to systems of this sort.

There have been other computational studies of complexes pairing thiourea with proton acceptors, albeit not imines. An early study involving a water molecule<sup>42</sup> identified a geometry akin to **A1**, where both NH groups of thiourea engage in a HB with the proton acceptor O. The small basis set found an interaction energy below 5 kcal/mol. Full-fledged anions of course form stronger complexes<sup>43</sup> but again show a predilection for a structure like **A1**. On the other hand, when the anion contains two proton acceptor atoms, as for example in acetate, structures of the **B2** or **D1** sort emerge, containing two separate NH $\cdots$ X HBs. This same bonding pattern of **A1** for a single proton acceptor and **B2** for 2 acceptor atoms was also noted later<sup>44</sup> for more complicated systems, and for nitro groups<sup>45</sup>.

#### Overview

There are several geometrical themes that appear with some regularity. The first type, comprising **A1**, **C3** and **D2**, has a pair of nearly symmetric NH $\cdots$ N HBs, with both NH groups of thiourea approaching the imine N from above and below its molecular plane.

The presence of either an OH or NH<sub>2</sub> group on the imine reduces the interaction energy from that in **A1**, presumably by withdrawing electron density from the N lone pair. A second arrangement combines a linear NH $\cdots$ N with a CH $\cdots$ S HB, as in the **A2**, **C2**, **D3** collection, where the OH and NH<sub>2</sub> groups again weaken the binding. Still another type of geometry is characterized by **A5**, **C4** and **D6**, in which the S approaches the imine's CH<sub>2</sub> group. All of these are bound by between 1.7 and 1.9 kcal/mol. There is a fine balance between a S $\cdots$ C tetrel bond, as in **A5**, and bifurcated CH $\cdots$ S HBs as in **C4** and **D6**. There are only two stacked structures, **A4** and **B4**. Their interaction energies are 5.2 and 6.3 kcal/mol, respectively, but their stability rests on different specific interactions. For example, while **A4** contains a NH $\cdots$  $\pi$ (CS) HB, **B4** relies on a N<sub>lp</sub> $\rightarrow\sigma^*$ (CN) transfer coupled with a back transfer from  $\pi$ (CN) to  $\sigma^*$ (CS).

### 5-3. 3. Energy Partitioning

As another means of analyzing the nature of the interactions in the various heterodimers, the total interaction energy was dissected into its components. SAPT calculations were carried out at the HF/aug-cc-pVDZ level of theory. The contributions of each of the attractive components are illustrated in Figure 5-7. In most cases, particularly where the interaction is primarily of HB type, the electrostatic attraction represents the largest contribution, exceeding 20 kcal/mol in certain cases. Induction and dispersion are smaller, and comparable to one another. The exceptions to this behavior are observed in the stacked structures and those containing a tetrel bond, i.e. **A4**, **A5**, **B4**, **C4**, **D5**, and **D6**. In these cases, the electrostatic contribution is reduced and dispersion makes a much larger percentage contribution, comparable to or even exceeding ES. The sum of all of the

components including exchange repulsion yields the total interaction energy, shown as the yellow bar in Figure 5-7. This SAPT sum matched rather closely with the CCSD(T)/aug-cc-pVDZ quantity, with a correlation coefficient of 0.94.

#### 5-3. 4. Electron Density Shifts

The formation of any molecular interaction causes the electron density to shift, both internal within each molecule, and externally from one molecule to the other. Each sort of noncovalent bond manifests itself in a characteristic shift, a fingerprint if you will. These shifts are displayed in Figure 5-8 for the complexes of urea with  $\text{CH}_2\text{NH}$ . Each was generated by subtracting the densities of the individual isolated monomers from that of the entire complex. Blue regions designate an area where density is gained as a result of the formation of the complex, losses are shown in red.

The pattern illustrated for complex **A1** fits into the classic picture of HBs: Density is lost around the bridging protons, and is acquired in the region of the lone pair of the proton accepting atom, with additional gain seen in the vicinity of the proton-donating atom. This same pattern is evident in the HBs of structures **A2** and **A3**. Although NBO suggests the interaction in **A5** is best described as a  $\text{S}\cdots\text{C}$  tetrel bond, the prominent red losses around the two CH protons, and the blue gain near the S atom, might argue instead for a bifurcated HB, consistent with AIM data. The pattern for stacked configuration **A4** is perhaps a bit more complicated. It confirms the presence of a  $\text{NH}\cdots\text{S}$  HB as suggested by AIM, although NBO places the source of the density as the CS  $\pi$  bond, not obvious in Figure 5-8. There is also little direct evidence of transfer from  $\pi(\text{CN})$  to  $\sigma^*(\text{CS})$  as predicted by NBO.

The electron density shifts of the B, C, and D complexes are displayed in the Supplementary Information, Figure 5-9-Figure 5-11. As for the A structures, HBs exhibit the same characteristic pattern. The **B4** structure is particularly interesting. NBO describes charge transfers from the imine NC  $\pi$  bond to the thiourea CS  $\sigma^*$  antibond which is not easily seen in the density shift. Nor is the NBO transfer in the reverse direction from the thiourea N lone pair to the CN  $\sigma^*$  antibond readily apparent. The AIM prediction of a C $\cdots$ N bond path is similarly not confirmed in the density shift pattern. With this exception, though, the density shift patterns are entirely consistent with the NBO and AIM interpretations of bonding.

### 5-3. 5. Effect of Complexation on Imine Geometry

It is reasonable to suppose that one of the most important effects of the thiourea catalyst upon the imine might be to prepare it for reaction, perhaps by affecting the strength of the C-N bond. One measure of this bond strength is the length of this bond. Table 5-6 displays the change undergone by this bond, in units of mÅ, within the context of each dimer. Taking the A dimers with CH<sub>2</sub>NH as an example, the CN bond stretches between 1 and 2 mÅ for all structures with the exception of **A3**, where the bond contracts by 2.5 mÅ. A similar contraction occurs in **B3**. What these two geometries share in common, differing from all other dimers, is the participation of the imine NH in a HB.

Another configuration which suffers a significant contraction of the C-N bond length is **D3**. This structure combines a strong NH $\cdots$ N to the imine N proton acceptor, with a CH $\cdots$ S HB. This same motif occurs as well in **A2** and **C2**. The latter shows a small C-N contraction, but the former undergoes a bond lengthening, so this particular combination

of HBs cannot be considered as universally shrinking the C-N bond.

In summary, most of the complexes produce a lengthening of the C-N bond, particularly the most strongly bound. In many, but not all of these, the imine N acts as proton acceptor. If, on the other hand, the imine CH simultaneously acts as proton donor, there is a tendency for this rule to be reversed. Participation of the imine NH also has a tendency to shorten the C-N bond. But it is stressed that these are only general rules, with several exceptions noted.

#### 5-4. Discussion

There are a wide range of different geometries when thiourea combines with each sort of substituted imine. The most strongly bound of these contain one or more HBs. One type is characterized by a pair of nearly symmetric  $\text{NH}\cdots\text{N}$  HBs, with both NH groups of thiourea approaching the imine N from above and below its molecular plane. Another arrangement combines a linear  $\text{NH}\cdots\text{N}$  with a  $\text{CH}\cdots\text{S}$  HB. The sulfur atom approaches the imine's  $\text{CH}_2$  group in a third category, which is supplemented by a stacked arrangement in a fourth. The interaction energies vary from as little as 2 kcal/mol for the structures containing a bifurcated  $\text{CH}_2\cdots\text{S}$  HB up to a maximum of 13.5 kcal/mol for the  $\text{NHCHOH}$  imine which combines a  $\text{NH}\cdots\text{O}$  and  $\text{OH}\cdots\text{S}$  pair of HBs.

In most cases, particularly where the interaction is primarily of HB type, the electrostatic attraction makes the largest contribution to the binding, with induction and dispersion comparable to one another. In the stacked structures and those containing a tetrel bond, on the other hand, the electrostatic contribution is reduced and dispersion makes a much larger percentage contribution. Electron density shift patterns are consistent with the

formulation of the interaction on the basis of HBs. The formation of the complex typically elongates the imine C-N bond by 0.001 - 0.004 Å, but there are certain arrangements wherein this bond is contracted.

Of the various imines examined here, one of them NHCHOH has available to it more than a single geometry. That is, the configuration examined and illustrated in Figure 5-3 has both the NH and OH hydrogen atoms cis to the CH. But either of these could also be trans to the CH, which could conceivably alter some of the trends discussed above. In order to check to see whether any such reversal might occur, a full set of calculations was carried out for the structure wherein the NH group is rotated around to lie trans to the CH. The five minima identified in the complex of this variant of NHCHOH are illustrated in Figure 5-6. The binding themes were found to be quite similar to the all-cis isomer in Figure 5-3, and indeed of all of the imines. The global minimum **E1** is like **B1**, again one in which a OH··S HB is supplemented by a NH··O interaction, with very similar interaction energy. The second minimum contains a NH··N/CH··S pair, just as in **A2/C2/D3**. And **E3** contains a bifurcated NH··N pair of HBs, quite similar to **A1**. Further reinforcing the similarities, SAPT decomposition of the interaction energies of these five E structures reveals nearly identical patterns as is evident in Figure 5-7, and electron density shifts mimic those of the other imines.

Finally, as was mentioned earlier, interaction energies have all been corrected for basis set superposition error. The counterpoise corrections are rather small, all less than 0.6 kcal/mol, some as small as 0.2 kcal/mol at the MP2/aug-cc-pVQZ level. On a percentage basis, these corrections amount to less than 5% in most cases.

## References

- (1) Dalko, P. I.; Moisan, L. *Angew. Chem. Int. Ed.* **2004**, *43*, 5138.
- (2) Seayad, J.; List, B. *Organic & Biomolecular Chemistry* **2005**, *3*, 719.
- (3) Dalko, P. I. In *Enantioselective Organocatalysis Reactions and Experimental Procedure*, Dalko, P. I., Ed. Wiley-VCH: Weinheim, 2007.
- (4) Mukherjee, S.; Yang, J. W.; Hoffmann, S.; List, B. *Chem. Rev.* **2007**, *107*, 5471.
- (5) MacMillan, D. W. C. *Nature* **2008**, *455*, 304.
- (6) Francis, M. B.; Finney, N. S.; Jacobsen, E. N. *J. Am. Chem. Soc.* **1996**, *118*, 8983.
- (7) Sigman, M. S.; Jacobsen, E. N. *J. Am. Chem. Soc.* **1998**, *120*, 4901.
- (8) Sigman, M. S.; Vachal, P.; Jacobsen, E. N. *Angew. Chem. Int. Ed.* **2000**, *39*, 1279.
- (9) Vachal, P.; Jacobsen, E. N. *Org. Lett.* **2000**, *2*, 867.
- (10) Yoon, T. P.; Jacobsen, E. N. *Angew. Chem. Int. Ed.* **2005**, *44*, 466.
- (11) Okino, T.; Nakamura, S.; Furukawa, T.; Takemoto, Y. *Org. Lett.* **2004**, *6*, 625.
- (12) Taylor, M. S.; Jacobsen, E. N. *J. Am. Chem. Soc.* **2004**, *126*, 10558.
- (13) Esrafil, M. D.; Mohammadian-Sabet, F. *Chem. Phys. Lett.* **2015**, *634*, 210.
- (14) Azofra, L. M.; Alkorta, I.; Scheiner, S. *J. Phys. Chem. A* **2015**, *119*, 535.
- (15) Zhou, F.; Liu, R.; Li, P.; Zhang, H. *New J. Chem.* **2015**, *39*, 1611.
- (16) Fanfrlík, J.; Přáda, A.; Padělková, Z.; Pecina, A.; Macháček, J.; Lepšík, M.; Holub, J.; Růžička, A.; Hnyk, D.; Hobza, P. *Angew. Chem. Int. Ed.* **2014**, *53*, 10139.
- (17) Desiraju, G. R.; Nalini, V. *J. Mater. Chem.* **1991**, *1*, 201.
- (18) Iwaoka, M.; Takemoto, S.; Tomoda, S. *J. Am. Chem. Soc.* **2002**, *124*, 10613.
- (19) Nziko, V. d. P. N.; Scheiner, S. *J. Phys. Chem. A* **2015**, *119*, 5889.
- (20) Werz, D. B.; Gleiter, R.; Rominger, F. *J. Am. Chem. Soc.* **2002**, *124*, 10638.



- (21) Sanz, P.; Mó, O.; Yáñez, M. *Phys. Chem. Chem. Phys.* **2003**, *5*, 2942.
- (22) Cozzolino, A. F.; Vargas-Baca, I.; Mansour, S.; Mahmoudkhani, A. H. *J. Am. Chem. Soc.* **2005**, *127*, 3184.
- (23) Nziko, V. d. P. N.; Scheiner, S. *J. Org. Chem.* **2015**, *80*, 2356.
- (24) Bleiholder, C.; Werz, D. B.; Koppel, H.; Gleiter, R. *J. Am. Chem. Soc.* **2006**, *128*, 2666.
- (25) Gleiter, R.; Werz, D. B.; Rausch, B. J. *Chem. Eur. J.* **2006**, *9*, 2676.
- (26) Nziko, V. d. P. N.; Scheiner, S. *J. Phys. Chem. A* **2014**, *118*, 10849.
- (27) Sánchez-Sanz, G.; Alkorta, I.; Elguero, J. *Mol. Phys.* **2011**, *109*, 2543.
- (28) Wu, C. H.; Ramamoorthy, A.; Gierasch, L. M.; Opella, S. J. *J. Am. Chem. Soc.* **1995**, *117*, 6148.
- (29) Frisch, M. J.; Trucks, G. W.; Schlegel, H. B.; Scuseria, G. E.; Robb, M. A.; Cheeseman, J. R.; Scalmani, G.; Barone, V.; Mennucci, B.; Petersson, G. A.; Nakatsuji, H.; Caricato, M.; Li, X.; Hratchian, H. P.; Izmaylov, A. F.; Bloino, J.; Zheng, G.; Sonnenberg, J. L.; Hada, M.; Ehara, M.; Toyota, K.; Fukuda, R.; Hasegawa, J.; Ishida, M.; Nakajima, T.; Honda, Y.; Kitao, O.; Nakai, H.; Vreven, T.; Montgomery, J., J. A.; Peralta, J. E.; Ogliaro, F.; Bearpark, M.; Heyd, J. J.; Brothers, E.; Kudin, K. N.; Staroverov, V. N.; Kobayashi, R.; Normand, J.; Raghavachari, K.; Rendell, A.; Burant, J. C.; Iyengar, S. S.; Tomasi, J.; Cossi, M.; Rega, N.; Millam, J. M.; Klene, M.; Knox, J. E.; Cross, J. B.; Bakken, V.; Adamo, C.; Jaramillo, J.; Gomperts, R.; Stratmann, R. E.; Yazyev, O.; Austin, A. J.; Cammi, R.; Pomelli, C.; Ochterski, J. W.; Martin, R. L.; Morokuma, K.; Zakrzewski, V. G.; Voth, G. A.; Salvador, P.; Dannenberg, J. J.; Dapprich, S.; Daniels, A. D.; Farkas,

O.; Foresman, J. B.; Ortiz, J. V.; Cioslowski, J.; Fox, D. J. *Gaussian 09*, Revision B.01; Wallingford, CT, 2009.

- (30) Boys, S. F.; Bernardi, F. *Mol. Phys.* **1970**, *19*, 553.
- (31) Helgaker, T.; Klopper, W.; Koch, H.; Noga, J. *J. Chem. Phys.* **1997**, *106*, 9639.
- (32) Mishra, B. K.; Karthikeyan, S.; Ramanathan, V. *J. Chem. Theory Comput.* **2012**, *8*, 1935.
- (33) Szalewicz, K.; Jeziorski, B. Symmetry-adapted perturbation theory of intermolecular interactions. In *Molecular Interactions. From Van der Waals to Strongly Bound Complexes*, Scheiner, S., Ed. Wiley: New York, 1997; pp 3.
- (34) Moszynski, R.; Wormer, P. E. S.; Jeziorski, B.; van der Avoird, A. *J. Chem. Phys.* **1995**, *103*, 8058.
- (35) Werner, H.-J.; Knowles, P. J.; Manby, F. R.; Schütz, M.; Celani, P.; Knizia, G.; Korona, T.; Lindh, R.; Mitrushenkov, A.; Rauhut, G.; Adler, T. B.; Amos, R. D.; Bernhardsson, A.; Berning, A.; Cooper, D. L.; Deegan, M. J. O.; Dobbyn, A. J.; Eckert, F.; Goll, E.; Hampel, C.; Hesselmann, A.; Hetzer, G.; Hrenar, T.; Jansen, G.; Köppl, C.; Liu, Y.; Lloyd, A. W.; Mata, R. A.; May, A. J.; McNicholas, S. J.; Meyer, W.; Mura, M. E.; Nicklaß, A.; Palmieri, P.; Pflüger, K.; Pitzer, R.; Reiher, M.; Shiozaki, T.; Stoll, H.; Stone, A. J.; Tarroni, R.; Thorsteinsson, T.; Wang, M.; Wolf, A. *MOLPRO*, Version 2006; 2010.
- (36) Reed, A. E.; Weinhold, F.; Curtiss, L. A.; Pochatko, D. J. *J. Chem. Phys.* **1986**, *84*, 5687.
- (37) Reed, A. E.; Curtiss, L. A.; Weinhold, F. *Chem. Rev.* **1988**, *88*, 899.
- (38) Bader, R. F. W. *Atoms in Molecules, A Quantum Theory*. Clarendon Press: Oxford, 1990; Vol. 22, p 438.

- (39) Carroll, M. T.; Chang, C.; Bader, M. F. W. *Mol. Phys.* **1988**, *63*, 387.
- (40) Keith, T. A. *AIMALL*, TK Gristmill Software: Overland Park KS, 2013.
- (41) Zheng, W.-R.; Fu, Y.; Shen, K.; Liu, L.; Guo, Q.-X. *Journal of Molecular Structure: THEOCHEM* **2007**, *822*, 103.
- (42) Weiqun, Z.; Wen, Y.; Lihua, Q. *Journal of Molecular Structure: THEOCHEM* **2005**, *730*, 133.
- (43) Jose, D. A.; Singh, A.; Das, A.; Ganguly, B. *Tetrahedron Lett.* **2007**, *48*, 3695.
- (44) Fleming, E. M.; Quigley, C.; Rozas, I.; Connon, S. J. *J. Org. Chem.* **2008**, *73*, 948.
- (45) Zheng, W.; Xu, J.; Huang, T.; Yang, Q.; Chen, Z. *Res Chem Intermed* **2011**, *37*, 31.

Table 5-1 Electron density ( $10^{-2}$  au) at indicated AIM bond critical point

A1	NH··N	1.66	B1	OH··S	2.98	C1	NH··N	3.04	D1	NH··N	2.08
	NH··N	1.66		NH··O	2.50		OH··S	2.74		NH··N	1.97
A2	NH··N	2.97	B2	NH··N	2.21	C2	NH··N	2.34	D2	NH··N	1.66
	OH··S	1.06		NH··O	1.36		CH··S	1.07		NH··N	1.58
A3	NH··N	2.74	B3	NH··N	2.76	C3	NH··N	1.78	D3	NH··N	2.94
	NH··S	1.36		NH··S	1.44		NH··N	1.04		CH··O	1.05
A4	NH··S	0.95	B4	C··N	0.79	C4	CH··S	0.55	D4	NH··N	1.97
										NH··S	1.49
A5	CH··S	0.56							D5	NH··N	1.24
	CH··S	0.56								CH··S	0.71
									D6	CH··S	0.59

Table 5-2 Interaction energies (kcal/mol) for complexes of thiourea with  $\text{CH}_2\text{NH}$  calculated with aug-cc-pV(X)Z basis set.

MP2					CCSD(T)	
X	D	T	Q	CBS	D	CBS
A1	9.11	9.73	9.97	10.15	8.62	9.66
A2	8.86	9.67	9.95	10.15	8.36	9.65
A3	8.45	9.31	9.58	9.78	7.84	9.17
A4	4.81	5.45	5.66	5.81	4.23	5.23
A5	1.70	1.89	1.96	2.01	1.59	1.90

Table 5-3 Interaction energies (kcal/mol) for complexes of thiourea with  $\text{NHCHOH}$ .

MP2					CCSD(T)	
X	D	T	Q	CBS	D	CBS
B1	12.10	13.31	13.76	14.09	11.51	13.50
B2	9.62	10.12	10.36	10.54	9.40	10.32
B3	9.20	10.08	10.36	10.56	8.60	9.96
B4	5.84	6.44	6.67	6.84	5.35	6.35

Table 5-4 Interaction energies (kcal/mol) for complexes of thiourea with CH<sub>2</sub>NOH.

MP2					CCSD(T)	
X	D	T	Q	CBS	D	CBS
C1	12.26	13.58	13.97	14.25	11.54	13.53
C2	6.44	7.17	7.42	7.60	6.16	7.32
C3	6.57	7.10	7.30	7.45	6.29	7.17
C4	1.63	1.82	1.89	1.94	1.54	1.85

Table 5-5 Interaction energies (kcal/mol) for complexes of thiourea with CH<sub>2</sub>NNH<sub>2</sub>.

MP2					CCSD(T)	
X	D	T	Q	CBS	D	CBS
D1	9.07	9.71	9.97	10.16	8.54	9.63
D2	8.48	9.02	9.24	9.40	8.05	8.97
D3	8.07	8.87	9.14	9.34	7.61	8.88
D4	7.71	8.73	9.05	9.28	6.88	8.45
D5	4.02	4.66	4.88	5.04	3.61	4.63
D6	1.56	1.75	1.82	1.87	1.43	1.74

Table 5-6 Changes in C-N bond length of imines (mÅ) caused by formation of indicated heterodimer

	A	B	C	D
1	2.2	4.0	1.9	-0.7
2	2.1	0.2	-0.7	2.3
3	-2.5	-2.7	0.8	-4.2
4	1.2	1.5	-0.3	4.8
5	1.0			2.9
6				0.0

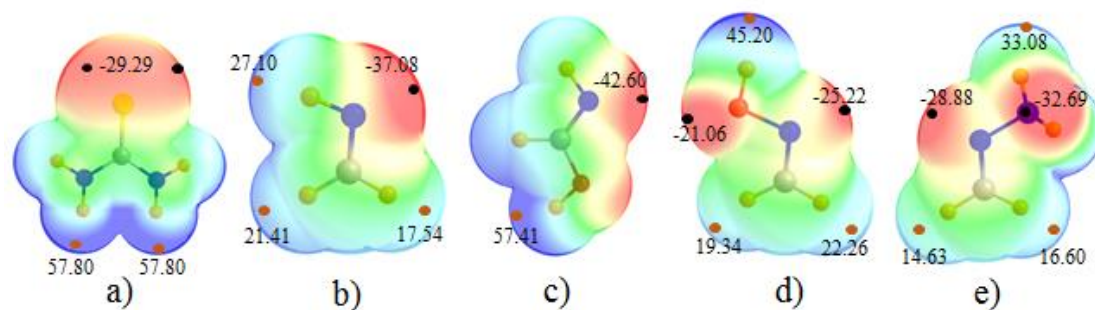


Figure 5-1 Molecular electrostatic potentials (MEPs) of a) thiourea, b)  $CH_2NH$ , c)  $NHCHOH$ , d)  $CH_2NOH$ , and e)  $CH_2NNH_2$ , all on a surface corresponding to  $1.5 \times$  vdW radii. Colors vary from  $-0.04$  au (red) to  $+0.04$  au (blue). Red/black dots indicate positions of  $V_{s,max}$

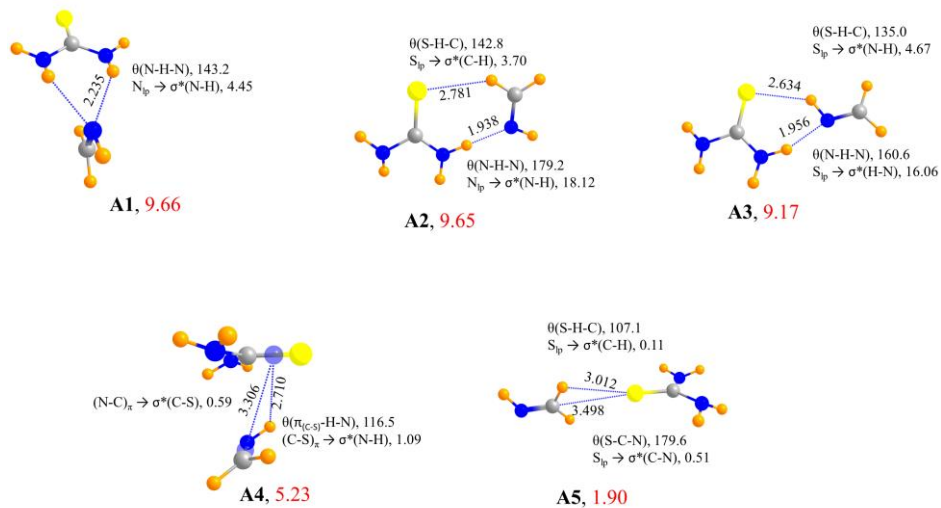


Figure 5-2 Optimized geometries of complexes of thiourea with  $\text{CH}_2\text{NH}$ . Red number refers to interaction energy (kcal/mol) evaluated at the CCSD(T)/CBS level. Distances are in Å, and angles in degs. The NBO value of  $E(2)$  is in kcal/mol.

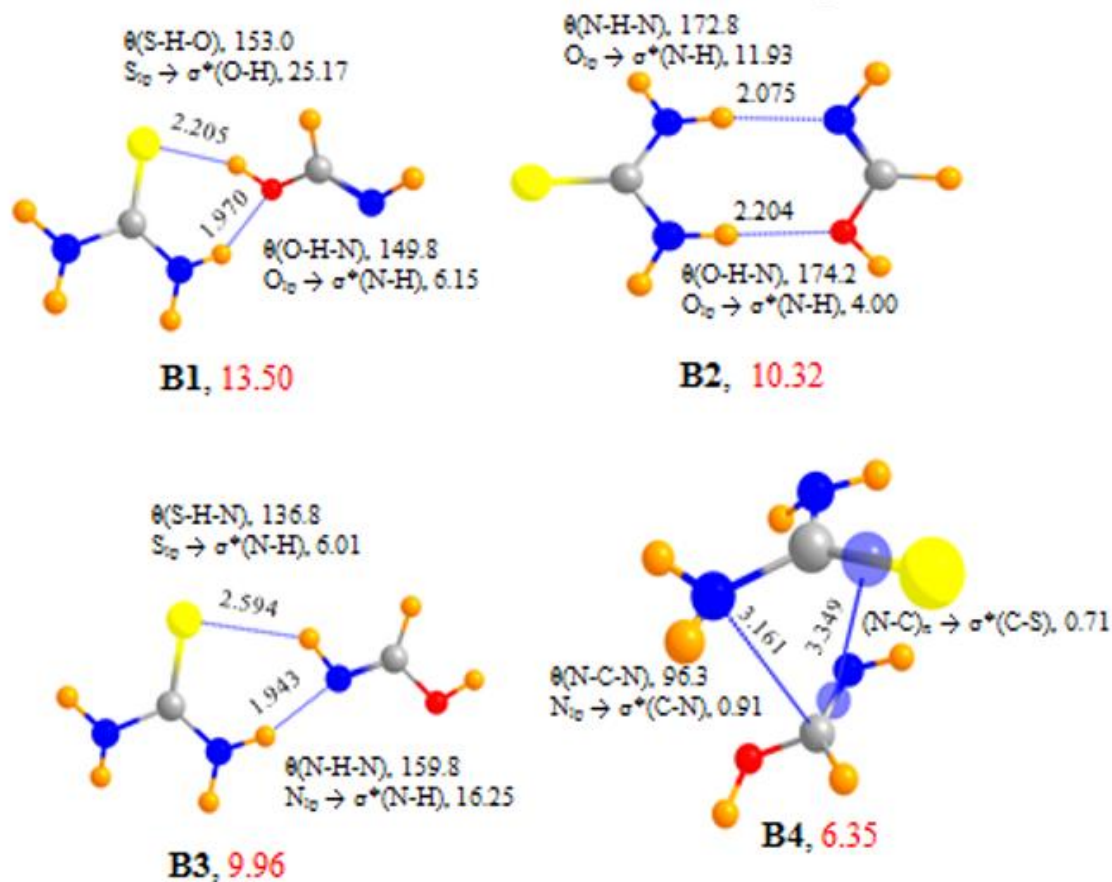


Figure 5-3 Optimized geometries of complexes of thiourea with NHCHOH. Red number refers to interaction energy (kcal/mol) evaluated at the CCSD(T)/CBS level. Distances are in Å, and angles in degs. The NBO value of E(2) is in kcal/mol.



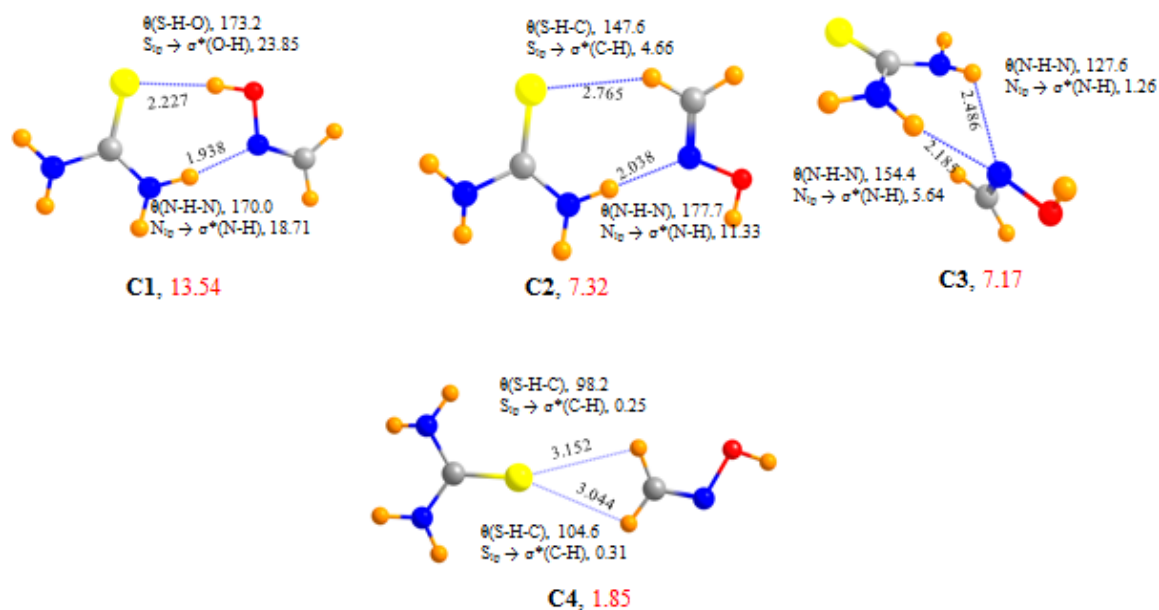


Figure 5-4 Optimized geometries of complexes of thiourea with  $\text{CH}_2\text{NOH}$ . Red number refers to interaction energy (kcal/mol) evaluated at the CCSD(T)/CBS level. Distances are in Å, and angles in degs. The NBO value of  $E(2)$  is in kcal/mol.

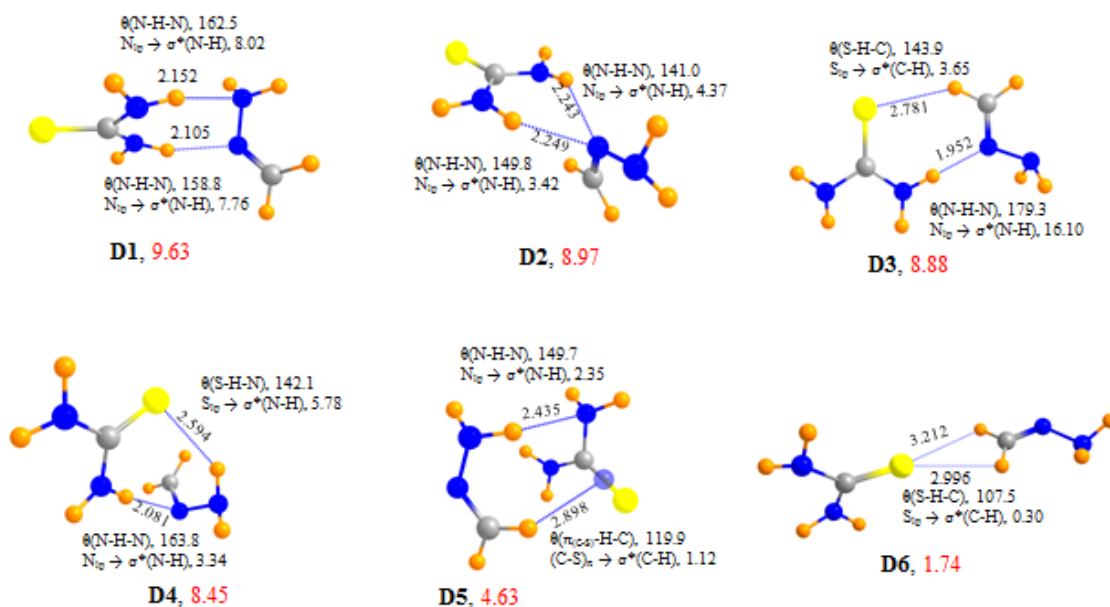


Figure 5-5 Optimized geometries of complexes of thiourea with  $\text{CH}_2\text{NNH}_2$ . Red number refers to interaction energy (kcal/mol) evaluated at the CCSD(T)/CBS level. Distances are in Å, and angles in degs. The NBO value of E(2) is in kcal/mol.

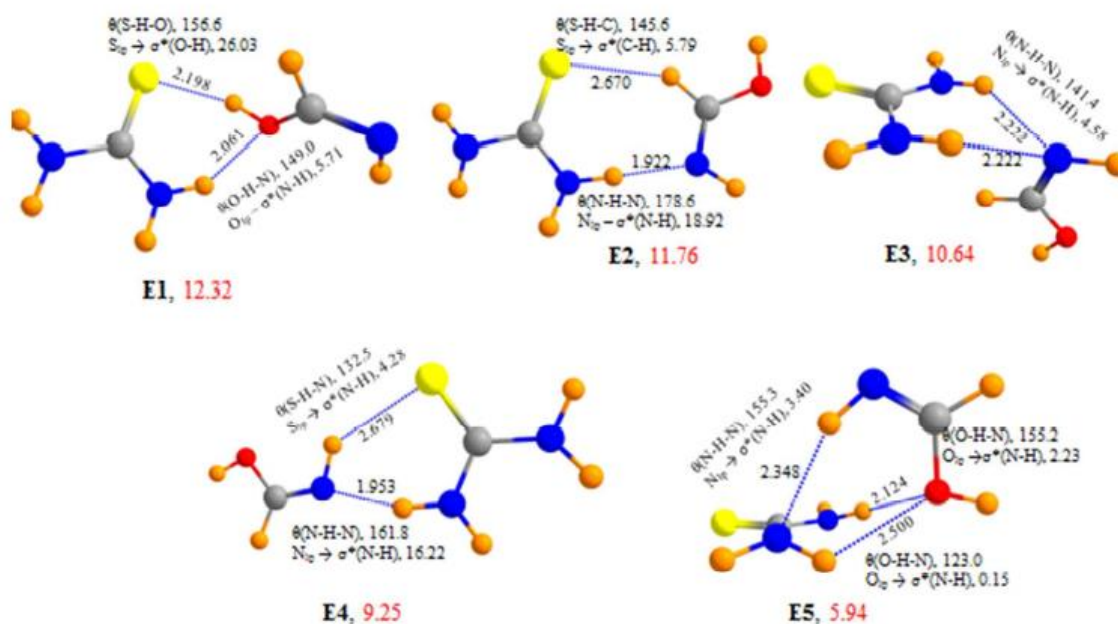


Figure 5-6 Optimized geometries of complexes of thiourea with  $\text{NHCHOH}$  with NH trans to CH number refers to interaction energy (kcal/mol) evaluated at the CCSD(T)/CBS level. Distances are in Å, and angles in degs. The NBO value of E(2) is in kcal/mol.

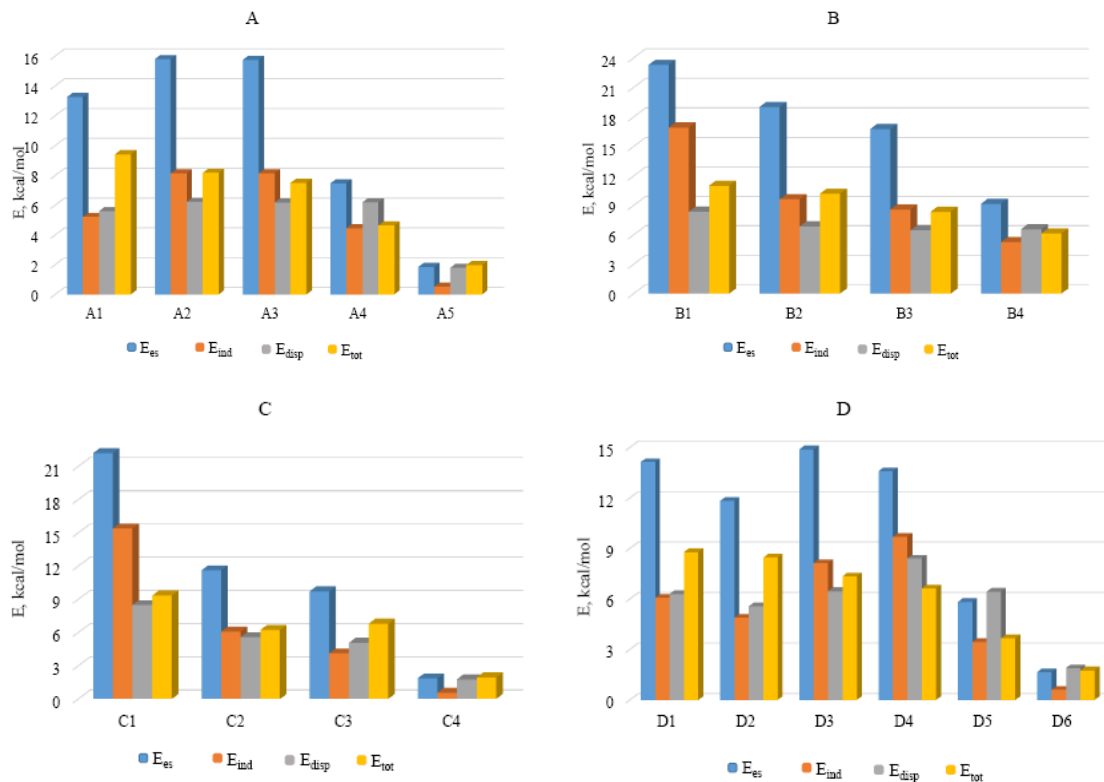


Figure 5-7 SAPT partitioning of interaction energies in complexes of thiourea with a)  $\text{CH}_2\text{NH}$ , b)  $\text{NHCHOH}$ , c)  $\text{CH}_2\text{NOH}$ , and d)  $\text{CH}_2\text{NNH}_2$ .

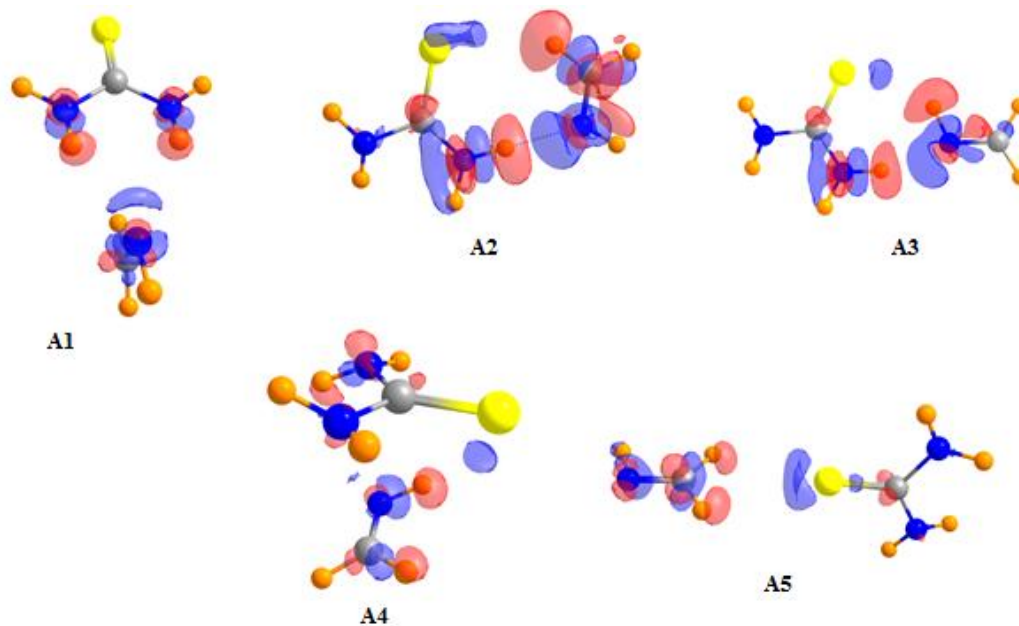


Figure 5-8 Calculated electron density shifts calculated at MP2/aug-cc-pVDZ level for complexes of thiourea with  $\text{CH}_2\text{NH}$ . Blue and red regions refer respectively to gain and loss of electron density upon complexation. Contours represent  $\pm 0.001$  au.

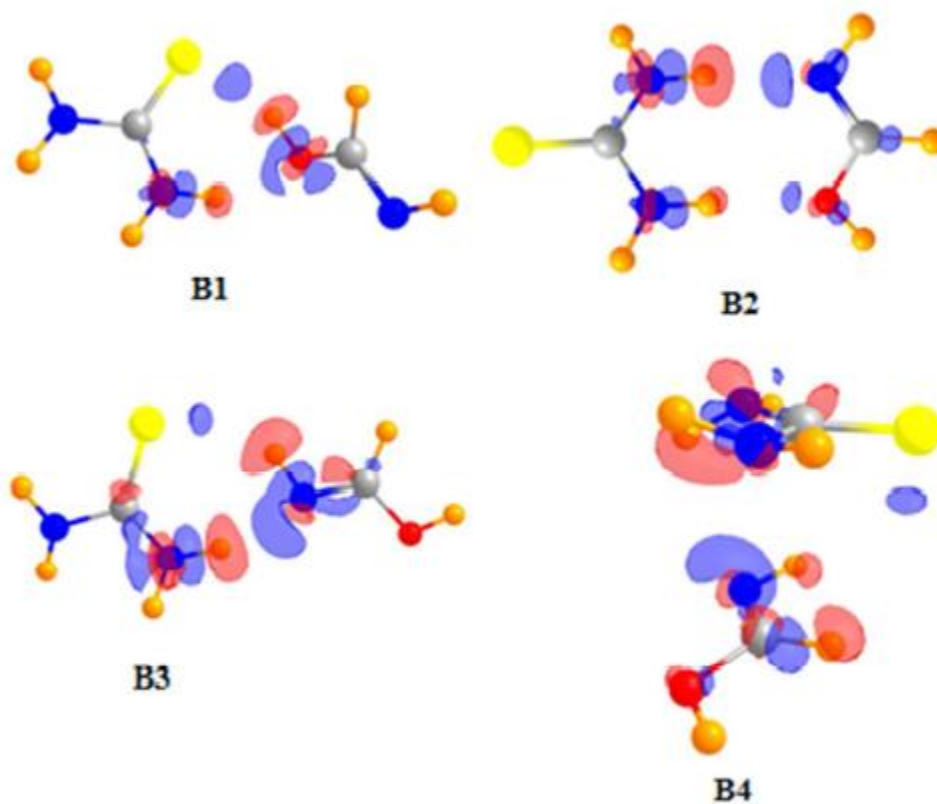


Figure 5-9 Calculated electron density shifts calculated at MP2/aug-cc-pVDZ level for complexes of thiourea with NHCHOH. Blue and red regions refer respectively to gain and loss of electron density upon complexation. Contours represent  $\pm 0.001$  au.

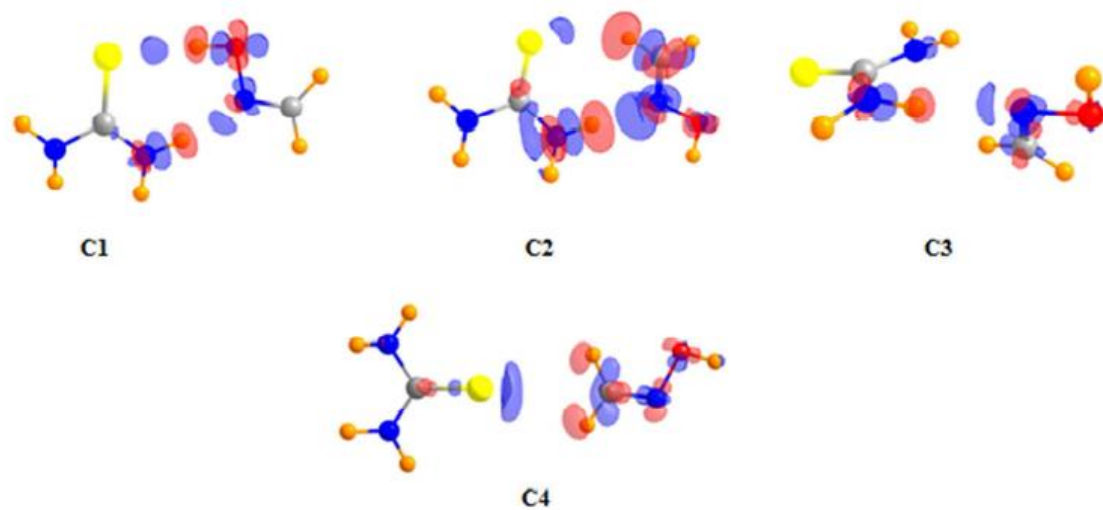


Figure 5-10 Calculated electron density shifts calculated at MP2/aug-cc-pVDZ level for complexes of thiourea with  $\text{CH}_2\text{NOH}$ . Blue and red regions refer respectively to gain and loss of electron density upon complexation. Contours represent  $\pm 0.001$  au.

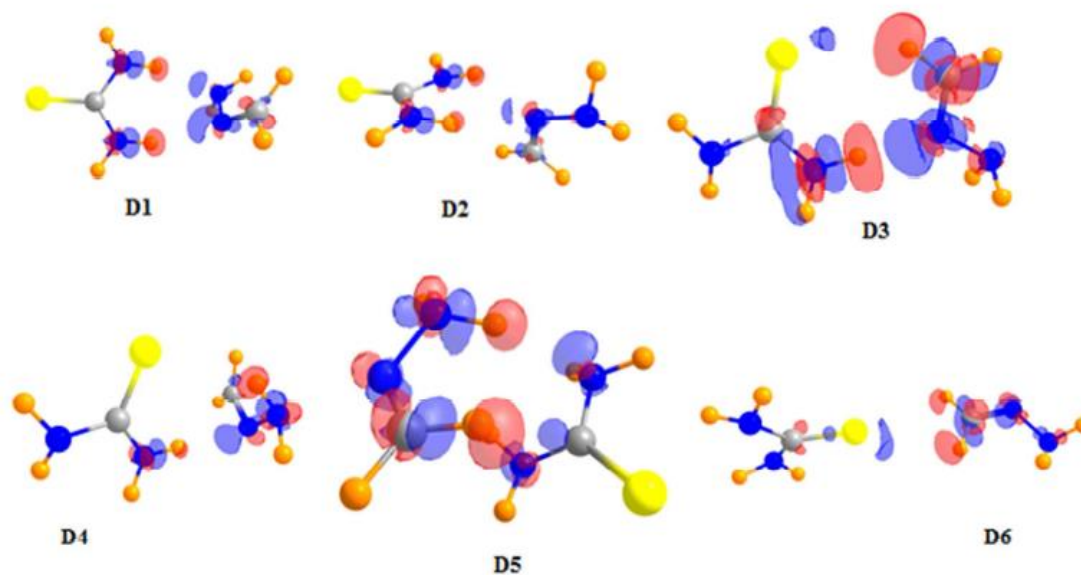


Figure 5-11 Calculated electron density shifts calculated at MP2/aug-cc-pVDZ level for complexes of thiourea with  $\text{CH}_2\text{NNH}_2$ . Blue and red regions refer respectively to gain and loss of electron density upon complexation. Contours represent  $\pm 0.001$  au.

## CHAPTER 6

COMPARISON OF  $\pi$ -HOLE TETREL BONDING WITH  $\Sigma$ -HOLE HALOGENBONDS IN COMPLEXES OF XCN (X = F, CL, BR, I) AND NH<sub>3</sub><sup>1</sup>**Abstract**

In addition to the standard halogen bond formed when NH<sub>3</sub> approaches XCN (X=F,Cl,Br,I) along its molecular axis, a perpendicular approach is also possible, toward a  $\pi$ -hole that is present above the X-C bond. MP2/aug-cc-pVDZ calculations indicate the latter geometry is favored for X=F, and the  $\sigma$ -hole structure is preferred for the heavier halogens. The  $\pi$ -hole structure is stabilized by charge transfer from the NH<sub>3</sub> lone pair into the  $\pi^*(\text{CN})$  antibonding orbital, and is characterized by a bond path from the N of NH<sub>3</sub> to the C atom of XCN, a form of tetrel bond. The most stable 2:1 NH<sub>3</sub>/XCN heterotrimer for X=F and Cl is cyclic and contains a tetrel bond augmented by a pair of NH $\cdots$ N H-bonds. For X=Br and I, the favored trimer is noncyclic, stabilized by a tetrel and a halogen bond.

**6-1. Introduction**

Noncovalent interactions play important roles in a wide range of chemical and biochemical processes such as molecular recognition, conformational changes, and molecular stacking in crystals<sup>1-3</sup>. The hydrogen bond (HB) has emerged as the most widely studied type of noncovalent interaction. Its original formulation that involved only O, N and F atoms has been expanded over the years to include C, Cl, S, and P as proton donor

---

<sup>1</sup> Coauthored by Vincent de Paul Nzuwah Nziko and Steve Scheiner. Reproduced with permission from *Phys. Chem. Chem. Phys.* **2016**, *18*, 3581-3590. Copyright 2016, Royal Society of Chemistry.



atoms<sup>4-13</sup>. There are also other types of noncovalent interactions in which the bridging atom is not H but rather a member of group IV, V, VI or VII, commonly denoted as tetrel<sup>14-17</sup>, pnictogen<sup>18-27</sup>, chalcogen<sup>28-36</sup>, and halogen bonds<sup>37-46</sup>, respectively.

These bond types share certain structural and electronic features. Along the extension of the Z-Y bond (Z = an electronegative atom and Y = a group IV, V, VI, or VII atom) their molecular electrostatic potential (MEP) usually contains a positive region, frequently referred to as a  $\sigma$ -hole. This idea has been expanded in the sense that the electron density of certain molecules is thinned out above the molecular plane, which accounts for a region of positive MEP in that area, sometimes denoted a  $\pi$ -hole. Whether in or out of the molecular plane, these areas of positive MEP are drawn toward sources of electron density in a neighboring molecule, typically either a lone pair or a  $\pi$ -bond.

Cyanogen halides (X-CN, X = F, Cl, Br or I) play an important role in chemical reactions especially in electrophilic substitution reactions in which CN acts as an electrophile. This reaction is particularly important in biopolymer modification and in protein and peptide fragmentation<sup>47-49</sup>. In organic synthesis, these compounds serve<sup>50, 51</sup> as a source of an extra carbon atom in the synthesis of guanidines and hydroxyguanidines when reacted with primary and/or hydroxylamines<sup>52</sup>. The cyanogen halides are also used<sup>53</sup> in the synthesis of nitriles, especially aryl nitriles.

Due to the importance of the C $\equiv$ N group, it has generated substantial examination of its electron donation to neighboring molecules via its N lone pair. Also well considered is its indirect effect on noncovalent interactions via its electron-withdrawing ability to strengthen  $\sigma$ -holes on neighboring atoms. However, there has been very little study of its

interactions with other molecules which are oriented perpendicular to it. In current lexicon, can the  $\text{-C}\equiv\text{N}$  group generate a region of positive electrostatic potential above itself, one that could be characterized as a  $\pi$ -hole? If that is the case, how strong might its interactions be with an incoming electron donor molecule? Also, given the strength of  $\text{C}\equiv\text{N}$  as an electron-withdrawing agent, it would deepen the  $\sigma$ -hole of the X atom on a  $\text{XC}\equiv\text{N}$  molecule on which it occurs. Would the ensuing  $\sigma$ -hole bond through this X atom be competitive with a potential  $\pi$ -hole interaction? And finally, how might the formation of either the  $\sigma$  or  $\pi$ -hole complex affect the ability of the XCN molecule to engage in an interaction with a third molecule?

While interactions involving  $\sigma$ -holes have drawn very extensive study, there is much less examination of  $\pi$ -hole analogues available in the literature<sup>54-66</sup>. There has been some recent study of  $\pi$ -holes connected with the  $\text{-NO}_2$  group<sup>67-75</sup>, for example, or noble gas systems such as  $\text{XeF}_4$  and  $\text{Xe(OMe)}_4$ <sup>76</sup>. But the  $\text{C}\equiv\text{N}$  group remains virtually unexplored in terms of its potential for  $\pi$ -hole interactions.

This work considers the halogen cyanides XCN where X spans the F, Cl, Br, I range of halogen atoms. In terms of  $\sigma$ -hole interactions, F is known as a very reluctant halogen-bonding atom, while I forms very strong halogen bonds, with Cl and Br intermediate. On the other hand, there is little known about how these halogens might affect the MEP above the  $\text{C}\equiv\text{N}$  axis, and the ability of this region to engage in  $\pi$ -hole interactions. The set of XCN molecules thus offers a useful means of comparison of  $\sigma$  and  $\pi$ -hole bonding.  $\text{NH}_3$  is chosen as the common electron donor, not only here but in numerous other studies<sup>44, 65, 70, 75, 77-80</sup> of these sorts of interactions. By adding a second  $\text{NH}_3$  molecule to the XCN/ $\text{NH}_3$

heterodimer, it becomes possible to examine the cooperativity of both sorts of noncovalent bonds. To the best of our knowledge this set of systems represents the first study of  $\pi$ -hole interaction with direct involvement of sp-hybridized carbon.

## 6-2. Methods

Gaussian 09, Rev D.01 and B.01<sup>81</sup> was used to carry out the ab initio calculations. Geometries of all species were fully optimized at the MP2 level with the aug-cc-pVDZ basis set for all atoms except for I for which the aug-cc-pVDZ-PP set was adopted to account for relativistic effects. Minima were confirmed by the lack of any imaginary frequencies. Interaction energies were computed as the difference in energy between the optimized complex and the sum of monomer energies, within the complex geometry reference frame. Three-body components for the trimer systems ( $\Delta^3E$ ) were evaluated via Eqs (1) and (2).

$$\Delta^3E(ABC) = E_{\text{int}}(ABC) - (\Delta^2E(AB) + \Delta^2E(AC) + \Delta^2E(BC)) \quad (1)$$

$$\Delta^2E(AB) = E_{AB} - (E_A + E_B) \quad (2)$$

Higher level calculations expanded the basis set to aug-cc-pVTZ and aug-cc-pVQZ, using the MP2/aug-cc-pVDZ geometries. CCSD(T) was also employed with the aug-cc-pVDZ basis set. One can extrapolate the data from the ordered DZ, TZ, QZ basis sets to an estimate of complete basis set (CBS) results. Extrapolation was based on the idea<sup>82</sup> that correlation energy is roughly proportional to  $X^{-3}$  for basis sets of the aug-cc-pVXZ type. Utilizing a two-step method with triple and quadruple sets<sup>83</sup>:

$$\Delta E_{\text{MP2/CBS}} = (64 \Delta E_{\text{MP2/aug-cc-pVQZ}} - 27 \Delta E_{\text{MP2/aug-cc-pVTZ}}) / 37 \quad (3)$$

A correction was added to account for discrepancies between MP2 and CCSD(T)

$$E_{\text{CCSD(T)/CBS}} = E_{\text{MP2/CBS}} + (E_{\text{CCSD(T)/aug-cc-pVDZ}} - E_{\text{MP2/aug-cc-pVDZ}}) \quad (4)$$

All interaction energies were corrected for basis set superposition error using the standard counterpoise method <sup>84</sup>. Natural Bond Order (NBO) treatment of charge transfer <sup>85-87</sup> was carried out via the M06-2X DFT method with the aug-cc-pVDZ basis set, as this procedure includes electron correlation and was designed so as to treat intermolecular interactions with some accuracy. Atoms in Molecules (AIM) analysis <sup>88, 89</sup> of the wave function was performed via the AIMall package <sup>90</sup> to assess the presence of bond paths. The total interaction energy was dissected into various components by symmetry-adapted perturbation theory (SAPT) <sup>91-93</sup> using the MOLPRO program <sup>93</sup>, at the PBE0 DFT level <sup>94-96</sup> with the aug-cc-pVDZ set. Maxima and minima of the molecular electrostatic potential were derived via the WFA-SAS program <sup>97</sup>, using the MP2/aug-cc-pVDZ electron density.

### 6-3. Results

#### 6-3. 1. Monomers

The MEP of each XCN monomer is illustrated in Figure 6-1, where red and blue regions indicate negative and positive potentials, respectively. These MEPs share certain features. All exhibit a red negative region along the projection of the C-N bond, corresponding to a N lone pair. There is a positive region on the opposite end of each molecule, a  $\sigma$ -hole along the C-X bond. There is another positive area located above the X-C bond, which might be referred to as a  $\pi$ -hole. The magnitudes of these potentials can be assessed via the maxima and minima on the  $\rho=0.001$  au isodensity surfaces, which are

indicated by the black and blue dots, respectively. As one progresses to larger halogen atoms,  $F \rightarrow Cl \rightarrow Br \rightarrow I$ , the value of the minimum near N becomes slightly more negative, varying from -27.2 to -31.6 kcal/mol, which can be explained by the progressively smaller electron-withdrawing power of the halogen. More sensitive to the identity of X is the magnitude of the  $\pi$ -hole which reaches as high as 28.2 kcal/mol for  $X=F$  and drops down to only 10.7 kcal/mol for  $X=I$ . Also sensitive to the halogen, but varying in the opposite direction is the magnitude of the  $\sigma$ -hole, which is only +14.5 kcal/mol for  $X=F$  but increases all the way up to +47.9 kcal/mol for  $X=I$ .

### 6-3. 2. Heterodimers

One would expect that nucleophilic  $NH_3$ , and specifically its lone pair, to approach one of the two positive regions of  $XCN$ . And in fact, this expectation is confirmed. The two sorts of minima obtained are illustrated in Figure 6-2. In the upper set of structures, the N lone pair approaches the  $\pi$ -hole lying above the C-X bond, while the second set of geometries fall in the category of standard  $\sigma$ -hole halogen bonds. The interatomic distances in Figure 6-2 conform to the pattern of MEP maxima: These distances get longer for the  $F \rightarrow Cl \rightarrow Br \rightarrow I$  progression of the  $\pi$ -hole configurations, and shorter for the  $\sigma$ -holes.

These distances are displayed in Table 6-1 and Table 6-2, along with the counterpoise-corrected interactions energies in the first column. The halogen bonds get very much stronger as the halogen atom becomes larger, but the  $\pi$ -hole interaction energies in Table 6-1 are less sensitive to halogen atom, again fitting the MEP patterns in Figure 6-1. Very similar patterns may be noted in the electronic markers of the noncovalent bond. The blue numbers in Figure 6-2 correspond to the energetic manifestation of the charge

transfer from the N lone pair to the  $\pi^*(\text{CN})$  antibonding orbital for the  $\pi$ -hole complexes, and to  $\sigma^*(\text{CX})$  for the  $\sigma$ -bonded congeners. This quantity increases dramatically in the order  $\text{F} < \text{Cl} < \text{Br} < \text{I}$  for the  $\sigma$ -hole structures, but diminishes slowly for the  $\pi$ -hole geometries. The same applies to the electron densities at the appropriate AIM bond critical points, displayed after the / mark in Figure 6-2. The corresponding bond paths in the  $\pi$ -hole dimers connect N of  $\text{NH}_3$  with the C atom. For this reason, these structures might be considered a sort of tetrel bond, although the presence of such a bond path does not necessarily prove<sup>98</sup> the existence of a noncovalent bond.

Along with the charge transfer in the  $\sigma$ -hole complexes into the  $\sigma^*(\text{CX})$  antibonding orbital one can see the lengthening of this bond reported in the last column of Table 6-2, again increasing as the halogen becomes larger. In contrast, the  $\text{C}\equiv\text{N}$  bond of  $\text{XCN}$  shows only marginal changes in length upon formation of the  $\pi$ -hole complexes in Table 6-1. It is worth noting that neither NBO nor AIM data are consistent with any sort of  $\text{NH}\cdots\text{N}$  H-bond in the  $\pi$ -hole complexes, despite a  $\text{H}\cdots\text{N}$  distance of less than 3 Å (see Figure 6-2). Comparison of the energetics of the two sorts of complexes shows that the halogen-bonded  $\text{NCX}\cdots\text{NH}_3$  structures are favored for  $\text{X}=\text{Cl}$ ,  $\text{Br}$ , and  $\text{I}$ , but that there is a strong preference for the tetrel bond for  $\text{FCN}$ . This distinction again conforms to the increasing/decreasing magnitude of the  $\pi/\sigma$  hole maximum in the  $\text{XCN}$  sequence. Similar observations apply to both the NBO and AIM measures of the noncovalent bond strength: these quantities are larger for the  $\sigma$ -hole complexes for  $\text{X}=\text{Cl}$ ,  $\text{Br}$ , and  $\text{I}$ , but the reverse is true for  $\text{X}=\text{F}$ .

The nature of the bonding in complexes such as these can also be examined through the lens of electron density shifts. These shifts, displayed in Figure 6-3 for the four  $\pi$ -hole

complexes, were evaluated as the difference between the total electron density of the complex, minus the sum of the densities of the two monomers, located in the same positions as in the dimer. The yellow regions correspond to an increase of density accruing from complexation, while depletions are signaled by green. The dominant feature of these diagrams is the yellow buildup of density in the region of the N lone pair, coupled with the green loss above the C-X bond, consistent with the idea of the interaction with the XCN  $\pi$ -hole. Note that the extent of these two regions diminishes as one goes from left to right, from F to I. This pattern is consistent with the AIM data concerning the strength of the N $\cdots$ C tetrel bond.

Another interesting feature of Figure 6-3 is the reduced involvement of the central C atom with heavier halogens. That is, as one moves from left to right in Figure 6-3, the green depletion region over the XCN molecule shifts away from the C and toward the halogen. This green region above the C is rather extensive for FCN, but shrinks to a far smaller area for ICN.

The density shifts in Figure 6-3 also show indications of a HB between two of the NH<sub>3</sub> protons and the XCN N atom, albeit a weak one. This interaction is marked by the small green loss of density around these bridging H atoms and a yellow gain above the N atom. On the other hand, AIM does not suggest the presence of a H-bond path, even a weak one, nor was there any significant NBO charge transfer from N to  $\sigma^*(\text{NH})$ . One may conclude that any such HB would indeed be a weak one, with negligible contribution to the total binding.

Decomposition of the total interaction energies can add insights into the nature of

the bonding. The SAPT procedure partitions the total attractive forces into electrostatic (ES), induction (IND), and dispersion (DISP), leaving exchange (EX) as the repulsive term which prevents coalescence into a single entity. Perusal of the data in Table 6-3 shows that ES and IND make the largest contributions to the  $\pi$ -hole complexes, roughly equal to one another, with DISP are not far behind. These quantities are largest for X=F, and roughly equivalent for the three other halogens. In the  $\sigma$ -hole complexes of Table 6-4, on the other hand, all of the terms grow rapidly as the halogen atom becomes heavier. The ES term for X=I is some 12 times larger than for X=F, and this ratio is 40 for induction energy. ES is the largest contributor for F, but it is far exceeded by IND for Br and I; DISP is the smallest of the three attractive terms. In conclusion, the  $\pi$ -hole complexes are characterized by a nearly equivalent ES, IND, and DISP, and a low sensitivity to the identity of X. The nature of the halogen atom makes a huge difference in the  $\sigma$ -hole complexes, with all three attractive terms becoming more so for the heavier atoms; it is IND that makes the dominant contribution for Br and I. In most cases, the total SAPT interaction in the final column of Table 6-3 and Table 6-4 matches quite closely the supermolecular quantities in Table 6-1 and Table 6-2. The sole exception is the  $\text{NCI}\cdots\text{NH}_3$   $\sigma$ -hole complex where the former exceeds the latter by several kcal/mol. This difference may be associated with the very large induction energy for this complex in the final row of Table 6-4.

Of course, MP2/aug-cc-pVDZ does not represent the final word in terms of the interaction energies. It is worthwhile to examine how the interaction energetics might be affected if higher levels of theory were applied. The first few columns of Table 6-5 and Table 6-6 show that enlargement of the basis set first to triple and then to quadruple- $\zeta$  leads



to small enhancements of the interaction energies at the MP2 level. Extrapolation to the complete basis set then yields another small increment. Including electron correlation via CCSD(T), on the other hand, produces smaller interaction energies than does MP2, although this decrement is fairly small. The CCSD(T) data with a complete basis set, reported in the last columns of Table 6-5 and Table 6-6, are close to but a bit larger than the MP2/aug-cc-pVDZ results, generally closer to MP2/aug-cc-pVTZ.

### 6-3. 3. Heterotrimers

It is of interest to gauge the effect that a second  $\text{NH}_3$  molecule might exert upon the  $\pi$ -hole heterodimers. The optimized geometries adopted by the  $(\text{NH}_3)_2\text{XCN}$  heterotrimers that contain such a  $\pi$ -bond are displayed in Figure 6-4. T1 pairs the tetrel and halogen-bonded structures of the dimer together in a single trimer. The latter XB is replaced by a second  $\pi$ -hole bond in T2. Instead of XCN as central molecule, it is  $\text{NH}_3$  that serves this function in T3. T4 and T5 are cyclic in that each molecule interacts directly with both of the remaining molecules. T4 combines a tetrel bond with a pair of  $\text{NH}\cdots\text{N}$  HBs. The geometry of T5 is similar except that the third  $\text{NH}_3$  molecule is inverted, i.e. it engages in a HB with the other  $\text{NH}_3$  unit via the smaller lobe of its N lone pair.

The interaction energies of the five trimer structures are reported in Table 6-7 for all of the  $\text{XCN}(\text{NH}_3)_2$  heterotrimers. For both FCN and ClCN, cyclic structure T4 is most stable; however, the preferred trimer is T1 for BrCN and ICN. This preference is likely a result of the very strong halogen bonds in which the latter two molecules engage, an interaction which is only present in T1. It may be noted that T1 does not represent a minimum on the surface of the FCN trimer, a consequence of the very weak XB formed

by FCN. The inverse HB present in T5 is weak enough that this configuration is the least stable in all cases, and is not even present for ICN.

In both T1 and T2, the central XCN molecule serves as double electron acceptor. One would hence expect some degree of negative cooperativity. This anticipation is confirmed by comparison of the interaction energies with those in parentheses in Table 6-7. The latter quantities represent a simple sum of the pertinent interaction energies in the dimers:  $\sigma$ -hole +  $\pi$ -hole for T1 and 2 x  $\pi$ -hole for T2. The actual interaction energies are somewhat smaller than the sums, consistent with negative cooperativity. This negative cooperativity is verified by comparison of the NBO/AIM data for the trimers and the dimers. Taking X=Cl as an example, the NBO charge transfer is 0.99 kcal/mol in the dimer of Figure 6-4 to Figure 6-7, but is reduced below 0.6 kcal/mol in T1 and T2. The BCP density is similarly diminished and in fact the bond path disappears entirely for T2. The  $\sigma$ -hole charge transfer energy is 3.25 kcal/mol for the  $\text{NCCl}\cdots\text{NH}_3$  dimer, and it diminishes but only slightly in T1; likewise, for  $\text{pBCP}$ . Very similar trends are observed for the other XCN dimers and trimers.

Rather than comparing the structures of the heterotrimers to fully optimized dimers, another view of the cooperativity may be achieved by a multi-body analysis in which pairwise interaction energies are evaluated within the geometry of the optimized trimer. The difference between the sum of all three pairwise interaction energies (whether the geometry is cyclic or linear) and the total interaction energy of the trimer is equal to a three-body term,  $\Delta^3E$ , which can be equated with an energetic measure of cooperativity. These three-body terms are listed in Table 6-8 where negative quantities refer to an enhancement

of the interaction and hence to a positive cooperativity.  $\Delta^3E$  is slightly positive for T2, consistent with the negative cooperativity. On the other hand,  $\Delta^3E$  is slightly negative for T1 although negative cooperativity might be anticipated there. This apparent contradiction may be related to the incorporation into the formalism of a small but repulsive two-body interaction between the two  $\text{NH}_3$  molecules which are far apart. A similar inter- $\text{NH}_3$  repulsion may be similarly responsible for the small values of  $\Delta^3E$  for T2 which might otherwise be more positive. T3-T5 all display positive cooperativity, most notably T4 which is the most stable trimer in a number of cases.

#### 6-4. Discussion and Conclusion

$\text{NH}_3$  can approach the XCN molecules from one of two directions. A standard  $\sigma$ -hole halogen bond is formed if the  $\text{NH}_3$  approaches the X atom along the NCX axis. The strength of this bond grows rapidly in the usual  $\text{F} < \text{Cl} < \text{Br} < \text{I}$  sequence, ranging from 1.1 kcal/mol for  $\text{X}=\text{F}$  to 8.2 kcal/mol for I. There is also a region of positive MEP above the axis of the XCN molecule. The maximum of this  $\pi$ -hole area is larger than that of the  $\sigma$ -hole for FCN, but the opposite is true for the other XCN molecules. Unlike the sensitivity of the MEP  $\pi$  maximum to the identity of X, the interaction energies of the  $\pi$ -hole dimers are fairly uniform in the range between 2.4 and 3.1 kcal/mol. The  $\pi$ -hole complex is more stable than the  $\sigma$ -hole analogue for FCN, but it is the  $\sigma$ -hole structure that is preferred for the other XCN molecules.

NBO analysis traces the stability of the  $\pi$ -hole geometries in large measure to charge transfer from the  $\text{NH}_3$  lone pair to the  $\pi^*(\text{CN})$  antibonding orbital, whose behavior parallels the energetics of binding. The AIM topology of the electron density ascribes the

interaction to a bond between the N of  $\text{NH}_3$  and C of  $\text{XCN}$ , and also scales nicely with  $E_{\text{int}}$ . The electrostatic component of the total interaction energy is the largest, but induction and dispersion are not far behind. Like the total interaction, the components are also relatively insensitive to the identity of X. This behavior differs markedly from the halogen-bonded dimers where both ES and IND grow quickly with the size of the halogen atom, and IND exceeds ES for Br and I; DISP is considerably smaller.

A second  $\text{NH}_3$  molecule has several options for binding to the  $\text{NH}_3/\text{XCN}$  heterotrimer. The resulting trimer may contain both a  $\sigma$  and  $\pi$ -hole arrangement, or two of the latter, with the two  $\text{NH}_3$  molecules on opposite sides of  $\text{XCN}$ . There are also three different geometries wherein the two  $\text{NH}_3$  units engage in HBs with one another. For  $\text{X}=\text{F}$  and  $\text{Cl}$ , the preferred structure is one of the latter, which includes i) a  $\pi$ -hole interaction, ii) a  $\text{NH}\cdots\text{N}$  HB between the two  $\text{NH}_3$  molecules, and iii) a  $\text{NH}\cdots\text{N}$  HB to the  $\text{XCN}$  N atom. The strength of the halogen bonds for  $\text{X}=\text{Br}$  and  $\text{I}$  is an overwhelming factor so that the most stable heterotrimer contains this bond as well as a tetrel bond. The energetics, as well as the NBO and AIM characteristics, obey the expected cooperativity trends in that they are enhanced or diminished respectively when a given molecule serves as electron donor and acceptor, or as double acceptor.

As mentioned earlier, the  $\pi$ -hole characteristics of the  $\text{C}\equiv\text{N}$  group have not been explored previously at any length, so comparison with other data in the literature is difficult. On the other hand, there have been a number of studies of the  $-\text{NO}_2$  group which together offer a point of comparison. The  $\pi$ -hole of the  $\text{NO}_2$  group is centered directly over the N atom<sup>69, 72, 73, 75</sup> so dimers of relevant molecules tend to place an electronegative atom

of one molecule over the N of the other. There are indications that these interactions tend to be dominated by dispersion. Like XCN, the  $\pi$ -hole over the NO<sub>2</sub> subunit in XNO<sub>2</sub> becomes weaker in the order Cl > Br > I<sup>70, 73</sup>, but this trend is stronger than in the case of XCN. When placed on a phenyl ring, the NO<sub>2</sub> group engages in  $\pi$ -hole complexes with a variety of nucleophiles with binding energies that range up to more than 6 kcal/mol<sup>71</sup>, wherein AIM places the bond to the N atom in most cases, but also to the phenyl C to which the NO<sub>2</sub> group is connected. In addition to a lone pair, the  $\pi$ -bonding pair of a simple alkene or alkyne<sup>67</sup> can also interact with the  $\pi$ -hole of NO<sub>2</sub>, in which case the dispersion energy exceeds the ES component.

With specific respect to the NH<sub>3</sub> nucleophile, interaction energies of XNO<sub>2</sub> with NH<sub>3</sub> are slightly larger than is the case for XCN<sup>73</sup>. Overall, the XNO<sub>2</sub> series has similar behavior as XCN<sup>75</sup>. The halogen-bonded structure is favored for X=Br and I, but the  $\pi$ -hole preferred for X=Cl. Unlike the situation for XCN, trimers of the T1 type display both positive and negative cooperativity, depending upon the nature of X. Curiously, BrNO<sub>2</sub> favors the  $\sigma$ -hole halogen bond with NH<sub>3</sub> but the  $\pi$ -hole is preferred<sup>74</sup> for certain other nucleophiles.

## References

1. P. Auffinger, F. A. Hays, E. Westhof and P. S. Ho, *Proc. Nat. Acad. Sci., USA*, 2004, **101**, 16789-16794.
2. A. D. Buckingham, P. W. Fowler and J. M. Hutson, *Chem. Rev.*, 1988, **88**, 963-988.

3. M. G. Chudzinski, C. A. McClary and M. S. Taylor, *J. Am. Chem. Soc.*, 2011, **133**, 10559-10567.
4. M. Nishio, Y. Umezawa, K. Honda, S. Tsuboyama and H. Suezawa, *CrystEngComm*, 2009, **11**, 1757-1788.
5. B. J. van der Veken, S. N. Delanoye, B. Michielsens and W. A. Herrebout, *J. Mol. Struct.*, 2010, **976**, 97-104.
6. S. Scheiner, Y. Gu and T. Kar, *J. Mol. Struct. (Theochem)*, 2000, **500**, 441-452.
7. Y. Gu, T. Kar and S. Scheiner, *J. Mol. Struct.*, 2000, **552**, 17-31.
8. M. Domagala and S. J. Grabowski, *Chem. Phys.*, 2010, **367**, 1-6.
9. E. Arunan, G. R. Desiraju, R. A. Klein, J. Sadlej, S. Scheiner, I. Alkorta, D. C. Clary, R. H. Crabtree, J. J. Dannenberg, P. Hobza, H. G. Kjaergaard, A. C. Legon, B. Mennucci and D. J. Nesbitt, *Pure Appl. Chem.*, 2011, **83**, 1637-1641.
10. Z. Latajka and S. Scheiner, *J. Chem. Phys.*, 1987, **87**, 5928-5936.
11. H. S. Biswal, E. Gloaguen, Y. Loquais, B. Tardivel and M. Mons, *J. Phys. Chem. Lett.*, 2012, **3**, 755-759.
12. S. Scheiner, S. J. Grabowski and T. Kar, *J. Phys. Chem. A*, 2001, **105**, 10607-10612.
13. E. Kryachko and S. Scheiner, *J. Phys. Chem. A*, 2004, **108**, 2527-2535.
14. D. Mani and E. Arunan, *Phys. Chem. Chem. Phys.*, 2013, **15**, 14377-14383.
15. D. Mani and E. Arunan, *J. Phys. Chem. A*, 2014, **118**, 10081-10089.
16. S. J. Grabowski, *Phys. Chem. Chem. Phys.*, 2014, **16**, 1824-1834.
17. A. Bauzá, T. J. Mooibroek and A. Frontera, *Angew. Chem. Int. Ed.*, 2013, **52**, 12317-12321.
18. M. D. Esrafil and F. Mohammadian-Sabet, *Chem. Phys. Lett.*, 2015, **638**, 122-127.

19. H. Zhuo and Q. Li, *Phys. Chem. Chem. Phys.*, 2015, **17**, 9153-9160.
20. I. Alkorta, J. Elguero and S. J. Grabowski, *Phys. Chem. Chem. Phys.*, 2015, **17**, 3261-3272.
21. J. E. Del Bene, I. Alkorta and J. Elguero, *J. Phys. Chem. A*, 2014, **119**, 224-233.
22. S. Sarkar, M. S. Pavan and T. N. Guru Row, *Phys. Chem. Chem. Phys.*, 2015, **17**, 2330-2334.
23. M. Solimannejad, E. Bayati and M. D. Esrafil, *Mol. Phys.*, 2014, **112**, 2058-2062.
24. G. Sanchez-Sanz, C. Trujillo, I. Alkorta and J. Elguero, *Phys. Chem. Chem. Phys.*, 2014, **16**, 15900-15909.
25. S. J. Grabowski, *Chem. Eur. J.*, 2013, **19**, 14600-14611.
26. S. Zahn, R. Frank, E. Hey-Hawkins and B. Kirchner, *Chem. Eur. J.*, 2011, **17**, 6034-6038.
27. S. Scheiner, *Int. J. Quantum Chem.*, 2013, **113**, 1609-1620.
28. A. Lange, M. Günther, F. M. Büttner, M. O. Zimmermann, J. Heidrich, S. Hennig, S. Zahn, C. Schall, A. Sievers-Engler, F. Ansideri, P. Koch, M. Laemmerhofer, T. Stehle, S. A. Laufer and F. M. Boeckler, *J. Am. Chem. Soc.*, 2015, **137**, 14640-14652.
29. J. W. Keller, *J. Phys. Chem. A*, 2015, **119**, 10390-10398.
30. V. d. P. N. Nziko and S. Scheiner, *J. Phys. Chem. A*, 2014, **118**, 10849-10856.
31. S. P. Thomas, K. Satheeshkumar, G. Mugesh and T. N. Guru Row, *Chem. Eur. J.*, 2015, **21**, 6793-6800.
32. V. d. P. N. Nziko and S. Scheiner, *J. Org. Chem.*, 2015, **80**, 2356-2363.
33. A. Bauzá, I. Alkorta, A. Frontera and J. Elguero, *J. Chem. Theory Comput.*, 2013, **9**, 5201-5210.

34. M. Iwaoka and N. Isozumi, *Molecules*, 2012, **17**, 7266-7283.
35. G. Sánchez-Sanz, C. Trujillo, I. Alkorta and J. Elguero, *ChemPhysChem.*, 2012, **13**, 496–503.
36. U. Adhikari and S. Scheiner, *J. Phys. Chem. A*, 2012, **116**, 3487-3497.
37. W. Zierkiewicz, D. C. Bieńko, D. Michalska and T. Zeegers-Huyskens, *J. Comput. Chem.*, 2015, **36**, 821-832.
38. M. Tawfik and K. J. Donald, *J. Phys. Chem. A*, 2014, **118**, 10090-10100.
39. A. Mukherjee, S. Tothadi and G. R. Desiraju, *Acc. Chem. Res.*, 2014, **47**, 2514-2524.
40. S. J. Grabowski, *Chem. Phys. Lett.*, 2014, **605-606**, 131-136.
41. A. J. Stone, *J. Am. Chem. Soc.*, 2013, **135**, 7005-7009.
42. A. Bauzá, D. Quiñonero, P. M. Deyà and A. Frontera, *CrystEngComm*, 2013, **15**, 3137-3144.
43. P. Politzer and J. S. Murray, *ChemPhysChem.*, 2013, **14**, 278-294.
44. J. A. Joseph and S. A. C. McDowell, *J. Phys. Chem. A*, 2015, **119**, 2568-2577.
45. D. Hauchecorne and W. A. Herrebout, *J. Phys. Chem. A*, 2013, **117**, 11548-11557.
46. G. Desiraju, R., P. S. Ho, L. Kloo, C. Legon Anthony, R. Marquardt, P. Metrangolo, P. Politzer, G. Resnati and K. Rissanen, in *Pure Appl. Chem.* 2013, vol. 85, pp. 1711-1713.
47. W. A. Schroeder, J. B. Shelton and J. R. Shelton, *Arch. Biochem. Biophys.*, 1969, **130**, 551-555.
48. R. Kaiser and L. Metzka, *Anal. Biochem.*, 1999, **266**, 1-8.
49. G. Lunn and E. B. Sansone, *Anal. Biochem.*, 1985, **147**, 245-250.



50. D. N. Deaton, A. M. Hassell, R. B. McFadyen, A. B. Miller, L. R. Miller, L. M. Shewchuk, F. X. Tavares, D. H. Willard and L. L. Wright, *Bioorg. Med. Chem. Lett.*, 2005, **15**, 1815-1819.
51. B. B. Snider and S. M. O'Hare, *Tetrahedron Lett.*, 2001, **42**, 2455-2458.
52. J. March, *Advanced Organic Chemistry: Reactions, Mechanisms, and Structure*, Wiley, New York, 1985.
53. T. K. Brotherton and J. W. Lynn, *Chem. Rev.*, 1959, **59**, 841-883.
54. A. Bauzá, T. J. Mooibroek and A. Frontera, *ChemPhysChem.*, 2015, **16**, 2496-2517.
55. A. Bauzá and A. Frontera, *ChemPhysChem.*, 2015, **16**, 3625-3630.
56. A. Bauzá and A. Frontera, *ChemPhysChem.*, 2015, **16**, 3108-3113.
57. H. Wang, C. Li, W. Wang and W. J. Jin, *Phys. Chem. Chem. Phys.*, 2015, **17**, 20636-20646.
58. Y. Geboes, F. D. Proft and W. A. Herrebout, *J. Phys. Chem. A*, 2015, **119**, 5597-5606.
59. S. J. Grabowski, *ChemPhysChem.*, 2015, **16**, 1470-1479.
60. F. Zhou, R. Liu, P. Li and H. Zhang, *New J. Chem.*, 2015, **39**, 1611-1618.
61. I. Alkorta, J. Elguero and J. E. Del Bene, *J. Phys. Chem. A*, 2013, **117**, 10497-10503.
62. L. M. Azofra, I. Alkorta and S. Scheiner, *Phys. Chem. Chem. Phys.*, 2014, **16**, 18974-18981.
63. L. M. Azofra, I. Alkorta and S. Scheiner, *Theor. Chem. Acc.*, 2014, **133**, 1-8.
64. N. Ma, Y. Zhang, B. Ji, A. Tian and W. Wang, *ChemPhysChem.*, 2012, 1411-1414.

- 65. J. S. Murray, P. Lane, T. Clark, K. E. Riley and P. Politzer, *J. Mol. Model.*, 2012, **18**, 541-548.
- 66. J. E. Del Bene, I. Alkorta and J. Elguero, *J. Phys. Chem. A*, 2013, **117**, 11592-11604.
- 67. A. Bauzá and A. Frontera, *Chem. Phys. Lett.*, 2015, **633**, 282-286.
- 68. S. Roy, A. Bauza, A. Frontera, R. Banik, A. Purkayastha, M. G. B. Drew, B. M. Reddy, B. Sridhar, S. K. Das and S. Das, *CrystEngComm*, 2015, **17**, 3912-3916.
- 69. C. Trujillo, G. Sanchez-Sanz, I. Alkorta and J. Elguero, *New J. Chem.*, 2015, **39**, 6791-6802.
- 70. T. Lang, X. Li, L. Meng, S. Zheng and Y. Zeng, *Struct. Chem.*, 2015, **26**, 213-221.
- 71. A. Bauza, T. J. Mooibroek and A. Frontera, *Chem. Commun.*, 2015, **51**, 1491-1493.
- 72. M. Solimannejad, N. Nassirinia and S. Amani, *Struct. Chem.*, 2013, **24**, 651-659.
- 73. G. Sánchez-Sanz, C. Trujillo, M. Solimannejad, I. Alkorta and J. Elguero, *Phys. Chem. Chem. Phys.*, 2013, **15**, 14310-14318.
- 74. A. Bauzá, R. Ramis and A. Frontera, *J. Phys. Chem. A*, 2014, **118**, 2827-2834.
- 75. M. Solimannejad, V. Ramezani, C. Trujillo, I. Alkorta, G. Sánchez-Sanz and J. Elguero, *J. Phys. Chem. A*, 2012, **116**, 5199-5206.
- 76. A. Bauza and A. Frontera, *Phys. Chem. Chem. Phys.*, 2015, **17**, 24748-24753.
- 77. I. Alkorta, J. Elguero and J. E. Del Bene, *Chem. Phys. Lett.*, 2015, **641**, 84-89.
- 78. K. Haupa, A. Bil and Z. Mielke, *J. Phys. Chem. A*, 2015, **119**, 10724-10734.
- 79. D. M. Bittner, D. P. Zaleski, S. L. Stephens, N. R. Walker and A. C. Legon, *ChemPhysChem.*, 2015, **16**, 2630-2634.

80. Q. Li, H. Zhuo, X. Yang, J. Cheng, W. Li and R. E. Loffredo, *ChemPhysChem.*, 2014, **15**, 500-506.
81. M. J. Frisch, G. W. Trucks, H. B. Schlegel, G. E. Scuseria, M. A. Robb, J. R. Cheeseman, G. Scalmani, V. Barone, B. Mennucci, G. A. Petersson, H. Nakatsuji, M. Caricato, X. Li, H. P. Hratchian, A. F. Izmaylov, J. Bloino, G. Zheng, J. L. Sonnenberg, M. Hada, M. Ehara, K. Toyota, R. Fukuda, J. Hasegawa, M. Ishida, T. Nakajima, Y. Honda, O. Kitao, H. Nakai, T. Vreven, J. Montgomery, J. A., J. E. Peralta, F. Ogliaro, M. Bearpark, J. J. Heyd, E. Brothers, K. N. Kudin, V. N. Staroverov, R. Kobayashi, J. Normand, K. Raghavachari, A. Rendell, J. C. Burant, S. S. Iyengar, J. Tomasi, M. Cossi, N. Rega, J. M. Millam, M. Klene, J. E. Knox, J. B. Cross, V. Bakken, C. Adamo, J. Jaramillo, R. Gomperts, R. E. Stratmann, O. Yazyev, A. J. Austin, R. Cammi, C. Pomelli, J. W. Ochterski, R. L. Martin, K. Morokuma, V. G. Zakrzewski, G. A. Voth, P. Salvador, J. J. Dannenberg, S. Dapprich, A. D. Daniels, O. Farkas, J. B. Foresman, J. V. Ortiz, J. Cioslowski and D. J. Fox, Wallingford, CT, Revision B.01 edn., 2009.
82. T. Helgaker, W. Klopper, H. Koch and J. Noga, *J. Chem. Phys.*, 1997, **106**, 9639-9646.
83. B. K. Mishra, S. Karthikeyan and V. Ramanathan, *J. Chem. Theory Comput.*, 2012, **8**, 1935-1942.
84. S. F. Boys and F. Bernardi, *Mol. Phys.*, 1970, **19**, 553-566.
85. A. E. Reed, F. Weinhold, L. A. Curtiss and D. J. Pochatko, *J. Chem. Phys.*, 1986, **84**, 5687-5705.
86. A. E. Reed, L. A. Curtiss and F. Weinhold, *Chem. Rev.*, 1988, **88**, 899-926.

87. E. D. Glendening, C. R. Landis and F. Weinhold, *J. Comput. Chem.*, 2013, **34**, 1429-1437.
88. R. F. W. Bader, *Atoms in Molecules, A Quantum Theory*, Clarendon Press, Oxford, 1990.
89. R. F. W. Bader, M. T. Carroll, J. R. Cheeseman and C. Chang, *J. Am. Chem. Soc.*, 1987, **109**, 7968-7979.
90. T. A. Keith, TK Gristmill Software, Overland Park KS2013.
91. K. Szalewicz and B. Jeziorski, in *Molecular Interactions. From Van der Waals to Strongly Bound Complexes*, ed. S. Scheiner, Wiley, New York1997, pp. 3-43.
92. R. Moszynski, P. E. S. Wormer, B. Jeziorski and A. van der Avoird, *J. Chem. Phys.*, 1995, **103**, 8058-8074.
93. H.-J. Werner, P. J. Knowles, F. R. Manby, M. Schütz, P. Celani, G. Knizia, T. Korona, R. Lindh, A. Mitrushenkov, G. Rauhut, T. B. Adler, R. D. Amos, A. Bernhardsson, A. Berning, D. L. Cooper, M. J. O. Deegan, A. J. Dobbyn, F. Eckert, E. Goll, C. Hampel, A. Hesselmann, G. Hetzer, T. Hrenar, G. Jansen, C. Köppl, Y. Liu, A. W. Lloyd, R. A. Mata, A. J. May, S. J. McNicholas, W. Meyer, M. E. Mura, A. Nicklaß, P. Palmieri, K. Pflüger, R. Pitzer, M. Reiher, T. Shiozaki, H. Stoll, A. J. Stone, R. Tarroni, T. Thorsteinsson, M. Wang and A. Wolf, Version 2006 edn., 2010.
94. J. P. Perdew, K. Burke and M. Ernzerhof, *Phys. Rev. Lett.*, 1996, **77**, 3865-3868.
95. L. M. Azofra and S. Scheiner, *Phys. Chem. Chem. Phys.*, 2014, **16**, 5142-5149.
96. L. M. Azofra and S. Scheiner, *J. Chem. Phys.*, 2014, **140**, 034302.
97. F. A. Bulat, A. Toro-Labbé, T. Brinck, J. S. Murray and P. Politzer, *J. Mol. Model.*, 2010, **16**, 1679-1691.

98. J. Poater, M. Solà and F. M. Bickelhaupt, *Chem. Eur. J.*, 2006, **12**, 2902-2905.

Table 6-1 Energetic and geometric aspects of  $\pi$ -hole complexes  $\text{XCN}\cdots\text{NH}_3$

X	$E_{\text{int}}$ kcal/mol	$R(\text{C}\cdots\text{N})$ Å	$\Delta r(\text{C}\equiv\text{N})$ Å	$\theta(\text{N}\cdots\text{CN})$ degs
F	3.14	2.867	0.0002	96.0
Cl	2.53	3.046	0.0000	87.5
Br	2.43	3.072	0.0002	87.0
I	2.44	3.104	0.0016	86.0

Table 6-2 Energetic and geometric aspects of  $\sigma$ -hole complexes  $\text{NCX}\cdots\text{NH}_3$

X	$E_{\text{int}}$ kcal/mol	$R(\text{X}\cdots\text{N})$ Å	$\Delta r(\text{X}-\text{C})$ Å
F	1.06	3.141	-0.0025
Cl	3.95	2.950	0.0051
Br	5.62	2.880	0.0130
I	8.24	2.852	0.0297

Table 6-3 SAPT components (kcal/mol) of total interaction energy of  $\pi$ -hole complexes  $\text{XCN}\cdots\text{NH}_3$

X	ES	IND	DISP	$\delta^{\text{HF}}$	EX	TOTAL
F	-6.52	-6.03	-3.08	-0.33	13.30	-2.65
Cl	-4.26	-3.63	-2.77	-0.22	8.85	-2.03
Br	-4.06	-4.04	-2.81	-0.23	9.19	-1.95
I	-4.07	-4.75	-3.14	0.02	9.61	-2.33

Table 6-4 SAPT components (kcal/mol) of total interaction energy of  $\sigma$ -hole complexes  
 $\text{NCX} \cdots \text{NH}_3$

X	ES	IND	DISP	$\delta^{\text{HF}}$	EX	TOTAL
F	-1.66	-1.35	-0.81	-0.09	2.99	-0.92
Cl	-7.58	-10.14	-2.84	-0.82	18.13	-3.25
Br	-12.09	-26.34	-4.02	-1.36	38.93	-4.88
I	-19.18	-53.72	-5.45	8.41	57.24	-12.71

Table 6-5 Interaction Energies (kcal/mol) of  $\pi$ -hole complexes  $\text{XCN} \cdots \text{NH}_3$  calculated at various levels.

	MP2/aug-cc-pV(X)Z					
X	D	T	Q	CCSD(T)/ aug-cc-pVDZ	MP2/CBS	CCSD(T)/CBS
F	3.14	3.56	3.78	2.92	3.94	3.72
Cl	2.53	2.93	3.00	2.28	3.05	2.80
Br	2.43	2.87	2.99	2.18	3.08	2.83
I	2.44	2.88	3.05	2.19	3.17	2.92

Table 6-6 Interaction Energies (kcal/mol) of  $\sigma$ -hole complexes  $\text{NCX} \cdots \text{NH}_3$  calculated at various levels

	MP2/aug-cc-pV(X)Z					
X	D	T	Q	CCSD(T)/ aug-cc-pVDZ	MP2/CBS	CCSD(T)/CBS
F	1.06	1.14	1.22	1.06	1.28	1.28
Cl	3.95	4.28	4.52	3.79	4.70	4.54
Br	5.62	6.01	6.23	5.31	6.39	6.08
I	8.24	8.65	9.17	7.67	9.55	8.98

Table 6-7 Interaction energies (kcal/mol) of five heterotrimer geometries of  $\text{XCN}(\text{NH}_3)_2$ 

	T1 <sup>a</sup>	T2 <sup>a</sup>	T3	T4	T5
F	-	5.66(6.28)	6.26	8.58	5.00
Cl	6.12(6.48)	4.88(5.06)	5.28	7.48	4.33
Br	7.71(8.05)	4.71(4.86)	5.11	7.26	4.23
I	10.38(10.68)	4.72(4.88)	5.05	7.21	-

<sup>a</sup>value in parentheses equals sum of dimer interactionsTable 6-8 Three-body term  $\Delta 3E$  (kcal/mol) of heterotrimers of  $\text{XCN}(\text{NH}_3)_2$ 

	T1	T2	T3	T4	T5
F	-	0.08	-0.19	-1.10	-0.34
Cl	-0.08	0.01	-0.04	-0.86	-0.21
Br	-0.09	0.02	-0.03	-0.85	-0.19
I	-0.10	0.03	-0.01	-0.88	-

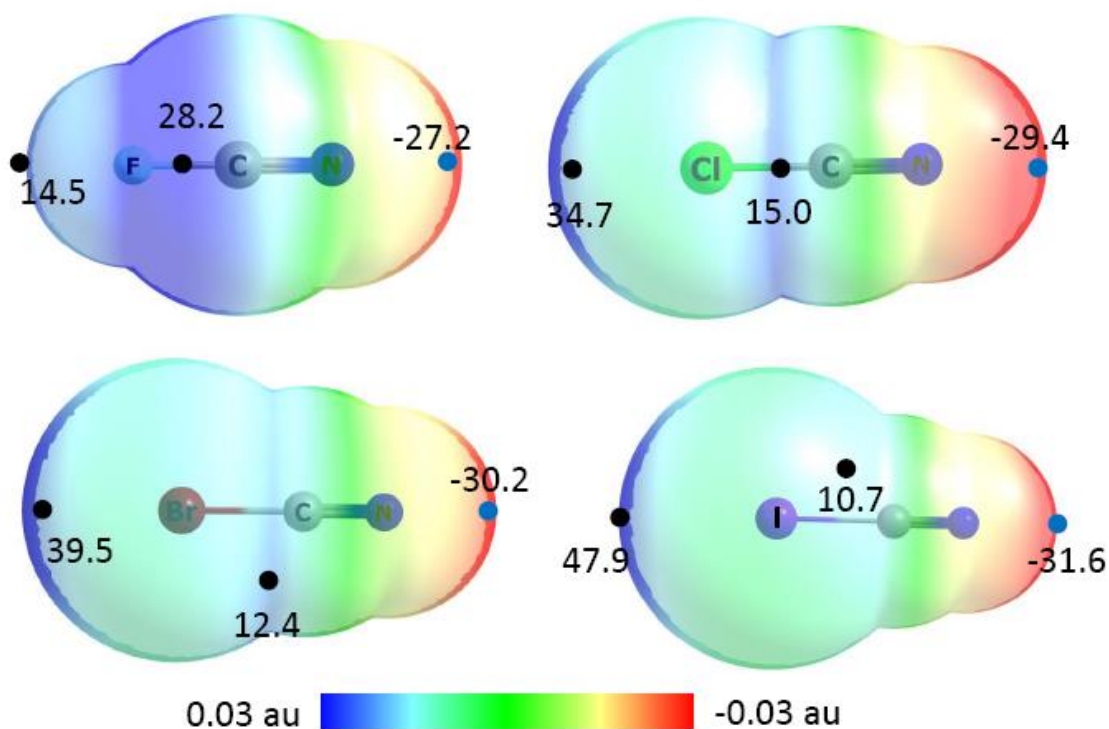


Figure 6-1 Molecular electrostatic potentials (MEPs) of XCN molecules. Black and blue dots respectively indicate positions of maxima and minima on the 0.001 au isodensity surface, with values displayed in kcal/mol.

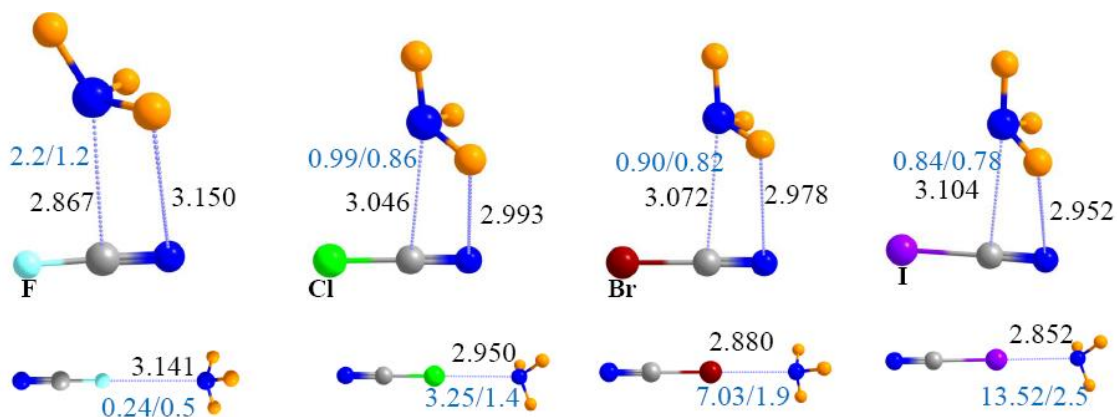


Figure 6-2 Optimized geometries of  $\pi$ -hole (top) and  $\sigma$ -hole (bottom) dimers of  $\text{NH}_3$  with XCN. Distances are in Å. Blue numbers refer to NBO values of  $E(2)$ , in kcal/mol, for transfer from N lone pair to  $\pi^*(\text{CN})$  (top) and  $\sigma^*(\text{XC})$  (bottom). Number to right of slash indicates the interaction energy.



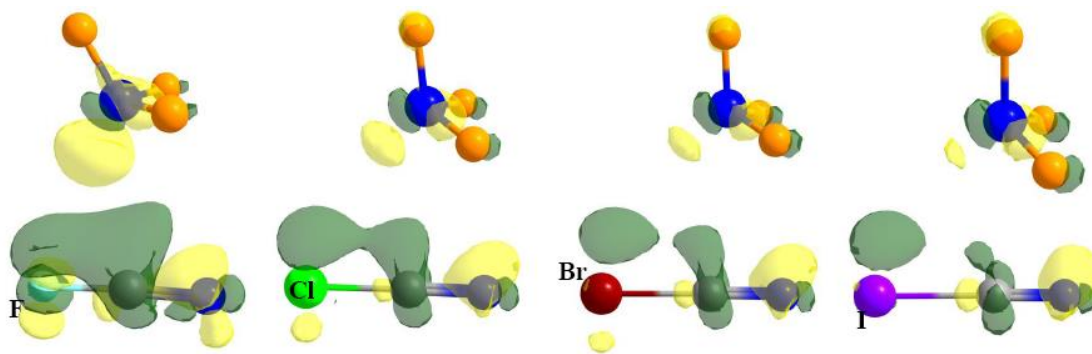


Figure 6-3 Electron density shifts that arise from formation of  $\pi$ -hole complexes. Yellow and green regions respectively correspond to gain and loss of electron density, on the  $\pm 0.0005$  au contour.

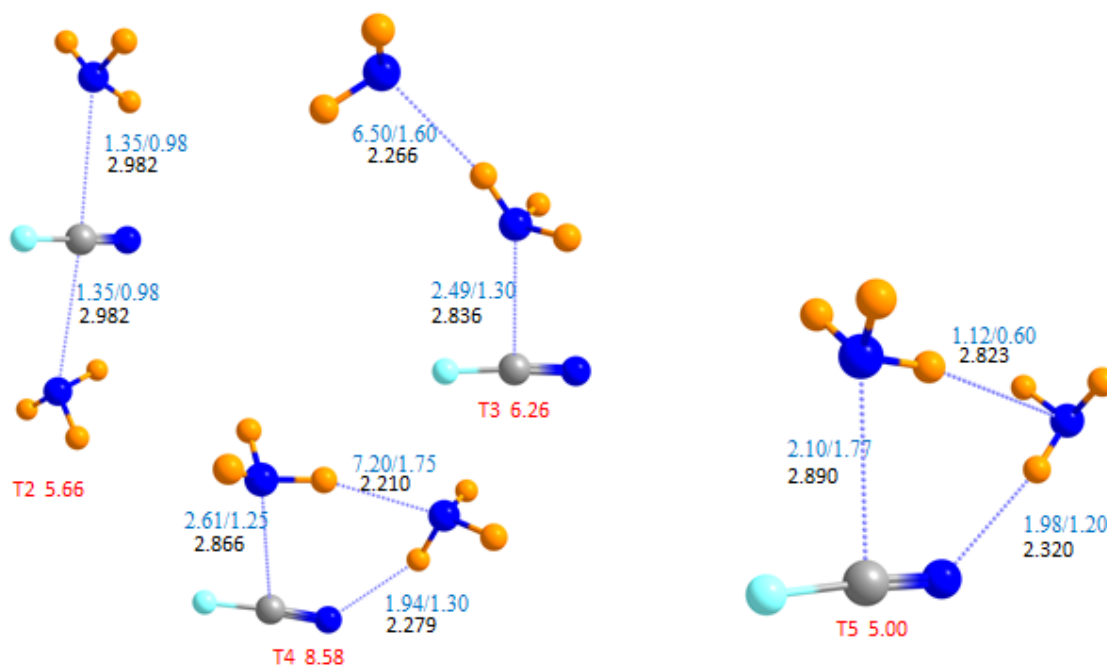


Figure 6-4 Optimized geometries of 2:1 heterotrimers of  $\text{NH}_3$  with  $\text{FCN}$ . Red number indicates total interaction energy in kcal/mol. Distances are in Å in black. Blue numbers refer to NBO values of  $E(2)$ , in kcal/mol, for transfer from N lone pair to  $\pi^*(\text{CN})$  or  $\sigma^*(\text{XC})$ .

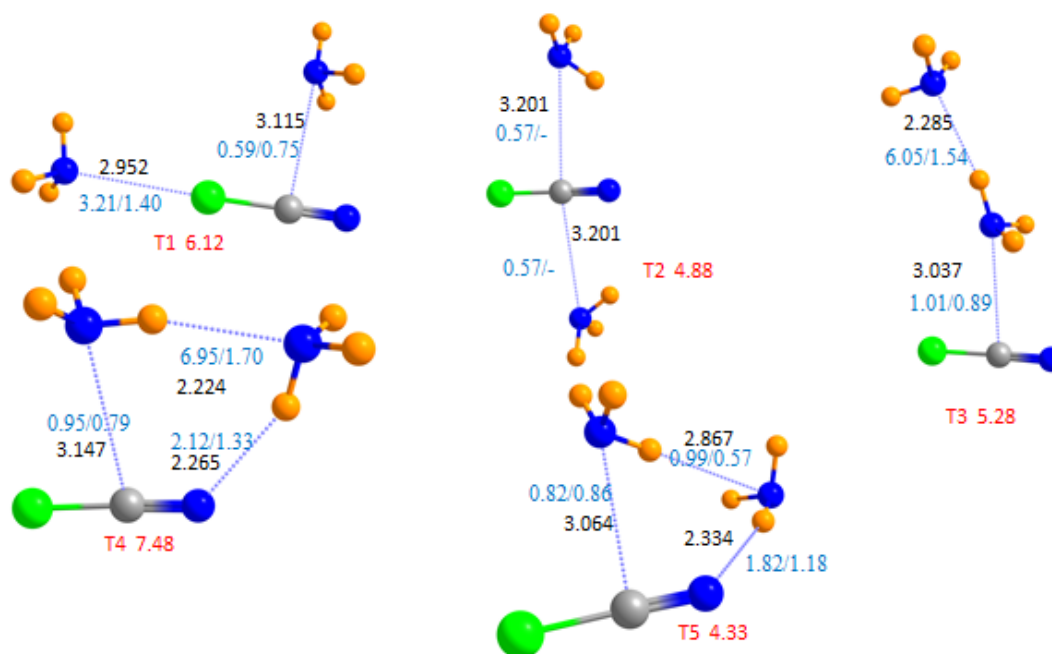


Figure 6-5 Optimized geometries of 2:1 heterotrimers of  $\text{NH}_3$  with  $\text{ClCN}$ . Red number indicates total interaction energy in kcal/mol. Distances are in Å in black. Blue numbers refer to NBO values of  $E(2)$ , in kcal/mol, for transfer from N lone pair to  $\pi^*(\text{CN})$  or  $\sigma^*(\text{XC})$

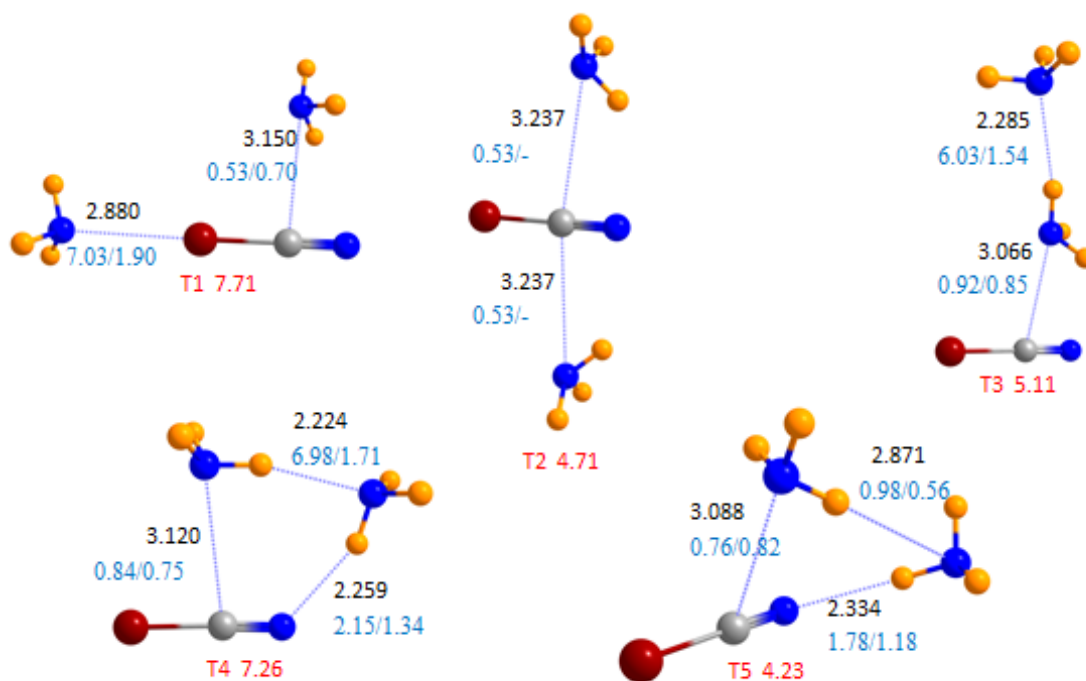


Figure 6-6 Optimized geometries of 2:1 heterotrimers of  $\text{NH}_3$  with  $\text{BrCN}$ . Red number indicates total interaction energy in kcal/mol. Distances are in Å in black. Blue numbers refer to NBO values of  $E(2)$ , in kcal/mol, for transfer from N lone pair to  $\pi^*(\text{CN})$  or  $\sigma^*(\text{XC})$

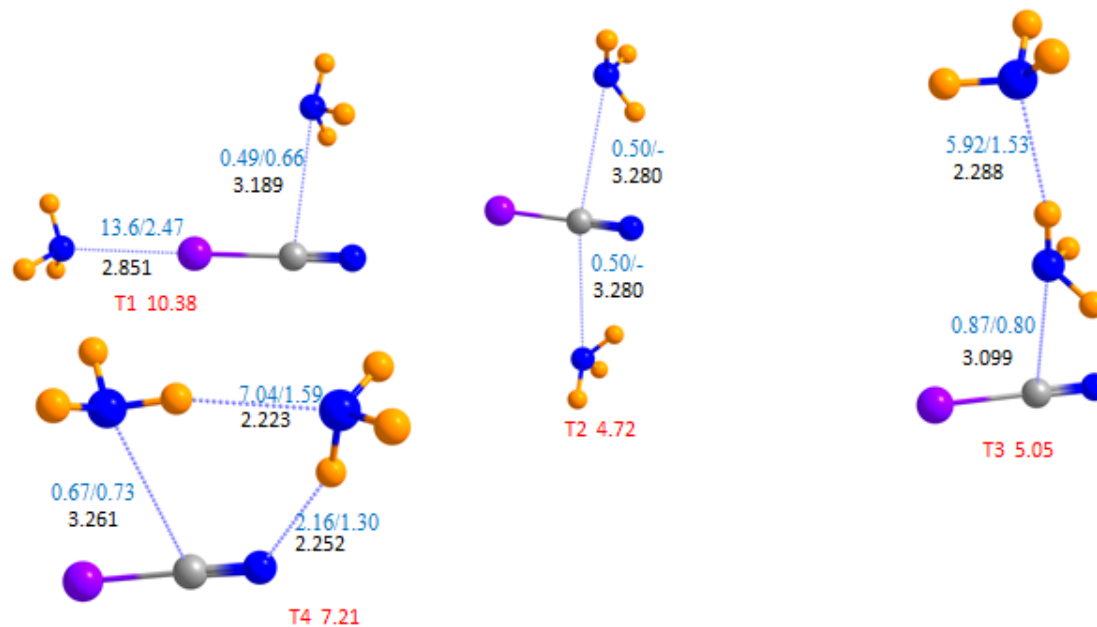


Figure 6-7 Optimized geometries of 2:1 heterotrimers of  $\text{NH}_3$  with  $\text{ICN}$ . Red number indicates total interaction energy in kcal/mol. Distances are in Å in black. Blue numbers refer to NBO values of  $E(2)$ , in kcal/mol, for transfer from N lone pair to  $\pi^*(\text{CN})$  or  $\sigma^*(\text{XC})$ .

## CHAPTER 7

### CATALYSIS OF THE AZA-DIELS-ALDER REACTION BY HYDROGEN AND HALOGEN BONDS<sup>1</sup>

#### Abstract

The combination of  $\text{H}_2\text{C}=\text{NH}$  and *cis*-1,3-butadiene to form a six-membered ring was examined by quantum calculations. The energy barrier for this reaction is substantially lowered by the introduction of an imidazolium catalyst with either a H or halogen (X) atom in the 2-position, which acts via a H or halogen bond to the N atom of the imine, respectively. X=I has the largest effect, and Cl the smallest; Br and H are roughly equivalent. The catalyst retards the formation of the incipient N-C bond from imine to diene while simultaneously accelerating the C-C bond formation. The energy of the  $\pi^*$  LUMO of the imine is lowered by the catalyst, which thereby enhances charge transfer from the diene to the imine. Assessment of free energies suggests catalytic rate acceleration by as much as four to six orders of magnitude.

#### 7-1. Introduction

Organocatalysts have found widespread use in the synthesis of natural products and pharmaceutically relevant molecules from readily available small organic precursor molecules. This method of synthesis is cost effective, operationally simple, and easy<sup>1-2</sup> to handle. Those organocatalysts that interact with their substrate through a hydrogen bond

---

<sup>1</sup> Coauthored by Vincent de Paul Nzuwah Nziko and Steve Scheiner. Reproduced with permission from *J. Org. Chem.* **2016**, *81*, 2589-2597. Copyright 2016, American Chemical Society.

(HB) have been especially widely developed and used. For example the Jacobsen group<sup>3</sup> has successfully used chiral bifunctional urea to catalyze the Povarov reaction that involves an imine and an enamine. BINOL is another widely used organocatalyst which acts as both proton donor and acceptor<sup>4-7</sup> through the intermediate of a HB that has been applied to a variety of reactions including hydride transfer.

There has been growing interest in other sorts of organocatalysts that proceed via noncovalent interactions other than H-bonding. Organic molecules that have the potential to form halogen bonds (XBs) have been a recent source of exploration due to the high linearity and strength of these bonds, comparable and sometimes stronger than a H-bond<sup>8-11</sup>. An important step in applications of the use of XBs in catalysis occurred in 2008 when Bolm et al<sup>12</sup> demonstrated that fluorinated alkyl halides could catalyze the reduction of substituted quinolines by Hantzsch esters. Various other applications of XB activation followed shortly thereafter<sup>13-16</sup>.

The Diels-Alder reaction has proven over the years to be an effective synthetic strategy for building stereochemically well-defined unsaturated 6-membered rings. The first organocatalyst applied to the Diels-Alder reaction was developed by MacMillan and coworkers<sup>17</sup> in 2000. This catalyst is believed to work through the formation of a HB and proceeds by a LUMO-lowering activation mechanism. The Diels-Alder reaction has continued its development over the years and a number of additional catalysts<sup>18-20</sup> have found application, especially Lewis acids like  $\text{AlCl}_3$ .

The Aza Diels-Alder reaction described in Scheme 1 offers an alternative route for one-step synthesis of functionalized nitrogen-containing heterocyclic rings from readily

available imines, coupled with diene components. The regioselectivity, diastereoselectivity, and enantioselectivity of the resulting heterocyclic rings are easily controlled <sup>21</sup> via this procedure. Just as in the standard Diels-Alder reaction, chiral Lewis acids play an important catalytic role in the aza Diels-Alder reaction. Unfortunately, most Lewis acids end up trapped by the basic nitrogen atoms, either of the starting imine or the final heterocyclic product, thereby hindering the catalytic activity <sup>22</sup> of these Lewis acids. In order to overcome this drawback, a new generation of catalyst would be very useful. Following up on the Huber group's finding <sup>23</sup> that a bis(2-iodoimidazolium) salt could catalyze a Diels-Alder reaction, Takeda and co-workers considered <sup>24</sup> a range of related X-bonding agents in connection with the slightly different aza-Diels-Alder reaction. After noting that a reaction of this sort would not occur in the presence of perfluoroiodobenzene, they found success with a set of more powerful X-bonding 2-halogenoimidazolium salts. Their comparison of closely related catalysts suggested that the reaction rate ought to match the expected order of XB strength; viz.  $I > Br > Cl$ , but left certain other issues incompletely resolved, and they suggested further studies of the details of the reaction mechanism. For example, they were unable to extract any information concerning the transition states of these reactions, nor their energies.

The present work attempts to provide detailed information about this reaction, and specifically about the involvement of any XBs in its catalysis. Quantum calculations are applied in order to take advantage of their ability to elucidate fine details of the structure and energy of transient species such as the transition state, as well as any intermediates in the course of the reaction. These methods are also amenable to analysis of the electronic

structure of these species, providing information such as the amount of charge transfer or the energies of frontier molecular orbitals. In this manner, these methods allow one to focus on the mechanism by which a XB is capable of catalyzing the reaction. So as to maximize contact with experimental information, this work focuses on the aza-Diels-Alder reaction studied recently by Takeda et al <sup>24</sup>. As such we report here the first computational work pertaining to the use of an organocatalyst to catalyze the Diels-Alder reaction via XB formation. The direct influence of the strength of the XB is studied by a comparison of I with Br and Cl as the halogen atom on the catalyst. In order to extract further information about the influence of a XB, we also consider an analogous catalyst which replaces the halogen by H, i.e. comparison of XB with HB.

## 7-2. Computational methods

All computations were carried out with Gaussian 09, Rev D.01 and B.01 <sup>25</sup>. Geometry optimization and frequency calculations were performed using the M06-2X density functional <sup>26</sup> with the aug-cc-pVDZ basis set, and ECP aug-cc-PVDZ for I to account for relativistic effects. The performance of this computationally affordable level of theory has been shown to be suitable for the geometric, electronic and energetic features of the Diels-Alder (DA) reaction <sup>27-29</sup>. Additional calculations were carried out at the MP2 level, as detailed below. The stationary points were characterized by frequency calculations, and all transition states were confirmed to have a single imaginary frequency corresponding to the formation of the expected bonds. The NBO method <sup>30-32</sup> was used to measure the charge transfer involved in this reaction. The interaction energy was dissected using symmetry-adapted perturbation theory (SAPT) methods <sup>33-35</sup>.



So as to examine the essence of the reaction, free of complicating substituent effects, model reactants and catalysts were studied here.  $\text{H}_2\text{C}=\text{NH}$  and *cis*-1,3-butadiene were chosen as reactants that ultimately coalesce to form a six-membered ring. The imidazolium catalysts placed an X atom (X=I, Br, Cl) in the 2-position, along with methyl groups on the two N atoms so as to closely mimic the cations examined earlier<sup>24</sup>. The halogen atom was replaced by H so as to compare the results of H-bonding on this reaction.

### 7-3. Results

Figure 7-1 outlines the steps in the reaction of interest, and the definition of the various relevant energy terms. The reaction begins with all three units: diene, imine, and catalyst separate and distinct. The first step refers to the binding of the catalyst to the imine, which stabilizes the system by an amount  $E_1$ . The imine-catalyst pair then interacts with the diene substrate forming an encounter complex  $\text{diene}\cdots\text{Im}\cdots\text{cat}$ , further lowering the total energy by  $E_2$ . The reaction then proceeds through a transition state TS which requires energy  $E_3$  from the encounter complex. The reaction next proceeds to form the heterocyclic six-membered ring, still bound to the catalyst,  $\text{product}\cdots\text{cat}$ , liberating  $E_6$  units of energy. The final step, requiring  $E_7$ , separates the product from the regenerated catalyst which can now go on to reinitiate the reaction with a new substrate. Overall, starting from the beginning with separate diene, imine, and catalyst, the total reaction energy  $E_{\text{reac}}$ , can be expressed in terms of the other quantities, e.g.  $E_{\text{reac}} = E_1 + E_2 + E_3 + E_6 + E_7$ . The quantity  $E_5$  represents the energy of the TS relative to the starting reactants, which can be considered the activation energy of the entire reaction.  $E_5$  can also be expressed as the sum of other terms:  $E_5 = E_1 + E_2 + E_3$ .

### 7-3. 1. Geometries

Some of the pertinent geometries are exhibited in Figure 7-2. The upper set of structures corresponds to the uncatalyzed aza-Diels-Alder reaction in which the imine first forms an encounter complex with the diene. After overcoming the transition state, the six-membered heterocyclic ring is formed as product. Immediately below this set of structures is the same reaction in the presence of a H-bonding imidazolium catalyst, and the I-substituted analogues are shown directly below. The encounter complexes on the left show how the imine approaches the diene from above with its C and N atoms directly above the two terminal CH<sub>2</sub> groups of the diene. At the same time, the H/I atoms of the catalyst engage in a H/halogen bond with the imine N atom. The transition states follow the natural course of a closer approach of the imine to the diene, as the C-C and C-N bonds between them begin to form, still retaining the H/halogen bonds to the catalyst. These same noncovalent bonds are present in the product-catalyst complex following the full formation of the C-C and C-N bonds which characterize the six-membered heterocyclic ring. All that remains is the disengagement of the catalyst from this product.

Some of the geometrical parameters in Figure 7-2 suggest the influence of the catalyst. First considering the initial encounter complex, the R(N··C) and R(C··C) distances are 3.306 and 3.250 Å, respectively in the uncatalyzed structure. The H bond from the imine N to the H-bonding catalyst is rather short, 2.163 Å, suggesting a good deal of binding strength. This HB “tips” the imine, so that the R(N··C) distance to the diene is shortened and the R(C··C) counterpart is lengthened. The I-substituted catalyst on the other hand, shortens both of these bonds, although the contraction is a bit greater for R(C··C).

Turning next to the transition states,  $R(N\cdots C)=1.969\text{ \AA}$  and  $R(C\cdots C)=2.406\text{ \AA}$  in the uncatalyzed process. The former is lengthened and the latter shortened with the HB catalyst, the reverse of the effect of this catalyst upon the encounter complex. The I-substituted catalyst also lengthens  $R(C\cdots N)$  and contracts  $R(C\cdots C)$ , and to a greater extent than does the HB catalyst. One might say that the presence of either catalyst alters the synchronicity of the formation of the two incipient bonds, delaying the formation of C-N while hastening the formation of C-C. Considering the H-bonding catalyst,  $R(H\cdots N)$  to the imine is equal to  $2.163\text{ \AA}$  in the encounter complex, and becomes shorter, and presumably stronger as the reaction proceeds, culminating in a HB length of less than  $2\text{ \AA}$  in the product. The  $I\cdots N$  halogen bond is shortest in the transition state.

These interatomic distances are displayed in Table 7-1 along with the equivalent data for the Cl and Br-substituted imidazolium catalysts. There are certain trends apparent in a comparison of the three halogen atoms. Most notable is the shortening of the  $R(N\cdots X)$  halogen bond distance as one proceeds from Cl to Br to I in all structures: encounter complex, TS, and product. This contraction is clear evidence of strengthening interaction since the halogen radius is increasing in this progression. This halogen bond becomes shorter as the reaction proceeds in most cases, although this is not a strong trend.

As the reaction proceeds through transition state and product, the  $R(N\cdots C)$  and  $R(C\cdots C)$  bonds of course become shorter. But the presence of a catalyst affects the timing of the reaction. Beginning with the encounter complex, in comparison to the uncatalyzed reaction in the first column of Table 7-1, the  $R(N\cdots C)$  bond is shorter, and the  $R(C\cdots C)$  bond longer (with the exception of the I substituent). Within the transition state, the catalyst has

the opposite effect, lengthening  $R(N\cdots C)$  and contracting  $R(C\cdots C)$ . In other words, the catalyst appears to delay the formation of the former bond while hastening the latter. This trend is not very sensitive to the nature of the catalyst, although I shows the greatest effect in this regard. Because of differential effects by each catalyst, it may be noted that the  $N\cdots C$  bond is longer than  $C\cdots C$  for the transition states of Cl and I, but roughly equal for H and Br.

A perhaps more quantitative way of discussing the progress of the reaction is as follows. The  $N\cdots C$  distance in the encounter complex (of the uncatalyzed process) is 3.306 Å. This same distance is 1.461 Å in the product, so there is a total change of 1.845 Å occurring upon reaction. The  $N\cdots C$  distance in the TS is 1.969, which is 1.337 Å smaller than that in the encounter complex. The percentage change of this distance in the TS, relative to the total change required for full reaction is thus  $1.337/1.845 = 0.725$ . This same fractional change in the TS relative to the final product in the catalyzed reactions are smaller, in the range between 0.56 and 0.61, confirming more quantitatively the delay in the formation of the N-C bond. Application of the analogous formula for the C-C bond leads to a fractional formation in the TS of 0.49 in the uncatalyzed reaction, and 0.64-0.69 when a catalyst is present, reaffirming the acceleration of the formation of this bond by the catalyst.

In addition to monitoring the progress of the incipient bonds between the imine and diene, one can also consider the bond length changes within the diene itself. The three  $R(CC)$  bonds in the optimized diene are 1.337, 1.476, and 1.337 Å, respectively, corresponding to the alternating double-single-double nature of these bonds. After the

reaction is complete, these three bond lengths are 1.507, 1.336 and 1.509 Å, respectively (where the last one corresponds to C<sub>3</sub>C<sub>4</sub>, adjacent to the N). As anticipated by the transitions between single and double bond character in the aza-Diels-Alder reaction, the central bond shortens (by 0.140 Å) and the two terminal bonds elongate (by 0.17 Å).

The bond lengths in the transition state serve as a gauge of the progress of each bond toward its eventual bond length in the product. Considering the uncatalyzed reaction first, the three C-C bond lengths in the diene are equal to 1.373, 1.413, and 1.390, which respectively represent 21, 45, and 30% of their full changes upon reaching the product. The presence of a catalyst alters these percentage changes to 25, 48 and 25%, respectively. In other words, the catalyst speeds up the progress of the first two bonds toward their eventual length, while simultaneously retarding the progress of the third bond (the one adjacent to the N atom in the final product). This effect is largely insensitive to the particular nature of the catalyst, with only small differences from one catalyst to the other.

### 7-3. 2. Energetics

The computed values of the various energies defined in Figure 7-1 are reported in Table 7-2, first for the uncatalyzed reaction in the first row, encompassing only the imine and diene. The imidazole-catalyzed quantities are listed in the ensuing four rows, headed by the identity of the atom on the imidazole catalyst, whether H or one of the halogens. Comparison of these quantities provides insight into the activity of each catalyst. The first column corresponds to the strength of the interaction between the imidazole and the imine. The H-bonding pair is bound by 12.9 kcal/mol. Replacing H by Cl weakens this binding while I-substitution strengthens the interaction by some 6 kcal/mol; Br has a small

weakening effect. The binding of this catalyst-imine pair to the diene,  $E_2$ , is considerably weaker. Without a catalyst at all, the diene and imine are bound by 3.9 kcal/mol, whereas the catalyst-imine pair binds slightly more strongly, by 4-6 kcal/mol. This cooperative effect can be attributed to the fact that the imine N atom serves as electron donor to the catalyst (whether HB or XB) while accepting charge from the  $\pi$ -system of the diene.

Transition to the TS from the fully bound system ( $E_3$ ), requires some 17.4-18.7 kcal/mol, and is rather insensitive to the presence of a catalyst or the nature of the substituent. The same can be said of  $E_4$ , which differs from  $E_3$  only by the binding of the diene to the catalyst-imine pair. It might be noted that neither  $E_3$  nor  $E_4$  show a strong effect from the presence of a catalyst, regardless of its substituent.

The most important quantity in Table 7-2 is  $E_5$ , which corresponds to the activation energy of the reaction. This term is equal to 13.8 kcal/mol for the uncatalyzed process, but is much smaller for the various catalysts. In fact, for the I-substituted imidazolium, the transition state is more stable than the separate reactants, leading to a negative value of  $E_5$ . Comparison of the preceding terms in Table 7-2 leads to insights into how the catalysts reduce the activation energy. The binding energy  $E_2$  of the diene is more negative for the catalyzed reaction, but only slightly. The energy needed to transit from the encounter complex to the transition state,  $E_3$ , is barely affected by the presence of any of the catalysts. The biggest difference between uncatalyzed and catalyzed reactions resides in the binding of the imine to the catalyst,  $E_1$ . This quantity varies from a minimum of 9 kcal/mol for Cl up to 18.5 kcal/mol for I; H lies between with a binding energy of 12.9 kcal/mol. It is this strong binding of the catalyst, whether by H-bond or halogen bond, that can be taken as

primarily responsible for the reduction of  $E_5$ . Indeed, the strength of the I-bond, 18.5 kcal/mol, is large enough that the transition state in which this I-bond is present lies lower in energy than the unassociated reactants where this I-bond is absent. The growing strength of the halogen bond,  $\text{Cl} < \text{Br} < \text{I}$ , thus matches the reduction of  $E_5$ , with that of H intermediate between Br and I.

Continuing the reaction beyond the transition state, the ensuing formation of the product-catalyst complex is quite exothermic, nearly -60 kcal/mol, and largely independent of the presence of a catalyst. The last step in the catalyzed process is the separation of the catalyst from the product,  $E_7$ , which amounts to between 10 and 20 kcal/mol. These dissociation energies are slightly larger than  $E_1$ , representing the binding of the catalyst to the imine, but obey the same trend: Again the I-bonded species requires the most energy to pull apart, and Cl the least. Following the removal of the catalyst, the final reaction energies are all equally exothermic, -43.3 kcal/mol.

There are of course several ways of understanding the energetics of catalysis in a reaction such as this. One prescription which has shown itself useful is commonly dubbed the activation strain model<sup>27, 36-39</sup>, and is illustrated by the red energies in Figure 7-1. The transition from the separate reactants to the transition state is envisioned as occurring in two conceptual steps. The first process requires that each of the reactants be deformed into the precise internal geometries they will eventually adopt in the transition state, requiring an amount of energy labeled  $E_{\text{def}}^\ddagger$ . The second step stabilizes the system by an energy  $E_{\text{int}}^\ddagger$  when the properly deformed reactants are allowed to combine together to assemble the transition state. The sum of the latter two terms adds up to the activation energy  $E_5$ , as

indicated in Figure 7-1.

Both  $E_{\text{def}}^{\ddagger}$  and  $E_{\text{int}}^{\ddagger}$  are displayed in the last two columns of Table 7-2. Considering the first row of the table, the deformation energy of the uncatalyzed reaction is 17.3 kcal/mol, which is barely compensated by the interaction energy of only 3.6 kcal/mol, leaving a barrier of 14 kcal/mol. The deformation energies of the catalyzed reactions are larger, 22-27 kcal/mol. But the interaction energies are far more stabilizing than in the uncatalyzed case, between 18 and 32 kcal/mol. In the I case, for example, the interaction energy of 32 kcal/mol actually exceeds the deformation energy, which leads to the negative activation energy. One may thus conclude that the reduction in  $E_5$  arising from the presence of the catalysts can be attributed to the high interaction energies that result from bringing the pre-deformed species together in order to assemble the transition state. If one considers either  $E_1$  or  $E_7$  as a measure of the binding energy of the H/X bond between the catalyst and the imine N atom, then this noncovalent bond can be thought of as responsible for roughly half of the total  $E_{\text{int}}^{\ddagger}$ .

Figure 7-3 illustrates the activation strain model visually, wherein the blue downward arrows represent  $E_{\text{int}}^{\ddagger}$  and the final activation energies  $E_5$  are shown in red. The deformation energy on the left is broken down into the strain of each of the subunits. The deformation energy of the catalyst in brown is very small, less than 2 kcal/mol in all cases. The strain undergone by the diene (black) is the largest of the three, and is 2 or 3 kcal/mol larger in the four catalyzed cases than in the uncatalyzed reaction. The (green) deformation energy of the imine is smaller, less than 9 kcal/mol, and is also larger in the catalyzed situations. The greatest imine strain (8.7 kcal/mol) occurs for the I-catalyst, as compared



to about 6.7 kcal/mol for the other three catalyst processes. But as indicated above, the largest single factor that differentiates one reaction from the next is the interaction energy, characterized by the blue downward arrows of very different length, which is the primary factor in the effect of catalyst upon activation energy.

### 7-3. 3. Electronic Structure Analysis

It is clear that one important effect of the catalyst is its formation of a H/X bond with the imine N atom. One can also inquire as to the effect of each catalyst upon other factors that influence the stability of the transition state. In particular, how might the catalyst affect the interactions between the imine and the diene within the transition state? The energetic manifestation of the charge transfer taking place between the imine and diene within the TS can be accessed via the NBO formalism which evaluates the second order perturbation energy for the transfer between any given pair of orbitals. Table 7-3 displays these values of  $E(2)$  which shows first that there is a good deal of transfer in both directions. The transfers involve the  $\pi$ -systems of the two molecules. Charge is shifted from the occupied  $\pi$ -orbitals of each molecule to the vacant  $\pi^*$  antibonding orbitals of the other. The diene contains a pair of  $\pi$  bonds (and antibonds), and the imine has a single pair involving the C-N bond.

Comparison of the first two rows of Table 7-3 suggest the transfer from diene to imine is considerably larger than that for the reverse process. The imine→diene transfer is relatively insensitive to the presence or absence of a catalyst, or the nature of the latter. The diene→imine transfer, however, is rather strongly dependent upon the catalyst. This transfer amounts to 50 kcal/mol in the non-catalyzed process, but rises to as much as 74

kcal/mol when a catalyst is present. In fact, the value of this quantity in the first row of Table 7-3 correlates rather well with reduction in the  $E_5$  activation energies in Table 7-2, with order: uncatalyzed < Cl < Br < H < I. One can thus conclude that one means by which the catalysts help to accelerate the reaction is via the facilitation of charge transfer from diene to imine. This trend is sensible in that the H/X bond acts to suck density away from the imine, thereby allowing the latter to act as a better electron acceptor from the diene.

The last four rows of Table 7-3 break down the total charge transfer into the individual interorbital quantities. One can see that this is generally an asymmetric process, in that one of the two C=C bonds of the diene transfers considerably more charge to the imine than does the other, and this same bond is also a better sink for transfer from the imine. Note that C<sub>3</sub>C<sub>4</sub>, the C=C bond that is closest to the imine N, has stronger  $\pi(\text{C}_3\text{C}_4) \rightarrow \pi^*(\text{NC})$  interactions with the imine for the uncatalyzed process in the first column of Table 7-3. However, this situation reverses, during catalysis and it is the C<sub>1</sub>C<sub>2</sub> bonding orbital that shows the largest transfer to the imine. This trend is consistent with the intermolecular distances in Table 7-1. In the uncatalyzed transition state, the imine N is considerably closer to the diene than is the imine C atom, which would facilitate the greater transfer from the C<sub>3</sub>=C<sub>4</sub> bond. In the catalyzed processes, on the other hand, this distinction vanishes and in fact it is the imine C atom that is closer to the diene in a number of cases. This trend is most obvious for the I-catalyst where  $R(\text{C} \cdots \text{C})$  is some 0.2 Å shorter than is  $R(\text{N} \cdots \text{C})$ , and the transfer from  $\pi(\text{C}_1\text{C}_2)$  is nearly 5 times larger than  $E(2)$  from  $\pi(\text{C}_3\text{C}_4)$ .

In addition to the transfer between individual orbitals, it is of interest to consider the transfer between the overall chemical groups participating in the reaction. As may be

seen in the first column of Table 7-4, only 2 me of charge transfer from the diene to the imine in the uncatalyzed encounter complex, and there is even less transfer within the transition state. The presence of a cationic catalyst absorbs a certain amount of charge, as evident by the values of less than unity in the third row of Table 7-4. In the encounter a greater share of the positive charge winds up on the imine than on the diene, consistent with the greater proximity of the former. However, this situation changes drastically as the reaction proceeds to the transition state, where the imine becomes negatively charged, despite the influence of the positively charged catalyst. This negative charge arises via transfer from the diene which takes on a fairly large positive charge. This transfer from diene to imine is consistent with the NBO analysis above. The lower section of Table 7-4 reflects the change in the group charges on going from encounter complex to transition state. Note that the catalyst itself undergoes very little change, but it does act to facilitate the transfer from the diene which becomes more positive and the imine which becomes more negative. With respect to trends, the loss of charge by the diene follows the same  $\text{Cl} < \text{Br} < \text{I}$  order as do many other quantities here, with the H-catalyst similar to Br.

Frontier molecular orbitals offer another lens through which to view this reaction. The primary interaction would be expected between the HOMO of the diene and the LUMO of the imine, both of which are of  $\pi$ -type. The energy of the HOMO of the diene is -0.3393 au. As indicated in the first entry of Table 7-5, the LUMO energy of the imine is +0.0108 au, leading to a gap between them of 0.3501 au. The succeeding entries in the first row of Table 7-5 indicate that the association of the imine with each catalyst lowers its LUMO energy, by an amount varying between 0.100 au for Cl up to 0.124 au for I. This lowering

would also reduce the HOMO-LUMO gap which would serve to facilitate the electron transfer. In fact, there is a certain degree of correlation between the reduction of this gap and the activation energy  $E_5$ . Specifically, the LUMO energy reduction follows the same  $\text{Cl} < \text{Br} < \text{I}$  order as does activation energy drop. On the other hand, the HOMO-LUMO gap for I and H are very nearly the same, although I is a much more effective catalyst, so this correlation is imperfect. The second row of Table 7-5 lists the comparable information about the more tightly localized NBO LUMO. Their energies are all about 0.05 au higher than the canonical equivalent, and follow a similar  $\text{Cl} < \text{Br} < \text{I}$  pattern; the gap reduction in the NBO LUMO is a bit larger for I than for H, better reflecting the superior catalytic activity of I.

With respect to the binding of the catalyst to the imine, so important to the acceleration of the reaction, one can partition this interaction into its component parts. Table 7-6 displays the results of a SAPT partitioning of the total interaction energy into its three attractive parts. For H and Cl, the electrostatic component is largest, followed by induction and then dispersion. However, induction overtakes electrostatic attraction as the largest component for the larger halogens Br and I. Indeed, in the latter case, induction is twice the magnitude of ES. Dispersion makes a smaller, but not negligible contribution in all cases. In terms of trends, the transition from Cl to Br results in an increase in all of the components, a trend which accelerates when Br is replaced by the larger I. The large induction and dispersion energy for I is consistent with its much greater size and polarizability, as well as with prior calculations<sup>40</sup>.

### 7-3. 4. Higher Level of Theory and Second Conformation

It is important to be sure that the patterns and principles arising from the DFT calculations are truly correct, and reflect the real process. For this reason, the calculation of all energies was repeated by the MP2 method, using geometries obtained by M06/2X, all with the same aug-cc-pVDZ basis set. These results are reported in

Table 7-9 and can be compared directly with the DFT data in Table 7-2. The association energies of each catalyst with the imine,  $E_1$ , are changed very little by the DFT to MP2 transition. The same may be said of the dissociation of the catalyst from the final product,  $E_7$ . The MP2 values of the latter quantity are a bit bigger than the DFT quantities but obey the same trend. This similarity of  $E_1$  and  $E_7$ , confirms the two methods are in agreement about the strengths of the various H or halogen bonds.  $E_2$  quantities match well also, again with the proviso that MP2 binding energies are slightly larger, so the two methods are in accord about the binding of the diene. The largest disagreement occurs in the activation energies  $E_5$ . The transition from M06-2X to MP2 reduces this barrier in the uncatalyzed process by 7 kcal/mol, with slightly larger reductions for the four catalyzed reactions. These reductions are quite uniform from one catalyst to the next, so the M06-2X order of reaction barriers stands up very well against MP2 results. The energy released upon going from transition state to product,  $E_6$ , is somewhat less negative for MP2, but by a uniform amount of 8-9 kcal/mol, again preserving the DFT patterns. Importantly, the upshot of any differences between the two methods, the final reaction energy  $E_{\text{react}}$ , is virtually identical for the two methods, differing by only 1.0 kcal/mol.

With respect to the deformation and interaction energies within the transition state, the application of MP2 to the M06-2X geometries reduces  $E_{\text{def}}^{\dagger}$  by a nearly uniform amount

of 4 kcal/mol.  $E_{\text{int}}^{\ddagger}$  becomes more negative, but again by similar amounts from one catalyst type to the other, about 5-7 kcal/mol. In summary, then, the conclusions concerning catalysis derived from the activation strain model are essentially unchanged by the upgrade from M06-2X to MP2.

When the imine approaches the diene, there are two geometric possibilities. As indicated in Figure 7-2, the NH proton can adopt a position in toward the two central C=C atoms of the diene. In contrast to this endo orientation, this proton could in principle also lie in the opposite or exo direction, away from the C=C bond. In order to examine this second possibility, parallel calculations were carried out for this exo orientation, and the results are reported in Table 7-10 to Table 7-14.

Comparison with the corresponding endo data in Table 7-1 to Table 7-6 reveals only minor changes for the most part. Considering first the encounter complex, Table 7-10 shows that in most cases, the change from endo to exo elongates the  $R(\text{N}\cdots\text{C})$  distance, but engenders only a small change in the H/X-bond distance. (The exo encounter complexes differ from the endo cases in that there is a tendency for the diene to associate more closely with the aromatic catalyst than with the imine. This tendency is greatest for the X=H and Cl cases, although the energetic change associated with this relocation is slight.) The  $R(\text{N}\cdots\text{C})$  stretch persists in the TS albeit to a smaller extent; very little change is observed in the products.

With respect to the energetics in Table 7-11, the binding of the diene to the imine $\cdots$ catalyst complex,  $E_2$ , is enhanced a bit in the exo structure particularly for H and Cl, but the energy jump from the encounter complex to the TS,  $E_3$ , is also raised. As a

consequence, the important total energy barrier  $E_5$  is changed by only small amounts. For example, the energy barrier in the uncatalyzed exo reaction is 3.5 kcal/mol higher than for endo, but the changes to the catalyzed energy barriers are even smaller, less than 2 kcal/mol. With respect to the deformation and interaction energies in the TS, these quantities are also changed by little, less than 2 kcal/mol in most cases.

The switch from endo to exo has some effect on the NBO charge transfers in the transition states, but again these are generally quite small, and confirm the prior finding that a good deal more transfer takes place from the  $\pi$  orbitals of the diene to the imine  $\pi^*$  orbital than in the reverse direction. The same can be said concerning the group charges in Table 7-4 and Table 7-13. Even less affected by the endo $\rightarrow$ exo change are the orbital energies in Table 7-5 and Table 7-14, which confirms the prior conclusion that the catalysts reduce the energy barrier in part by a lowering of the energy of the  $\pi^*$  LUMO of the imine. In summary, the calculations for the exo reaction repeat the findings of the endo geometries in all but the finest quantitative detail.

### 7-3. 5. Free Energies

Using standard thermochemical formulae, it is possible to evaluate the free energy quantities that parallel the electronic energies of Table 7-2. Table 7-7 and Table 7-8 display these free energies ( $T=25\text{ C}$ ,  $p=1\text{ atm}$ ) for each reaction step defined in Figure 7-1 for the endo and exo geometries, respectively. Inclusion of entropic effects leads to free energies that are generally more positive than  $E$  but the trends observed in the latter quantities remain largely intact. The reactions characterized by  $G_1$  and  $G_2$  experience the largest positive changes since they involve the association of two separate species into a single

entity. But they also exhibit the large halogen-bond energy associated with I, with  $G_1$  following the same trend as did  $E_1$ :  $I > H > Br > Cl$ , and with very similar increments.  $G_6$ , the drop in energy upon going from the transition state down to the product-catalyst complex, is only slightly less negative than  $E_6$ , both very exothermic quantities of more than -50 kcal/mol.

With respect to  $G_5$ , these quantities are again larger than  $E_5$ . Inclusion of entropy mutes to a certain extent the dramatic catalytic effects of Table 7-2, but confirms the catalytic reduction in activation free energy, especially that associated with the I substituent. Indeed,  $G_5$  also follows the same  $I > H > Br > Cl$  pattern as does the binding energy  $E_1$ . The free energies in Table 7-7 and Table 7-8 may be used to estimate reaction rate accelerations by the catalysts. Assuming an Arrhenius-type relation  $\exp\{-(E_{cat} - E_{uncat})/RT\}$ , the speedup of the reaction by the I-catalyst amounts to  $5 \times 10^4$  for the endo geometry; this acceleration is even larger,  $2 \times 10^6$ , for the exo structure. The catalytic speedup of the H and Br catalysts are smaller, only one order of magnitude for endo, but  $2 \times 10^4$  and  $3 \times 10^2$  respectively for exo. In summary, the catalytic reduction of the activation energy is somewhat more prominent for the exo structures, accelerating the rate by as much as 6 orders of magnitude.

In order to be an effective catalyst, the entity must not only reduce the activation energy, but also release its grip upon the product at the conclusion of the reaction. This dissociation corresponds to  $E_7$  in Figure 7-1. While these quantities are fairly large in Table 7-2, in the 10-20 kcal/mol range, they are greatly reduced by the impact of entropy. As indicated in Table 7-7 and Table 7-8,  $G_7$  is less than 7 kcal/mol, and even slightly



exothermic in several instances. In most cases  $G_7$  is smaller for the exo structure than for endo, reinforcing the smaller values of  $G_5$  for the former geometry.

#### 7-4. Discussion and Summary

After first forming a fairly loosely bound encounter complex, the imine and diene go on to a transition state where the incipient C-N and C-C bonds are some 2.0-2.4 Å in length. This transition state lies 14 kcal/mol higher in energy than the separated reactants. The presence of the imidazolium catalyst has a number of effects upon the reaction. Whether H, Cl, Br, or I-substituted imidazolium, the catalyst binds tightly to the imine-diene complex. In doing so, it reduces the activation energy from 14 down to less than 5 kcal/mol. The I-substituted imidazolium is most effective in this regard, and Cl the least; H and Br are roughly equivalent. The high effectiveness of I-substitution is thus intimately connected with the strength of halogen bonds including I. Br-bonds are somewhat weaker, and Cl-bonds weaker still, consistent with the trends observed in catalytic rate acceleration. Within the context of the activation strain model, the reduction of the barrier by the catalyst is a result of the high interaction energy connected with the approach of the pre-deformed species as they form the transition state. This stabilization far exceeds any increase in the deformation energy needed by the reactants to achieve their transition state structure.

The catalyst also alters the timing of the reaction, by slowing the formation of the N-C bond while hastening C-C formation. There is a good deal of  $\pi \rightarrow \pi^*$  charge transfer in both directions between the imine and diene in the transition state, although the diene( $\pi$ )  $\rightarrow$  imine( $\pi^*$ ) transfer is considerably larger. This transfer is amplified by the imidazolium catalyst, and the degree of amplification also follows the energetic trend: Cl < H ~ Br < I.

The catalyst also depresses the energy of the electron-accepting  $\pi^*$  LUMO of the imine, thereby facilitating the charge transfer from the diene.

The catalyst exerts its influence in multifold ways. In the most obvious and direct effect, the H/X bond stabilizes the transition state. The catalyst also facilitates the transfer of charge from the diene to the imine in the transition state. This effect is manifest in both the total charges of the groups themselves, but also in the energies of charge transfer between specific orbitals ( $\pi_{\text{diene}} \rightarrow \pi^*_{\text{imine}}$ ). The H/X bond to the catalyst facilitates this transfer by lowering the energy of the  $\pi^*_{\text{imine}}$  antibonding orbital, thereby reducing the HOMO-LUMO energy gap.

The effect of the catalysts upon the reaction rate has been considered here via a comparison of the transition state energy with that of the reactants, prior to any association occurring. If one were to consider instead the reaction as beginning after the reactants have already bound to one another, then one might conclude that the catalysts have very little effect upon the activation energy, even raising it by a small amount in some cases. This distinction reconfirms the importance of the binding energy of the catalyst to the acceleration of this reaction. The strong catalytic effect of the I-substituted catalyst can thus be directly attributed to the strength of halogen bonds involving this element.

In order to obtain a detailed understanding of the aza-Diels Alder reaction on a molecular level, it is first necessary to study the system without the complicating effects of surrounding molecules that would interact with the reacting system in various ways. The introduction of solvent would cause a multitude of interactions, of a rapidly fluctuating nature, making it extremely difficult to extract the underlying intramolecular effects on the

catalysis process. Moreover, each particular solvent would result in differing interactions and effects. It is for this reason that solvation has not been included to this point, but is envisioned as a large scale future endeavor.

## References

- (1) Reddi, Y.; Sunoj, R. B. *ACS Catalysis* **2015**, *5*, 5794.
- (2) Maruoka, K.; List, B.; Yamamoto, H.; Gong, L.-Z. *Chem. Commun.* **2012**, *48*, 10703.
- (3) Xu, H.; Zuend, S. J.; Woll, M. G.; Tao, Y.; Jacobsen, E. N. *Science* **2010**, *327*, 986.
- (4) Grayson, M. N.; Pellegrinet, S. C.; Goodman, J. M. *J. Am. Chem. Soc.* **2012**, *134*, 2716.
- (5) Simón, L.; Goodman, J. M. *J. Am. Chem. Soc.* **2008**, *130*, 8741.
- (6) Simón, L.; Paton, R. S. *J. Org. Chem.* **2015**, *80*, 2756.
- (7) Marcelli, T.; Hammar, P.; Himo, F. *Chem. Eur. J.* **2008**, *14*, 8562.
- (8) Bauzá, A.; Mooibroek, T. J.; Frontera, A. *ChemPhysChem*. **2015**, *16*, 2496.
- (9) Politzer, P.; Murray, J. S. A unified view of halogen bonding, hydrogen bonding and other s-hole interactions. In *Noncovalent Forces*, Scheiner, S., Ed. Springer: Dordrecht, Netherlands, 2015; Vol. 19, pp 357.
- (10) Del Bene, J. E.; Alkorta, I.; Elguero, J. *J. Phys. Chem. A* **2014**, *118*, 2360.
- (11) Scheiner, S. *Int. J. Quantum Chem.* **2013**, *113*, 1609.
- (12) Bruckmann, A.; Pena, M. A.; Bolm, C. *Synlett* **2008**, *2008*, 900.
- (13) Coulembier, O.; Meyer, F.; Dubois, P. *Polymer Chemistry* **2010**, *1*, 434.

- (14) Walter, S. M.; Kniep, F.; Herdtweck, E.; Huber, S. M. *Angew. Chem. Int. Ed.* **2011**, *50*, 7187.
- (15) Kniep, F.; Jungbauer, S. H.; Zhang, Q.; Walter, S. M.; Schindler, S.; Schnapperelle, I.; Herdtweck, E.; Huber, S. M. *Angew. Chem. Int. Ed.* **2013**, *52*, 7028.
- (16) He, W.; Ge, Y.-C.; Tan, C.-H. *Org. Lett.* **2014**, *16*, 3244.
- (17) Ahrendt, K. A.; Borths, C. J.; MacMillan, D. W. C. *J. Am. Chem. Soc.* **2000**, *122*, 4243.
- (18) Berkessel, A.; Vogl, N. *Eur. J. Org. Chem.* **2006**, *2006*, 5029.
- (19) Shirakawa, H.; Sano, H. *Synthesis* **2014**, *46*, 1788.
- (20) Jiang, X.; Wang, R. *Chem. Rev.* **2013**, *113*, 5515.
- (21) Kobayashi, S., Jørgensen, K. A. *Cycloaddition Reactions in Organic Synthesis*. Wiley-VCH: Weinheim, 2002.
- (22) Jungbauer, S. H.; Walter, S. M.; Schindler, S.; Rout, L.; Kniep, F.; Huber, S. M. *Chem. Commun.* **2014**, *50*, 6281.
- (23) Takeda, Y.; Hisakuni, D.; Lin, C.-H.; Minakata, S. *Org. Lett.* **2015**, *17*, 318.
- (24) Frisch, M. J.; Trucks, G. W.; Schlegel, H. B.; Scuseria, G. E.; Robb, M. A.; Cheeseman, J. R.; Scalmani, G.; Barone, V.; Mennucci, B.; Petersson, G. A.; Nakatsuji, H.; Caricato, M.; Li, X.; Hratchian, H. P.; Izmaylov, A. F.; Bloino, J.; Zheng, G.; Sonnenberg, J. L.; Hada, M.; Ehara, M.; Toyota, K.; Fukuda, R.; Hasegawa, J.; Ishida, M.; Nakajima, T.; Honda, Y.; Kitao, O.; Nakai, H.; Vreven, T.; Montgomery, J., J. A.; Peralta, J. E.; Ogliaro, F.; Bearpark, M.; Heyd, J. J.; Brothers, E.; Kudin, K. N.; Staroverov, V. N.; Kobayashi, R.; Normand, J.; Raghavachari, K.; Rendell, A.; Burant, J. C.; Iyengar, S. S.; Tomasi, J.; Cossi, M.; Rega, N.; Millam, J. M.; Klene, M.; Knox, J. E.; Cross, J. B.;

Bakken, V.; Adamo, C.; Jaramillo, J.; Gomperts, R.; Stratmann, R. E.; Yazyev, O.; Austin, A. J.; Cammi, R.; Pomelli, C.; Ochterski, J. W.; Martin, R. L.; Morokuma, K.; Zakrzewski, V. G.; Voth, G. A.; Salvador, P.; Dannenberg, J. J.; Dapprich, S.; Daniels, A. D.; Farkas, O.; Foresman, J. B.; Ortiz, J. V.; Cioslowski, J.; Fox, D. J. *Gaussian 09*, Revision B.01; Wallingford, CT, 2009.

(25) Zhao, Y.; Truhlar, D. G. *Theor. Chem. Acc.* **2008**, *120*, 215.

(26) Levandowski, B. J.; Houk, K. N. *J. Org. Chem.* **2015**, *80*, 3530.

(27) Pieniazek, S. N.; Clemente, F. R.; Houk, K. N. *Angew. Chem. Int. Ed.* **2008**, *47*, 7746.

(28) Gayatri, G. *Ind. J. Chem.* **2011**, *50A*, 1579.

(29) Reed, A. E.; Weinhold, F.; Curtiss, L. A.; Pochatko, D. J. *J. Chem. Phys.* **1986**, *84*, 5687.

(30) Reed, A. E.; Curtiss, L. A.; Weinhold, F. *Chem. Rev.* **1988**, *88*, 899.

(31) Glendenning, E. D.; Landis, C. R.; Weinhold, F. *J. Comput. Chem.* **2013**, *34*, 1429.

(32) Szalewicz, K.; Jeziorski, B. Symmetry-adapted perturbation theory of intermolecular interactions. In *Molecular Interactions. From Van der Waals to Strongly Bound Complexes*, Scheiner, S., Ed. Wiley: New York, 1997; pp 3.

(33) Moszynski, R.; Wormer, P. E. S.; Jeziorski, B.; van der Avoird, A. *J. Chem. Phys.* **1995**, *103*, 8058.

(34) Werner, H.-J.; Knowles, P. J.; Manby, F. R.; Schütz, M.; Celani, P.; Knizia, G.; Korona, T.; Lindh, R.; Mitrushenkov, A.; Rauhut, G.; Adler, T. B.; Amos, R. D.; Bernhardsson, A.; Berning, A.; Cooper, D. L.; Deegan, M. J. O.; Dobbyn, A. J.; Eckert, F.; Goll, E.; Hampel, C.; Hesselmann, A.; Hetzer, G.; Hrenar, T.; Jansen, G.; Köppl, C.; Liu,

- Y.; Lloyd, A. W.; Mata, R. A.; May, A. J.; McNicholas, S. J.; Meyer, W.; Mura, M. E.; Nicklaß, A.; Palmieri, P.; Pflüger, K.; Pitzer, R.; Reiher, M.; Shiozaki, T.; Stoll, H.; Stone, A. J.; Tarroni, R.; Thorsteinsson, T.; Wang, M.; Wolf, A. *MOLPRO*, Version 2006; 2010.
- (35) Wolters, L. P.; Bickelhaupt, F. M. *WIRE: Comput. Mol. Sci.* **2015**, *5*, 324.
- (36) Fernandez, I.; Bickelhaupt, F. M. *Chem. Soc. Rev.* **2014**, *43*, 4953.
- (37) Hayden, A. E.; Houk, K. N. *J. Am. Chem. Soc.* **2009**, *131*, 4084.
- (38) van Zeist, W.-J.; Bickelhaupt, F. M. *Org. Biomol. Chem.* **2010**, *8*, 3118.
- (39) Nziko, V. d. P. N.; Scheiner, S. *Phys. Chem. Chem. Phys.* **2016** *18* 3581.

Table 7-1 Interatomic distances (Å)Interatomic distances (Å)

	none	H	Cl	Br	I
encounter complex					
R(N··C)	3.306	3.165	3.237	3.218	3.202
R(C··C)	3.250	3.499	3.290	3.472	3.074
R(N··H/X)	-	2.163	2.780	2.738	2.607
TS					
R(N··C)	1.969	2.147	2.205	2.146	2.243
R(C··C)	2.406	2.143	2.098	2.160	2.077
R(N··H/X)	-	2.002	2.737	2.644	2.525
product					
R(N··C)	1.461	1.469	1.468	1.469	1.474
R(C··C)	1.531	1.527	1.529	1.528	1.527
R(N··H/X)	-	1.962	2.731	2.623	2.552

Table 7-2 Energetics (kcal/mol) of aza-Diels-Alder reaction with various substitutions on catalyst

	E <sub>1</sub>	E <sub>2</sub>	E <sub>3</sub>	E <sub>4</sub>	E <sub>5</sub>	E <sub>6</sub>	E <sub>7</sub>	E <sub>react</sub>	E <sub>def</sub> <sup>†</sup>	E <sub>int</sub> <sup>†</sup>
none	0	-3.91	17.69	13.78	13.78	-57.07	0	-43.30	17.30	-3.56
H	-12.86	-5.57	18.62	13.05	0.18	-57.45	13.97	-43.30	24.35	-24.17
Cl	-9.27	-4.54	18.46	13.92	4.65	-58.12	10.17	-43.30	22.17	-17.54
Br	-11.70	-5.61	18.68	13.07	1.37	-58.57	13.91	-43.30	23.27	-21.87
I	-18.48	-3.93	17.40	13.47	-5.02	-58.63	20.35	-43.30	26.54	-31.56

Table 7-3 NBO values of E(2) (kcal/mol) between imine and diene within the TS

	none	H	Cl	Br	I
diene $\rightarrow$ imine	49.99	64.94	58.57	61.85	73.81
imine $\rightarrow$ diene	27.47	25.04	25.48	23.89	21.66
$\pi(\text{C}_3\text{C}_4)^a \rightarrow \pi^*(\text{NC})$	31.99	19.29	22.26	18.91	12.96
$\pi(\text{C}_1\text{C}_2) \rightarrow \pi^*(\text{NC})$	18.00	45.65	36.31	42.94	60.85
$\pi(\text{NC}) \rightarrow \pi^*(\text{C}_3\text{C}_4)$	23.56	15.41	17.44	14.86	10.85
$\pi(\text{NC}) \rightarrow \pi^*(\text{C}_1\text{C}_2)$	3.91	9.63	8.04	9.03	10.81

<sup>a</sup>C<sub>3</sub>C<sub>4</sub> refers to C=C bond of diene that is close to imine N, and C<sub>1</sub>C<sub>2</sub> to the other double bond

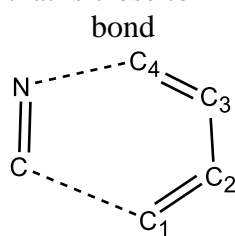


Table 7-4 NBO group charges (e)NBO group charges (e)

	non	H	Cl	Br	I
encounter complex					
imine	-0.002	0.027	0.014	0.043	0.097
diene	0.002	0.008	0.010	0.003	0.014
cat	-	0.965	0.976	0.953	0.888
TS					
imine	0.000	-0.098	-0.071	-0.072	-0.062
diene	0.000	0.140	0.097	0.136	0.206
cat	-	0.958	0.974	0.936	0.856
$\Delta q = q(\text{TS}) - q(\text{encounter complex})$					
imine	0.002	-0.125	-0.085	-0.116	-0.160
diene	-0.002	0.131	0.087	0.133	0.192
cat	-	-0.007	-0.002	-0.017	-0.032



Table 7-5 Energy eigenvalues (au) of the  $\pi^*$  imine LUMO in complex with indicated catalyst

	none	H	Cl	Br	I
canonical LUMO	+0.0108	-0.1138	-0.0888	-0.0961	-0.1134
NBO LUMO	+0.0666	-0.0600	-0.0366	-0.0447	-0.0633

Table 7-6 Attractive SAPT components (kcal/mol) of the interaction energy between imine and catalyst, prior to introduction of diene

	H	Cl	Br	I
ES	-16.22	-12.47	-16.98	-37.41
IND	-5.98	-9.56	-21.77	-70.82
DISP	-3.86	-3.50	-4.67	-19.68
total	-12.68	-8.21	-9.99	-17.78

Table 7-7 Free energies (kcal/mol) of aza-Diels-Alder reaction in the endo conformation with various substitutions on catalyst, evaluated at 298 K and 1 atm.

endo	G <sub>1</sub>	G <sub>2</sub>	G <sub>3</sub>	G <sub>4</sub>	G <sub>5</sub>	G <sub>6</sub>	G <sub>7</sub>	G <sub>react</sub>
none	0	5.30	23.05	28.34	28.34	-52.85	0	-24.51
H	-3.77	4.60	26.23	30.83	27.06	-53.75	2.18	-24.51
Cl	-0.06	8.19	23.16	31.35	31.29	-56.31	0.51	-24.51
Br	-1.54	4.63	24.37	29.00	27.45	-55.63	3.67	-24.51
I	-7.73	8.61	20.97	29.58	21.85	-53.29	6.93	-24.51

Table 7-8 Free energies (kcal/mol) of aza-Diels-Alder reaction in the exo conformation with various substitutions on catalyst, evaluated at 298 K and 1 atm.

exo	G <sub>1</sub>	G <sub>2</sub>	G <sub>3</sub>	G <sub>4</sub>	G <sub>5</sub>	G <sub>6</sub>	G <sub>7</sub>	G <sub>react</sub>
none	0	5.30	26.92	32.22	32.22	-56.73	0	-24.51
H	-3.77	2.74	27.43	30.17	26.40	-53.72	2.81	-24.51
Cl	-0.06	2.83	28.91	31.74	31.68	-55.05	-1.14	-24.51
Br	-1.54	5.88	24.45	30.33	28.79	-51.89	-1.41	-24.51
I	-7.73	8.85	22.50	31.35	23.62	-51.55	3.42	-24.51

Table 7-9 Energies (kcal/mol) computed at the MP2 level with the aug-cc-pVDZ basis set for the

Endo	E <sub>1</sub>	E <sub>2</sub>	E <sub>3</sub>	E <sub>4</sub>	E <sub>5</sub>	E <sub>6</sub>	E <sub>7</sub>	E <sub>react</sub>	E <sub>def</sub> <sup>‡</sup>	E <sub>int</sub> <sup>‡</sup>
none	0	-4.73	11.88	7.15	7.15	-49.41	0	-42.26	14.05	-6.88
H	-13.91	-7.09	11.03	3.93	-9.97	-48.63	16.35	-42.26	20.29	-30.26
Cl	-9.67	-5.87	11.12	5.25	-4.42	-49.4	11.57	-42.26	18.4	-22.82
Br	-12.87	-7.29	10.83	3.53	-9.34	-49.97	17.05	-42.26	19.35	-28.69
I	-16.81	-8.47	9.86	1.38	-15.42	-50.31	23.47	-42.26	22.51	-37.93

Table 7-10 Interatomic distances (Å) of exo conformation

	none	H	Cl	Br	I
encounter complex					
R(N··C)	3.306	3.747	5.588	3.799	3.604
R(C··C)	3.250	3.743	5.129	3.277	3.261
R(N··H/X)	-	2.097	2.824	2.749	2.654
TS					
R(N··C)	2.063	2.194	2.160	2.206	2.287
R(C··C)	2.235	2.097	2.140	2.097	2.049
R(N··H/X)	-	1.913	2.714	2.628	2.514
product					
R(N··C)	1.461	1.469	1.468	1.479	1.489
R(C··C)	1.531	1.527	1.529	1.534	1.532
R(N··H/X)	-	1.962	2.731	2.641	2.570

Table 7-11 Energetics (kcal/mol) of Diels-Alder reaction in the exo conformation

exo	E <sub>1</sub>	E <sub>2</sub>	E <sub>3</sub>	E <sub>4</sub>	E <sub>5</sub>	E <sub>6</sub>	E <sub>7</sub>	E <sub>react</sub>	E <sub>def</sub> <sup>†</sup>	E <sub>int</sub> <sup>†</sup>
none	0	-3.91	21.26	17.34	17.34	-60.64	0	-43.30	21.5	-4.24
H	-12.86	-9.74	23.19	13.45	0.59	-57.44	13.56	-43.30	25.77	-25.19
Cl	-9.27	-10.51	25.88	15.37	6.10	-59.62	10.23	-43.30	23.78	-17.54
Br	-11.7	-6.38	20.85	14.47	2.77	-55.04	8.97	-43.30	24.74	-21.96
I	-18.48	-3.85	18.67	14.82	-3.66	-54.47	14.84	-43.30	27.17	-30.82

Table 7-12 NBO values of E(2) (kcal/mol) between imine and diene within the TS in the exo.

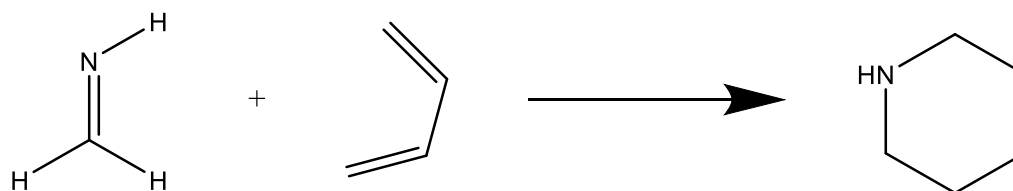
	none	H	Cl	Br	I
diene → imine	51.96	66.80	60.42	67.74	79.35
imine → diene	28.33	26.61	26.39	24.96	21.53
$\pi(\text{C}_3\text{C}_4) \rightarrow \pi^*(\text{NC})$	16.61	12.72	13.84	12.44	9.71
$\pi(\text{C}_1\text{C}_2) \rightarrow \pi^*(\text{NC})$	35.35	54.08	46.58	55.30	69.64
$\pi(\text{NC}) \rightarrow \pi^*(\text{C}_3\text{C}_4)$	21.10	15.09	16.33	13.98	9.96
$\pi(\text{NC}) \rightarrow \pi^*(\text{C}_1\text{C}_2)$	7.23	11.52	10.06	10.98	11.57

Table 7-13 NBO charges in the exo conformation

	encounter complex				
	none	H	Cl	Br	I
imine	-0.002	0.037	0.020	0.040	0.092
diene	0.002	0.001	0.001	0.006	0.007
cat		0.962	0.979	0.953	0.902
	TS				
	none	H	Cl	Br	I
imine	-0.003	-0.065	-0.076	-0.079	-0.068
diene	0.003	0.104	0.102	0.145	0.218
cat		0.961	0.974	0.934	0.849
	$\Delta q = q(\text{TS}) - q(\text{encounter complex})$				
imine	0.000	-0.102	-0.096	-0.120	-0.159
diene	0.000	0.102	0.101	0.139	0.212
cat	0.000	0.000	-0.005	-0.020	-0.052

Table 7-14 Energy eigenvalues (au) of the  $\pi^*$  imine LUMO in complex with indicated catalyst in

	none	H	Cl	Br	I
LUMO	+0.0105	-0.1117	-0.0883	-0.1081	-0.1111
NBOLUMO	+0.0655	-0.0523	-0.0352	-0.0407	-0.0534



Scheme 7-1Aza Diels-Alder Reaction

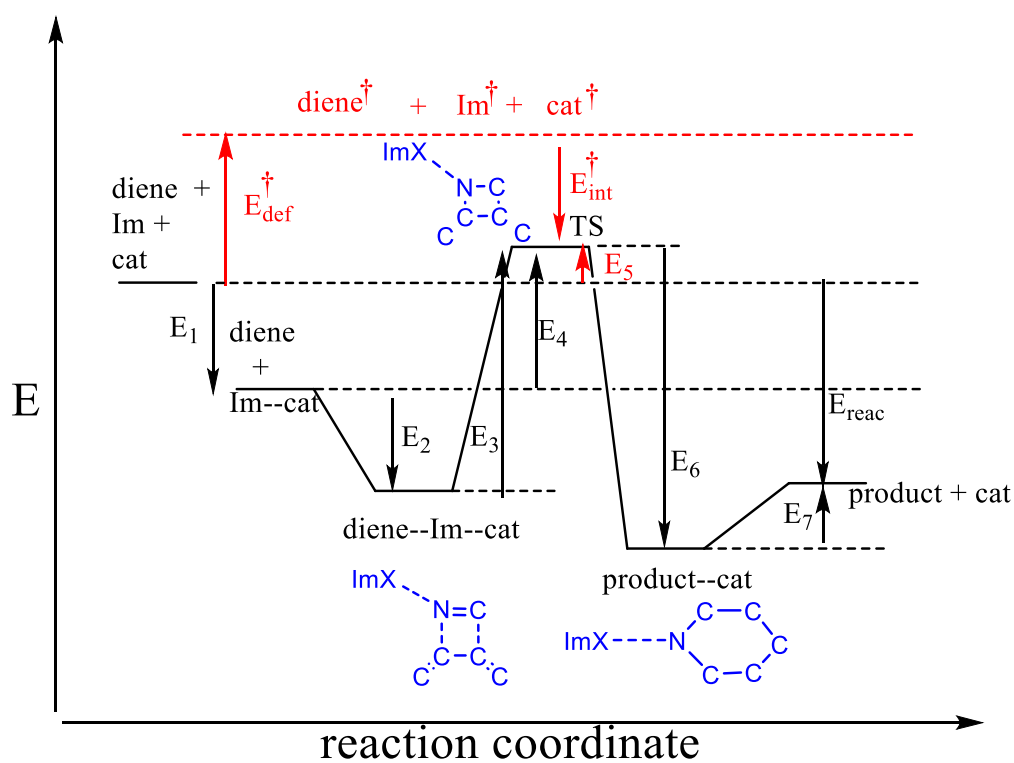


Figure 7-1 Energy diagram of aza-Diels-Alder reaction of diene with imine (Im) and catalyst (cat)

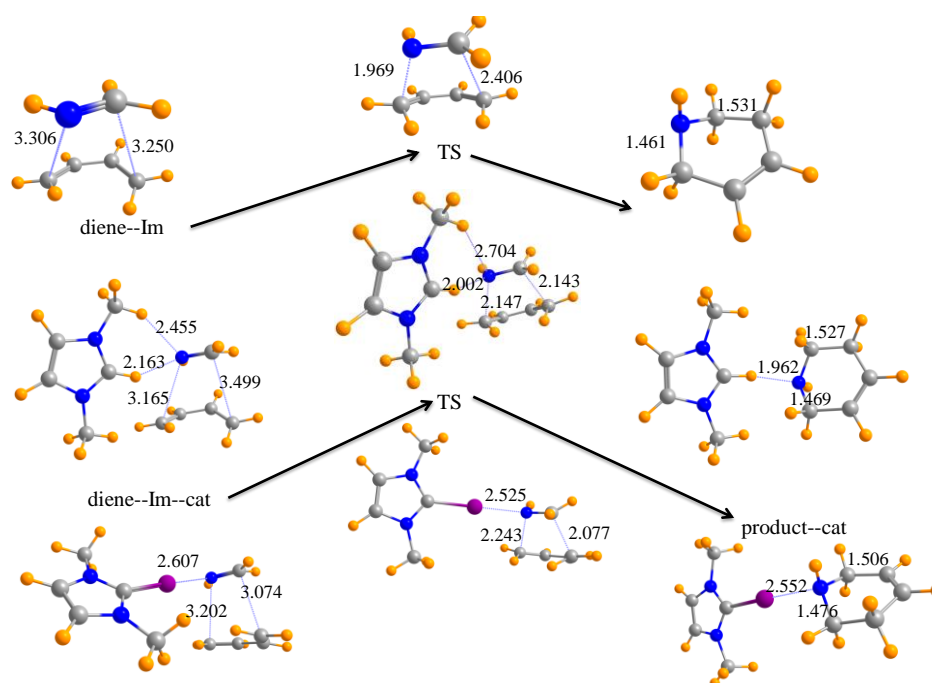


Figure 7-2 Encounter complex, transition state (TS) and product with no catalyst (top), H-bonding catalyst (middle), and I-bonding catalyst (bottom). Distances in Å.

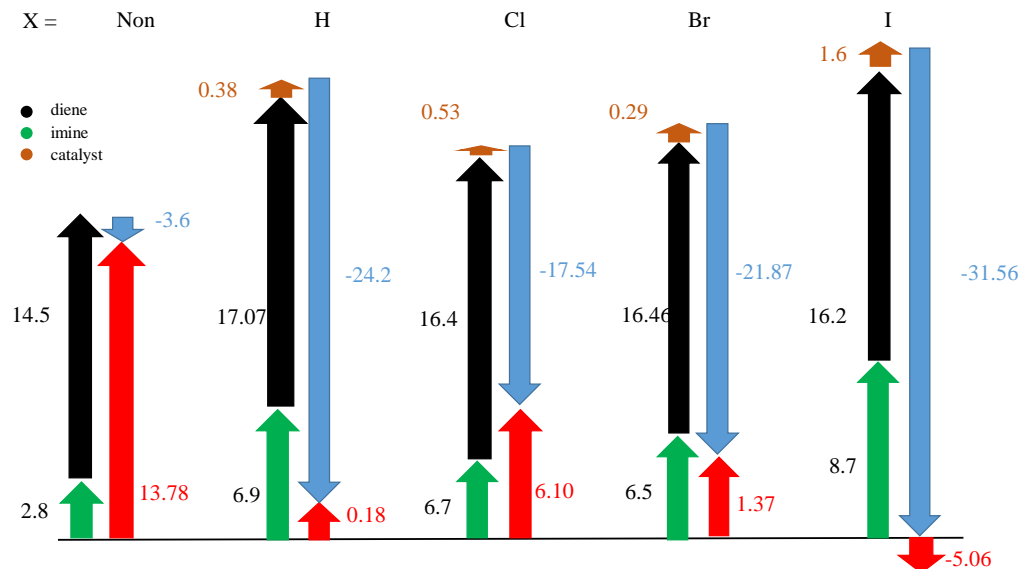


Figure 7-3 Deformation energies (kcal/mol) of imine (green) and diene (black), catalyst (brown), and interaction energy (blue) of reaction with indicated catalyst. Total activation energy in red.

CHAPTER 8  
EFFECT OF ANGULAR DEFORMATION ON THE ENERGETICS OF THE S<sub>N</sub>2  
REACTION<sup>1</sup>

**Abstract**

Quantum calculations are applied to a number of model S<sub>N</sub>2 reactions. The halides F-, Cl-, and Br- were allowed to attack the central C atom of a set of CH<sub>2</sub>RI molecules, with R= H, CH<sub>3</sub>, CH=CH<sub>2</sub>, C≡CH, and C≡N. For each system the X··C··I angle was distorted in set increments from the optimized value, and the activation energy computed for each angle. The energy of the transition state rose in conjunction with this deformation. However, the distortion energy of the initial X··CH<sub>2</sub>RI reaction complex was similar in magnitude. As a result, the activation energy of the reaction was quite insensitive to angular deformation.

**8-1. Introduction**

The bimolecular nucleophilic substitution reaction (S<sub>N</sub>2) is one of the most useful and fundamental reactions in organic synthesis <sup>1-7</sup>. The Williamson ether synthesis in which an alkoxide reacts with an alkyl halide is a typical S<sub>N</sub>2 reaction. This reaction also plays a key role in biochemical reactions like methyl group transfer in which S-adenosyl methionine serves as co-substrate <sup>8-11</sup>.

Due to the versatility of this reaction, it has been intensively scrutinized in a number

---

<sup>1</sup>Coauthored by Vincent de Paul Nzuwah Nziko and Steve Scheiner. Reproduced with permission from *Eur. J. Org. Chem.* **2016**, 23, 3964-3968. Copyright 2016, ChemPubSoc Europe.



of experimental and theoretical studies over the years. It's been shown that  $S_N2$  reactions can result either in inversion and/or retention of configuration at the central atom <sup>12</sup>. The former proceeds through a backside attack and the latter through the front side attack on the central atom. Generally, the backside mechanism proceeds through a lower transition state energy and it is therefore kinetically dominant and more efficient. Efforts have been made to understand the factors that affect this reaction <sup>13-17</sup>, including solvent effects, and nucleophile and leaving group electronegativity <sup>18-22</sup>. For example, Bento and Bickelhaupt <sup>23, 24</sup> used relativistic density functional theory to ascertain that backside  $S_N2$  barriers increase as the halide nucleophile becomes less electronegative:  $F^- < Cl^- < Br^- < I^-$ , and obeys the opposite trend for the leaving group:  $CH_3F > CH_3Cl > CH_3Br > CH_3I$ .

With respect to the common backside mechanism, it is believed that the system strives toward linearity at the transition state, where the central C atom CA lies along the axis between the leaving group (LG) and the incoming nucleophile (Nu), viz.  $\theta(Nu^- \cdots CA \cdots LG)$  tends toward  $180^\circ$ . Unlike the situation where this reaction takes place between initially separate reactants in solution, when the various species are free to adopt their most stable orientations relative to one another, there are certain restrictions associated with a biological setting. In the context of an enzyme, the overall three-dimensional structure of the protein is the result of a host of interactions between various parts of the molecule. For example, H-bonds which prefer a linear geometry, are seldom free to adopt this arrangement within a protein, but instead must make compromises and adjust their structure accordingly. The same sorts of restrictions would be expected between the nucleophile and substrate with respect to  $S_N2$  reactions, which would prevent the linear

approach that is intrinsically preferred. The methyl transfer reaction that takes place in glycine N-methyltransferase serves as one example. Soriano et al showed using QM/MM calculations that the transition state angle for the transfer of the methyl group from SAM to glycine in both neutral and basic solutions are  $172.4^\circ$  and  $170.9^\circ$ , which deviate from linearity by about  $10^\circ$ <sup>25</sup>. In this particular example, there would appear to be a H-bond between Arg175 and Gly137 which keeps the nucleophile from its preferred trajectory in attacking SAM at  $180^\circ$ , but other systems might certainly have other factors that cause angular deformations.

It is thus important to understand how angular distortions from linearity might affect the energetics and thus the rates of the  $S_N2$  reaction. How, and by how much, is the activation energy of this reaction affected by angular deformation? How is the sensitivity of the energy barrier to deformation in turn affected by the nature of the attacking nucleophile, or by the groups attached to the central C atom? This work attempts to provide answers to these questions through a set of carefully designed quantum calculations. A range of nucleophiles are considered, in conjunction with a variety of different chemical groups attached to the central C. The range of properties considered in the set of systems examined is chosen so as to be broad enough to cover a wide swath of chemistry and biochemistry.

## 8-2. Theoretical Methods

Calculations made use of the Gaussian 09 package of codes<sup>26</sup>. Geometries were optimized at the ab initio MP2 level using the aug-cc-pVDZ basis set which have together been shown to be of high accuracy when applied to molecular systems of this sort<sup>27-29</sup>.

Each system was composed of a tetravalent carbon (CA), bound to a leaving group (LG). A nucleophile (Nu) was allowed to approach CA from its backside relative to LG. An  $S_N2$  reaction profile was traced out by reducing  $R(\text{Nu}\cdots\text{CG})$  in small decrements. For each such fixed distance, the geometry of the entire system was fully optimized. The peak of this profile was deemed to be the transition state. Angular distortions were introduced by imposing a fixed angle  $\theta(\text{Nu}\cdots\text{CA}\cdots\text{LG})$  upon the system. The reaction profile was traced out as before, with the addition of the restriction to this particular angle  $\theta$ . Its peak was deemed to be the transition state for this angle  $\theta$ .

Systems chosen for study are presented in Scheme 1. The leaving group (LG) was chosen to be I. The central C (CA) is bound to two H atoms, plus one additional group. This group varies from methyl, to ethyl, vinyl, ethynyl, and cyano. In other words, the pendant group may contain single, double, or triple bonds, as well as a heteroatom. The approaching nucleophile took the form of one of the halides:  $\text{F}^-$ ,  $\text{Cl}^-$  or  $\text{Br}^-$ .

### 8-3. Results

The transition states obtained for the case where  $\text{F}^-$  serves as the attacking nucleophile are exhibited in Figure 8-1 for each of the various substituents. The fluoride locates itself nearly opposite the I leaving group. The  $\theta(\text{F}\cdots\text{C}\cdots\text{I})$  angle is  $180^\circ$  for the H substituent but deviates from linearity by as much as  $14^\circ$  in the case of the ethyl group. For each system, it is this optimized angle which is taken as the undistorted geometry. The structures for the other systems examined with  $\text{Cl}^-$  and  $\text{Br}^-$  nucleophiles were quite similar. The undistorted angles are displayed in Table 8-1 for all systems. Their deviation from  $180^\circ$  tends to grow along with the size of the approaching halide nucleophile. In order to

measure the sensitivity of the reaction to angular distortion, each complex was distorted from its fully optimized geometry in  $2^\circ$  increments. As indicated above, the reaction profile was mapped out by holding fixed the angle  $\theta$ , and optimizing the geometry of each structure for each  $R(X\cdots CA)$ . The salient energetic quantities in each reaction profile are indicated in Scheme 2. Beginning with the fully separate nucleophile  $X^-$  and the  $CRH_2I$  molecule, these two species first come together to form an reaction complex  $X^-\cdots CRH_2I$ , with a binding energy of  $E_0$ . From that point, the system requires an energy  $E_2$  to attain the transition state  $(X\cdots CRH_2\cdots I)^-$ .  $E_1$  refers to the energy of the transition state relative to the separated reactants. The red energy levels in Scheme 2 refer to the same structures, but with a deformation imposed upon their angular preference. As such, these red levels are placed higher in energy than are the undistorted black energy levels. Like their unprimed counterparts,  $E_2'$  and  $E_1'$  again correspond to the energy of the (distorted) transition state, relative to the reaction complex, and unassociated reactants, respectively.

The calculated quantities for the activation barriers are reported in Table 8-2, where  $\Delta\theta$  refers in each case to the distortion of this angle from linearity. Focusing first on the values of  $E_1$ , there is a fairly sharp rise in this barrier, relative to the separated reactants, as angular distortions are imposed upon each system. The dependence of  $E_1$  upon angular distortion is displayed in Figure 8-2 where the curves resemble parabolas.

And indeed, these data may be fit well by a quadratic function of the form in Eq (1)

$$E_1 = \frac{1}{2} k(\Delta\theta)^2 \quad (1)$$

The values of the distortion constant  $k$  are reported in Table 8-3, along with the correlation coefficient for its fitting. In terms of scale, a value of  $k = 8 \text{ cal}\cdot\text{mol}^{-1}\text{deg}^{-2}$  in Table 8-3, a typical value, would correspond to a rise in  $E_1$  by 3.6 kcal/mol caused by a

distortion  $\Delta\theta$  of  $30^\circ$ . Inspection of the R=H curves in Figure 8-2 indicates that the bromide and chloride curves are less steep than the fluoride. This trend is confirmed by the larger values of  $k$  for  $F^-$  than for the other two halides in Table 8-3. With regard to R, the methyl group exhibits the greatest sensitivity to angular distortion, followed by ethyl, and then H. The triple-bonded species are least sensitive, with the exception of when they are coupled with bromide. An alternate, and more common, means of assessing the barrier for a reaction such as this begins not with the separated reactants, but rather with the reaction complex. This barrier corresponds to the  $E_2$  quantity in Scheme 2. Inspection of Table 8-2 suggests that this barrier is rather insensitive to angular distortions, typically remaining constant to within less than 1 kcal/mol, even after the introduction of as much as a  $30^\circ$  deformation. Taking the reaction of  $Cl^-$  with  $CH_3I$  as an example,  $E_2$  diminishes from 10.87 kcal/mol in its undistorted geometry to 10.22 when the  $Cl\cdots C\cdots I$  angle is  $30^\circ$  removed from linearity. It is perhaps puzzling at first sight to note such discrepant behavior between the two measures of activation energy. This difference can be explained by a glance at Scheme 2 wherein the black energies refer to an undistorted geometry, while distortions are indicated by the red quantities and the primed quantities. Considering first the  $X^-\cdots CRH_2I$  reaction complex, it of course becomes less stable upon introducing an angular distortion. But the same is true of the  $(X\cdots CRH_2\cdots I)^-$  transition state. If the distortion energies of the two geometries are similar, then only small changes can be anticipated in their energy difference  $E_2$ .  $E_1$ , on the other hand, takes as its starting point the fully separated reactants, with no possibility of distortion energy. The destabilization of the transition state thus cannot be compensated by any such rise in energy of the reactants, so the deformation will

universally raise  $E_1$ .

#### 8-4. Discussion and Summary

The calculations have indicated that a distortion of the preferred angle of attack of the nucleophile toward the central C atom in an  $S_N2$  reaction induces a strain energy into the system. Angular deformations raise the transition state energy, proportional to  $(\Delta\theta)^2$ . Depending upon the particular system, a  $30^\circ$  distortion increments this energy by between 2.5 and 5.2 kcal/mol. With respect to the variations on the theme of halide attacking the  $CH_2RI$  molecule, the sensitivity to angular deformation appears to be a function of both the nature of the halide and the R group. For example, the methyl group is most sensitive to angle for  $F^-$  and  $Br^-$  nucleophiles, but the vinyl group takes this distinction for  $Cl^-$ . There is a general trend of  $F^- > Cl^- > Br^-$  but  $Br^- > Cl^-$  for both the triple bonded  $C\equiv CH$  and  $C\equiv N$  groups. This rise in energy of the transition state increases the barrier of the reaction when the fully separated reactants are taken as the initial point of the reaction.

On the other hand, the idea of taking the infinitely separated reactants as a starting point for the reaction is not relevant to a situation as might occur within an enzyme. In such a case, the nucleophile is already engaged with the central C atom to a certain extent even before the reaction begins. It therefore is more sensible to begin the process with the nucleophile already in striking distance of the central C atom, with the leaving group still covalently bonded to it. And indeed, this sort of structure serves as the traditional starting point for a host of studies of the  $S_N2$  reaction<sup>30-35</sup>, even in the gas phase. In this context, the imposition of an angular deformation has a minor, perhaps even negligible, effect on the activation energy. The reason for this lack of sensitivity to angular strain arises from

the fact that the initial structure for the reaction, analogous to an reaction complex, suffers from strain energy, just as does the transition state. And perhaps more importantly, this strain energy is roughly equal in the two geometries. As a result of both the starting point and transition state rising in energy by similar amounts, the activation energy is barely affected by the angular deformation.

The effects of angular distortion have been extensively studied for another reaction, that involving the transfer of a proton along a pre-existing H-bond<sup>37-41</sup>. For this reaction, bends of the H-bond typically lead to increases in the transfer barrier, and quite sizable ones at that. These barrier increments were observed not only in E1, but also in E2, with reference to Scheme 2. That is, the barrier to proton transfer rises as a result of an angular deformation, whether one considers the barrier with reference to the separated reactants, or to the pre-formed H-bonded reaction complex. In other words, the angular deformation yields a much more substantial destabilization of the transition state than of the reaction complex. This result is different from the S<sub>N</sub>2 reaction examined here, where the reaction barrier E<sub>2</sub> is barely affected by angular distortion.

On a final note concerning the level of theory, a very recent set of calculations<sup>42</sup> observed that MP2 energy barriers for the S<sub>N</sub>2 reaction of the attack of F<sup>-</sup> on the CH<sub>3</sub>I molecule were quite similar to those computed using the much more accurate CCSD(T). This result adds to our confidence in the calculations described above.

## References

- 1 G. Vayner, K.N. Houk, W.L. Jorgensen, and J. I. Brauman *J. Am. Chem.*, **2004**, 126, 9054-9058
- 2 E.D. Hughes and C.K. Ingold, *J. Chem. Soc.*, **1935**, 244-255
- 3 R.J.S. Francis, A. Carey, (fifth ed.)Springer, New York, **2007**
- 4 J.I. Brauman, W.N. Olmstead and C.A. Lieder, *J. Am. Chem. Soc.*, **1974**, 96 4030-4031
- 5 J. A. Dodd, K. E. Salomon, W. E. Tumas and J. I. Brauman, *Pure Appl. Chem.*, **1984**, 56 1809-1818
- 6 W. D. Allen, H. F. Schaefer, A. G. Csaszar, and G. Tarczay *Chem.-Eur. J.*, **2003**, 9, 2173-2192
- 7 A. Dedieu and A. Veillard *J. Am. Chem. Soc.*, **1972**, 94, 6730-6738
- 8 S. C. Chen, C. H. Huang, S. J. Lai, J. S. Liu, P. K. Fu and S. T Tseng. *Scientific Reports* **2015**, 5, 10100.
- 9 D. O'Hagan and J. W. Schmidberger, *Nat. Prod. Rep.*, **2010**, 27, 900-918
- 10 M. Fujioka, K. Konishi and Y. Takata, *Biochemistry*, **1988**, 27, 7658-7664
- 11 Y. Takata, K. Konishi, T. Gomi and M. Fujioka, *J. Biol. Chem.*, **1994**, 269, 5537-5542
- 12 A.P. Bento and F.M. Bickelhaupt, *J. Org. Chem.*, **2008**, 73, 7290-7299
- 13 G. N. Merrill, S. Gronert, and S. R. Kass, *J. Phys. Chem. A.*, **1997**, 101, 208-218
- 14 M. L. Chabiny, S. L. Craig, C. K. Regan, and J. I. Brauman, *Science.*, **1998**, 279, 1882-1886.
- 15 B. Ensing, and M. L Klein, *Proc. Nat. Acad. Sci., USA* **2005**, 102, 6755-6759.



- 16 J. Xie, R. Otto, J. Mikosch, J. Zhang, R. Wester and W. L. Hase, *Acc. Chem. Res.*, **2014**, 47, 2960-2969.
- 17 J. Zhang, L. Yang, J. Xie and W. L. Hase, *J. Phys. Chem. Lett.*, **2016**, 7, 660-665.
- 18 S. Liu, H. Hu and L.G. Pedersen, *J. Phys. Chem. A*, **2010**, 114, 5913-5918
- 19 S.L. Craig and J.I. Brauman, *J. Am. Chem. Soc.*, **1996**, 118, 6786-6787
- 20 K.C. Westaway, Y. Gao and Y. Ren Fang, *J. Org. Chem.*, **2003**, 68, 3084-3089
- 21 J.R. Pliego and J.M. Riveros, *J. Phys. Chem. A*, **2004**, 108, 2520-2526
- 22 J.R. Pliego and D. Piló-Veloso, *J. Phys. Chem. B.*, **2007**, 111, 1752-1758
- 23 A. P. Bento and F. M. Bickelhaupt, *Chem.-Asian J.*, **2008**, 3, 1783-1792
- 24 A. P. Bento, M. Sola and F. M. Bickelhaupt, *J. Comput. Chem.*, **2005**, 26, 1497-1504
- 25 A. Soriano, R. Castillo, C. Christov, J. Andres and V. Moliner, *Biochemistry.*, **2006**, 45, 14917-14925
- 26 Frisch, M. J.; Trucks, G. W.; Schlegel, H. B.; Scuseria, G. E. Robb, M. A.; Cheeseman, J. R.; Scalmani, G.; Barone, V.; Mennucci, B.; Petersson, G. A.; et al. Gaussian 09, revision B.01; Gaussian, Inc.: Wallingford, CT, **2009**.
- 27 V.P.N Nziko and S. Scheiner, *J. Phys. Chem. A.*, **2014**, 118, 10849-10856
- 28 V.P.N Nziko and S. Scheiner, *J. Phys. Chem. A.*, **2015**, 119, 5889-5899
- 29 D. Hauchecorne and W. A. Herrebout, *J. Phys. Chem. A.*, **2013**, 117, 11548-11557
- 30 W. N. Olmstead, and J. I. Brauman, *J. Am. Chem. Soc.*, **1977**, 99, 4219-4228
- 31 A. Merkel, Z. Havlas, and R. Zahradnik, *J. Am. Chem. Soc.*, **1988**, 110, 8355-8359
- 32 A. P. Bento, M. Solà and F. M. Bickelhaupt, *J. Chem. Theory Comput.*, **2008**, 4, 929-940

- 33 P. Manikandan, J. Zhang and W. L. Hase, *J. Phys. Chem. A.*, **2012**, 116, 3061-3080.
- 34 A. A. Ahmadi, and A. Fattahi, *Comput. Theor. Chem.*, **2015**, 1067, 71-83.
- 35 J. Xie and W. L. Hase, *Science.*, **2016**, 352, 32-33.
- 36 E. A. Hillenbrand, and S. Scheiner, *J. Am. Chem. Soc.*, **1984**, 106, 6266-6273.
- 37 S. Scheiner, and E. A. Hillenbrand, *Proc. Nat. Acad. Sci.*, USA **1985**, 82, 2741-2745.
- 38 S. Cybulski, S. Scheiner, *J. Am. Chem. Soc.*, **1987**, 109, 4199-4206.
- 39 S. Cybulski, and S. Scheiner, *J. Am. Chem. Soc.*, **1989**, 111, 23-31.
- 40 S. Scheiner, and L. Wang, *J. Am. Chem. Soc.*, **1993**, 115, 1958-1963
- 41 S. Scheiner, *Acc. Chem. Res.*, **1994**, 27, 402-408.
- 42 J. Zhang, L. Yang, and L. Sheng, *J. Phys. Chem., A* **2016**, 120, 3613-3622.

Table 8-1  $\theta(\text{F}\cdots\text{C}\cdots\text{I})$  angle in the transition state for  $(\text{X}\cdots\text{CH}_2\text{R}\cdots\text{I})^-$ 

	$\text{F}^-$	$\text{Cl}^-$	$\text{Br}^-$
$\text{R}=\text{H}$	179.9	180.0	180.0
$\text{CH}_3$	165.9	163.6	163.1
$\text{CH}=\text{CH}_2$	169.4	166.5	166.0
$\text{C}\equiv\text{CH}$	167.7	166.2	165.7
$\text{C}\equiv\text{N}$	172.5	169.5	168.9

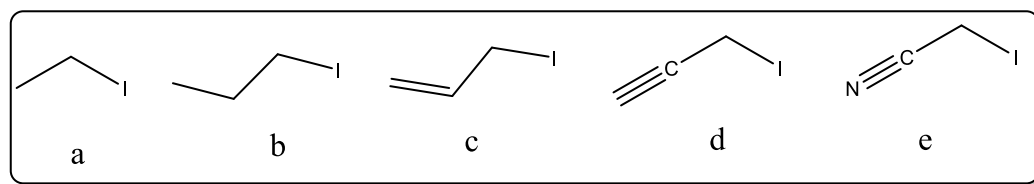
Table 8-2 Calculated energy barriers to  $\text{S}_{\text{N}}2$  reaction (kcal/mol)

	$\Delta\theta$	$\text{F}^-$		$\text{Cl}^-$		$\text{Br}^-$	
		$\text{E}_1$	$\text{E}_2$	$\text{E}_1$	$\text{E}_2$	$\text{E}_1$	$\text{E}_2$
$\text{R}=\text{H}$	0	0.10	16.17	6.64	10.87	6.79	9.86
	10	0.63	15.71	7.56	10.66	7.71	9.70
	20	2.73	15.55	9.79	10.41	9.90	9.40
	30	5.93	16.16	12.32	10.22	12.57	9.18
$\text{CH}_3$	0	5.23	18.85	11.83	11.65	12.76	10.36
	10	3.22	18.84	10.27	12.42	11.12	11.37
	20	3.58	18.58	10.16	12.43	11.28	11.20
	30	5.38	18.44	11.46	12.21	12.55	10.96
$\text{CH}=\text{CH}_2$	0	4.97	21.65	8.94	12.95	9.03	11.46
	10	5.21	21.30	8.40	13.86	8.21	12.23
	20	5.63	21.14	9.44	14.03	9.18	12.6
	30	7.53	21.12	12.24	13.76	10.62	12.34
$\text{C}\equiv\text{CH}$	0	0.99	17.24	4.63	9.43	6.78	8.39
	10	0.33	17.57	3.75	10.69	6.41	9.61
	20	1.04	17.55	4.25	11.35	7.51	10.24
	30	2.72	17.63	5.82	11.66	9.31	10.44
$\text{C}\equiv\text{N}$	0	0.81	26.34	5.02	16.21	6.03	14.58
	10	0.21	25.85	4.47	17.05	5.95	15.40
	20	1.25	25.31	5.44	17.4	7.41	15.76
	30	3.37	25.24	7.73	17.56	9.57	15.91

Table 8-3 Distortion constant  $k$  (cal·mol<sup>-1</sup>deg<sup>-2</sup>) fit to Eq (1)

	F <sup>-</sup>		Cl <sup>-</sup>		Br <sup>-</sup>	
	$k$	$R^2$ <sup>a</sup>	$k$	$R^2$	$k$	$R^2$
R=H	9.2	1.0	7.4	1.0	6.1	1.0
CH <sub>3</sub>	11.5	1.0	8.8	0.99	8.3	0.97
CH=CH <sub>2</sub>	9.8	0.99	9.3	0.94	6.5	0.99
C≡CH	7.4	1.0	5.7	1.0	6.9	1.0
C≡N	8.7	1.0	7.0	1.0	7.4	1.0

<sup>a</sup>correlation coefficient



Scheme 8-1 Molecules considered for  $S_N2$  reaction involving replacement of I by nucleophile.

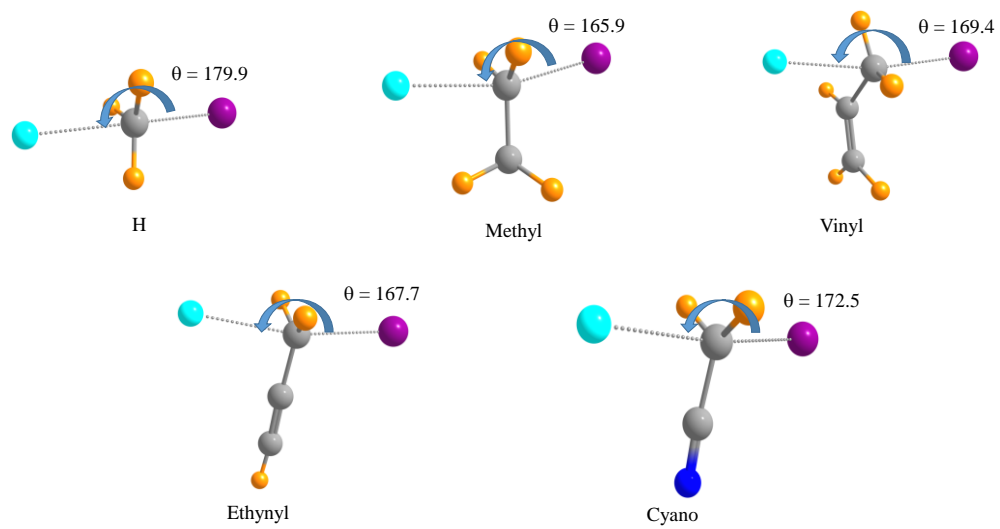


Figure 8-1 Transition state geometries of  $S_N2$  reactions, with  $F^-$  as nucleophile.

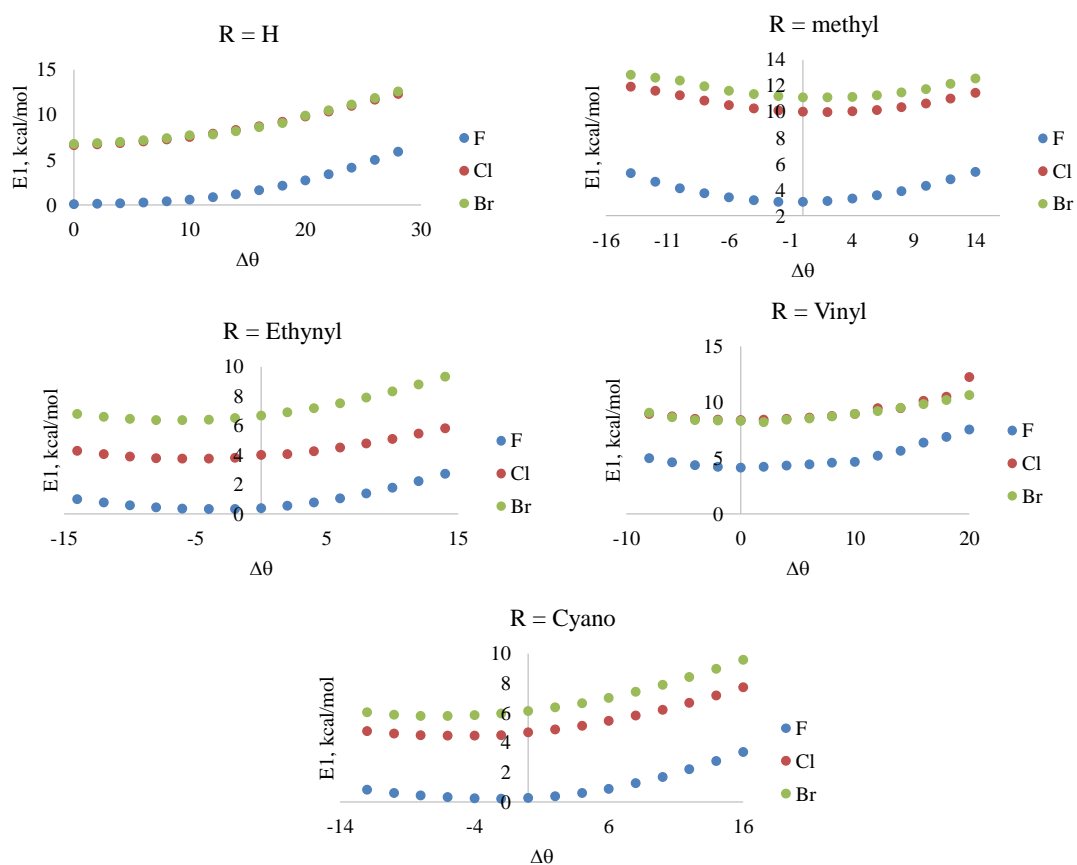


Figure 8-2 Dependence of activation energy  $E_1$  to angular distortion.

## CHAPTER 9

## SUMMARY

In this work, electronic and energetic as well as the catalytic importance of various types of non-covalent interactions has been presented. In chapter 2, sulfur tetrafluoride ( $\text{SF}_4$ ), a tetravalent S was used as the bridging atom for chalcogen bond formation involving various amines as electron donors. The amines used in this study were, both alkyl (ammonia, methyl, dimethyl and trimethyl amine) and heteroaromatic amines (pyridine, pyridazine, pyrazine, pyrimidine and imidazole). All of these amines, engage in strong chalcogen-bonds with  $\text{SF}_4$ . The methyl group substituent effect of alkyl amines was examined and it was established that the binding energy is very sensitive to the number of methyl groups. Ammonia with a binding energy of 6.6 kcal/mol had the weakest interaction amongst the alkyl amines while trimethyl amine had a binding energy of 14.4 kcal/mol. A comparison between alkyl and heteroaromatic amines revealed that, the latter are less sensitive to the nature of the ring and all the binding energies range between 7 and 9 kcal/mol. SAPT analysis of these complexes uncovered induction as the major attractive component of the binding energy. This induction energy is associated with transfer of charges primarily from the N-lone pair of the amine to the  $\sigma^*(\text{S-F})$  antibonding orbital of  $\text{SF}_4$ . The dimethylamine- $\text{SF}_4$  complex was so strong that it was said to approach the covalent bond regime. Its  $\text{R}(\text{N-S})$  distance is only 2.16 Å and the binding energy is 13 kcal/mol. The charge transferred from dimethylamine to  $\text{SF}_4$  upon formation of the chalcogen bond is 0.23 e, exceeding what is normally observed in a non-covalent bond. Charge rearrangement analysis shows that the charge transfer from the amine to the  $\text{SF}_4$



molecule is ultimately distributed among all four F-atoms, as well as the central S atom.

When one of the fluorine atoms of sulfur tetrafluoride, is replaced by a phenyl group, there is a strong preference for this group to occupy an equatorial position. No true minimum was observed in the gas phase when the phenyl group was made to occupy an apical position of the tetravalent sulfur. Ortho substitution of the phenyl group by an ether  $-\text{CH}_2\text{OCH}_3$  group further support the preference for the equatorial position. The latter structure was mainly stabilized by intramolecular chalcogen bond of the  $\text{S} \cdots \text{O}$  type, with O-atom as electron donor. This chalcogen bond also existed when the substituted phenyl group occupied apical position of tetravalent S, and accounts for the existence of this configuration in the gas phase. Addition of a second ether ( $-\text{CH}_2\text{OCH}_3$ ) group in the second ortho position of the phenyl ring led to the formation of disubstituted molecule. The apical geometry of this disubstituted molecule contains two  $\text{O} \cdots \text{S}$  chalcogen bonds in its most stable structure. In addition to the ether substituents, further substitution of the phenyl ring had only minor effects on the properties and energetics. All substituents, whether nominally electron-donating or withdrawing, and in any position on the phenyl ring, strengthen the  $\text{O} \cdots \text{S}$  chalcogen bond.

Both  $\text{SF}_2$  and  $\text{SF}_4$  engage in  $\text{S} \cdots \pi$  chalcogen bonds with a range of unsaturated hydrocarbons. Irrespective of the number of  $\text{C}=\text{C}$  bond present in a molecule such as butadiene or benzene, the S-atom is situated directly above one specific C double bond. The binding energies vary from a minimum of 3.3 kcal/mol for  $\text{SF}_4 \cdots \text{ethene}$  up to 6.6 kcal/mol for  $\text{SF}_2 \cdots \text{cis-butadiene}$ . Charge transfer from the  $\pi$  bond of the alkene to the  $\sigma^*(\text{S}-\text{F}_1)$  antibonding orbital is the primary source of the binding, wherein F1 lies directly

opposite the alkene. However, there are also lesser contributions from transfer to the other  $\sigma^*(\text{SF}_2)$  antibond. Additional transfer can originate from secondary C=C  $\pi$ -bonds as in butadiene. S sulfur lone pair of  $\text{SF}_2$  can align itself so as to transfer charge into the  $\pi^*$  MOs of the alkene, in what amounts to a back transfer, augmenting the strength of the chalcogen bond.

This dissertation also examined the wide range of different geometries when thiourea combines with each sort of substituted imine. In these complexes, the most strongly bound of these contain one or more hydrogen bonds. One type is characterized by a pair of nearly symmetric  $\text{NH}\cdots\text{N}$  HBs, with both NH groups of thiourea approaching the imine N from above and below its molecular plane. In a secondary structure, the arrangement combines a linear  $\text{NH}\cdots\text{N}$  with a  $\text{CH}\cdots\text{S}$  hydrogen bond. A third category of complex structure represent one in which the sulfur atom of thiourea approaches the imine methylene group. This structure is supplemented by a stacked arrangement. The bifurcated  $\text{CH}_2\cdots\text{S}$  hydrogen bond had the lowest interaction energy while a maximum of 13.5 kcal/mol was observed for the  $\text{NHCHOH}$  imine which combines a  $\text{NH}\cdots\text{O}$  and  $\text{OH}\cdots\text{S}$  pair of hydrogen bonds. Symmetry adapted perturbation theory analysis of the interaction energies of these complexes reveals nearly identical patterns with the electrostatic component emerging as the major contributor. Electron density shift patterns are consistent with the formulation of the interaction on the basis of HBs. The formation of the complex typically elongates the imine C-N bond by 0.001 - 0.004 Å, but there are certain complex arrangements wherein this bond is contracted.

Another aspect of this dissertation looked into the interaction of ammonia and

cyanogen halides (XCN). Ammonia can approach the XCN molecules from one of two directions. A typical  $\sigma$ -hole halogen bond is generated when the ammonia approaches the halogen atom along the NCX axis. This interaction ranges from 1.1 kcal/mol for X=F to 8.2 kcal/mol for I and it follows the  $F < Cl < Br < I$  trend. Above the axis of the XCN molecule, there exist a region of positive molecular electrostatic potential which is referred to as a  $\pi$ -hole. Quantitatively, the maximum potential of this  $\pi$ -hole area is larger than that of the  $\sigma$ -hole for FCN, but the reverse is true for the other cyanogen halogens. Unlike the  $\sigma$ -hole complexes, the  $\pi$ -hole dimers are fairly uniform in the range between 2.4 kcal/mol in the ICN:NH<sub>3</sub> complex and 3.1 kcal/mol in the FCN:NH<sub>3</sub> complexes. Electronic analysis notably the NBO analysis traces the stability of the  $\pi$ -hole geometries in large measure to charge transfer from the ammonia lone pair to the  $\pi^*(CN)$  antibonding orbital whose behavior is proportional to the energetics of binding. The Atoms In Molecule (AIM) topology analysis of the electron density confirms the interaction between the N-atom of ammonia and C-atom of cyanogen halide and also varies proportionately with the interaction energy. This behavior differs markedly from the halogen-bonded dimers where both ES and IND grow quickly with the size of the halogen atom, and IND exceeds ES for Br and I; DISP is considerably smaller. The  $\pi$ -hole characteristics of the C $\equiv$ N group have not been explored previously at any length, so comparison with other data in the literature is difficult. On the other hand, there have been a number of studies of the -NO<sub>2</sub> group which together offer a point of comparison. The  $\pi$ -hole of the NO<sub>2</sub> group is centered directly over the N atom<sup>1-4</sup> so dimers of relevant molecules tend to place an electronegative atom of one molecule over the N of the other. There are indications that these interactions

tend to be dominated by dispersion. Like XCN, the  $\pi$ -hole over the NO<sub>2</sub> subunit in XNO<sub>2</sub> becomes weaker in the order Cl > Br > I<sup>3,5</sup> but this trend is stronger than in the case of XCN. When placed on a phenyl ring, the NO<sub>2</sub> group engages in  $\pi$ -hole complexes with a variety of nucleophiles with binding energies that range up to more than 6 kcal/mol<sup>7</sup>, wherein AIM places the bond to the N atom in most cases, but also to the phenyl C to which the NO<sub>2</sub> group is connected. In addition to a lone pair, the  $\pi$ -bonding pair of a simple alkene or alkyne<sup>8</sup> can also interact with the  $\pi$ -hole of NO<sub>2</sub>, in which case the dispersion energy exceeds the ES component.

Application of such interactions notably in catalysis constituted a major part of this work. In chapter 7, we examined an Aza-Diels- Alder reaction catalyzed by a halogenated imidazolium salt. The halogenated imidazolium catalyst first form a loosely bound encounter complex with the imine and the diene. The transition state of the uncatalyzed reaction is 14 kcal/mol higher in energy than the separated reactants. In the presence of the catalyst, this transition state drops down to less than 5kcal/mol. In this regard, the Iodine substituted imidazolium salt is the most effective and the chlorine substituted imidazolium the least. The activation energy due to the H and Br are roughly the same. The high effectiveness of I-substitution is thus intimately connected with the strength of halogen bonds including I. Br-bonds are somewhat weaker, and Cl-bonds weaker still, consistent with the trends observed in catalytic rate acceleration. Activation-strain model of this reaction enabled the attestation that the reduction of the barrier by the catalyst is a result of the high interaction energy connected with the approach of the pre-deformed species as they form the transition state. The catalyst also alters the order of bond formation at the

transition state, by slowing the formation of N-C bond while hastening C-C formation. The catalyst exerts its influence in multifold ways. In the most obvious and direct effect, the H/X bond stabilizes the transition state. The catalyst also facilitates the transfer of charge from the diene to the imine in the transition state. This effect is manifest in both the total charges of the groups themselves, but also in the energies of charge transfer between specific orbitals ( $\pi_{\text{diene}} \rightarrow \pi^*_{\text{imine}}$ ). The H/X bond to the catalyst facilitates this transfer by lowering the energy of the  $\pi^*_{\text{imine}}$  antibonding orbital, thereby reducing the HOMO-LUMO energy gap.

In the last chapter of this work, the effect of angular deformation on the energetics of the  $\text{S}_{\text{N}}2$  reaction was considered. The calculations have indicated that a distortion of the preferred angle of attack of the nucleophile toward the central C atom in an  $\text{S}_{\text{N}}2$  reaction induces a strain energy into the system. Depending upon the particular system, a  $30^\circ$  distortion increments this energy by between 2.5 and 5.2 kcal/mol. With respect to the variations on the theme of halide attacking the  $\text{CH}_2\text{RI}$  molecule, the sensitivity to angular deformation appears to be a function of both the nature of the halide and the R group. For example, the methyl group is most sensitive to angle for  $\text{F}^-$  and  $\text{Br}^-$  nucleophiles, but the vinyl group takes this distinction for  $\text{Cl}^-$ . There is a general trend of  $\text{F}^- > \text{Cl}^- > \text{Br}^-$  but  $\text{Br}^- > \text{Cl}^-$  for both the triple bonded  $\text{C}\equiv\text{CH}$  and  $\text{C}\equiv\text{N}$  groups. This rise in energy of the transition state increases the barrier of the reaction when the fully separated reactants are taken as the initial point of the reaction.

In a nutshell, this dissertation has explained some of the fundamental properties and application of non-covalent interactions notably hydrogen, halogen, chalcogen and tetrel

bond. In some cases, a comparative analysis of these interactions has been made. This work has provided some insightful mechanistic results in imine reduction chemistry as well as Aza-Diels-Alder reaction. This will serve as a good guide in chemistry especially in the development of novel catalyst. For example, the study of the effect of halogenated imidazolium salts as catalyst in the Diels-alder reaction presented here represents the first computational attempt to rationalize the use of such compounds in chemical catalysis. This particular work can trigger the development of novel catalyst for other types of organic reactions that make use of non-covalent interactions. The study of the effect of angular deformation on the energetics of the  $S_N2$  reaction will find good applications in enzymes catalysis especially reactions involving  $S_N2$  mechanism like methyl transfer reactions. This work provides the basis of  $S_N2$  enzyme catalyzed reactions though in a simplified version. The work on intramolecular S---O chalcogen interactions will be helpful in the development of novel fluorinating agents as well as understanding the role of such interactions in molecular frameworks.

## References

- (1) C. Trujillo, G. Sanchez-Sanz, I. Alkorta and J. Elguero, *New J. Chem.*, 2015, **39**, 6791-6802
- (2) M. Solimannejad, N. Nassirinia and S. Amani, *Struct. Chem.*, 2013, 24, 651-659.
- (3) G. Sánchez-Sanz, C. Trujillo, M. Solimannejad, I. Alkorta and J. Elguero, *Phys. Chem. Chem. Phys.*, 2013, **15**, 14310-14318.
- (4) M. Solimannejad, V. Ramezani, C. Trujillo, I. Alkorta, G. Sánchez-Sanz and J.

Elguero, *J. Phys. Chem. A*, 2012, **116**, 5199-5206.

(5) T. Lang, X. Li, L. Meng, S. Zheng and Y. Zeng, *Struct. Chem.*, 2015, **26**, 213-221.



(6) Bauza, T. J. Mooibroek and A. Frontera, *Chem. Commun.*, 2015, **51**, 1491-1493.

A. Bauzá and A. Frontera, *Chem. Phys. Lett.*, 2015, **633**, 282-286.


## APPENDICES



## Appendix A. Copyright permissions

[Home](#)
[Account Info](#)
[Help](#)
[Live Chat](#)



**ACS Publications**  
Most Trusted. Most Cited. Most Read.


**Title:** Chalcogen Bonding between Tetravalent SF<sub>4</sub> and Amines  
**Author:** Vincent de Paul N. Nziko, Steve Scheiner  
**Publication:** The Journal of Physical Chemistry A  
**Publisher:** American Chemical Society  
**Date:** Nov 1, 2014  
Copyright © 2014, American Chemical Society


Logged in as:  
 Vincent de Paul Nzuwah Nziko  
[LOGOUT](#)


## Quick Price Estimate


Permission for this particular request is granted for print and electronic formats, and translations, at no charge. Figures and tables may be modified. Appropriate credit should be given. Please print this page for your records and provide a copy to your publisher. Requests for up to 4 figures require only this record. Five or more figures will generate a printout of additional terms and conditions. Appropriate credit should read: "Reprinted with permission from {COMPLETE REFERENCE CITATION}. Copyright {YEAR} American Chemical Society." Insert appropriate information in place of the capitalized words.

**I would like to...** 

**Requestor Type** 

**Portion** 

**Format** 

**Will you be translating?** 

**Select your currency**

**Quick Price**

This service provides permission for reuse only. If you do not have a copy of the article you are using, you may copy and paste the content and reuse according to the terms of your agreement. Please be advised that obtaining the content you license is a separate transaction not involving Rightslink.

To request permission for a type of use not listed, please contact [the publisher](#) directly.

Copyright © 2016 [Copyright Clearance Center, Inc.](#) All Rights Reserved. [Privacy statement](#). [Terms and Conditions](#).  
 Comments? We would like to hear from you. E-mail us at [customercare@copyright.com](mailto:customercare@copyright.com)



RightsLink®

[Home](#)[Account Info](#)[Help](#)ACS Publications  
Most Trusted. Most Cited. Most Read.

**Title:** Chalcogen Bonding between Tetravalent SF<sub>4</sub> and Amines  
**Author:** Vincent de Paul N. Nziko, Steve Scheiner  
**Publication:** The Journal of Physical Chemistry A  
**Publisher:** American Chemical Society  
**Date:** Nov 1, 2014

Copyright © 2014, American Chemical Society

Logged in as:

Vincent de Paul Nzuwah Nziko

[LOGOUT](#)**PERMISSION/LICENSE IS GRANTED FOR YOUR ORDER AT NO CHARGE**

This type of permission/license, instead of the standard Terms & Conditions, is sent to you because no fee is being charged for your order. Please note the following:

- Permission is granted for your request in both print and electronic formats, and translations.
- If figures and/or tables were requested, they may be adapted or used in part.
- Please print this page for your records and send a copy of it to your publisher/graduate school.
- Appropriate credit for the requested material should be given as follows: "Reprinted (adapted) with permission from (COMPLETE REFERENCE CITATION). Copyright (YEAR) American Chemical Society." Insert appropriate information in place of the capitalized words.
- One-time permission is granted only for the use specified in your request. No additional uses are granted (such as derivative works or other editions). For any other uses, please submit a new request.

[BACK](#)[CLOSE WINDOW](#)

Copyright © 2016 Copyright Clearance Center, Inc. All Rights Reserved. [Privacy statement](#). [Terms and Conditions](#).  
Comments? We would like to hear from you. E-mail us at [customer@copyright.com](mailto:customer@copyright.com)



# RightsLink®

[Home](#)
[Account Info](#)
[Help](#)


**ACS Publications**  
Most Trusted. Most Cited. Most Read.

**Title:** Intramolecular S···O Chalcogen Bond as Stabilizing Factor in Geometry of Substituted Phenyl-SF<sub>3</sub> Molecules

**Author:** Vincent de Paul N. Nziko, Steve Scheiner

**Publication:** The Journal of Organic Chemistry

**Publisher:** American Chemical Society

**Date:** Feb 1, 2015

Copyright © 2015, American Chemical Society

Logged in as:

Vincent de Paul Nzuwah Nziko

[LOGOUT](#)

## Quick Price Estimate

Permission for this particular request is granted for print and electronic formats, and translations, at no charge. Figures and tables may be modified. Appropriate credit should be given. Please print this page for your records and provide a copy to your publisher. Requests for up to 4 figures require only this record. Five or more figures will generate a printout of additional terms and conditions. Appropriate credit should read: "Reprinted with permission from {COMPLETE REFERENCE CITATION}. Copyright {YEAR} American Chemical Society." Insert appropriate information in place of the capitalized words.

**I would like to...** ?

reuse in a Thesis/Dissertation ▼

**Requestor Type** ?

Author (original work) ▼

**Portion** ?

Full article ▼

**Format** ?

Print and Electronic ▼

**Will you be translating?** ?

No ▼

**Select your currency**

USD - \$ ▼

**Quick Price**

[Click Quick Price](#)

This service provides permission for reuse only. If you do not have a copy of the article you are using, you may copy and paste the content and reuse according to the terms of your agreement. Please be advised that obtaining the content you license is a separate transaction not involving Rightslink.

[QUICK PRICE](#)

[CONTINUE](#)

To request permission for a type of use not listed, please contact [the publisher](#) directly.

Copyright © 2016 [Copyright Clearance Center, Inc.](#) All Rights Reserved. [Privacy statement.](#) [Terms and Conditions.](#)  
Comments? We would like to hear from you. E-mail us at [customercare@copyright.com](mailto:customercare@copyright.com)



**RightsLink®**

Home

Account  
Info

Help



**ACS Publications**  
Most Trusted. Most Cited. Most Read.

**Title:** Intramolecular S...O Chalcogen Bond as Stabilizing Factor in Geometry of Substituted Phenyl-SF<sub>3</sub> Molecules

**Author:** Vincent de Paul N. Nziko, Steve Scheiner

**Publication:** The Journal of Organic Chemistry

**Publisher:** American Chemical Society

**Date:** Feb 1, 2015

Copyright © 2015, American Chemical Society

Logged in as:

Vincent de Paul Nzuwah Nziko

LOGOUT

#### PERMISSION/LICENSE IS GRANTED FOR YOUR ORDER AT NO CHARGE

This type of permission/license, instead of the standard Terms & Conditions, is sent to you because no fee is being charged for your order. Please note the following:

- Permission is granted for your request in both print and electronic formats, and translations.
- If figures and/or tables were requested, they may be adapted or used in part.
- Please print this page for your records and send a copy of it to your publisher/graduate school.
- Appropriate credit for the requested material should be given as follows: "Reprinted (adapted) with permission from (COMPLETE REFERENCE CITATION). Copyright (YEAR) American Chemical Society." Insert appropriate information in place of the capitalized words.
- One-time permission is granted only for the use specified in your request. No additional uses are granted (such as derivative works or other editions). For any other uses, please submit a new request.

BACK

CLOSE WINDOW

Copyright © 2016 Copyright Clearance Center, Inc. All Rights Reserved. [Privacy statement](#). [Terms and Conditions](#). Comments? We would like to hear from you. E-mail us at [customercare@copyright.com](mailto:customercare@copyright.com)



# RightsLink®

[Home](#)
[Account Info](#)
[Help](#)


**ACS Publications**  
Most Trusted. Most Cited. Most Read.

**Title:** S...n Chalcogen Bonds between SF<sub>2</sub> or SF<sub>4</sub> and C–C Multiple Bonds

**Author:** Vincent de Paul N. Nziko, Steve Scheiner

**Publication:** The Journal of Physical Chemistry A

**Publisher:** American Chemical Society

**Date:** Jun 1, 2015

Copyright © 2015, American Chemical Society

Logged in as:

Vincent de Paul Nzuwah Nziko

[LOGOUT](#)

## Quick Price Estimate

Permission for this particular request is granted for print and electronic formats, and translations, at no charge. Figures and tables may be modified. Appropriate credit should be given. Please print this page for your records and provide a copy to your publisher. Requests for up to 4 figures require only this record. Five or more figures will generate a printout of additional terms and conditions. Appropriate credit should read: "Reprinted with permission from {COMPLETE REFERENCE CITATION}. Copyright {YEAR} American Chemical Society." Insert appropriate information in place of the capitalized words.

**I would like to...** ?

reuse in a Thesis/Dissertation ▼

**Requestor Type** ?

Author (original work) ▼

**Portion** ?

Full article ▼

**Format** ?

Print ▼

**Will you be translating?** ?

No ▼

**Select your currency**

USD - \$ ▼

**Quick Price**

[Click Quick Price](#)

This service provides permission for reuse only. If you do not have a copy of the article you are using, you may copy and paste the content and reuse according to the terms of your agreement. Please be advised that obtaining the content you license is a separate transaction not involving Rightslink.

[QUICK PRICE](#)

[CONTINUE](#)

To request permission for a type of use not listed, please contact [the publisher](#) directly.

Copyright © 2016 [Copyright Clearance Center, Inc.](#) All Rights Reserved. [Privacy statement](#). [Terms and Conditions](#). Comments? We would like to hear from you. E-mail us at [customercare@copyright.com](mailto:customercare@copyright.com)



RightsLink®

Home

Account  
Info

Help



ACS Publications  
Most Trusted. Most Cited. Most Read.

**Title:** S...n Chalcogen Bonds between SF<sub>2</sub> or SF<sub>4</sub> and C–C Multiple Bonds  
**Author:** Vincent de Paul N. Nziko, Steve Scheiner  
**Publication:** The Journal of Physical Chemistry A  
**Publisher:** American Chemical Society  
**Date:** Jun 1, 2015  
Copyright © 2015, American Chemical Society

Logged in as:  
Vincent de Paul Nzuwah Nziko  
[LOGOUT](#)

#### PERMISSION/LICENSE IS GRANTED FOR YOUR ORDER AT NO CHARGE

This type of permission/license, instead of the standard Terms & Conditions, is sent to you because no fee is being charged for your order. Please note the following:

- Permission is granted for your request in both print and electronic formats, and translations.
- If figures and/or tables were requested, they may be adapted or used in part.
- Please print this page for your records and send a copy of it to your publisher/graduate school.
- Appropriate credit for the requested material should be given as follows: "Reprinted (adapted) with permission from (COMPLETE REFERENCE CITATION). Copyright (YEAR) American Chemical Society." Insert appropriate information in place of the capitalized words.
- One-time permission is granted only for the use specified in your request. No additional uses are granted (such as derivative works or other editions). For any other uses, please submit a new request.

[BACK](#)

[CLOSE WINDOW](#)

Copyright © 2016 Copyright Clearance Center, Inc. All Rights Reserved. [Privacy statement](#). [Terms and Conditions](#).  
Comments? We would like to hear from you. E-mail us at [customercare@copyright.com](mailto:customercare@copyright.com)



# RightsLink®

[Home](#)
[Account Info](#)
[Help](#)


**ACS Publications**  
Most Trusted. Most Cited. Most Read.

**Title:** Interactions between Thiourea and Imines. Prelude to Catalysis  
**Author:** Vincent de Paul N. Nziko, Steve Scheiner  
**Publication:** The Journal of Organic Chemistry  
**Publisher:** American Chemical Society  
**Date:** Oct 1, 2015  
Copyright © 2015, American Chemical Society

Logged in as:  
Vincent de Paul Nzuwah Nziko  
[LOGOUT](#)

## Quick Price Estimate

Permission for this particular request is granted for print and electronic formats, and translations, at no charge. Figures and tables may be modified. Appropriate credit should be given. Please print this page for your records and provide a copy to your publisher. Requests for up to 4 figures require only this record. Five or more figures will generate a printout of additional terms and conditions. Appropriate credit should read: "Reprinted with permission from {COMPLETE REFERENCE CITATION}. Copyright {YEAR} American Chemical Society." Insert appropriate information in place of the capitalized words.

I would like to... ?

reuse in a Thesis/Dissertation ▼

Requestor Type ?

Author (original work) ▼

Portion ?

Full article ▼

Format ?

Electronic ▼

Will you be translating? ?

No ▼

Select your currency

USD - \$ ▼

Quick Price

Click Quick Price

This service provides permission for reuse only. If you do not have a copy of the article you are using, you may copy and paste the content and reuse according to the terms of your agreement. Please be advised that obtaining the content you license is a separate transaction not involving Rightslink.

[QUICK PRICE](#)

[CONTINUE](#)

To request permission for a type of use not listed, please contact [the publisher](#) directly.

Copyright © 2016 [Copyright Clearance Center, Inc.](#) All Rights Reserved. [Privacy statement](#). [Terms and Conditions](#).  
Comments? We would like to hear from you. E-mail us at [customer@copyright.com](mailto:customer@copyright.com)



RightsLink®

Home

Account  
Info

Help



ACS Publications  
Most Trusted. Most Cited. Most Read.

**Title:** Interactions between Thiourea and Imines. Prelude to Catalysis  
**Author:** Vincent de Paul N. Nziko, Steve Scheiner  
**Publication:** The Journal of Organic Chemistry  
**Publisher:** American Chemical Society  
**Date:** Oct 1, 2015

Copyright © 2015, American Chemical Society

Logged in as:  
Vincent de Paul Nzuwah Nziko

LOGOUT

#### PERMISSION/LICENSE IS GRANTED FOR YOUR ORDER AT NO CHARGE

This type of permission/license, instead of the standard Terms & Conditions, is sent to you because no fee is being charged for your order. Please note the following:

- Permission is granted for your request in both print and electronic formats, and translations.
- If figures and/or tables were requested, they may be adapted or used in part.
- Please print this page for your records and send a copy of it to your publisher/graduate school.
- Appropriate credit for the requested material should be given as follows: "Reprinted (adapted) with permission from (COMPLETE REFERENCE CITATION). Copyright (YEAR) American Chemical Society." Insert appropriate information in place of the capitalized words.
- One-time permission is granted only for the use specified in your request. No additional uses are granted (such as derivative works or other editions). For any other uses, please submit a new request.

BACK

CLOSE WINDOW

Copyright © 2016 Copyright Clearance Center, Inc. All Rights Reserved. [Privacy statement](#). [Terms and Conditions](#).  
Comments? We would like to hear from you. E-mail us at [customer@copyright.com](mailto:customer@copyright.com)





RightsLink®

Home

Create Account

Help



ACS Publications  
Most Trusted. Most Cited. Most Read.

**Title:** Catalysis of the Aza-Diels–Alder Reaction by Hydrogen and Halogen Bonds  
**Author:** Vincent de Paul N. Nziko, Steve Scheiner  
**Publication:** The Journal of Organic Chemistry  
**Publisher:** American Chemical Society  
**Date:** Mar 1, 2016

Copyright © 2016, American Chemical Society

**LOGIN**  
If you're a [copyright.com](#) user, you can login to RightsLink using your [copyright.com](#) credentials. Already a [RightsLink](#) user or want to [learn more?](#)

#### PERMISSION/LICENSE IS GRANTED FOR YOUR ORDER AT NO CHARGE

This type of permission/license, instead of the standard Terms & Conditions, is sent to you because no fee is being charged for your order. Please note the following:

- Permission is granted for your request in both print and electronic formats, and translations.
- If figures and/or tables were requested, they may be adapted or used in part.
- Please print this page for your records and send a copy of it to your publisher/graduate school.
- Appropriate credit for the requested material should be given as follows: "Reprinted (adapted) with permission from (COMPLETE REFERENCE CITATION). Copyright (YEAR) American Chemical Society." Insert appropriate information in place of the capitalized words.
- One-time permission is granted only for the use specified in your request. No additional uses are granted (such as derivative works or other editions). For any other uses, please submit a new request.

BACK

CLOSE WINDOW

Copyright © 2016 [Copyright Clearance Center, Inc.](#) All Rights Reserved. [Privacy statement.](#) [Terms and Conditions.](#)  
Comments? We would like to hear from you. E-mail us at [customercare@copyright.com](mailto:customercare@copyright.com)



# RightsLink®

[Home](#)
[Create Account](#)
[Help](#)


**ACS Publications**  
Most Trusted. Most Cited. Most Read.

**Title:** Catalysis of the Aza-Diels–Alder Reaction by Hydrogen and Halogen Bonds

**Author:** Vincent de Paul N. Nziko, Steve Scheiner

**Publication:** The Journal of Organic Chemistry

**Publisher:** American Chemical Society

**Date:** Mar 1, 2016

Copyright © 2016, American Chemical Society

[LOGIN](#)

If you're a [copyright.com](#) user, you can login to RightsLink using your copyright.com credentials. Already a RightsLink user or want to [learn more?](#)

## Quick Price Estimate

Permission for this particular request is granted for print and electronic formats, and translations, at no charge. Figures and tables may be modified. Appropriate credit should be given. Please print this page for your records and provide a copy to your publisher. Requests for up to 4 figures require only this record. Five or more figures will generate a printout of additional terms and conditions. Appropriate credit should read: "Reprinted with permission from {COMPLETE REFERENCE CITATION}. Copyright {YEAR} American Chemical Society." Insert appropriate information in place of the capitalized words.

I would like to... ?

reuse in a Thesis/Dissertation ▼

Requestor Type ?

Author (original work) ▼

Portion ?

Full article ▼

Format ?

Electronic ▼

Will you be translating? ?

No ▼

Select your currency

USD - \$ ▼

Quick Price

Click Quick Price

This service provides permission for reuse only. If you do not have a copy of the article you are using, you may copy and paste the content and reuse according to the terms of your agreement. Please be advised that obtaining the content you license is a separate transaction not involving Rightslink.

[QUICK PRICE](#)
[CONTINUE](#)

To request permission for a type of use not listed, please contact [the publisher](#) directly.

Copyright © 2016 [Copyright Clearance Center, Inc.](#) All Rights Reserved. [Privacy statement](#). [Terms and Conditions](#). Comments? We would like to hear from you. E-mail us at [customercare@copyright.com](mailto:customercare@copyright.com)



# RightsLink®

[Home](#)
[Create Account](#)
[Help](#)


**Title:** Effects of Angular Deformation on the Energetics of the SN2 Reaction

**Author:** Vincent Paul N. Nziko, Steve Scheiner

**Publication:** European Journal of Organic Chemistry

**Publisher:** John Wiley and Sons

**Date:** Jul 18, 2016

© 2016 WILEY-VCH Verlag GmbH & Co. KGaA, Weinheim

[LOGIN](#)

If you're a [copyright.com](#) user, you can login to RightsLink using your [copyright.com](#) credentials. Already a [RightsLink](#) user or want to [learn more?](#)

## Quick Price Estimate

**I would like to...** ?

reuse in a dissertation/thesis ▼

**Requestor Type** ?

Author of this Wiley article ▼

**Format** ?

Electronic ▼

**Portion** ?

Full article ▼

**Will you be translating?** ?

No ▼

**Select your currency**

USD - \$ ▼

**Quick Price**

Click Quick Price

### Content Delivery:

A copy of this content may be purchased following completion of your permissions order. High Res Image files - please contact [Wiley](#)

[QUICK PRICE](#)
[CONTINUE](#)

To request permission for a type of use not listed here, please select "I don't see my intended use" from the drop down option above.

[Information regarding permissions for developing countries.](#)

Copyright © 2016 [Copyright Clearance Center, Inc.](#) All Rights Reserved. [Privacy statement.](#) [Terms and Conditions.](#) Comments? We would like to hear from you. E-mail us at [customer@copyright.com](mailto:customer@copyright.com)



RightsLink®

[Home](#)[Account Info](#)[Help](#)

**Title:** Effects of Angular Deformation on the Energetics of the SN2 Reaction

**Author:** Vincent Paul N. Nziko, Steve Scheiner

**Publication:** European Journal of Organic Chemistry

**Publisher:** John Wiley and Sons

**Date:** Jul 18, 2016

© 2016 WILEY-VCH Verlag GmbH & Co. KGaA, Weinheim

Logged in as:

Vincent de Paul Nzuwah Nziko

Account #:  
3001070548

[LOGOUT](#)

### About Your Thesis / Dissertation

Please enter, completely and accurately, the following information regarding the thesis / dissertation you are currently working on. Any errors may delay or invalidate your license. All fields are required unless otherwise noted.

**Title of your thesis / dissertation**

COMPUTATIONAL CHEMISTRY OF NON-COVALEN

**Expected completion date**

Nov ▼

2016 ▼

**Estimated size (number of pages)**

250

[BACK](#)

[CONTINUE](#)

Copyright © 2016 [Copyright Clearance Center, Inc.](#) All Rights Reserved. [Privacy statement](#). [Terms and Conditions](#).  
Comments? We would like to hear from you. E-mail us at [customer@copyright.com](mailto:customer@copyright.com)

# JOHN WILEY AND SONS LICENSE TERMS AND CONDITIONS

Oct 13, 2016

This Agreement between Vincent de Paul Nzuwah Nziko ("You") and John Wiley and Sons ("John Wiley and Sons") consists of your license details and the terms and conditions provided by John Wiley and Sons and Copyright Clearance Center.

License Number	3967111255025
License date	Oct 13, 2016
Licensed Content Publisher	John Wiley and Sons
Licensed Content Publication	European Journal of Organic Chemistry
Licensed Content Title	Effects of Angular Deformation on the Energetics of the SN2 Reaction
Licensed Content Author	Vincent Paul N. Nziko, Steve Scheiner
Licensed Content Date	Jul 18, 2016
Licensed Content Pages	5
Type of use	Dissertation/Thesis
Requestor type	Author of this Wiley article
Format	Electronic
Portion	Full article
Will you be translating?	No
Title of your thesis / dissertation	COMPUTATIONAL CHEMISTRY OF NON-COVALENT INTERACTION AND ITS APPLICATION IN CHEMICAL CATALYSIS
Expected completion date	Nov 2016
Expected size (number of pages)	250
Requestor Location	Vincent de Paul Nzuwah Nziko 28 aggievillage apt K  LOGAN, UT 84341 United States Attn: Vincent de Paul Nzuwah Nziko
Publisher Tax ID	EU826007151
Billing Type	Invoice
Billing Address	Vincent de Paul Nzuwah Nziko 28 aggievillage apt K  LOGAN, UT 84341 United States Attn: Vincent de Paul Nzuwah Nziko
Total	0.00 USD
Terms and Conditions	

## TERMS AND CONDITIONS

This copyrighted material is owned by or exclusively licensed to John Wiley & Sons, Inc. or one of its group companies (each a "Wiley Company") or handled on behalf of a society with

<https://s100.copyright.com/AppDispatchServlet>

which a Wiley Company has exclusive publishing rights in relation to a particular work (collectively "WILEY"). By clicking "accept" in connection with completing this licensing transaction, you agree that the following terms and conditions apply to this transaction (along with the billing and payment terms and conditions established by the Copyright Clearance Center Inc., ("CCC's Billing and Payment terms and conditions"), at the time that you opened your RightsLink account (these are available at any time at <http://myaccount.copyright.com>).

#### Terms and Conditions

- The materials you have requested permission to reproduce or reuse (the "Wiley Materials") are protected by copyright.
- You are hereby granted a personal, non-exclusive, non-sub licensable (on a stand-alone basis), non-transferable, worldwide, limited license to reproduce the Wiley Materials for the purpose specified in the licensing process. This license, and any CONTENT (PDF or image file) purchased as part of your order, is for a one-time use only and limited to any maximum distribution number specified in the license. The first instance of republication or reuse granted by this license must be completed within two years of the date of the grant of this license (although copies prepared before the end date may be distributed thereafter). The Wiley Materials shall not be used in any other manner or for any other purpose, beyond what is granted in the license. Permission is granted subject to an appropriate acknowledgement given to the author, title of the material/book/journal and the publisher. You shall also duplicate the copyright notice that appears in the Wiley publication in your use of the Wiley Material. Permission is also granted on the understanding that nowhere in the text is a previously published source acknowledged for all or part of this Wiley Material. Any third party content is expressly excluded from this permission.
- With respect to the Wiley Materials, all rights are reserved. Except as expressly granted by the terms of the license, no part of the Wiley Materials may be copied, modified, adapted (except for minor reformatting required by the new Publication), translated, reproduced, transferred or distributed, in any form or by any means, and no derivative works may be made based on the Wiley Materials without the prior permission of the respective copyright owner. For STM Signatory Publishers clearing permission under the terms of the [STM Permissions Guidelines](#) only, the terms of the license are extended to include subsequent editions and for editions in other languages, provided such editions are for the work as a whole in situ and does not involve the separate exploitation of the permitted figures or extracts. You may not alter, remove or suppress in any manner any copyright, trademark or other notices displayed by the Wiley Materials. You may not license, rent, sell, loan, lease, pledge, offer as security, transfer or assign the Wiley Materials on a stand-alone basis, or any of the rights granted to you hereunder to any other person.
- The Wiley Materials and all of the intellectual property rights therein shall at all times remain the exclusive property of John Wiley & Sons Inc, the Wiley Companies, or their respective licensors, and your interest therein is only that of having possession of and the right to reproduce the Wiley Materials pursuant to Section 2 herein during the continuance of this Agreement. You agree that you own no right, title or interest in or to the Wiley Materials or any of the intellectual property rights therein. You shall have no rights hereunder other than the license as provided for above in Section 2. No right, license or interest to any trademark, trade name, service mark or other branding ("Marks") of WILEY or its licensors is granted hereunder, and you agree that you



shall not assert any such right, license or interest with respect thereto

- NEITHER WILEY NOR ITS LICENSORS MAKES ANY WARRANTY OR REPRESENTATION OF ANY KIND TO YOU OR ANY THIRD PARTY, EXPRESS, IMPLIED OR STATUTORY, WITH RESPECT TO THE MATERIALS OR THE ACCURACY OF ANY INFORMATION CONTAINED IN THE MATERIALS, INCLUDING, WITHOUT LIMITATION, ANY IMPLIED WARRANTY OF MERCHANTABILITY, ACCURACY, SATISFACTORY QUALITY, FITNESS FOR A PARTICULAR PURPOSE, USABILITY, INTEGRATION OR NON-INFRINGEMENT AND ALL SUCH WARRANTIES ARE HEREBY EXCLUDED BY WILEY AND ITS LICENSORS AND WAIVED BY YOU.
- WILEY shall have the right to terminate this Agreement immediately upon breach of this Agreement by you.
- You shall indemnify, defend and hold harmless WILEY, its Licensors and their respective directors, officers, agents and employees, from and against any actual or threatened claims, demands, causes of action or proceedings arising from any breach of this Agreement by you.
- IN NO EVENT SHALL WILEY OR ITS LICENSORS BE LIABLE TO YOU OR ANY OTHER PARTY OR ANY OTHER PERSON OR ENTITY FOR ANY SPECIAL, CONSEQUENTIAL, INCIDENTAL, INDIRECT, EXEMPLARY OR PUNITIVE DAMAGES, HOWEVER CAUSED, ARISING OUT OF OR IN CONNECTION WITH THE DOWNLOADING, PROVISIONING, VIEWING OR USE OF THE MATERIALS REGARDLESS OF THE FORM OF ACTION, WHETHER FOR BREACH OF CONTRACT, BREACH OF WARRANTY, TORT, NEGLIGENCE, INFRINGEMENT OR OTHERWISE (INCLUDING, WITHOUT LIMITATION, DAMAGES BASED ON LOSS OF PROFITS, DATA, FILES, USE, BUSINESS OPPORTUNITY OR CLAIMS OF THIRD PARTIES), AND WHETHER OR NOT THE PARTY HAS BEEN ADVISED OF THE POSSIBILITY OF SUCH DAMAGES. THIS LIMITATION SHALL APPLY NOTWITHSTANDING ANY FAILURE OF ESSENTIAL PURPOSE OF ANY LIMITED REMEDY PROVIDED HEREIN.
- Should any provision of this Agreement be held by a court of competent jurisdiction to be illegal, invalid, or unenforceable, that provision shall be deemed amended to achieve as nearly as possible the same economic effect as the original provision, and the legality, validity and enforceability of the remaining provisions of this Agreement shall not be affected or impaired thereby.
- The failure of either party to enforce any term or condition of this Agreement shall not constitute a waiver of either party's right to enforce each and every term and condition of this Agreement. No breach under this agreement shall be deemed waived or excused by either party unless such waiver or consent is in writing signed by the party granting such waiver or consent. The waiver by or consent of a party to a breach of any provision of this Agreement shall not operate or be construed as a waiver of or consent to any other or subsequent breach by such other party.
- This Agreement may not be assigned (including by operation of law or otherwise) by you without WILEY's prior written consent.

- Any fee required for this permission shall be non-refundable after thirty (30) days from receipt by the CCC.
- These terms and conditions together with CCC's Billing and Payment terms and conditions (which are incorporated herein) form the entire agreement between you and WILEY concerning this licensing transaction and (in the absence of fraud) supersedes all prior agreements and representations of the parties, oral or written. This Agreement may not be amended except in writing signed by both parties. This Agreement shall be binding upon and inure to the benefit of the parties' successors, legal representatives, and authorized assigns.
- In the event of any conflict between your obligations established by these terms and conditions and those established by CCC's Billing and Payment terms and conditions, these terms and conditions shall prevail.
- WILEY expressly reserves all rights not specifically granted in the combination of (i) the license details provided by you and accepted in the course of this licensing transaction, (ii) these terms and conditions and (iii) CCC's Billing and Payment terms and conditions.
- This Agreement will be void if the Type of Use, Format, Circulation, or Requestor Type was misrepresented during the licensing process.
- This Agreement shall be governed by and construed in accordance with the laws of the State of New York, USA, without regards to such state's conflict of law rules. Any legal action, suit or proceeding arising out of or relating to these Terms and Conditions or the breach thereof shall be instituted in a court of competent jurisdiction in New York County in the State of New York in the United States of America and each party hereby consents and submits to the personal jurisdiction of such court, waives any objection to venue in such court and consents to service of process by registered or certified mail, return receipt requested, at the last known address of such party.

#### **WILEY OPEN ACCESS TERMS AND CONDITIONS**

Wiley Publishes Open Access Articles in fully Open Access Journals and in Subscription journals offering Online Open. Although most of the fully Open Access journals publish open access articles under the terms of the Creative Commons Attribution (CC BY) License only, the subscription journals and a few of the Open Access Journals offer a choice of Creative Commons Licenses. The license type is clearly identified on the article.

##### **The Creative Commons Attribution License**

The [Creative Commons Attribution License \(CC-BY\)](#) allows users to copy, distribute and transmit an article, adapt the article and make commercial use of the article. The CC-BY license permits commercial and non-

##### **Creative Commons Attribution Non-Commercial License**

The [Creative Commons Attribution Non-Commercial \(CC-BY-NC\) License](#) permits use, distribution and reproduction in any medium, provided the original work is properly cited and is not used for commercial purposes.(see below)

##### **Creative Commons Attribution-Non-Commercial-NoDerivs License**

The [Creative Commons Attribution Non-Commercial-NoDerivs License](#) (CC-BY-NC-ND) permits use, distribution and reproduction in any medium, provided the original work is properly cited, is not used for commercial purposes and no modifications or adaptations are made. (see below)

Use by commercial "for-profit" organizations



Use of Wiley Open Access articles for commercial, promotional, or marketing purposes requires further explicit permission from Wiley and will be subject to a fee.

Further details can be found on Wiley Online Library

<http://olabout.wiley.com/WileyCDA/Section/id-410895.html>

**Other Terms and Conditions:**

**v1.10 Last updated September 2015**

Questions? [customercare@copyright.com](mailto:customercare@copyright.com) or +1-855-239-3415 (toll free in the US) or +1-978-646-2777.

---

## CURRICULUM VITAE

**Vincent de Paul N. Nziko**

Department of Chemistry and Biochemistry  
Utah State University, 0300 Old Main Hill  
Logan, UT 84322-0300  
[vpn.nziko@aggiemail.usu.edu](mailto:vpn.nziko@aggiemail.usu.edu)  
(435) 363 6747

---

**Education**

<b>Utah State University, UT</b>	2011-present
Ph.D., Chemistry	
<b>University of Buea, Cameroon</b>	
M.Sc., Chemistry/Pharmaceutical Chemistry	2008-2011
B.Sc., Chemistry/ Material Science	2005-2008

**Research Experience****Utah State University, UT (Ph.D. Research)**

**Project:** Computational study of non-covalent interaction and its application in organic, inorganic and bioorganic systems.

**University of Buea, Cameroon (M.Sc. Research)**

**Project:** Synthesis, Pharmacological Evaluation and Structure-Activity Relationship of Spiro [indole-3, 3'-Pyrrolidin]-2(1H)-ones.

**Teaching Experience**

**Sacred Heart College Douala-  
Cameroon (Archdiocese of  
Douala)**

**Organic Chemistry – Lecturer (Sep  
2009-Feb 2011)**

Prepared teaching material including problem set and quizzes.  
Addressed individual students' questions and needs

**Physical Chemistry – Lecturer (Sep 2009-  
Feb 2011)**

Prepared teaching material including problem set and quizzes.  
Addressed individual students' questions and needs

**Utah State University (2011-  
2016)**

**Principle of Chemistry I & II –  
Teaching Assistant**

Prepared teaching material including problem set and quizzes.  
Addressed individual students' questions and needs (spring 2016,  
2015, 2014, 2013 & fall 2015)

**Computational Chemistry – Teaching Assistant**

Supervised and Assist students with individual needs in completing  
their research class research projects (Fall 2015)

**Principle of Chemistry Lab I & II – Teaching Assistant**

Supervised and instruct students in principle of chemistry  
laboratory. Emphasized keeping complete and accurate scientific  
notes as well as laboratory safety. (Fall 2013 and summer 2015)

**Organic Chemistry Laboratory I & II**

Supervised and instruct students in organic Techniques.  
Emphasized keeping complete and accurate scientific notes as well  
as laboratory safety (fall 2011, 2012, spring 2011, 2012)

**University of Buea, Cameroon (2008-2011)**

**General Chemistry**

Prepared teaching material including problem set and quizzes.  
Addressed individual students' questions and needs (Oct. 2008 –  
June 2009)

**Organic Chemistry I & II-(part-time)**

Prepared teaching material including problem set and quizzes.  
Addressed individual students' questions and needs (Oct. 2009 –  
Feb 2011)

**Expertise:**

**Computational:** Quantum Chemical Calculations (electronic properties)- Density Functional Theory (DFT), *ab initio* calculations (open and closed shell systems), Molecular Dynamics, 2D and 3D Qualitative Structure Activity Relationship (QSAR), Binding/Bonding interactions, coupled-cluster, many-body perturbation, symmetry-adapted perturbation theories (SAPT), Energy decomposition analysis, Reaction Mechanism elucidation and Transition state search, Molecular Surface Energy, QM/MM, High-performance Computing, Ability to work with both organic, inorganic (metals) and biochemical molecules.

**Software:** GaussView5.0, Gaussian09 packages, ADF, NBO6, ChemCraft, AIM2000, ChemDraw, Spartan10, MOE, GROMACS, GAMESS, Molpro, VASP, NAMD/VMD

**Scripts/Programing (Beginner):** Python, Perl, FORTRAN, C++ and Shell

**Experimental:** UV-Spectroscopy, IR, NMR, and HPLC. Additional chromatographic technique includes TLC, Paper Chromatography

**Language:** English and French (Written and Spoken)

**Professional Organization:**

- American Chemical Society (ACS) member since 2012

**Departmental Service:**

- Member of the Utah State University Department of Chemistry and biochemistry Student Safety Committee since 2013

**Publications (16)**

1. Vincent de Paul N Nziko, Steve Scheiner “Catalysis of the Aza-Diels-alder reaction by Hydrogen and Halogen Bonds” *J. Org. Chem.* **2016** (doi: 10.1021/acs.joc.6b00344)
2. Vincent de Paul N Nziko, Steve Scheiner “Comparison of  $\pi$ -hole tetrel bonding with  $\sigma$ -hole halogen bonds in complexes of XCN (X = F, Cl, Br, I) and NH<sub>3</sub>” *Phys. Chem. Chem. Phys.*, **2016**, Advance Article DOI: 10.1039/C5CP07545A.
3. Vincent de Paul N Nziko, Steve Scheiner “Effects of Angular Deformation on the Energetics of the SN<sub>2</sub> Reaction” *Eur. J. Org. Chem.* **2016** (DOI: 10.1002/ejoc.201600712)
4. Vincent de Paul N Nziko, Steve Scheiner “Interaction between Thiourea and Imines. Prelude to catalysis” *J. Org. Chem.*, **2015**, 80 (20), 10334–10341
5. Okuma Kasende, Muya Jule, Vincent de Paul N Nziko, Steve Scheiner “Hydrogen-Bonded and Stacked geometries of the Temozolomide Dimer” *J. Mol. Mod.* **2016** 22: 27

6. Okuma Kasende, Vincent de Paul N Nziko, Steve Scheiner “H-bonding and Stacking Interactions between Chloroquine and Temozolomide” *int. j. quan. Chem.* **2016**
7. Vincent de Paul N Nziko, Steve Scheiner “S $\cdots$   $\pi$  Chalcogen Bonds between SF<sub>2</sub> or SF<sub>4</sub> and CC Multiple Bonds” *J. Phys. Chem. A*, **2015**, 119 (22), 5889–5897
8. Vincent de Paul N Nziko, Steve Scheiner “Intramolecular S $\cdots$ O Chalcogen Bond as Stabilizing Factor in Geometry of Substituted Phenyl-SF<sub>3</sub> Molecules” *J. Org. Chem.*, **2015**, 80 (4), 2356–2363
9. Marina Fosso, Madher N AlFindee, Qian Zhang, Vincent de Paul Nzuwah Nziko, Yukie Kawasaki, Sanjib K Shrestha, Jeremiah Bearss, Rylee Gregory, Jon Y Takemoto, Cheng-Wei Tom Chang “Structure–Activity Relationships for Antibacterial to Antifungal Conversion of Kanamycin to Amphiphilic Analogues” *J. Org. Chem.*, **2015**, 80 (9), 4398–4411
10. Vincent de Paul N Nziko, Marina Y Fosso, Cheng-Wei Tom Chang “Quantitative structure–activity relationship analysis of antibacterial cationic anthraquinone analogs using Hansch and Fujita models” *Med. Chem. Res.*, **2014**, 23(12), 5058-5062
11. Vincent de Paul N Nziko, Steve Scheiner “Chalcogen Bonding between Tetravalent SF<sub>4</sub> and Amines” *J. Phys. Chem. A*, 2014, 118 (45), 10849– 10856
12. Marina Y Fosso, Vincent de Paul N Nziko, Cheng-Wei Tom Chang “Chemical Synthesis of N-Aryl Glycosides” *J. Carb. Chem.*, **2012**, 31(8), 603-619
13. Qian Zhang, Madher N. Alfindee, Jaya P. Shrestha, Vincent de Paul Nzuwah Nziko, Yukie Kawasaki, Xinrui Peng, Jon Y. Takemoto, and Cheng-Wei Tom Chang “Practical and Divergent Synthesis of Three Classes of Antifungal Amphiphilic Kanamycin Derivatives” *J. Carb. Chem.*, **2016**
14. Jaya P Shrestha, Coleman Baker, Yukie Kawasaki, Yagya P Subedi, Vincent de Paul N.Nziko, Jon Y Takemoto, and Cheng-Wei Tom Chang “Synthesis and Bioorganic Investigation of Quinone based multi-cationic triazolium amphiphiles” *J. Med.Chem.*, **2016** (Submitted)
15. Okuma Kasende, Vincent de Paul N Nziko, Steve Scheiner” Interactions of Nucleic Acids with Temozolomide: Stacked, Perpendicular, and Coplanar Heterodimers” *J. Phys. Chem B.*, **2016**

16. Okuma Kasende, Vincent de Paul N Nziko, Steve Scheiner” Interactions between Temozolomide and Quercetin” *Struc. Chem.*, **2016**

#### Poster Presentation (05)

1. Vincent de Paul Nzuwah Nziko, Steve Scheiner “N-S vs  $\pi$ -S interactions: a computational study” *ABSTRACTS OF PAPERS OF THE AMERICAN CHEMICAL SOCIETY*. Vol. 251. 1155 16TH ST, NW, WASHINGTON, DC 20036 USA: AMER CHEMICAL SOC, **2016**.
2. Vincent de Paul Nzuwah Nziko, Steve Scheiner “DFT conformational study of phenylsulfur trifluoride and their properties” *ABSTRACTS OF PAPERS OF THE AMERICAN CHEMICAL SOCIETY*. Vol. 248. 1155 16TH ST, NW, WASHINGTON, DC 20036 USA: AMER CHEMICAL SOC, **2015**.
3. Anderson, Stacey N., Vincent de Paul Nzuwah Nziko, Cheng-Wei Tom Chang, and Alvan C. Hengge. "Enhancing safety in academic research laboratories: Creating a student based safety committee." *ABSTRACTS OF PAPERS OF THE AMERICAN CHEMICAL SOCIETY*, vol. 248. 1155 16TH ST, NW, WASHINGTON, DC 20036 USA: AMER CHEMICAL SOC, **2014**.
4. Nziko V.P.N.; Fosso M. Y.; Chang C.-W. T. “Structural Optimization of Kanamycin Analogs.” *ABSTRACTS OF HANSEN RETREAT*, September **2012**, Wellsville, UT
5. Joelle Ngo Hanna, Fidele Ntie-Kang, Vincent de Paul Nzuwah Nziko, Paul T Chongwain, Simon MM Efange “Computer-aided design and screening of oxazolyl thiosemicarbazones against multidrug-resistant tuberculosis: coupling 2D descriptors with topological differences” *4th ANDI Stakeholder Meeting and Donors Conference*, Addis-Ababa, Ethiopia; 10/**2011**